TU WIEN **bi.**

Doctoral Thesis

Investigation of different vortex shedding models, based on sensibility and probability methods to evolve probabilistic models

submitted in satisfaction of the requirements for the degree of
Doctor of Science in Civil Engineering
of the Vienna University of Technology, Faculty of Civil Engineering

Dissertation

Studie unterschiedlicher Wirbelablösemodelle auf Basis von Sensitivitäts- und Probabilitätsmethoden zur Generierung probabilistischer Modelle

ausgeführt zum Zwecke der Erlangung des akademischen Grades eines
Doktors der technischen Wissenschaft
eingereicht an der Technischen Universität Wien, Fakultät für Bauingenieurwesen
von

Dipl.-Ing. Emanuel Bombasaro
Matnr.: 0425766
aus Innsbruck, Österreich

Gutachter:

- Prof. Dr. techn. Christian Bucher
  Institut für Hochbau und Technologie
  Technische Universität Wien, Österreich

- Prof. Ing. Giovanni Solari
  Dipartimento di Ingegneria delle Costruzioni, dell'Ambiente e del Territorio
  Università degli Studi di Genova, Italia

Wien, im März 2011

Abstract

In order to obtain a full, sophisticated design for a structure each individual phenomenon has to be considered in a proper way as a partial model. Among these phenomena are: the stress distribution, the material properties, the dynamical behavior, the loads and many more. In this work the load model for the vortex shedding phenomenon – as it is one of the most complex aeroelastic phenomena in the field of wind engineering – is studied in order to guarantee and provide a proper and reliable model for designing structures against fatigue due to vortex induced vibrations.

After a general introduction to the topic of sophisticated structural design – by introducing design model chains – the vortex shedding phenomenon is discussed and it is according to the state of the art framed in the context of physics of the atmosphere. More specific atmospheric stratification conditions are probabilistically studied to obtain the real atmospheric turbulence intensity via measurements of the Monin-Obukhov length. The vortex shedding phenomenon is generally analyzed with a dimensional analysis and further in terms of the five most popular models: Ruscheweyh, Vickery and Basu, ESDU, Griffin and AIJ recommendations. Results of all models are compared on the base of measurements taken from literature and how well they represent the physical phenomenon of vortex shedding. These analyses are carried out with the help of the Bayesian model selection and response surface analysis as well as limit studies.

As preparation for a variance based sensitivity analysis, a detailed parameter study is carried out to obtain the necessary information and distributions of the determining parameters in vortex shedding. The aim of the sensitivity analysis is to determine which parameters are the most influential ones and for which parameters further investigation would be appropriate to improve the structural design.

In the last part a closed form solution to evaluate the occurrence probability of vortex shedding for every individual natural vibration mode of the structure is given. Followed by a study, of how the distribution of structural parameters influences the results obtained by the Vickery and Basu model and if this influence can be described by a function. The last step is an introduction of the fatigue lifetime analysis of the structure where the atmospheric stratification condition, the mean wind velocity and the structural parameters enter as probabilistic parameters.

In two examples the improvement and quality of using probabilistic vortex shedding models in the whole context of sophisticated structural design is shown.

Keywords:
atmospheric stratification condition, dimensional analysis, vortex shedding approaches, variance based sensitivity analysis, Bayesian model class selection, occurrence probability of vortex shedding, probabilistic fatigue analysis

Zusammenfassung

Um eine vollständige und durchdachte Modellierungskette für die Bemessung von Strukturen zu erhalten, ist jedes Teilphänomen als partielles Modell möglichst genau zu berücksichtigen. Partielle Modelle umfassen unter anderem die Spannungsverteilung, das Materialverhalten, das dynamische Verhalten der Struktur und die Belastung. In dieser Arbeit wird das Lastmodel für wirbelerregte Schwingung untersucht, um ein vollständiges und zuverlässiges Modell zur Ermittlung der Ermüdungsbeanspruchung durch wirbelerregte Schwingung zu garantieren. Die wirbelerregte Schwingung stellt eine der komplexesten Phänomene im Windingenieurwesen dar.

Die Arbeit beginnt mit einer generellen Einführung in das Thema sowie mit Überlegungen an der Modellierungskette. Weiters wird die wirbelerregte Schwingung im Kontext der Physik der Atmosphäre auf dem aktuellen Stand der Forschung diskutiert. Der Stratifikationszustand der Atmosphäre wird probabilistisch berücksichtigt, um die atmosphärische Turbulenz möglichst genau abzubilden. Dies erfolgt auf Grundlage von Messungen der Monin-Obukhov-Länge, von welcher Verteilungen des Stratifikationszustandes abgeleitet werden. Im nächsten Schritt wird das Phänomen der Wirbelablösung mit der Dimensionenanalyse studiert und dann werden fünf der gängigsten Modelle zur Beschreibung der Wirbelablösung eingeführt: Ruscheweyh, Vickery und Basu, ESDU, Griffin und AIJ-Empfehlungen. Die Ergebnisse aller Modelle werden mit Messungen aus der Literatur verglichen und auf ihre physikalische Aussagekraft bewertet. Diese Studien erfolgen mit Hilfe der Bayes-Modellselektionsmethode sowie mit Antwortflächen-Untersuchungen und Limitbildungen.

Im Anschluss daran wird eine detaillierte Untersuchung der involvierten Parameter durchgeführt, um deren jeweilige Verteilungen und Charakteristiken für eine varianzbasierte Sensitivitätsstudie bereitzustellen. Ziel der Sensitivitätsstudie ist die Feststellung, welche Parameter den höchsten Einfluss auf das Ergebnis haben, und somit kann auch gezeigt werden, welche Parameter mit besonderer Sorgfalt ermittelt werden sollen, um ein zufriedenstellendes Ergebnis zu erzielen.

Im letzen Abschnitt wird ein Modell vorgestellt, mit welchem die Auftrittswahrscheinlichkeit von Wirbelablösung für jeden Mode der Struktur ermittelt werden kann. Weiters wird untersucht, wie bedeutend der Einfluss der Strukturparameter, Strukturdämpfung und Eigenfrequenz der Struktur in das Modell nach Vickery und Basu eingehen, und ob der Einfluss funktional abbildbar ist. Zuletzt wird die Lebensdauer zufolge Ermüdung der Struktur mittels eines Modells, in welches der Stratifikationszustand der Atmosphäre, die mittlere Windgeschwindigkeit und die Strukturparameter als probabilistische Größen eingehen, vorgestellt.

Abschließend wird in einem Beispiel gezeigt, welche Verbesserungen und Qualitätssteigerungen erzielt werden können, wenn probabilistische Modelle zur Ermittlung der Ermüdungsbeanspruchung durch wirbelerregte Schwingung verwendet werden. In einem zweiten Beispiel wird die weiterhin vorhandene Unsicherheit in der Beanspruchungsermittlung durch Wirbelablösung an einem sehr hohen Brückenpylon diskutiert.

Schlagwörter:
Stratifikationszustand der Atmosphäre, Dimensionen-Analyse, Modelle zur Beschreibung wirbelerregter Schwingung, varianzbasierte Sensitivitätsanalyse, Bayessche Modelselektion, Auftrittswahrscheinlichkeit von Wirbelablösung, probabilistische Ermüdungsanalyse

Acknowledgements

. . . Eile heißt der Wind, der das Baugerüst umweht . . .

Bertold Brecht

. . . Wer baut auf Wind, baut auf Satans Erbarmen!

Wagner, Der Fliegende Holländer

Contents

List of Symbols

a_1, a_2 Wöhler curve parameters

a, c, F_0 model parameters of the Weibull model for P_h

a_j modal coefficient; *Vickery and Basu*

α limiting factor of rms response in number of D; *Vickery and Basu*

α_ε, β_ε, γ_ε atmospheric stratification condition density distribution parameter, $\varepsilon = d, n$

α_{ζ_s, n_j} quantile value of the deterministic model reaction

$a_{(n)}$ nth mode shape integral; $a_{(n)} = \int_h \phi_j^n \, \mathrm{d}z$

c_{dis} distribution of lift coefficients, c_l or c_{lat}

χ_v, χ_w non-dimensional quantities related to wind induced excitation

$\tilde{C}_L$ rms lift force coefficient depending on oscillation amplitude; *ESDU*

c_l rms lift force coefficient

c_L, c_D, c_M non-dimensional force coefficients; *lift, drag, rotation*

C_{L0} fluctuating lift amplitude; *Griffin and Skop*

c_{lat} exciting force coefficient; *Ruscheweyh*

$\tilde{C}_{L_j}$ mode generalized fluctuating force coefficient ; *ESDU*

$c_L{}'$, $c_D{}'$, $c_M{}'$ prime angular derivative of the non-dimensional force coefficients; *lift, drag, rotation*

$\mathrm{C}_{\varepsilon,\varepsilon}(z, z', n)$ coherence function at height z and z' for the lateral excitation $\varepsilon = v$ and wake excitation $\varepsilon = w$ spectrum

c_P non-dimensional pressure coefficient

c_p specific heat at constant pressure

C_r wind force coefficient at resonance; *AIJ*

$\mathcal{D}$ output dynamic data of a structural system

D structure representative dimension; cylinder diameter

δ_B bandwidth parameter associated with vortex shedding; *ESDU*

$\delta^s\Delta$ stress amplitudes interval step

$^e\Delta$ equivalent amplitude according to Goodman's relation

ΔL^{-1} inverse Monin-Obukhov length interval

δL^{-1} inverse Monin-Obukhov length interval step

$^s\Delta$ stress amplitude interval

ΔT time interval which falls into the spectral gap

$\Delta\bar{u}$ velocity interval

$\delta\bar{u}$ velocity interval steps

$\delta(X_i)$ error made by fixing random value X_i; Sobol'

$\bar{d}$ mean damage according to the Palmgren-Miner linear rule

$\bar{D}_{ref}$ diameter average over top third of structure

$\bar{D}(T)$ total mean damage according to the Palmgren-Miner linear rule

$D_v,\ D_w$ non-dimensional quantities related to the resonant part of the structural response excitation component

e wind loading effect

$\bar{e},\ e'$ $\bar{e}$ mean loading effect; e' fluctuation of the loading effect

ϵ equivalent surface roughness

ε desired exceeding probability when fixing X_i; Sobol'

η reduced amplitude; $\eta = \dfrac{y_{0,\sigma}}{D}$

f Coriolis parameter; $f = 2\Omega\sin\theta$, unit s^{-1}

$F,\ G,\ H$ non-linear solution functions; *Griffin and Skop*

$F_{\varepsilon,hl}$ wind induced force in direction $\varepsilon = x,\ y,\ \varphi$

$\bar{F}_{\varepsilon,hl}$ mean wind induced force in direction $\varepsilon = x,\ y,\ \varphi$

$F'_{\varepsilon,hl}$ fluctuating part of wind induced force in direction $\varepsilon = x,\ y,\ \varphi$

$^vF'_{y,hl}$ lateral turbulence fluctuating part of the wind induced force

$^wF'_{y,hl}$ wake contribution to the wind induced force, both in y direction

$\tilde{F}_j$ modal fluctuating lift force due to vortex shedding; *ESDU*

$F_{\hat{u}}$ cumulative distribution function of the maximum wind velocity in the structure's lifetime

g	acceleration of gravity; $g = 9.81\mathrm{m\ s^{-2}}$
Γ	lapse rate; $\Gamma = -\partial \bar{T}/\partial z$
γ	Euler Mascheroni constant $\gamma = 0.5772156649\ldots$
Γ_a	dry adiabatic lapse rate; $\Gamma_a = g/c_p$
g_P	peak factor
H	structure height
H_0	vertical heat flux, upwards stream positive
I_ε	component of turbulence intensity in direction $\varepsilon = u,\ v,\ w$
k	rate of change of $\tilde{C}_L$ with η; *ESDU*
K_a	aerodynamic damping parameter; *Vickery and Basu*
$K_{a,max}$	negative aerodynamic damping parameter; *Vickery and Basu*
$K_{a,max_{dis}}$	distribution for negativ aerodynamic damping $K_{a,max}$
κ	Karman constant; $\kappa = 0.4$
K_j	mode generalized stiffness; $K_j = \omega_j^2 M_j$
K_ϕ	constant of the mode shape; *Ruscheweyh*
k_s	maximum value of k with no modulation effects due to turbulence; *ESDU*
K_v', K_w', $\bar{K}_{yu}$	non-dimensional coefficients derived from the fluctuating part of the force term $F_{y,hl}'$
K_w^*, K_w	correlation length factors; *Ruscheweyh*
L	Monin-Obukhov length; $L = \dfrac{u_*^3}{\kappa \dfrac{g}{\bar{\bar{T}}}\dfrac{H_0}{\rho c_p}}$
l	correlation length in number of structural dimension D; *Vickery and Basu*
L'	correlation length; *Ruscheweyh*
$\lambda\left(I_u, \mathrm{S_{cr}}\right)$	critical velocity u_{crit} reduction function
Le	effective correlation length; *Ruscheweyh*
$1/L_{o,\varepsilon}$	the atmospheric stratification condition density distribution peak location parameter, $\varepsilon = d, n$
m	local mass per unit length
$m_{e,j}$	equivalent mass per unit length for mode j; $m_{e,j} = \dfrac{M_j}{\int_H \phi_j^2\,\mathrm{d}z}$
$\mathcal{M}_j$	class of model

M_j mode generalized structural mass; $M_j = \int_H m\phi_j^2 \,\mathrm{d}z$

m_j mode generalized mass per unit length; $m_j = \dfrac{1}{H} \int_H m\phi_j^2 \,\mathrm{d}z$

μ mass parameter; $\mu = \dfrac{\rho D^2}{8\pi^2 \,\mathrm{St}^2 m}$; *Griffin and Skop*

N number of base sample

n, ω general frequency; $\omega = 2\pi n$

n_j, ω_j natural frequency of mode j; $\omega_j = 2\pi n_j$

$\bar{N}$ mean number of cycles which will lead to failure

$\bar{n}$ mean stress cycles

n_s, ω_s frequency of vortex shedding; $\omega_s = 2\pi n_s$

ν kinematic viscosity of fluid; air $\nu = 15 \cdot 10^{-6}\mathrm{m}^2\,\mathrm{s}^{-1}$

$^s\nu$ expected frequency of the stress process

Ω earth rotation rate; $\Omega = 7.29 \cdot 10^{-5}\mathrm{s}^{-1}$

ϕ_j jth mode shape

$\phi(B, k)$ influence of bandwidth on response; *Vickery and Basu*

P_{hl} wind field configuration joint probability

$\pi_0, \ldots, \pi_{N-k}$ dimensionless variables

p, p_0 p local pressure; p_0 reference pressure

ψ_m function of the adiabatic wind shear in relation to the atmospheric condition

$P[x]$ cumulative distribution function or with subscript P_{sub}

$p[x]$ probability density function

$Q_1, \ldots, Q_k$ physical quantities

Q_v, Q_w non-dimensional quantities related to the quasi static part of the structural response excitation component

R inspected point in the structure

Re Reynolds number; $\mathrm{Re} = \dfrac{uD}{\nu}$

ρ density of fluid; air $\rho = 1.25\mathrm{kg}\,\mathrm{m}^{-3}$

$\rho_{\mathbf{X},\mathbf{Y}}$ Spearman's rank correlation coefficient

Ri	Richardson number; $\mathrm{Ri} = \dfrac{g}{\bar{\bar{T}}} \dfrac{\Gamma - \Gamma_a}{(\partial u / \partial z)^2}$
$r_{\mathbf{X},\mathbf{Y}}$	Pearson's correlation coefficient
s	wind induced nominal stress
S_{C_F}	spectral density due to vortex shedding and buffeting; *ESDU*
S_{C_L}	spectral density due to vortex shedding; *ESDU*
$\mathrm{S_{cr}}$	Scruton number; $\mathrm{S_{cr}} = \dfrac{4\pi m \zeta_s}{\rho D^2}$
${}^s\sigma$	variance of the stress process
s_L, s_D	stress bending points of the Wöhler curve
$\bar{s}$, s'	$\bar{s}$ mean wind induced stress; s' fluctuation of the wind induced stress
$\bar{s}_P$	stress due to permanent loads
$\mathcal{S}(R)$	functional dependency of the stress in the structural point R due to the along wind mean force $\bar{F}_{x,hl}(z)$
$S^*_\varepsilon(z, n)$	power spectrum of the wind induced lateral excitation $\varepsilon = v$ and wake excitation $\varepsilon = w$ component
$S^*_{\varepsilon,\varepsilon}(z, z', n)$	cross power spectrum of the wind induced lateral excitation $\varepsilon = v$ and wake excitation $\varepsilon = w$ component
St	Strouhal number; $\mathrm{St} = \dfrac{n_s D}{u}$
ρ_{steel}	steel density distribution
St_{dis}	distribution for Strouhal number St
S_{T,X_i}	total effect term for ith input variable
St^*	vortex shedding parameter; *Griffin and Skop*
s_u	ultimate stress strength of the material
$S_w(n)$	spectral force per unit length; *Vickery and Basu*
S_{X_i}, S_{X_i,X_j}	sensitivity index of first and second order
$\bar{T}$	mean atmospheric temperature
$\hat{T}_F$	mean fatigue life according to the Palmgren-Miner linear rule
θ	latitude; Genova $\theta \simeq 44°24'40''$
θ_j	parameter vector in parameter space $\Theta_j \subset \mathbb{R}^{N_j}$ defined by each model $\mathcal{M}_j$
T, T_{hl}	T time interval greater then ΔT; T_{hl} effective duration time
$\mathcal{U}$	user judgement on the initial plausibility of a model class

u_{crit}	flow velocity corresponding to the condition $n_s = n_j$; critical wind velocity
$\bar{u}_{ref}$	reference fluid velocity; reference height $z_{ref} = 10.0$m
u_*	shear velocity
u', v', w'	fluctuating part of flow velocity according to the x, y, z direction
u, v, w	flow velocity according to the x, y, z direction
$\bar{u}(z)$	mean flow velocity in x direction at height z
v^*	reduced lateral excitation component
w^*	reduced wake excitation component
$w(z,t)$	force per unit length; *Vickery and Basu*
$\mathbf{X}$	model input variable vector; $\mathbf{X} = [X_1, \ldots, X_k]^T$
X_i	model input variable in terms of sensitivity analysis
x, y, z, φ	x, y, z space coordinates and φ rotation; if two different points are indicated to the second coordinate a $'$ is added
$\mathbf{Y}$	model outcome vector; $\mathbf{Y} = [Y_1, \ldots, Y_N]^T$
$y_0(t)$	rms coordinate response in the time domain due to vortex shedding
Y_i	model outcome in terms of the sensitivity analysis
$Y_j(t)$	mode generalized across flow deflection amplitude
z_0	roughness length
ζ_a	aerodynamic damping ratio; *Vickery and Basu*
ζ_{aero}	aerodynamic damping ratio; *ESDU*
ζ_s	structural damping ratio

Subscripts

det	deterministic value to be multiplied with an error distribution
ε	subscript substitute character
h, k, l	integers, correspond to an element in a sequence
j	refers to the jth normal mode, if $j = 0$ it indicates stationarity; in case of sensitivity analysis it refers to the jth input variable; in case of model class selection to the jth model class
max	refers to expecting a maximum value
$meas.$	abbr. measurement; the variable is a measured value
σ	refers to the standard deviation; rms value

Chapter 1

Introduction

This propaedeutic chapter contains all knowledge needed to follow the complete work, but presupposes that the reader has already gained knowledge in the field of thermal atmospheric stratification and aerodynamics, especially vortex shedding. After a general introduction and motivation some fundamentals of thermal atmospheric stratification are given, followed by an introduction to vortex shedding and by aerodynamic parameters that were used, the chapter concludes with a short introduction to the field of sensitivity analysis and model class selection.

The current challenge in civil engineering can be reduced to two general aspects: first to determine the action and second to predict the resulting reaction of a structure; based on the obtained reaction a suitable design is devised. Determining the impacting action generally means to describe it with a conforming load model, which can be from extremely simple to extremely complicated. The same considerations are applicable for the reaction where again the structure is described with a model and so the reaction predicted. Obviously both the action and the reaction models can be split up further in more detailed partial models. Starting with these main observations we end up with a variety of partial models which are linked together to obtain a complete path from the impact to the reaction of a structure where the chain is categorically not straight forward in complex cases.

One central request for the design of sophisticated structures is to have this chain as well developed as possible, which is already available for a variety of problems, especially on the reaction side. This goal can be achieved by consequently enhancing the single partial models in a design chain or adding more partial models for neglected phenomena. Doing this in case of wind engineering the first problems starts to arise when trying to describe the wind field itself – without even think of the structure. Looking at the cutting edge a variety of different models exist, see [Solari, 2000]. Where the different wind field models range from extremely simple and consequently poor to demanding and logically excellent.

Making a further step and moving to applying the wind load on an immersed structure in the fluid flow the number of partial models increases drastically for two main reasons. First and probably the more important reason is the complexity of fluid structure interaction and second the amount of different observed phenomena in the aeroelastic field. Nearly all aeroelastic and aerodynamic phenomena introduce a loop in the design chain which again can range from minor importance to extremely impacting the whole reaction prediction procedure.

Without going into detail on what aerodynamic phenomena were taken into consider-

ation, we take a look at a schematic design chain for a general aerodynamic phenomenon which is shown in Fig. 1.1, where predominantly three loops can be identified. The first possible case is the interaction of structure motion with the aerodynamic behavior path 1 or with the wind field itself path 3 and in some special cases the aerodynamic characteristics itself can influence the wind field, path 2. The wind field is described with the mean velocity vector $u(\boldsymbol{x}, t)$ and the turbulence vector $I_u(\boldsymbol{x}, t)$, the load with $f(\boldsymbol{x}, t)$ and the structural reaction with $g(\boldsymbol{x}, t)$ all depending on space $\boldsymbol{x}$ and time t.
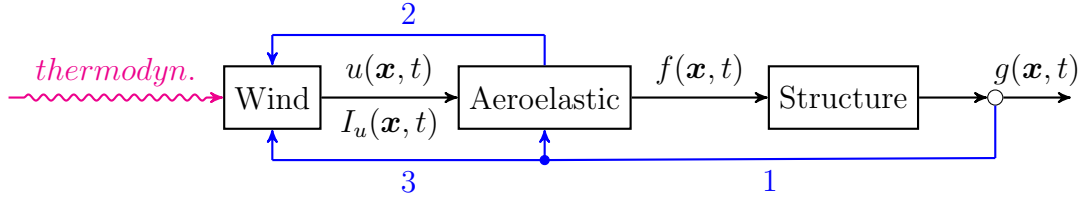
Figure 1.1 – Scheme from atmosphere to structural reaction with determining aeroelastic effects.

Fig. 1.1 makes clear that coming from the thermodynamic action in the atmosphere as a first step a wind model has to be created which then can be inserted into an aerodynamic model that applies the wind field impact on the structural model in order to obtain the structural reaction. Refining Fig. 1.1 and embedding the initial context of action and reaction leads to Fig. 1.2, where additionally the step from the reaction to the design is made.

Breaking it up and introducing verification as a separate model an additional loop is introduced as modifying the structural shape due to the design needs, changes the aerodynamic characteristics of the structure. In this work the action part will be studied exclusively so this part is split up where for the reaction and verification part only transfer functions $\mathcal{S}$ and $\mathcal{V}$ are representing possible paths.
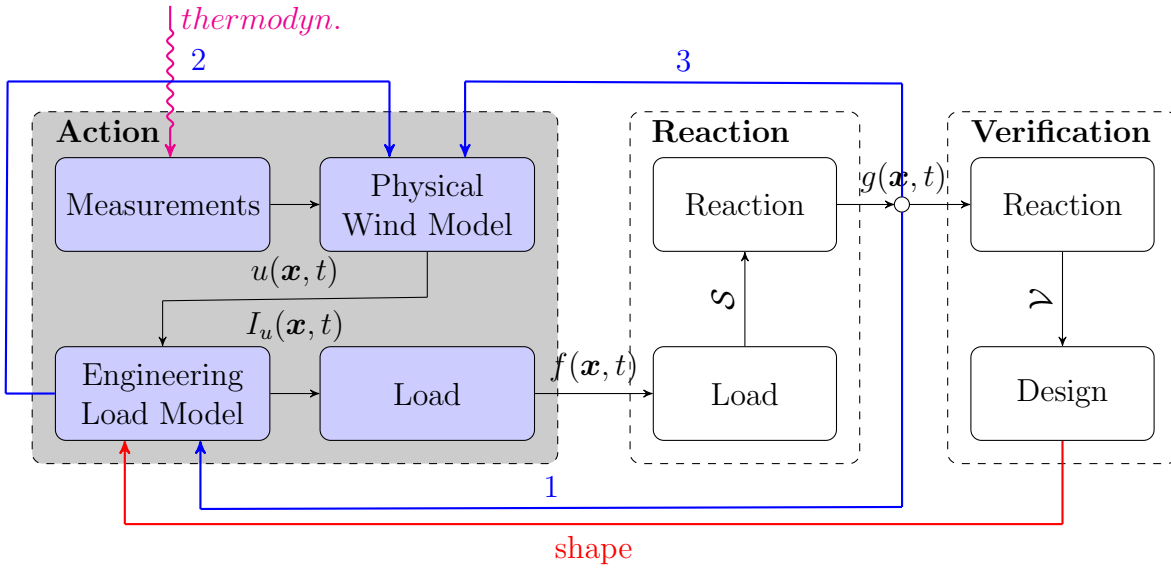
Figure 1.2 – Scheme for an aeroelastic structural engineering problem separated in action, reaction and design part.

Starting with the thermodynamical processes using an adequate partial model the physical happening has to be investigated which is done by measuring these physical circum-

stances. Based on these measured values a suitable wind model is derived where more or less phenomena can be taken into account. The wind partial model is typically a physical model as it is derived from general valid physical laws, which are mostly simplified. Normally the atmospheric stratification is not considered due to its complexity and so the turbulence intensity $I_u(\boldsymbol{x}, t)$ is only defined in a natural stratification condition which can lead to underestimating critical aerodynamic effects, see [Verboom and van Koten, 2010], [Kawecki and Żurański, 2005] and [Vickery and Clark, 1972].

The next step is to find a suitable model which describes in an most accurate way the aerodynamic behavior of the fluid-structure interaction and so creates an adequate load formulation. This partial model can be strictly derived from physical laws, but due to the complexity of these kind of phenomena it is normally a semi-empirical model and can therefore be considered to be an engineering model.

This load is then applied onto the structure where in a similar way the structural reaction is found and then used in the design process. In every single stage possible loops have to be considered in order to represent the nature of the underlying phenomena well.

By creating the different partial models step by step a model chain evolves which with all its loops allows to predict the structural reaction and thus in consequence allows to design a structure properly. N.B. that additionally the probabilistic character of influencing parameters has to be taken into account, not only for integrity purposes, but to consider also the probabilistic characteristics of natural phenomena.

The author remarks that simplicity can and should not be an argument for a model formulation, not even for a design rule and so agrees with [Verboom and van Koten, 2010] where additionally to this request the two very important arguments are given. First because accuracy and applicability is fare more important and second the need of hand computation possibility is lapsed, to these two arguments the indication that using simple models means to waste knowledge has to be added.

Vortex shedding

In the field of aeroelasticity a variety of different phenomena exist. One of the most complex is vortex shedding where the phenomenon itself is not fully understood yet and so the currently existing models are all semi-empirical. This fact leads the different models to overestimate and underestimate the vortex shedding reaction in an order of magnitude as shown in [Verboom and van Koten, 2010]. Additionally, the sensitive influence of the atmospheric turbulence intensity is mentioned with reference to [Hansen, 1998] where this influence is discussed in detail. In [Blackburn and Melbourn, 1993] the difficulty of predicting the real structural reaction using models derived from experimental results is discussed further and all possible effects and interactions of partial phenomena are elaborated.

Looking at selected literature a variety of studies were made, trying to explain unexpected failure of chimneys, beginning with [Ruscheweyh and Sedlacek, 1988], [Ruscheweyh, 1996], [Piccardo and Solari, 2000], [Kawecki and Żurański, 2005] and [Verboom and van Koten, 2010] where all of them clearly identified the atmospheric turbulence intensity to be the point of interest.

The only consequent approach is to introduce the turbulence intensity directly, deriving it from the stratification condition of the atmosphere allows to predict the fatigue lifetime of a structure properly. This work was begun in [Repetto and Solari, 2002] and was extended in [Repetto and Solari, 2007] and [Benedetti et al., 2010] to a sophisticated level.

Therefore an accurate study and enhancement of the existing vortex shedding models would be a useful contribution to the design chain and the reliability of vortex shedding exposed structures would be increased if the probabilistic characteristics of the determining parameters is included as well. The path chosen in this work is to start with an accurate dimensional analysis on all vortex shedding related parameters to evaluate possible relations between them. After studying the single approaches a model class selection is carried out on measured results to gain an idea of the validity of the approaches. In oder to quantify the influence of the parameters a variance based sensitivity study is performed. As a sophisticated vortex shedding occurrence probability itself is not available yet, an analytic probabilistic method is devised. Then a probabilistic study of the overestimating probability of a deterministic computed structural reaction is carried out to demonstrate the need of using probabilistic methods. Concluding, the model developed in [Repetto and Solari, 2002] and [Repetto and Solari, 2007] is used, where the distribution of possible atmospheric stratification conditions is improved on the basis of [Benedetti et al., 2010], to determine the deterministic fatigue lifetime of a structure. To take into account distributed parameters for the structural damping ratio and the structural natural frequency a Monte Carlo simulation [Bucher, 2009] is carried out.

The last step represents a highly sophisticated model chain for fatigue lifetime analysis, as it takes the majority of knowledge about the atmosphere into account, combines it with an enhanced vortex shedding model and through the Monte Carlo simulation also covers the probabilistic structural parameters. How to derive the probabilistic characteristics of the structure is not discussed in this work.

Organization of the Text

In order to define the preliminaries properly, the basics in atmospheric stratification, vortex shedding, sensitivity analysis and model class selection are given. These introductions are indicative and do not claim completeness.

The work is separated into three main parts, with the first part including the dimensional analysis of the determining parameters of the vortex shedding phenomenon, followed by a presentation of five different models for vortex shedding and an analysis of them relatively to each other and related to their phenomenological representation capacity. In the second part an accurate study of the probabilistic behavior of all parameters is made as basis to perform a variance based sensitivity analysis. The third and last part contains a method to evaluate the vortex shedding occurrence probability for a structure, a study of how distributed structural parameters influence the structural reaction and based on the work of [Repetto and Solari, 2007] a probabilistic model for fatigue analysis is presented.

Enclosed are furthermore two examples and some additional proofs and explanations are listed to conclude the work.

1.1 Thermal Atmospheric Stratification

After studying the earth atmosphere from a global point of view[1] when zooming down to the atmospheric boundary layer the thermal condition of the atmosphere is very important considering turbulence property changes.

In general, neutral thermal stratification is assumed which in the end simplifies the analysis of wind induced structural reactions quite a lot. In terms of aerodynamic effects

---

[1]Which is not discussed here, see [Stull, 1988], [Plate, 1982] and [Solari, 2000] for more details.

the absence of turbulence generally intensifies those effects, especially vortex shedding which has its highest impact in the case of total absence of turbulence.

Turbulent flow can be described by the following characteristics, found and directly taken from [Panofsky and Dutton, 1983]

1. Fluid velocity is chaotic and apparently a random function of both space and time.

2. Flow is strongly rotational and three-dimensional, with gradients occurring in all directions.

3. Nonlinearity is essential to turbulence and responsible for energy being distributed smoothly with wavelength.

4. Gradients are created in the turbulent flow by stretching of vortices, a process that moves kinetic energy to smaller wavelengths.

5. Turbulent flows are diffusive and intermittent.

In [Panofsky and Dutton, 1983] a wonderful example in allusion to the atmospheric boundary layer can be found. Consider a fluid layer heated from below; after a certain heat load a vertical steady circulation will have established; after heating further some periodic flows of increasing complexity will evolve ending such that the whole fluid layer becomes turbulent.

1.1.1 Thermal Condition in the Atmospheric Boundary Layer

We find the atmospheric boundary layer to be very sensitive to thermal conditions and thus this layer can produce stable, neutral and unstable stratification as described by the Richardson number, [Stull, 1988]

$$\text{Ri} = \frac{g}{\bar{\bar{T}}} \frac{\Gamma - \Gamma_a}{\left(\partial u / \partial z\right)^2}. \tag{1.1}$$

with $\bar{T}$ being the mean atmospheric temperature, Γ the laps rate and Γ_a the dry adiabatic lapse rate. As found in [Stull, 1988], [Panofsky and Dutton, 1983] and [Plate, 1982] we can alternatively describe the stratification with the Monin-Obukhov length [Obukhov, 1971]

$$L = \frac{u_*^3}{\kappa \frac{g}{\bar{\bar{T}}} \frac{H_0}{\rho c_p}}, \tag{1.2}$$

using u_* shear velocity, κ Karman constant as recommended in [Panofsky and Dutton, 1983] is usually taken near $\kappa = 0.4$ and H_0 vertical heat flux.

We can bring the dimensional quantity L in relation to the non-dimensional Richardson number Ri in the following way

$$\frac{z}{L} = \text{Ri} \quad \text{for } \text{Ri} \leqslant 0$$
$$\frac{z}{L} = \frac{\text{Ri}}{1 - 5\,\text{Ri}} \quad \text{for } 0 \leqslant \text{Ri} \leqslant 0.2 \tag{1.3}$$

and define the different stratification regions. Stratification is neutral for Ri $= 0$ and $1/L$ tending towards zero, stable for Ri > 0 and $1/L > 0$ and it is unstable for Ri < 0 and

$1/L < 0$. In the end it is worth mentioning that, as noted in [Repetto and Solari, 2007], high wind velocities force the atmosphere towards a neutral condition caused by mixing the fluid through turbulent flow, thus stable and unstable conditions can most likely be found at slow wind velocities $u < 10\text{m s}^{-1}$, see also [Stull, 1988] for further details.

Starting from the idea in [Repetto and Solari, 2007] where a reasonable distribution for $1/L$ as function of u is provided, in [Benedetti et al., 2010] this distribution is found by analyzing a high number of measurements. It is represented in the following form

$$p[1/L](u) = \begin{cases} \gamma_n\, e^{-\beta_n(1/L_{o,n} - 1/L)} + \gamma_d\, e^{-\beta_d(1/L_{o,d} - 1/L)} & \text{if } 1/L < 1/L_{o,d}, \\ \gamma_n\, e^{-\beta_n(1/L_{o,n} - 1/L)} + \gamma_d\, e^{-\alpha_d(1/L - 1/L_{o,d})} & \text{if } 1/L_{o,d} \leqslant 1/L < 1/L_{o,n}, \\ \gamma_n\, e^{-\alpha_n(1/L - 1/L_{o,n})} + \gamma_d\, e^{-\alpha_d(1/L - 1/L_{o,d})} & \text{if } 1/L \geqslant 1/L_{o,n}. \end{cases} \quad (1.4)$$

Furthermore, we find the values of the daily peak $1/L_{o,d}$ and the nightly peak $1/L_{o,n}$

$$\begin{aligned} 1/L_{o,d} &= -0.1454\, e^{-0.3363u}, \\ 1/L_{o,n} &= 0.0325\, e^{-0.2847u}. \end{aligned} \quad (1.5)$$

The function parameters for the day and the ones for the night are

$$\begin{aligned} \alpha_d &= 2.7833u^2 + 3.4009, & \alpha_n &= 0.0964u^4 + 2.7043u^2 + 2.3052, \\ \beta_d &= 2.6504u^2 + 3.7918, & \beta_n &= 0.0441u^4 + 5.5791u^2 + 2.3962, \\ \gamma_d &= \frac{0.55}{1/\alpha_d + 1/\beta_d}, & \gamma_n &= \frac{0.45}{1/\alpha_n + 1/\beta_n}. \end{aligned} \quad (1.6)$$

The parameters used here are different from the ones found in [Benedetti et al., 2010]. Some further work on the data was done by the author, see appendix B.

1.1.2 Wind Field and Turbulence Models

In neutral and stable atmospheric conditions we can express the height h of the atmospheric boundary layer

$$h = C\frac{u_*}{|f|}\frac{1}{1 + b\sqrt{\dfrac{u_*}{|f|L}}} \quad (1.7)$$

and in unstable atmospheric conditions

$$h = C\frac{u_*}{|f|}\left[1 + d\sqrt{\frac{u_*}{|fL|}}\right] \quad (1.8)$$

according to [Panofsky and Dutton, 1983] for the values $C = 1/6$, $b = 0.1$ and $d = 0.25$ as recommended in [Repetto and Solari, 2007]. The Coriolis parameter $f = 2\Omega \sin\theta$ with the earth rotation rate Ω and the latitude θ. The shear velocity can be computed according to [Stull, 1988]

$$u_* = \left[\overline{u'w'} + \overline{v'w'}\right]^{1/4} \quad (1.9)$$

with $\overline{u'w'}$ and $\overline{v'w'}$ being the co-variances of the fluctuating part of flow velocity. Or it is solved as an inverse problem of Eq. (1.10) when $\bar{u}(z)$ is know for a certain z. Furthermore we can express the mean wind velocity $\bar{u}(z)$

$$\bar{u}(z) = \frac{u_*}{\kappa} \left[\ln \frac{z}{z_0} - \psi_m \left(\frac{z}{L} \right) \right] \tag{1.10}$$

with the roughness length z_0 and ψ_m being a function of the adiabatic wind shear in relation to the atmospheric condition, in stable[2]

$$\psi_m(\frac{z}{L}) = -5\frac{z}{L} \tag{1.11}$$

and in unstable atmosphere

$$\psi_m(\frac{z}{L}) = \ln \left(\frac{1+x^2}{2} \right) + 2\ln \left(\frac{1+x}{2} \right) - 2\arctan(x) + \frac{\pi}{2}, \quad x = \left(1 - 15\frac{z}{L} \right)^{1/4}, \tag{1.12}$$

see [Panofsky and Dutton, 1983] and [Arya, 1984].

The standard deviation of the turbulence components in stable and neutral atmosphere can be expressed as [Repetto and Solari, 2007]

$$\sigma_\varepsilon = \alpha_\varepsilon(z)u_*, \quad \varepsilon = u, v, w \tag{1.13}$$

where in neutral and stable atmosphere

$$\alpha_\varepsilon(z) = \alpha_{\varepsilon 0} \left(1 - \frac{z}{h} \right), \quad \varepsilon = u, v, w \tag{1.14}$$

and in unstable atmosphere for $\varepsilon = u, v$

$$\alpha_\varepsilon(z) = \begin{cases} \alpha_{\varepsilon 0} \left(1 - \frac{1}{30}\frac{h}{L} \right)^{1/3} & \text{if } \frac{z}{h} \leqslant 0.1, \\ 0.6 \left(-2\frac{h}{L} \right)^{1/3} & \text{if } 0.1 < \frac{z}{h} \leqslant 0.8 \end{cases} \tag{1.15}$$

and for $\varepsilon = w$

$$\alpha_w(z) = \begin{cases} \alpha_{w0} \left(1 - 3\frac{h}{L} \right)^{1/3} & \text{if } \frac{z}{h} \leqslant 0.0655 + 0.333L/h, \\ 0.6 \left(-2\frac{h}{L} \right)^{1/3} & \text{if } 0.0655 + 0.333L/h < \frac{z}{h} \leqslant 0.8. \end{cases} \tag{1.16}$$

We find in [Solari and Piccardo, 2001] $\alpha_{\varepsilon 0}$ which fulfills the identity $\alpha_{\varepsilon 0} = \alpha_\varepsilon(0)$

$$\alpha_{u0} = \sqrt{6 - 1.1 \arctan \left[\ln(z_0) + 1.75 \right]} \tag{1.17}$$

and $\alpha_{v0} = 0.75\alpha_{u0}$ and $\alpha_{w0} = 0.50\alpha_{u0}$; z_0 in meters.

From [Solari and Piccardo, 2001] we obtain the ratio for the turbulence intensity I_ε to be

$$I_\varepsilon(z) = \frac{\sigma_\varepsilon(z)}{\bar{u}(z)} \tag{1.18}$$

---

[2]As limit case $1/L = 0$ also considered valid for neutral atmospheric conditions.

and now substitute Eq. (1.10) and Eq. (1.13) into Eq. (1.18) and obtain for the case $\varepsilon = u, v$

$$I_u(z) = \frac{\alpha_u(z)\kappa}{\ln\dfrac{z}{z_0} - \psi_m\left(\dfrac{z}{L}\right)}, \quad I_v(z) = \frac{\alpha_v(z)\kappa}{\ln\dfrac{z}{z_0} - \psi_m\left(\dfrac{z}{L}\right)} \tag{1.19}$$

which describes the long and cross wind component of turbulence intensity, which are used in the vortex shedding approaches studied.

1.1.3 Behavior of Turbulence Intensity in the Monin-Obukhov Range

We are now interested in the behavior of Eq. (1.19) according to different atmospheric conditions at limit stages, see [Panofsky and Dutton, 1983], [Stull, 1988] and [Plate, 1982] for further explanations on the atmospheric stratification.

Stable atmospheric condition

As a first step we would like to find out, if an atmospheric condition with total absence of turbulence exists and if so, at which Monin-Obukhov length $1/L$. Starting with a general limit computation we obtain

$$\lim_{1/L \to \infty} I_u(z) = \frac{\alpha_{\varepsilon 0}\left(1 - \dfrac{z}{h}\right)\kappa}{\ln\dfrac{z}{z_0} + 5\dfrac{z}{L}} = 0 \tag{1.20}$$

in order to solve the equation we need to know how the boundary layer height behaves at the limit

$$\lim_{1/L \to \infty} h = C\frac{u_*}{|f|}\frac{1}{1 + b\sqrt{\dfrac{u_*}{|f|L}}} = 0. \tag{1.21}$$

This shows that in stable atmospheric conditions there could be a total absence of turbulence which is a very critical condition for vortex shedding. Moving to the second step we try to see if the value $1/L$ has to be infinite to satisfy Eq. (1.19) to be zero;

$$1/L = \frac{C^2 u_*^2 - 2Cu_*|f|z + |f|^2 z^2}{u_*|f|z^2 b^2} \ll \infty \tag{1.22}$$

Neutral atmospheric condition

$$\lim_{1/L \to 0} I_u(z) = \frac{\alpha_{\varepsilon 0}\left(1 - \dfrac{z}{h}\right)\kappa}{\ln\dfrac{z}{z_0} + 5\dfrac{z}{L}} = \frac{\alpha_{\varepsilon 0}\kappa\left(Cu_* - |f|z\right)}{Cu_*\ln\left(\dfrac{z}{z_0}\right)} \simeq \frac{1}{\ln\left(\dfrac{z}{z_0}\right)} \tag{1.23}$$

in order to solve this we need to know how the boundary layer height behaves at the limit

$$\lim_{1/L \to 0} h = C\frac{u_*}{|f|}\frac{1}{1 + b\sqrt{\dfrac{u_*}{|f|L}}} = \frac{Cu_*}{|f|}. \tag{1.24}$$

We see that in a neutral atmospheric condition the intensity of turbulence tents to a constant value which is the one found in most publications, especially [Solari and Piccardo, 2001], for values $\alpha_{\varepsilon 0\kappa} \approx 1$ and $|f|z \ll 0$ which are generally valid.

Unstable atmospheric condition

First we have to find in which region we are moving about by looking at the ratio z/h, and then the limit of a part of the numerator is computed

$$\lim_{1/L \to -\infty} \frac{h}{L} = C\frac{u_*}{|f|L}\left(1 + d\sqrt{\frac{u_*}{|fL|}}\right) = -A \to -\infty \text{ as } 1/\text{L} \to -\infty \qquad (1.25)$$

and so $z/h < 0.1$ will hold true for sure. We find that $\lim\limits_{1/L \to -\infty} \psi_m = B \to \infty$ as $1/\text{L} \to -\infty$ and by looking at the functions we find that A grows faster than B, see section A.1,

$$\lim_{1/L \to -\infty} I_u(z) = \frac{\alpha_{\varepsilon 0}\left(1 - \dfrac{1}{30}\dfrac{h}{L}\right)^{1/3}\kappa}{\ln\dfrac{z}{z_0} - \psi_m\left(\dfrac{z}{L}\right)} \sim \frac{\alpha_{\varepsilon 0}\kappa\left(1 + \dfrac{A}{30}\right)^{1/3}}{\ln\dfrac{z}{z_0} + B}, \ A, B \to \infty \qquad (1.26)$$

out of which we can see $\alpha_{\varepsilon 0}\kappa\left(1 + \dfrac{A}{30}\right)^{1/3} \geq \ln\dfrac{z}{z_0} + B$ and so we find the turbulence intensity to be somewhere in-between

$$\frac{1}{\ln\left(\dfrac{z}{z_0}\right)} \leq I_u(z) \lesssim 2.5 \text{ for reasonable values of } 1/L \qquad (1.27)$$

again assuming that $\alpha_{\varepsilon 0}\kappa \approx 1$ and of course $1/L \leq 0$ for the lower limit.

1.2 Vortex Shedding

Immersing a body in a fluid flow a wake is consequently formed leewards. When studying this wake for a circular sectioned body, it seems to have a special regularity, as we can see in Fig. 1.3[3] and we find the wake to be vortex like, furthermore we notice a body being fixed with elastic supports, starting to oscillate regularly in a direction transverse to the fluid flow direction.

These regular vortices impose a dynamic load onto the body which in case of dynamical sensitive structures can lead to resonance phenomena. Supplementary the development of vortices are in favor in the case of absence of atmospheric turbulence. Generally, the vortex shedding excitation is random and becomes more and more sinusoidal as the frequency ratio approaches $n_s = n_j$, see section 1.2.2 and section 1.2.4 for more details and some particular phenomena.

The phenomenon of vortex shedding is described and studied in many publications and shows to be quite complicate to be handled properly in context of structural engineering. Some very detailed explanations can be found in [Simiu and Scanlan, 1996], [Sockel, 1994] and [Blevins, 2001] and many more; an overview and some preliminaries are given in the following sections.

---

[3]The image has not been published anywhere but the research related to the image has been submitted to Physics of Fluids, by S. Kumar, C. Cantu, and B. Gonzalez, *An Experimental Study of Flow around a spinning cylinder* Physics of Fluids (submitted).
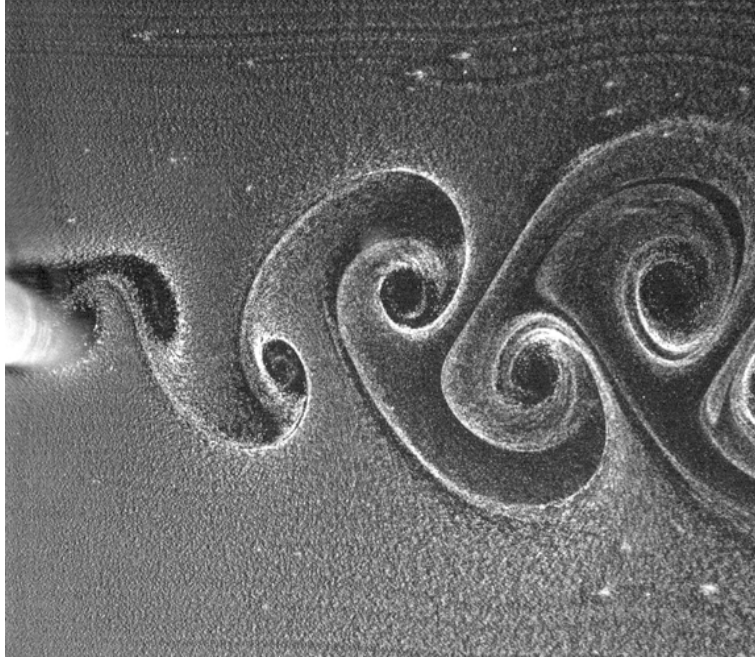
Figure 1.3 – Wake behind a cylinder immersed in a fluid flow showing extraordinarily regular vortices.

To understand the phenomenon even more clearly let us carry out a kind of thought experiment. We study an imaginary chimney with configuration ad libitum, standing somewhere exposed to the atmospheric fluid flow for which we can also impose all parameters.

As we increase the fluid flow velocity and measure the vortex shedding frequency we will notice the effect already shown in [Strouhal, 1878]. What we see is the vortex frequency to be depending on the fluid velocity and the chimney's diameter related to each other via the Strouhal number, see section 1.2.1. Contemporaneously we notice the vortex shedding frequency to lock-in as the vortex shedding frequency n_s tends closer to the chimney's natural frequency n_j, see section 1.2.2.

Now we observe the force on the base of the chimney and we totally cancel out every possible existing vortex shedding effect. By increasing the fluid velocity we notice that the force is increasing and thus depending on the fluid velocity, generally represented as lift coefficient, see section 1.2.3.

Finally we investigate the displacement on the top of the chimney and we notice straightaway that when the chimney oscillates arbitrarily it does this with quite a small amplitude, when oscillating harmonically the amplitude is considerably big. Starting to increase the fluid velocity we notice the chimney to oscillate arbitrarily and as we increase the fluid velocity and therefore n_s tends closer to n_j the oscillation is temporarily arbitrary and harmonic to become totally harmonic in the lock-in region. Stopping to increase the fluid velocity in the lock-in region let us observe the auto limiting behavior of the phenomenon too.

Being a thought experiment we now perform an infinite set of experiments and we start varying the chimneys structural damping ratio ζ_s and observe the maximum values of the top response. We notice that the factor between the mean and maximum rms value is a function of ζ_s, see section 1.2.4. In addition we change the turbulence of the fluid and notice a similar behavior, this is represented by the aerodynamic damping ratio, which describes the negative contribution to the structural damping ratio and thus makes the vortex shedding effect even worse.

Detailed explanations of vortex shedding can be found in [Simiu and Scanlan, 1996], [CNR, 2009] and [Vickery and Basu, 1983b]. We remember that the structural damping ratio is set in a relation to the structural mass, diameter and fluid density through the Scruton number S_{cr},

$$S_{cr} = \frac{4\pi m \zeta_s}{\rho D^2} \tag{1.28}$$

a similar relation exist for the aerodynamic damping ratio, which is called aerodynamic damping parameter.

1.2.1 Strouhal Number

Strouhal found and publicated in [Strouhal, 1878] the regularity of the vortex shedding and that the vortex shedding effect can be described in terms of a non-dimensional number

$$St = \frac{n_s D}{u} \tag{1.29}$$

which is called Strouhal number with n_s the frequency of full cycles of vortex shedding, D the characteristic dimension of the body and u the mean flow velocity. Furthermore, the Strouhal number is a characteristic constant for different cross-sections enveloped by the flow, see [Simiu and Scanlan, 1996]. In Fig. 1.4 the Strouhal number function in the range $10^4 \leq Re \leq 10^8$ for a circular cylinder is shown according to the data fit done by [ESDU96030, 1996] which also takes the surface roughness of the body into account.
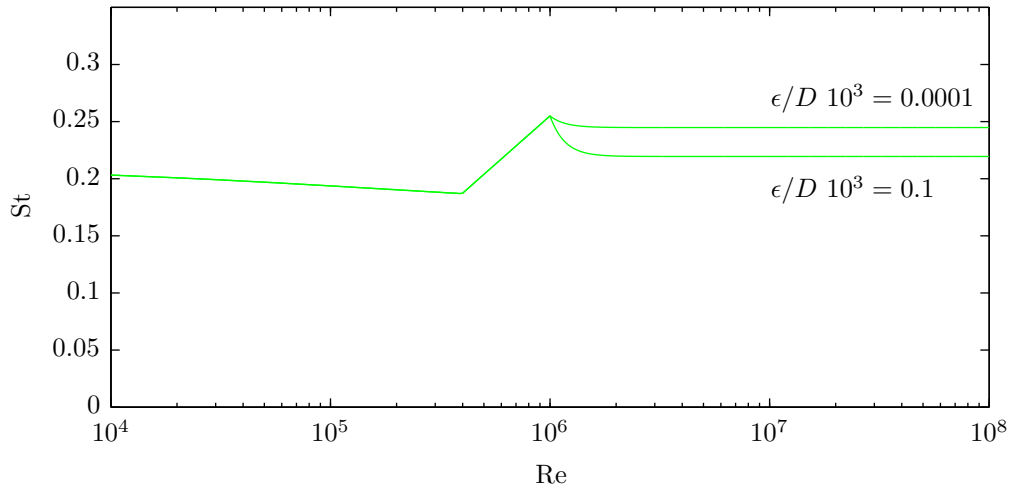
Figure 1.4 – Influence of Reynolds number on the Strouhal number for circular cylinders with different surface roughness.

We find the values for the Strouhal number to be

$$St = \begin{cases} 0.175 + 0.035\, e^{-2.9\cdot 10^{-4}\,(\log_{10} Re)^{4.77}} & \text{if } 5.6 \leq \log_{10} Re \\ 0.187 + 0.17\,[\log_{10} Re - 5.6] & \text{if } 5.6 < \log_{10} Re \leq 6 \\ 0.255\,\left[a + (1-a)\,e^{-15\,(\log_{10} Re - 6)}\right] & \text{if } \quad 6 < \log_{10} Re \end{cases} \tag{1.30}$$

with

$$a = 0.96\,\left[0.8 + 0.2\,e^{-0.12\,(E+3)^{2.6}}\right] \quad \text{and} \quad E = \begin{cases} \log_{10}\left(\frac{\epsilon}{D}10^3\right) & \text{if } -3 < E \\ -3 & \text{if } -3 > E \end{cases} \tag{1.31}$$

which shows that the often used fixed value of $St = 0.2$ corresponds quite well with the results found in Fig. 1.4.

1.2.2   Lock-in Phenomenon

We consider the following case: we immerse a rigid, circular cylinder elastically supported into a fluid flow and start to increase the fluid velocity. As we know from Eq. (1.29) and by considering the Strouhal number St to be constant over the whole Reynolds number range, we suspect the structure to vibrate exactly with the vortex shedding frequency n_s. This is true until we reach the natural frequency n_j of the structure itself. From
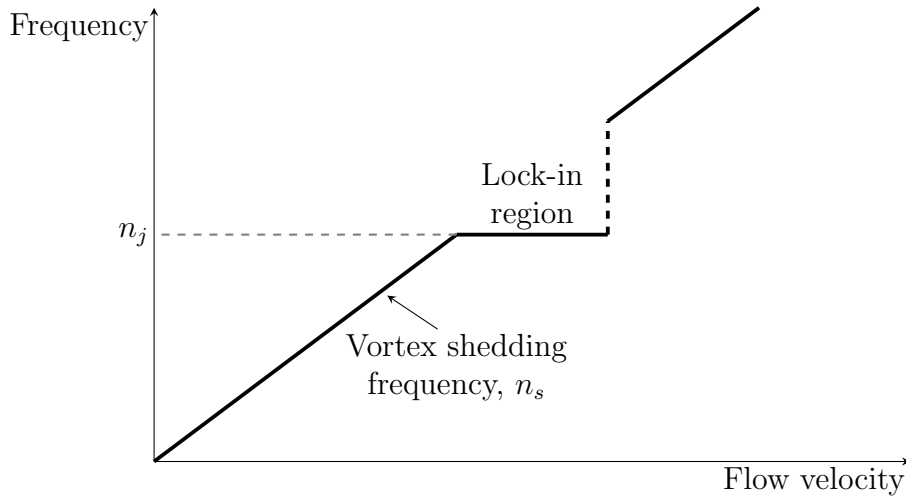
Figure 1.5 – Development of the vortex shedding frequency with wind velocity over elastic structure.

this point on the vortex shedding frequency is locked-in and the frequency stays constant for a certain fluid velocity domain to then return back onto the linear path given by Eq. (1.29), see Fig. 1.5. So, the natural frequency of the body controls the aeroelastic phenomena which we can also call synchronization. As mentioned in [Simiu and Scanlan, 1996] no completely successful analytical models are found to describe these phenomena properly and generally validly, but the problem can be handled sophistically with the help of semi-empirical models.

1.2.3   Lift Force Coefficient

Thinking of an object immersed in a fluid flowing at velocity u, a pressure p will act onto the surface of the body. By simply applying Bernoulli's law we find $1/2\rho u^2 + p = const.$ valid for all streamlines in the immediate vicinity of the object, see [Simiu and Scanlan, 1996]. If the pressure p is integrated over the surface the forces and moments acting on the body are obtained which can then be represented in coordinative orientated vectors and so we can formulated a non-dimensional pressure coefficient c_P

$$c_P = \frac{p - p_0}{\frac{1}{2}\rho u^2} \tag{1.32}$$

with p_0 being the reference pressure far upstream and u the mean reference fluid velocity.

It is obvious that c_P is strongly depending on the shape and the velocity u in other words of the Reynolds number. If looking at aerodynamical problems related to civil engineering the shape is mostly imposed upon by other than aerodynamic design objectives

but still or exactly therefore special care has to be taken on the size and the derivate of the pressure coefficients which mainly determine the behavior of the structure regarding to aerodynamic phenomena.

Expressing the non-dimensional pressure coefficient in force terms leads to

$$c_L = \frac{F_L}{\frac{1}{2}\rho u^2 D}, \quad c_D = \frac{F_D}{\frac{1}{2}\rho u^2 D}, \quad c_L = \frac{M}{\frac{1}{2}\rho u^2 D^2} \tag{1.33}$$

with D as a typical reference dimension of the structure.
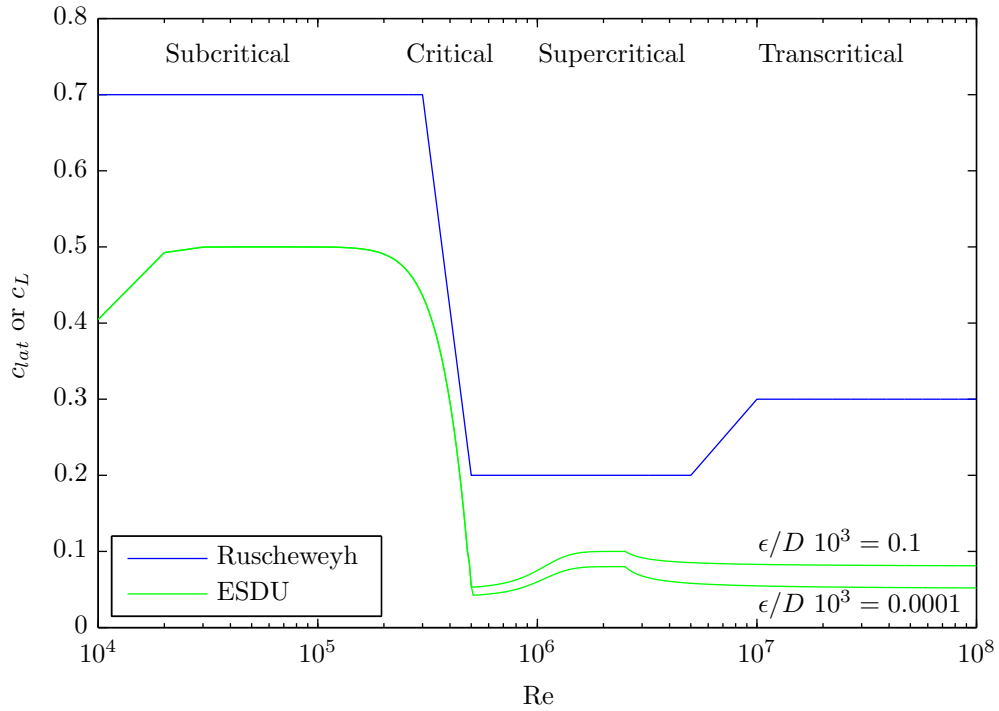
Figure 1.6 – Influence of Reynolds number on different lift force coefficients for circular cylinders with different surface roughness.

If the flow is turbulent, independent of whether the turbulence is caused by oncoming turbulence or induced by aerodynamic phenomena, the coefficients become time dependent and thus the coefficients either have to be represented in spectral form or as rms values which logically have a lack of information. The reason rms values are used is the easy handling of these values and the spectra of the values are closely related to the aerodynamic phenomena and therefore cannot be formulated generally. In Fig. 1.6 we see rms values for the lift force coefficients for two different approaches and the separation of the different regime regions, *subcritical, critical, supercritical and transcritical.*

We find rms values for the lift coefficients which are determining the vortex shedding phenomena in [ESDU96030, 1996] and Ruscheweyh [Sockel, 1994], both based on experiments, see Fig. 1.6. The main difference between the values provided by ESDU and Ruscheweyh are that Ruscheweyh used the maximum value rms [Ruscheweyh, 1985] which means having the peak factor already included in the lift force coefficient whereas ESDU interpolated the measured values and so derived a function which is passing through the measured value cloud. Secondly, Ruscheweyh is not taking the surface roughness into account which ESDU does.

1.2.4 Peak Factor

When studying the vortex excitation generally, the maximum rms value of the displacement is of interest, so the rms value has to be transformed in order to obtain the maximum value. The values for the two limits, sinusoidal reaction – lock-in and random excitation, which is shown to be Gaussian, see [Vickery and Basu, 1983b], can be found to be $g_P = \sqrt{2}$ in the sinusoidal case and $g_P = 3.87$ in the random case. g_P is called the peak factor and transforms the mean rms value by multiplication into the maximum rms value, see chapter 2 where the peak factor is applied to the different models.

Of course we are not only interested in the limit values, but we would like to know how the peak factor behaves on the whole response range. We find two interpolation functions one in [Daly, 1986] and one in [CNR, 2009] which is represented in Eq. (1.34) and used for all approaches.

$$g_P = \sqrt{2} \left\{ 1 + \arctan^{1.4} \left[0.7 \left(\frac{\mathrm{S_{cr}}}{4\pi K_a} \right)^{2.5} \right] \right\} \tag{1.34}$$

Both formulations give the value of the peak factor g_P as function of the relation between ζ_s or $\mathrm{S_{cr}}$ and the aerodynamic damping ζ_a or K_a.

1.3 Sensitivity Analysis

By using a variance based sensitivity analysis we have a method where the uncertainty of the output of a model can be apportioned to the uncertainties of the input parameters, see [Saltelli, 2008]. Furthermore, we are using a combination of uncertainty analysis with sensitivity analysis, which is not only recommended, but provides the possibility to understand the relation between input and output parameters before making an accurate probability analysis, maybe already with a reduced number of parameters.

1.3.1 First Order Sensitivity Indices

Starting with a generic model

$$Y = f(X_1, X_2, \ldots, X_k) \tag{1.35}$$

where each X_i has a non-null range of variation or uncertainty, we are now interested in the change of the output Y if we would fix one value X_i at a particular value x_i^*. According to [Saltelli, 2008] we formulate $V_{X_{\sim i}}(Y|X_i = x_i^*)$ which is the resulting variance of Y of all factors $X_{\sim i}$ devoid X_i, which is called conditional variance. Quite obvious by fixing one variable the total output variance $V(Y)$ decreases and we can imagine using $V_{X_{\sim i}}(Y|X_i = x_i^*)$ as a measure of relative importance of X_i. In order to make this measure valid and not influenced by the selection of x_i^* we take the average of all possible values for x_i^* and we write $E_{X_i}(V_{X_{\sim i}}(Y|X_i))$ which is always lower or equal to $V(Y)$.

We call the conditional variance $V_{X_i}(E_{X_{\sim i}}(Y|X_i))$ the first order effect of X_i on Y and the sensitivity measure

$$S_{X_i} = \frac{V_{X_i}(E_{X_{\sim i}}(Y|X_i))}{V(Y)} \tag{1.36}$$

as the first order sensitivity index of X_i on Y, with $0 \leq S_{X_i} \leq 1$ where high values indicate the variable to be important.

1.3.2   Higher Order Sensitivity Indices

As the model discussed in the following is not an additive model we will have the need of also studying higher order sensitivity indices, presupposing as before[4]

$$\frac{V_{X_i,X_j}\left(E\left(Y|X_i,X_j\right)\right)}{V\left(Y\right)}, \quad i \neq j \tag{1.37}$$

as conditioned variance we find $V_{X_i}\left(E\left(Y|X_i,X_j\right)\right) = V_i + V_j = V_{ij}$ with $V_i = V_{X_i}\left(E\left(Y|X_i\right)\right)$ and $V_j = V_{X_j}\left(E\left(Y|X_i\right)\right)$. The term V_{ij} represents the interaction between X_i and X_j which furthermore captures the influence on Y which cannot be superposed by the single effects of X_i or X_j. Again we can express the higher order sensitivity index

$$S_{X_i,X_j} = \frac{V_{X_i,X_j}\left(E\left(Y|X_i,X_j\right)\right)}{V\left(Y\right)} - S_{X_i} - S_{X_j}. \tag{1.38}$$

We have now found a method to capture even the mixed influence, in the above case the second order terms, but it is not guaranteed that there are no higher terms influencing the model outcome, but again we can express a condition which allows us to understand the percentage of knowledge gained[5]

$$\sum_i S_i + \sum_i \sum_{j>i} S_{ij} + \sum_i \sum_{j>i} \sum_{l>j} S_{ijl} + \ldots S_{123\ldots k} = 1.0. \tag{1.39}$$

This implies we have to compute $2^k - 1$ sensitivity indices in order to understand a model with k variables totally. This can lead to quite a high computational effort, to work around this the total effects are described in the next section. Due to the high computational effort in chapter 5 only the first order sensitivity indices and the total effects were computed.

1.3.3   Total Effects

What we do now is to start again with the idea used before and bring it to an extreme extend. We now compute the conditioned variance for all variables less than one

$$\frac{V_{\mathbf{X}_{\sim X_i}}\left(E\left(Y|\mathbf{X}_{\sim X_i}\right)\right)}{V\left(Y\right)} \tag{1.40}$$

which contains all terms of any order which do not include X_i. We remember that the sum made up in Eq. (1.39),

$$S_{T,X_i} = 1 - \frac{V_{\mathbf{X}_{\sim X_i}}\left(E\left(Y|\mathbf{X}_{\sim X_i}\right)\right)}{V\left(Y\right)} \tag{1.41}$$

must contain all effects made by X_i independent of the order and is accordingly called total effect term of variable X_i.

As found in [Saltelli, 2008] we understand the measure of total effect as a factor which shows how the output variance changes by changing the parameter of its range of variation. The case $S_{T,Xi} = 0$ is a sufficient and necessary condition for X_i to be a non-influential factor.

---

[4]We dropped the indices of E but we still keep in mind the average is now taken over $E_{X_{\sim i}, X_{\sim j}}$.

[5]For simplicity we removed the X in the index of the sensitive indices S_{X_i}.

In particular in [Sobol' et al., 2007] it can be found that the total effect also allows to estimate the possibly made error $\delta(X_i)$ when fixing the value, this is shown for uniform random distributions only; for an arbitrary $\varepsilon > 0$ with probability exceeding $1 - \varepsilon$

$$\delta(X_i) < \left(1 + \frac{1}{\varepsilon}\right) S_{T,X_i} \tag{1.42}$$

in this case setting $\varepsilon = 0.5$, $\delta(X_i) < 3S_{T,X_i}$ holds with a probability exceeding 0.50.

1.3.4 Correlation Coefficients

With the help of correlation coefficients we try to understand the dependency of the model's outcome on the model's input; we use two different correlation coefficients.

The Pearson Correlation Coefficient

The Pearson correlation coefficient shows us the linear dependency of two sets of variables, $\mathbf{X}$ and $\mathbf{Y}$. We find

$$r_{\mathbf{X},\mathbf{Y}} = \frac{E(\mathbf{X}|\mathbf{Y}) - E(\mathbf{X})E(\mathbf{Y})}{\sqrt{E(\mathbf{X}^2) - E(\mathbf{X})^2}\sqrt{E(\mathbf{Y}^2) - E(\mathbf{Y})^2}} \tag{1.43}$$

where $-1 \leq r_{\mathbf{X},\mathbf{Y}} \leq 1$ and if $r_{\mathbf{X},\mathbf{Y}} = 0$ there is no correlation, if $r_{\mathbf{X},\mathbf{Y}} = -1$ or $r_{\mathbf{X},\mathbf{Y}} = 1$ we have a perfect linear dependency, found in [Rodgers and Nicewander, 1988].

Spearman's Rank Correlation Coefficient

Spearman's rank correlation coefficient is a correlation measure based on the rank of two variable sets $\mathbf{X}$ and $\mathbf{Y}$. If R_i is the rank of $\mathbf{Y}$ corresponding to that pair $(\mathbf{X}, \mathbf{Y})$ we find

$$\rho_{\mathbf{X},\mathbf{Y}} = \frac{12}{N(N^2 - 1)} \sum_{i=1}^{N} \left(i - \frac{N+1}{2}\right)\left(R_i - \frac{N+1}{2}\right) \tag{1.44}$$

where $-1 \leq \rho_{\mathbf{X},\mathbf{Y}} \leq 1$ and if $\rho_{\mathbf{X},\mathbf{Y}} = 0$ there is no correlation, if $\rho_{\mathbf{X},\mathbf{Y}} = -1$ or $\rho_{\mathbf{X},\mathbf{Y}} = 1$ we can describe the dependency with the help of a monotonic function, found in [Hazewinkel, 1987].

1.3.5 Annotation

In [Saltelli, 2008] and more detailed in [Saltelli, 2004] we find a very effective way of computing the single sensitive indices S_{X_i} or S_{X_i,X_j} and the total effects S_{T,X_i}, starting with creating a matrix of the size $(N, 2k)$ containing N times two variable sets. N is called the base sample and k again the number of model input variables. We store this data in two matrices A and B each containing half of the variable sets and we create a matrix C_i formed by all columns of B except the ith column which is taken from A.

We compute the model output $Y_A = f(A)$, $Y_B = f(B)$ and $Y_{C_i} = f(C_i)$ and can now estimate the sensitivity indices

$$S_{X_i} = \frac{V_{X_i}(E_{X_{\sim i}}(Y|X_i))}{V(Y)} = \frac{\frac{1}{N}Y_A \cdot Y_{C_i} - f_0^2}{\frac{1}{N}Y_A \cdot Y_A - f_0^2} \tag{1.45}$$

$$S_{X_i, X_j} = \frac{V_{X_i, X_j}\left(E\left(Y|X_i, X_j\right)\right)}{V\left(Y\right)} - S_{X_i} - S_{X_j} = \frac{\frac{1}{N} Y_A \cdot Y_{C_{ij}} - f_0^2}{\frac{1}{N} Y_A \cdot Y_A - f_0^2} - S_{X_i} - S_{X_j} \quad (1.46)$$

where in the second case we create the matrix C_{ij} with all columns of B except the ith and jth column which are taken from A; according to [Saltelli, 2004] this can even be done in the same way for higher order terms. The total effect term can be computed in analogy

$$S_{T, X_i} = 1 - \frac{V_{\mathbf{X}_{\sim X_i}}\left(E\left(Y|\mathbf{X}_{\sim X_i}\right)\right)}{V\left(Y\right)} = 1 - \frac{\frac{1}{N} Y_B \cdot Y_{C_i} - f_0^2}{\frac{1}{N} Y_A \cdot Y_A - f_0^2} \quad (1.47)$$

with

$$f_0^2 = \left(\frac{1}{N} \sum_{j=1}^{N} Y_A^{(j)}\right)^2 \quad (1.48)$$

1.4 Model Class Selection

When comparing different models the Bayesian method gives us a very useful method for model comparison which is used since Laplace, see [MacKay, 1992]. With further developments done in this field we now have a very general probability based method to compare different models relative to a set of measurements.

Following [Beck and Yuen, 2004] we denote $\mathcal{D}$ the output data from a structural system and based on $\mathcal{D}$ we now select the most plausible class of models out of a set N_M of possible model classes $\mathcal{M}_1, \mathcal{M}_2, \ldots, \mathcal{M}_{N_M}$. As we want to obtain the plausibility of a single model class we need the conditional probability of the class of models based on the set of data $\mathcal{D}$. This can be achieved with the help of Bayes' theorem in the form,

$$P(\mathcal{M}_j|\mathcal{D}, \mathcal{U}) = \frac{p(\mathcal{D}|\mathcal{M}_j, \mathcal{U})P(\mathcal{M}_j|\mathcal{U})}{p(\mathcal{D}|\mathcal{U})}, \quad j = 1, 2, \ldots, N_M \quad (1.49)$$

where

$$p(\mathcal{D}|\mathcal{U}) = \sum_{j=1}^{N_M} p(\mathcal{D}|\mathcal{M}_j, \mathcal{U})P(\mathcal{M}_j|\mathcal{U}) \quad (1.50)$$

using the theorem of total probability, with $\mathcal{U}$ being introduced to this method as the user judgement on the plausibility of the model class which expresses a prior probability $P(\mathcal{M}_j|\mathcal{U})$, with the condition

$$\sum_{j=1}^{N_M} P(\mathcal{M}_j|\mathcal{U}) = 1. \quad (1.51)$$

The evidence for a model class $\mathcal{M}_j$ provided by the data $\mathcal{D}$ is $p(\mathcal{D}|\mathcal{M}_j, \mathcal{U})$, where $\mathcal{U}$ is irrelevant in $p(\mathcal{D}|\mathcal{M}_j, \mathcal{U})$. The most plausible model class is the one that maximizes $p(\mathcal{D}|\mathcal{M}_j, \mathcal{U})P(\mathcal{M}_j|\mathcal{U})$ with respect to j.

An interesting fact is that we can use $p(\mathcal{D}|\mathcal{M}_j, \mathcal{U})P(\mathcal{M}_j|\mathcal{U})$ not only for the selection of the most probable class of model, but also for the response prediction based on all model classes.

1.4.1   Evidence, Ockham Factor

We find the evidence for $\mathcal{M}_j$ provided by the data $\mathcal{D}$ based on the theorem of total probability

$$p(\mathcal{D}|\mathcal{M}_j) = \int_{\Theta_j} p(\mathcal{D}|\theta_j, \mathcal{M}_j) p(\theta_j|\mathcal{M}_j)\,\mathrm{d}\theta_j, \quad j = 1, 2, \ldots, N_M \tag{1.52}$$

where θ_j is the parameter vector in the parameter space $\Theta_j \subset \mathbb{R}^{N_j}$ defined by each model $\mathcal{M}_j$. In global identifiable cases, see [Beck and Katafygiotis, 1998], and with a large enough amount of data $\mathcal{D}$ Laplace's method for asymptotic approximation, [Papadimitriou et al., 1997], can be used and leads to

$$p(\mathcal{D}|\mathcal{M}_j) \approx p(\mathcal{D}|\hat{\theta}_j, \mathcal{M}_j) p(\hat{\theta}_j|\mathcal{M}_j) (2\pi)^{N_j/2} \left|\mathbf{H}_j(\hat{\theta}_j)\right|^{-1/2}, \quad j = 1, 2, \ldots, N_M, \tag{1.53}$$

with N_j being the number of uncertain parameters for the model class $\mathcal{M}_j$, the optimal parameter vector $\hat{\theta}_j$ which is the most probable value inside Θ_j and $\mathbf{H}_j(\hat{\theta}_j)$ the Hessian matrix of $-\ln\left[p(\mathcal{D}|\theta_j, \mathcal{M}_j) p(\theta_j|\mathcal{M}_j)\right]$ with respect to θ_j evaluated at $\hat{\theta}_j$.

We recognize $p(\mathcal{D}|\hat{\theta}_j, \mathcal{M}_j)$ to be the likelihood factor and $p(\hat{\theta}_j|\mathcal{M}_j) (2\pi)^{N_j/2} \left|\mathbf{H}_j(\hat{\theta}_j)\right|^{-1/2}$ to be the Ockham factor according to [Gull, 1988], which represents a penalty against parametrization.

According to [Taylor and Kitching, 2010] we use the Fisher matrix as approximation for the Hessian matrix $\mathbf{H}_j(\hat{\theta}_j)$, which shows to give numerically stable and admissible results.

Chapter 2

Vortex Shedding Approaches

This chapter introduces five approaches to describe vortex shedding phenomena by starting with a dimensional analysis to understand how the different determining parameter interact with each other and to show a possibility to base all approaches on the same set of parameters. After the dimensional analysis the vortex shedding models that were investigated are present, followed by the descriptions of the approaches. The investigated models are: H. Ruscheweyh [Sockel, 1994], B. J. Vickery and R. Basu [Vickery and Basu, 1983c] in a closed form solution given by the author, ESDU [ESDU96030, 1996], wake oscillator [Griffin, 1975] and AJI recommendations [AIJ, 2006].

The problem of vortex shedding can be described in different ways and thus the field of approaches available is quite wide. The basic problem when trying to figure out a valuable and sophisticated approach is the complexity of the phenomenon itself and so the only way to achieve a satisfying model is to do it in a semi-empirical way.

As semi-empirical models still have to be dimensional independent a dimensional analysis is done as a first step. This does not only allow us to understand better how the different parameters determine the process on a pure physical basis, but also make us realize that the wind velocity can be eliminated when introducing a critical velocity ratio term.

In the literature four recognized models can be found and in particular a very new one in [AIJ, 2006], which were selected by the author not only on the basis of sophistication but also based on which preliminary ideas and assumptions the models are developed on.

Vortex shedding is a non-linear phenomenon which the approaches have to take into account in order to find a proper solution. Ruscheweyh considers this non-linearity in the effective correlation length Le; Vickery and Basu do so by using a non-linear aerodynamic damping parameter ζ_a; ESDU modifies the mode generalized fluctuating force coefficient $\tilde{C}_{L_j}$; Griffin is using non-linear solution functions F, G, H for the differential equation and in the AJI recommendations a non-linear term for the Scruton number related to the natural frequency of the structure is included.

2.1 Abstract Parameter Study

In order to get a basic idea of the determining parameters in vortex shedding we diagram the input parameters categorized into geometry, dynamic, fluid and atmosphere; adding some already known non-dimensional quantities and some derived parameters completes the diagram, see Fig. 2.1, which should help to understand and underline the complexity of vortex shedding phenomena.
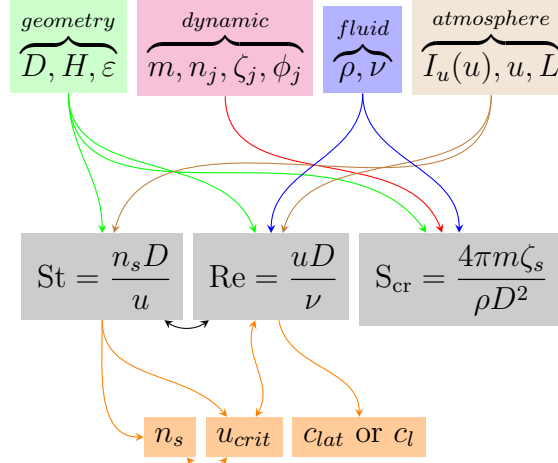
Figure 2.1 – Diagram showing the independent parameters, how they indirectly depend on each oder via non-dimensional relations and how characteristic values are derived.

2.2 Dimensional Analysis

Looking at the parameters in Fig. 2.1 we see that a general non-dimensional formulation would be very useful in order to gauge the different approaches properly and therefore we start with basic dimensional analysis;

$$\pi_0 = \bar{f}\left(Q_1, \ldots, Q_k, \pi_1, \ldots, \pi_{N-k}\right), \tag{2.1}$$

where the Vaschy Buckingham π-Theorem [Barenblatt, 1996] is satisfied and which we can rewrite in the form

$$\pi_0 = \mathcal{F}\left(\pi_1, \ldots, \pi_{N-k}\right). \tag{2.2}$$

As a first step we write the exponent matrix, using L for length, M for mass and T for time dimensions;

$$
\begin{array}{c|ccccccccccc}
 & y & D & H & \varepsilon & m & n_j & \zeta_s & \phi_j & \rho & \nu & I_u & u \\
\hline
\text{L} & 1 & 1 & 1 & 1 & -1 & 0 & 0 & 1 & -3 & 2 & 0 & 1 \\
\text{M} & 0 & 0 & 0 & 0 & 1 & 0 & 0 & 0 & 1 & 0 & 0 & 0 \\
\text{T} & 0 & 0 & 0 & 0 & 0 & -1 & 0 & 0 & 0 & -1 & 0 & -1
\end{array}
\tag{2.3}
$$

So we have $N + 1 = 12$ number of physical quantities Q_i and we find the rank k of the matrix in Eq. (2.3) to be $k = 3$. Now $N - k = 8$ dimensionless dependent variables $Q_{k+1}, \ldots, Q_N$ have to be associated with the dimensionally independent quantities $Q_1, \ldots, Q_k$. We select

$$Q_1 = D, \quad Q_2 = \rho, \quad Q_3 = \nu \tag{2.4}$$

which have no ulterior meaning[1] since we are trying to find suitable values for the dimensionless variables $\pi_0, \ldots, \pi_{N-k}$. Adding some physical knowledge, we find the dimensional dependent quantities $\pi_0, \ldots, \pi_{N-k}$ as follows – which is what we wanted to obtain in first place.[2]

$$\pi_0 = \frac{y_0}{D}, \ \pi_1 = \frac{m}{\rho D^2}, \ \pi_2 = \frac{n_j D^2}{\nu}, \ \pi_3 = \frac{a_{(n,h)}}{a_{(m,h)}}, \ \pi_4 = \frac{H}{D}, \ \pi_5 = \frac{\epsilon}{D}, \ \pi_6 = \zeta_s, \ \pi_7 = I_u. \tag{2.5}$$

---

[1]The reason we do not used u as dimensionally independent quantity becomes clear a few steps further.

[2]π_3 will be explained in detail later.

Applying the Vaschy Buckingham π-Theorem works and thus we were able to find the right dimensional independent quantities and we are now able to express the whole structural property using non-dimensional quantities; u is hidden in the dimensional dependent quantity π_2.

2.2.1 Annotations to the Dimensional Dependent Quantities

The dimensional dependent quantities $\pi_0, \pi_1, \pi_4, \pi_5, \pi_6, \pi_7$ are self-explanatory, however the quantity π_2 is a bit tricky as it includes a multiplication of a kind of Strouhal number St and the Reynolds number.[3]

$$\pi_2 = \frac{n_j D^2}{\nu} = \frac{n_j D}{u} \frac{uD}{\nu} \text{ in case of } n_s = n_j \text{ we know } \mathrm{St} = \mathcal{F}_{\mathrm{St}}(\mathrm{Re}) = \frac{n_s D}{u} \qquad (2.6)$$

and so for a given velocity u_{crit} we are able to obtain with the help of π_2 the Reynolds number as well as the Strouhal number for the case $n_s = n_j$; rewriting the condition yields

$$\pi_2 - \mathrm{St} \cdot \mathrm{Re} = 0; \qquad (2.7)$$

as the Strouhal number St does not exist in a closed form, Eq. (2.7) has to be solved iteratively. Expressed in this form we find a stable and fast solution by using the Newton method.

Now the only problem is that u is being cancelled and thus does not appear anymore because we are investigating the structure at $u = u_{crit}$ which is given by the condition $n_s = n_j$. To work around this to still have u as an independent variable is to introduce the ratio u/u_{crit} to be a dimensional dependent quantity in our case $\pi_6 = u/u_{crit}$ and thus the condition can be rewritten as

$$\mathrm{St}\big|_{n_s} = \mathcal{F}_{\mathrm{St}}(\pi_6 \cdot \mathrm{Re}). \qquad (2.8)$$

Now at least with the identity $n_s/n_j \cdot \mathrm{St}_j/\mathrm{St}_s = u/u_{crit}$ we can study the resulting behavior in relative variation to the fluid velocity u where the absolute value is again cancelled; more correctly it must be a dependent quantity as well.

When making dimensional analysis allusions to the models studied we see the need for the modal shape function ϕ_j which in itself is a function and thus no physical quantity, but it can be shown that for $\phi_1 = 1 - \cos(\pi z/2/h)$ and all other possible mode functions, see section A.2,

$$a_{(n,h)} = \int_h \phi_j^n \, \mathrm{d}z = const. \cdot h, \quad n \in \mathbb{N}_0, \qquad (2.9)$$

and so of course we find a dimensionless quantity with the used definition[4] of $a_{(n,h)}$ on $a_{(m,b)}$

$$\pi_3 = \frac{a_{(n,h)}}{a_{(m,b)}}, \quad m, n \in \mathbb{N}_0. \qquad (2.10)$$

The different approaches indeed need diverse information which can simply be created by setting n and m properly; the integration length h and b is normally over the whole structural length, except for the approach by Ruscheweyh where the integral must be known over the effective correlation length Le.

---

[3]Remember: St is a function of Re if the velocity u is expressed in Reynolds number Re.

[4]We use b instead of h to indicate a different integration length.

2.2.2   Conclusion

Summing up, we can express the vortex shedding phenomenon in the following non-dimensional form

$$\frac{y_{0,max}}{D} = \mathcal{F}\left(I_u, \zeta_s, \frac{m}{\rho D^2}, \frac{n_j D^2}{\nu}, \frac{a_{(n,h)}}{a_{(m,b)}}, \frac{H}{D}, \frac{\epsilon}{D}, \frac{u}{u_{crit}}\right). \tag{2.11}$$

The different approaches in non-dimensional form can be found in Tab. 2.1.

<div align="center">

Table 2.1 – Approaches represented in non-dimensional form

</div>

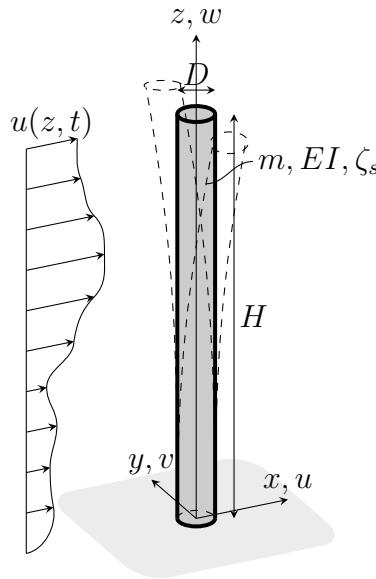| Approach	Non-dimensional Form
Ruscheweyh	$\dfrac{y_{0,max}}{D} = \mathcal{F}_{Ruscheweyh}\left(\zeta_s, \dfrac{m}{\rho D^2}, \dfrac{n_j D^2}{\nu}, \dfrac{a_{(1,Le)}}{a_{(1,H)}}, \dfrac{a_{(1,H)}}{a_{(2,H)}}, \dfrac{H}{D}, \dfrac{\epsilon}{D}\right)$
Vickery and Basu	$\dfrac{y_{0,max}}{D} = \mathcal{F}_{Vickery}\left(I_u, \zeta_s, \dfrac{m}{\rho D^2}, \dfrac{n_j D^2}{\nu}, \dfrac{a_{(2,H)}}{a_{(0,H)}}, \dfrac{H}{D}, \dfrac{\epsilon}{D}, \dfrac{u}{u_{crit}}\right)$
ESDU	$\dfrac{y_{0,max}}{D} = \mathcal{F}_{ESDU}\left(I_u, \zeta_s, \dfrac{m}{\rho D^2}, \dfrac{n_j D^2}{\nu}, \dfrac{a_{(2,H)}}{a_{(0,H)}}, \dfrac{H}{D}, \dfrac{\epsilon}{D}, \dfrac{u}{u_{crit}}\right)$
Wake Oscillator	$\dfrac{y_{0,max}}{D} = \mathcal{F}_{Wake}\left(\zeta_s, \dfrac{m}{\rho D^2}, \dfrac{n_j D^2}{\nu}, \dfrac{a_{(4,H)}}{a_{(2,H)}}, \dfrac{\epsilon}{D}\right)$
AIJ	$\dfrac{y_{0,max}}{D} = \mathcal{F}_{AIJ}\left(\zeta_s, \dfrac{m}{\rho D^2}, \dfrac{n_j D^2}{\nu}, \dfrac{\epsilon}{D}\right)$

2.3   Investigated Problem Set

Figure 2.2 – Scheme of a constant shaped oscillating circular cylindric steel structure immersed into a fluid flow

In order to be able to handle the approaches, some reduction to generality has to be made; at least we have to decide which type of structure we are investigating, otherwise the comparison can only be done in a very general way.

We are considering a steel chimney as shown in Fig. 2.2, with constant circular cross-section $D << H$ and the first mode shape with the shape function $\phi_1 = 1 - \cos(\pi z/2/H)$, is exposed to a fluctuating fluid flow. In addition, when performing the study we set the fluid flow to be constant over the complete height – this assumption is made according to [Vickery and Basu, 1983c] based on the observation that only the top third is determining the structure's reaction.

2.4   Ruscheweyh

The approach by Ruscheweyh [Sockel, 1994] and [Ruscheweyh, 1985] is a very simple model mostly based on experimental results. Via an explicit functional description of the correlation length which is found through experimental investigations the model is adjusted to represent obtained experimental results well; some practical experience can be found in [Ruscheweyh, 1990].

2.4.1   Correlation Length

The mechanism of vortex shedding is not distributed uniformly along the structural element. The exciting force cross correlation decreases as it is moving away from the antinode of the considered mode shape. This phenomenon is caused due to two effects, the first one being the non-uniform wind velocity distribution over the whole structural element and secondly by the lock-in effect. The lock-in effect also causes the maximum to be in the antinode point of the mode shape.

In the case of a cantilever the vortex shedding at the free end of the structure is disturbed and destroyed respectively by the three-dimensional flow around the top. Thus the maximum exciting force value is below the top.

We can describe the correlation curve with the help of the correlation length which is

$$L' = \frac{1}{c_{lat}} \int_H c_{y\sigma}(z)\,\mathrm{d}z, \qquad (2.12)$$

with $c_{y\sigma}(z)$ being the exciting force coefficient depending on the position on the structure and c_{lat} being the maximum value of $c_{y\sigma}(z)$. For a more detailed study see section 1.2.3 and [Ruscheweyh, 1985].

Once the structure is activated by vortex shedding, in the resonant phase the correlation length increases with the relative amplitude y_0/D. The synchronizing effect, the lock-in, as well as the increase of the correlation length are taken into account by this vortex resonance predicting model.

2.4.2   Mathematical Model

The model proposed by Ruscheweyh in [Sockel, 1994] is developed to predict the resonance amplitude y_0 due to vortex shedding by simplifying the vortex shedding phenomenon a fair bit.

The basic equation to compute the rms of the resonance amplitude is given by

$$\frac{y_{0,\sigma}}{D} = \frac{1}{\text{S}_{\text{cr}}} \frac{1}{\text{St}^2} \frac{\displaystyle\int_H c_{y\sigma}(z)\phi_j(z)\,\mathrm{d}z}{4\pi \displaystyle\int_H \phi_j^2(z)\,\mathrm{d}z}, \tag{2.13}$$

with, remembering Eq. (2.12),

$$\int_H c_{y\sigma}(z)\phi_j(z)\,\mathrm{d}z = c_{lat}\int^{L'} \phi_j(z)\,\mathrm{d}z, \tag{2.14}$$

based on the assumption that in the correlation length L' the value $c_{y\sigma}$ is nearly constant and equal to the maximum value c_{lat} and zero on the remaining part of the structure.

We now resubstitute and expand

$$\frac{y_{0,\sigma}}{D} = \frac{c_{lat}}{\text{S}_{\text{cr}}\,\text{St}^2} \frac{\displaystyle\int_H \phi_j(z)\,\mathrm{d}z}{4\pi\displaystyle\int_H \phi_j^2(z)\,\mathrm{d}z} \frac{\displaystyle\int^{L'} \phi_j(z)\,\mathrm{d}z}{\displaystyle\int_H \phi_j(z)\,\mathrm{d}z}, \tag{2.15}$$

and define

$$K_\phi = \frac{\displaystyle\int_H \phi_j(z)\,\mathrm{d}z}{4\pi\displaystyle\int_H \phi_j^2(z)\,\mathrm{d}z} = \text{constant of the mode shape} \tag{2.16}$$

and

$$K_w^* = \frac{\displaystyle\int^{L'} \phi_j(z)\,\mathrm{d}z}{\displaystyle\int_H \phi_j(z)\,\mathrm{d}z} = \text{correlation length factor} \tag{2.17}$$

The mode shape constant K_ϕ is identical to the definition made by Scruton [Scruton, 1963] and varies in the range of $0.1 - 0.14$. The K_w^* correlation length factor is depending on the correlation length L' itself and on the amplitude y_0/D and varies in a range of $0.0 - 1.0$.

Looking at the exciting force coefficient c_{lat} we notice that as well as $c_{y\sigma}$ both are rms values and so the calculated amplitude will also result as a rms value

$$\frac{y_{0,max}}{D} = g_P \cdot \frac{y_{0,\sigma}}{D}. \tag{2.18}$$

Ruscheweyh uses the same peak factor as we have described in section 1.2.4 in allusion to [Vickery and Basu, 1983b] and [Vickery and Basu, 1983a]. Now a very big step is done by Ruscheweyh by combining the peak factor g with the correlation length factor K_w^* to consequently obtain a closed form for all turbulence intensities I_u as well as for all Scruton numbers. This assumption still produces very convincing results.

$$K_w = K_w^* \cdot g_P = \frac{g_P \displaystyle\int^{L'} \phi_j(z)\,\mathrm{d}z}{\displaystyle\int_H \phi_j(z)\,\mathrm{d}z} = \frac{\displaystyle\int^{Le} \phi_j(z)\,\mathrm{d}z}{\displaystyle\int_H \phi_j(z)\,\mathrm{d}z} \tag{2.19}$$

with resulting $Le > L'$; and Le was found by approximation

$$\frac{Le}{D} = 2\,e^{1 + 1.4\frac{y_{0,max}}{D}}, \ \frac{y_{0,max}}{D} \le 0.6 \tag{2.20}$$

and is expressed by Ruscheweyh in an even simpler way by

$$\frac{Le}{D} = \begin{cases} 6 & \text{if} & \frac{y_{0,max}}{D} \le 0.1 \\ 4.8 + 12\frac{y_{0,max}}{D} & \text{if } 0.1 < \frac{y_{0,max}}{D} < 0.6 \\ 12 & \text{if} & \frac{y_{0,max}}{D} \ge 0.6 \end{cases} \tag{2.21}$$

which immediately implies that iterations have to be carried out in order to find the solution.

Here the main step carried out in the approach by Ruscheweyh should be noticed carefully. In Eq. (2.12) we expressed the length L' which gives use the same exciting force when integrated over the maximum value of $c_{y\sigma}$, c_{lat} over L', Eq. (2.14).

In Eq. (2.19) we find the integration length Le which takes the contribution of the peak factor g_P into account and so these two steps lead to the final result. The peak amplitude is then described as

$$\frac{y_{0,max}}{D} = K_\phi K_w \frac{c_{lat}}{\text{S}_{cr}\,\text{St}^2}. \tag{2.22}$$

2.4.3   Annotations

Furthermore, Eq. (2.22) holds true for structures with more than one vibration antinode and can be applied to more than one vibration mode, this advancement of K_ϕ and K_w is shown in detail in [CNR, 2009]. As already mentioned, in this study we are primarily interested in the influence of different parameters to the result. Hence, we are satisfied with a single mode shape and we find with $\phi_1 = 1 - \cos\left(\pi z/2/H\right)$

$$K_\phi = 0.128 \text{ and } K_w = \frac{Le/D\pi + 2H/D\cos\left(\frac{\pi}{2}\frac{Le/D}{H/D}\right) - 2H/D}{H/D(\pi - 2)}. \tag{2.23}$$

A notable fact is that using the commonly used approximation mode shape function $\phi_1 = (z/H)^2$ we find

$$K_\phi = 0.133 \text{ and } K_w = 3\frac{Le/D}{H/D}\left[1 - \frac{Le/D}{H/D} + \frac{1}{3}\left(\frac{Le/D}{H/D}\right)^2\right] \tag{2.24}$$

which, however, in the end does not lead to a really big overestimate, $\lesssim 5\%$ of the response, despite of using a poorer mode shape function.[5] When using this approach we insist in using $\phi_1 = 1 - \cos\left(\pi z/2/H\right)$ as mode shape function.

Ruscheweyh provides the possibility to reduce the exciting force coefficient c_{lat} for high critical wind velocities u_{crit}; this possibility is also not used here.

---

[5]Normally the mode shape function $\phi_1 = (z/H)^\xi$ is to prefer when dealing with taper stacks or non-uniformly distributed stiffness and/or mass, because by adjusting the value for ξ a well representing mode shape function can be found.

2.5 Vickery and Basu

The model by Vickery and Basu [Vickery and Clark, 1972] is a very complex approach based on both experimental results as well as fundamental physical principles. This makes the approach itself a bit more complicated but still allows to have a closed form solution. One of the main ideas is to apply the vortex shedding forces in the form of a force spectrum and perform simple modal analysis.

2.5.1 Mathematical Model

The concept of Vickery and Basu is based on the fundamental idea that the vortex shedding forces can be found by superposing the responses of all considered modes N in the form

$$y_0(z,t) = \sum_{j=1}^{N} a_j(t)\phi_j(z), \tag{2.25}$$

as seen in [Vickery and Basu, 1983c] mostly based on [Vickery and Basu, 1983b] and [Vickery and Clark, 1972].

Furthermore, the following assumptions are made when computing the response of each mode:

(i) Modeling the vortex shedding force as a normally distributed narrow band random force with the following characteristics is accurate enough and

- the force spectrum

$$\frac{nS_w(n)}{\sigma_w^2} = \frac{1}{\sqrt{B}} e^{-\left(\frac{1 - n/n_s}{B}\right)^2}, \tag{2.26}$$

is computed from the per unit length force $w(z,t)$. The variance results in

$$\sigma_w^2 = c_l^2 \frac{1}{2} \rho u^2 D^2, \tag{2.27}$$

which describes the phenomenon accurately enough in the vicinity of $n = n_s$. Of course the spectrum contains energy at lower frequencies which are primarily associated with turbulence in the flow while energy in high frequencies or high fluid velocities do not contribute significantly when n_s is close to n_j.

- Vickery and Basu also express the co-spectrum describing the vortex shedding correlation at two positions

$$S_{ww}(n,z_1,z_2) = \sqrt{S_w(n,z_1)} R(z_1,z_2)$$

$$R(z_1,z_2) = \cos\left(\frac{2r}{3l}\right) e^{-\left(\frac{r}{3l}\right)^2} \tag{2.28}$$

$$r = \frac{2|z_1 - z_2|}{D(z_1) + D(z_2)}$$

where $D(z_i)$ is the structural dimension at point z_i.

(ii) We describe the non-linear aerodynamic forces in dependency of the motion

$$w_d(z) = 4\pi \rho D^2 n_j K_a \left[1 - \left(\frac{y_{0,\sigma}}{\alpha D}\right)^2\right] \dot{y}_0 \tag{2.29}$$

where $K_a = \mathcal{F}(\text{St}, I_u, \text{Re})$ and will be successively discussed, see 2.5.2, and α is a limiting factor of rms response $y_{0,\sigma}$ in structural dimensions.

Based on the assumptions made in (i) and (ii) as well as comments in [Vickery and Clark, 1972] and [Vickery and Basu, 1983b] and neglecting the variation of the wind velocity over the height, see [Vickery and Basu, 1983c], we obtain a response equation in the form

$$\frac{y_{0,\sigma}}{D} = \frac{\dfrac{c_l \phi_j(H)}{8\pi^2 \text{St}^2} \dfrac{\rho D^2}{m} \sqrt{\dfrac{\sqrt{\pi} l}{2\frac{H}{D}}} \phi(B,k)}{\left[\dfrac{1}{H}\displaystyle\int_H \phi_j^2 \, \mathrm{d}z\right]^{\frac{1}{2}} \sqrt{\zeta_s - \dfrac{\rho D^2}{m} K_a \left[1 - \left(\dfrac{y_{0,\sigma}}{\alpha D}\right)^2\right]}} \tag{2.30}$$

with

$$\phi(B,k) = \frac{1}{\sqrt{B}} k^{\frac{3}{2}} e^{-\frac{1}{2}\left(\frac{1-k^{-1}}{B}\right)^2}. \tag{2.31}$$

$\phi(B,k)$ describes the influence of bandwidth on the response[6] and is derived from the spectrum of lift force due to vortex shedding, with the parameters $k = u/u_{crit}$ and $B = \sqrt{B_0^2 + 2I_u^2}$ as found in [Vickery and Basu, 1983b]; B_0 is in the range of $0.05 - 0.1$. In [Vickery and Basu, 1983c] a value of B around $0.10 - 0.30$ is assumed and it is mentioned that the peak response occurs for a value of $k = 1.1$ which means we need a higher flow velocity in order to obtain the maximal structural response; the maximum value is found at $\phi_{max}(B,k) = 2.5$.

The span-wise correlation parameter l can be found in [Simiu and Scanlan, 1996] to be $l = 2.5$ for $\text{Re} < 2 \cdot 10^5$ and $l = 1.0$ for $\text{Re} \geq 2 \cdot 10^5$.

With the use of some more assumptions a set of solutions can be found for this equation. Vickery and Basu mainly found these by looking at limit states of this function. In order to handle Eq. (2.30) in a proper way we solve it analytically starting with the expressions

$$\eta = \frac{y_{0,\sigma}}{D}, \quad \zeta_a = \frac{\rho D^2}{m} K_a, \quad c_1 = \frac{c_l \phi_j(H)}{8\pi^2 \text{St}^2} \frac{\rho D^2}{m}, \quad c_2 = \frac{\sqrt{\dfrac{\sqrt{\pi} l}{2\frac{H}{D}}} \phi(B,k)}{\left[\dfrac{1}{H}\displaystyle\int_H \phi_j^2 \, \mathrm{d}z\right]^{\frac{1}{2}}}. \tag{2.32}$$

Rewriting Eq. (2.30)

$$\eta = \frac{c_1 c_2}{\sqrt{\zeta_s - \zeta_a \left[1 - \left(\dfrac{\eta}{\alpha}\right)^2\right]}} \tag{2.33}$$

---

[6]Be aware of not confounding $\phi(B,k)$ with the mode shape function ϕ_j; $\phi(B,k)$ will always appear with functional parameters B and k.

gives us, using the first solution of the quadratic equation,

$$\eta = \frac{y_{0,\sigma}}{D} = \frac{1}{\sqrt{2}} \sqrt{\frac{-\zeta_s \alpha^2 + \zeta_a \alpha^2 + \sqrt{\zeta_s^2 \alpha^4 - 2\zeta_s \alpha^4 \zeta_a + \zeta_a^2 \alpha^4 + 4\zeta_a c_1^2 c_2^2 \alpha^2}}{\zeta_a}} \qquad (2.34)$$

the closed form solution for the vortex shedding phenomenon and again we find the maximum value by

$$\frac{y_{0,max}}{D} = g_P \cdot \frac{y_{0,\sigma}}{D}, \qquad (2.35)$$

with g_P in allusion to section 1.2.4. In section 7.2.2 we find this approach applied to tapered structures according to [Vickery and Clark, 1972] and [Vickery and Basu, 1983c].

2.5.2 Aerodynamic Damping Parameter

In Eq. (2.30) we used the aerodynamic damping parameter K_a and we noticed $K_a = \mathcal{F}(\text{St}, I_u, \text{Re})$; in [Vickery and Basu, 1983b] this parameter is found experimentally.

In [CICIND, 1999] a more accurate formulation of K_a is given which is based on the study by [Daly, 1986]. Thus K_a can be expressed as

$$K_a = K_{a,max} \left(1 - 3I_u\right) \qquad (2.36)$$

and $K_{a,max}$ can be found to be

$$K_{a,max}\left(\frac{u}{u_{crit}}\right) = \begin{cases} 0 & \text{if} \quad u/u_{crit} < 0.85, \\ a_t \left(3.5 \dfrac{u}{u_{crit}} - 2.95\right) & \text{if } 0.85 \leq u/u_{crit} < 1.00, \\ 0.55 a_t & \text{if } 1.00 \leq u/u_{crit} < 1.10, \\ a_t \left(2.75 - 2\dfrac{u}{u_{crit}}\right) & \text{if } 1.10 \leq u/u_{crit} < 1.30, \\ a_t \left(0.46 - 0.25\dfrac{u}{u_{crit}}\right) & \text{if } 1.30 \leq u/u_{crit} < 1.84, \\ 0 & \text{if } 1.84 \leq u/u_{crit}. \end{cases} \qquad (2.37)$$

with

$$a_t = a_1 a_2 a_3 a_4, \qquad (2.38)$$

and we set[7] $a_2 = 2.0$ considering u_{crit} to be smaller than 10m s^{-1},

$$a_1 = \begin{cases} 1.0 & \text{if} \quad \text{Re} < 10^4, \\ 1.8 & \text{if } 10^4 \leq \text{Re} < 10^5, \\ 1.0 & \text{if } 10^5 \leq \text{Re}. \end{cases} \qquad (2.39)$$

$$a_3 = 0.9 + 0.2 \left[\log_{10}\left(\frac{\epsilon}{D}\right) + 5\right], \qquad (2.40)$$

---

[7]This configuration is very conservative and the effect of this value is reduced by using the correction of [CICIND, 1999], see Eq. (2.36).

$$a_4 = \begin{cases} 1.0 & \text{if } H/D \geq 12.5, \\ 1.0 - 0.04 \left(12.5 - \dfrac{H}{D} \right) & \text{if } H/D < 12.5. \end{cases} \tag{2.41}$$

following [Simiu and Scanlan, 1996] and [Vickery and Basu, 1983b]. I_u as atmospheric turbulence, see section 1.1.

In addition, the limiting factor of rms response α is recommended in [CICIND, 1999] to be $\alpha = 0.4$ over the whole Reynolds number range.

2.5.3 Annotations

An important fact is that when Vickery and Basu solved Eq. (2.30) they did this in terms of limit value analysis. The considerations made in [Vickery and Basu, 1983c] are represented here; all equations are rewritten with the considerations made in Eq. (2.32).

(i) In the lock-in region, a region of large amplitudes and therefore of low mass and/or structural damping ratio the response is invariant of the factors c_1 and c_2 and thus invariant to the acting forces on the stationary structure.

$$\frac{y_{0,\sigma}}{D} \simeq \left[1 - \frac{\zeta_s}{\zeta_a} \right]^{\frac{1}{2}} \alpha \tag{2.42}$$

Thus the response is only determined by the nature of the non-linear aerodynamic damping and the reaction is more or less sinusoidal.

(ii) In the region of small amplitudes the reaction is random with a linear positive damping below that provided structurally

$$\frac{y_{0,\sigma}}{D} \simeq \frac{c_1 c_2}{[\zeta_s - \zeta_a]^{\frac{1}{2}}} \tag{2.43}$$

which has a nearly Gaussian trace.

(iii) In between these two regions we nearly find $\zeta_s = \zeta_a$ which means we are changing from a random regime into the sinusoidal regime. In this region the size of the amplitude is very sensitive to changes of ζ_s. In [Vickery and Basu, 1983c] it is still recommended to use the solution for the small amplitude region with the comment that after all both ζ_s and ζ_a are very insecure and poorly defined values and therefore it would be best to avoid entering the transition region at all.

2.6 ESDU

The idea provided by ESDU [ESDU96030, 1996] is trying to confront the problem from a more empirical point of view which shows the superposition of a broad band response and a narrow band response. This kind of phenomenon can easily be observed whenever vortex shedding occurs. At high amplitudes the structure is more or less oscillating in a constant sinusoidal form; in case of small amplitudes the oscillaton is more or less random; in between these two regions a mixture of both as well as an alternating oscillation in one or the other form can occur. The theoretical background is based on the research done by Vickery and Basu, an abstract of the main steps and equations of the ESDU approach are given here.

2.6.1 Mathematical Model

ESDU starts with the general equation of motion for an oscillating cylinder written in the mode generalized form

$$\left[-\omega_j^2 M_j + \mathrm{i}\omega_j \zeta_{s,j} 2\sqrt{M_j K_j} + K_j \right] Y_j = \tilde{F}_j. \tag{2.44}$$

Broad Band Response

We obtain the broad band response by assuming that the model force $\tilde{F}_j$ for small and moderate amplitudes is a combination of in phase and motional independent modal forces.

$$\left(\frac{y_{0,\sigma}}{D} \right)_B = \eta_B = \frac{\sqrt{n_j S_{C_F}}}{16\pi^{\frac{3}{2}}} \frac{\rho D^2}{m \dfrac{1}{H} \displaystyle\int_H \phi_j^2 \,\mathrm{d}z} \frac{1}{\sqrt{\zeta_s + \zeta_{aero}}} \left(\frac{u}{n_j D} \right)^2 \tag{2.45}$$

with

$$\zeta_{aero} = -\frac{\rho u^2 k}{4 m_j \omega_j^2} \frac{1}{H} \int_H \phi_j^2 \,\mathrm{d}z, \quad k = \frac{\mathrm{d}\tilde{C}_L}{\mathrm{d}\eta} \tag{2.46}$$

k_s is the max value of k which consists of a real and imaginary part, where the real part, which is out of phase with the motion, enriches the structure with a contribution to the stiffness but changes the resonant frequency only in a negligibly small way. The imaginary, in phase part, contributes in a negative way to the overall damping which here is expressed in the parameter ζ_{aero}.

In [ESDU96030, 1996] considerations made in [Vickery and Basu, 1984] were taken into account; if turbulence is of large scale the vortex shedding properties are depending on the instantaneous flow velocity k which can be found to be

$$k = \frac{k_s}{B_e} e^{-\dfrac{\left| \dfrac{u}{n_s D} - \dfrac{u}{n_j D} \right|}{B_e{}^2}}, \quad B_e = \sqrt{1 + 2\left(\frac{u}{n_j D} \right)^2 I_u{}^2} \tag{2.47}$$

with

$$k_s = 34 c_l^{n_k}, \quad n_k = 1.5 - 0.2\, e^{-100 c_l^3}. \tag{2.48}$$

The spectral density of the fluctuating side force coefficient $S_{C_F} = S_{C_B} + S_{C_L}$ is the sum of the buffeting spectrum S_{C_B} and the vortex shedding spectrum S_{C_L}. As all other studied model do not take into account buffeting we will discuss the effect of buffeting in section 3.5 and 3.6.1. The equations for the buffeting due to the lateral component of the turbulence spectrum S_{C_B} are not represented here.

$$n_j S_{F,j} = n_j S_{C_L} c_l^2 \int_0^1 \int_0^1 \phi_1(r_1)\phi_1(r_2)\, e^{-\left(\dfrac{|r_1 - r_2|}{L_{sn}} \right)^{1.5}} \cos\left(0.3|r_1 - r_2| \right) \,\mathrm{d}r_1 \,\mathrm{d}r_2 \tag{2.49}$$

using $n_j S_{C_L}$ as force spectral density for a circular cylinder

$$\frac{n_j S_{C_L}}{c_l^2} = \frac{4\delta_B \dfrac{n_j}{n_s}}{\pi} \left[\frac{1}{\left(1 - \dfrac{n_j}{n_s} \right)^2 + \left(2\delta_B \dfrac{n_j}{n_s} \right)^2} \right] \tag{2.50}$$

with δ_B as bandwidth parameter

$$\delta_B = 0.45 - 0.43\,e^{-118 I_u^{2.8}}. \tag{2.51}$$

L_{sn} is the length scale associated with vortex shedding

$$L_{sn} = \frac{0.4 L_s}{\left(1 - \frac{n_j}{n_s}\right)^2 + 0.4} \tag{2.52}$$

where L_s is the broad band spanwise correlation length in smooth flow, which is a function of Reynolds number, and the atmospheric turbulence; the tip effect was neglected.

Narrow Band Response

When approaching the lock-in region and $n_j = n_s$, the forces are in phase and sinusoidal due to vortex shedding and establish a constant amplitude

$$\left(\frac{y_{0,\sigma}}{D}\right)_N = \eta_N = \frac{1}{16\pi^2}\frac{\rho D^2}{m_j \zeta_s}\left(\frac{u}{n_j D}\right)^2 \tilde{C}_{L_j} \tag{2.53}$$

with $\tilde{C}_{L_j}$ being the mode generalized fluctuating force coefficient which is a non-linear function of η given by

$$\tilde{C}_{L_j} = \frac{1}{H}\int_H \frac{D(z)}{D}\left(\frac{u(z)}{u}\right)^2 \phi_j \tilde{C}_L. \tag{2.54}$$

Simplified for a constant fluid field, we obtain $\tilde{C}_L$ following a few steps, still being aware that $\tilde{C}_L$ is depending on η and thus can only be found in an iterative way:

$$\tilde{C}_L = \sqrt{\tilde{C}_{Lm}^2 + (f_r c_l)^2}, \quad f_r = \frac{2}{1 + e^{18 c_l \eta^2}} \tag{2.55}$$

and

$$\tilde{C}_{Lm} = \frac{b c_l\,(\,e^{c\eta} - 1)}{b + c_l\,(\,e^{c\eta} - 1)}\left[1 + \eta\frac{1 - e^{3\eta}}{1 + e^{3\eta}}\right],$$

$$b = 0.45\left(1 - e^{-0.00033\,(H/D)^{3.25}}\right), \quad c = 34 c_l^{n_k - 1} \tag{2.56}$$

with n_k as defined in Eq. (2.48).

Computed Response

We find the mixed response of broad band and narrow band response

$$\frac{y_{0,\sigma}}{D} = \eta = \sqrt{f_t \eta_N{}^2 + (1 - f_t)\,\eta_B{}^2} \tag{2.57}$$

with

$$c_t = \frac{1}{8}\left(1 + e^{-7.6\cdot 10^4 I_u^{3.6}}\right), \quad f_t = \begin{cases} c_t\left(\dfrac{\eta_N}{\eta_B} - 2\right) & \text{if } f_t \geqslant 0, \\ 0 & \text{if } f_t < 0. \end{cases} \tag{2.58}$$

And again we find the maximum value according to

$$\frac{y_{0,max}}{D} = g_P \cdot \frac{y_{0,\sigma}}{D}, \tag{2.59}$$

with g_P in allusion to section 1.2.4.

2.6.2 Annotations

To find the right value for $\tilde{C}_{L_j}$ we have to satisfy Eq. (2.53) and Eq. (2.54) in order to obtain equality in the form

$$16\pi^2\eta\frac{m_j\zeta_s}{\rho D^2}\left(\frac{n_j D}{u}\right)^2 = \tilde{C}_{L_j} = \frac{1}{H}\int_H \frac{D(z)}{D}\left(\frac{u(z)}{u}\right)^2 \phi_j\tilde{C}_L, \qquad (2.60)$$

where η_N is set to be the the structure reaction η. This can only be done iteratively; ESDU in [ESDU96031, 2000] does this by creating a set of possible values for η and then finding the maximal solution among them by linear interpolation of the values of η. What has to be mentioned and is noticed by the author is the numerical instability of this algorithm, which can be directly observed in the response surface plots in section 3.5.

The implementation of this approach has been based on the method described in [ESDU96030, 1996] and in accordance with the *visual basic* program code provided in an *excel* worksheet which is documented in [ESDU96031, 2000].

2.7 Wake Oscillator

O. M. Griffin, R. A. Skop et all. in [Skop and Griffin, 1973] describe the vortex shedding phenomenon with the help of a wake oscillator model related to maritime types of problems. The basic idea is that when the structure is activated in or around the lock-in effect region it behaves like a modified Van der Pol oscillator. The vortex shedding parameter St* which characterizes the structural activation is defined by Griffin and Votaw in [Griffin and Votaw, 1972]. It is an elementary parameter to describe the wake oscillator as well as the wake width and the formation length. Griffin and Votaw found that this value is used to describe in a suitable way the velocity fluctuations in the wake which in the end are used to explain the exciting forces in the wake oscillator equations.

2.7.1 Mathematical Model

We find the fundamental equation in allusion to [Griffin, 1975] and [Griffin and Skop, 1973b]

$$\ddot{C}_L + \omega_s^2 C_L - \left[C_{L0}^2 - C_L^2 - \left(\frac{\dot{C}_L}{\omega_s}\right)^2\right]\left(\omega_s G\dot{C}_L - n_s^2 H C_L\right) = \omega_s F\frac{\dot{y}}{D} \qquad (2.61)$$

with $C_L = C_{L0}\sin(\omega_s t)$ as solution for a self-excited, self-limited behavior and G, H and F obtained experimentally; the parameter ω_s shows to be the shedding frequency for a stationary cylinder and C_{L0} the fluctuating lift amplitude.

The equation of motion of a rigid mounted cylinder is

$$\frac{\ddot{y}}{D} + 2\zeta_s\frac{\dot{y}}{D} + \omega_1^2\frac{y}{D} = \mu\omega_1^2 C_L \qquad (2.62)$$

with μ the mass parameter and ω_1 as well as ζ_s to have the same values in a stationary or flowing fluid.

We find the solutions for Eq. (2.61) and Eq. (2.62) when both are in resonant oscillation

$$\begin{aligned}\frac{y}{D} &= A\sin\left(\omega t\right) \\ \frac{C_L}{C_{L0}} &= B\sin\left(\omega t + \varphi\right)\end{aligned} \qquad (2.63)$$

where we assume $\omega/\omega_s \approx 1.0$ and $\omega/\omega_1 \approx 1.0$ and A and B respectively are amplification factors for the cylinder displacement and fluctuating lift, φ is the phase between the cylinder displacement and the fluctuating lift. We found the entrained response to be

$$A = \frac{BC_L 0 \dfrac{\mu}{\zeta_s}}{\left(\delta^2 + 4\right)^{\frac{1}{2}}}$$

$$B^2 = 1 - \frac{\mu F}{G C_{L0}^2 \zeta_s} \frac{\delta}{\delta^2 + 4} \tag{2.64}$$

$$\varphi = \arctan\left(-\frac{2}{\delta}\right)$$

where δ must satisfy the cubic equation

$$\delta^3 - \Delta\delta^2 + \left(4 - \frac{\mu H F}{\zeta_s^2 G}\right)\delta - 4\left(\Delta - \frac{\mu F}{2\zeta_s^2}\right) = 0 \tag{2.65}$$

and δ and Δ are defined as

$$\delta = \frac{2}{\zeta_s}\left(\frac{\omega}{\omega_1} - 1\right), \quad \Delta = \frac{2}{\zeta_s}\left(\frac{\omega_s}{\omega_1} - 1\right). \tag{2.66}$$

In [Griffin and Skop, 1973a] and also in [Griffin and Skop, 1973b] we find experimental data and thus we are able to express the empirical parameters for a rigid cylinder

$$\log_{10} G = 0.25 - 0.21\frac{\zeta_s}{\mu},$$

$$\log_{10} h\left(\frac{\zeta_s}{\mu}\right)^2 = -0.24 + 0.66\frac{\zeta_s}{\mu}, \tag{2.67}$$

$$H = \zeta_s h, \quad F = 4G\frac{\zeta_s}{\mu h}.$$

Once we specify the relation for F we obtain the stable entrained response based on the solution to Eq. (2.65) to be $\delta \leqslant 0$.

To extend this approach from a rigid cylinder to an elastic cylinder Griffin and Skop choose the useful way to adopt a normal mode approach and we obtain

$$y_0(z, t) = \sum_{j=1}^{N} a_j(t)\phi_j(z) \tag{2.68}$$

which additionally allows use to superpose more than one mode N. Some basic mathematical operations can be found in [Griffin, 1975] which mainly deal with the extension to more than one mode which leads us to the solution with the assumptions made in [Griffin, 1985];

$$\frac{y_{0,max}}{D} = \frac{1.29\,\gamma_j}{\left[1 + 0.43\left(2\pi\,\mathrm{St}^2\,\mathrm{S_{cr}}\right)\right]^{3.35}} \tag{2.69}$$

these assumptions basically deal with the problem of high Reynolds numbers as well as the fluid to be air and give a closed form solution obtained from a set of wind tunnel tests. In Eq. (2.69) we compute

$$I_j = \frac{\displaystyle\int_H \phi_j^4(z)\,\mathrm{d}z}{\displaystyle\int_H \phi_j^2(z)\,\mathrm{d}z}, \quad \gamma_j = \frac{|\phi_j(z)|_{max}}{\sqrt{I_j}}, \tag{2.70}$$

where γ_j and I_j are kind of mode shape constants.

2.7.2 Annotations

In [Griffin, 1975] Griffin limits the validation of the above derived equations to $400 \leqslant$ Re $\leqslant 10^5$ which is truly fulfilled in maritime applications but is definitely not valid for fluid flow exposed structures where we normally start at Re $> 10^4$. One way to work around this is to adjust the parameter C_{L0} which as is explained in [Griffin, 1975] only effects the numerical parameters in Eq. (2.67) but not the functional dependence on ζ_s/μ. Eq. (2.69) includes a higher Reynolds number range as well as the possibility of the fluid to be air, see [Griffin and Skop, 1973a] and [Griffin, 1985].

2.8 AIJ Recommendations for Loads on Buildings

A further and very young approach can be found in [AIJ, 2006] which is mainly based on experimental data and describes the vortex shedding force. Considering the structural stiffness to be $m_1\omega_1^2$ we find the displacement on top of the structure, see section A.3,

$$\frac{y_{0,max}}{D} = \frac{20}{4\pi^2}\frac{\rho D^2}{m}C_r \tag{2.71}$$

where C_r is the wind force coefficient at resonance taken from Tab. 2.2. The approach is based on the spectral modal method with a fixed Strouhal number St $= 0.2$ for the vortex shedding and the power spectrum of the fluctuating wind loads based on the vibration amplitude.

The wind force coefficient C_r is separated into the three regions of Reynolds number Re, subcritical, critical, and supercritical and into two types of structures one with large amplitudes $m/D^2/\sqrt{\zeta_s} < 0.5$ and one with small amplitudes in which the structural damping ratio is modified, note the mutation of $1/\sqrt{\zeta_s}$.

Table 2.2 – Wind force coefficient C_r at resonance

$5n_jD^2$	$\dfrac{m}{D^2}\sqrt{\zeta_s} < 0.5$	$\dfrac{m}{D^2}\sqrt{\zeta_s} \geq 0.5$
$5n_jD^2 < 3$	$\dfrac{1.3}{\sqrt{\zeta_s}} + \dfrac{0.15}{\zeta_s}\dfrac{\rho D^2}{m}$	$\dfrac{1.7}{\sqrt{\zeta_s}}$
$3 \leq 5n_jD^2 < 6$	linier interpolation	linier interpolation
$6 \leq 5n_jD^2$	$\dfrac{0.53}{\sqrt{\zeta_s}} + \dfrac{0.02}{\zeta_s}\dfrac{\rho D^2}{m}$	$\dfrac{0.57}{\sqrt{\zeta_s}}$

2.9 Conclusion

Starting with the dimensional analysis as preparation for studying the individual approaches allows us to understand the relation between the different parameters properly. Furthermore, with the obtained dimensionless parameters it is possible to compare the different results on a uniform basis and to show which parameter relations determine the single models. Via the combination of the Strouhal number St and the Reynolds number Re a new dimensionless quantity π_2 was found, which proves the possibility of eliminating fluid velocity by substituting it with the dimensionless quantity π_6, critical velocity ratio u/u_{crit}.

Looking at the five presented approaches the difference and various possibilities of representing the vortex shedding phenomenon becomes obvious.

Chapter 3

Approach Diagnostics

After introducing the different approaches to model the vortex shedding phenomenon, we will analyze the different approaches in this chapter. Firstly, how they behave in the different parameter domains and then how well they fit measured data on real erected chimneys. Furthermore, a model class selection analysis is performed in order to see how the different approaches behave based on probabilistic model quality criteria. In order to get an idea of how the approaches cover a mixed parameter space the most meaningful response surfaces are shown and analyzed. The chapter concludes with a review of the ESDU approach due to the effect of contradictions detected in the results obtained by this approach.

Firstly, the approaches are studied in the damping domain, section 3.2, followed by a study of the influence of structural slenderness H/D, section 3.3 and concludes with section 3.4 of how well the different approaches capture the values measured given in section 3.1. To increase comprehension of the single approaches we take an additional careful look at the response surfaces and analyze them. In a two or three dimensional representation we are forced to fix the other parameters; the following values are chosen – these are in the first row the mean values of the values measured and represented in Tab. 3.1

$$\zeta_s = 0.004, \quad \frac{m}{\rho D^2} = 189, \quad \frac{n_j D^2}{\nu} = 300\ 240, \quad \frac{H}{D} = 25$$
$$I_u = 0.1, \quad \frac{\epsilon}{D} = 0.001, \quad \frac{u}{u_{crit}} = 1.0. \tag{3.1}$$

Fixing parameters or dimensionless quantities at a certain value can lead to problems when comparing the approaches with each other; whenever a value selected influences the characteristics it will be mentioned or the effect described.

3.1 Measured Values of Erected Chimneys

To obtain an idea of how real structures behave, a set of measurements was composed by researching publications, especially [Colaiuda and Currarino, 2007] where a numerousness database of chimneys is contained. All chimneys listed in Tab. 3.1 have constant shafts and the turbulence intensity I_u was computed according to the critical velocity u_{crit} with appearance probability $P = 0.95$ as defined in Eq. (4.10), in order to find a possible limit situation. See section 4.5 to find a detailed explanation. Thus it is plotted in all plots following and $u/u_{crit} = 1.0$ is assumed. The roughness of the surface is not known and

therefore not represented here. The dimensional parameters of the single chimneys can be found in Tab. 3.3.

Table 3.1 – Measured values of erected chimneys with the computed dimensionless quantities.

Description	No.	$\dfrac{y_{0,max}}{D}$ meas.	ζ_s	$\dfrac{m}{\rho D^2}$	$\dfrac{n_j D^2}{\nu}$	$\dfrac{H}{D}$
Strack "A" *Johns et al, 1972*	1	0.170	0.004	211.11	48 000	28.33
Venezuela *Exxon*	2	0.080	0.005	79.34	1 147 080	11.52
France *Exxon*	3	0.170	0.006	85.33	240 000	20.67
South Africa *Pritchard, 1984*	4	0.190	0.003	69.14	326 160	19.44
England *Exxon*	5	0.170	0.004	110.37	187 920	25.56
Ireland *Exxon*	6	0.320	0.003	88.16	223 440	20.71
Netherlands *Van Koten, 1979*	7	0.050	0.005	74.67	83 213	37.97
England *Exxon*	8	0.050	0.006	100.93	708 523	13.49
Poland *Ciesielski, 1992*	9	0.200	0.005	102.40	195 833	20.80
Poland *Ciesielski, 1992*	10	0.370	0.003	165.38	47 516	36.59
Germany	11	0.380	0.002	85.98	94 955	30.77

3.2 Behavior in the Damping Ratio Domain, ζ_s

In order to properly understand how the approaches work we start making some preliminary studies in the damping ratio domain which is the most significant domain when designing a dynamically sensitive structure. In Fig. 3.1 we can see all approaches as function of the structural damping ratio ζ_s or the Scruton number S_{cr} respectively as $m/\rho/D^2$ is constant, with fixed input values as well as imposed changes in $n_j D^2/\nu$ and $m/\rho/D^2$. We are changing two main dynamic input parameters of the structure, the natural frequency n_j and the structural mass per unit length m.

This way the effect of changing single values onto the result in the damping ratio domain becomes clear; the influence of all other determining parameters is shown in section 3.5. Furthermore, a range within which the response remains is given for structural damping ratios $\zeta_s > 0.01$; these results are obtained by finding the maximum values

via favorable combinations of the parameters and the minimum value via unfavorable combinations. Zero would obviously be the lowest value if single values would not be bound in certain ranges.

The behavior over the whole domain in terms of the Scruton number S_{cr} can be seen in Fig. 3.1; the decay itself in terms of a numerical derivation can be seen in Fig. 3.2. In addition, in Fig. 3.3 we can see the computed values minus the measured values and divided by the measured values for every single approach with the parameters of every chimney shown in Tab. 3.1 marked with the corresponding number.
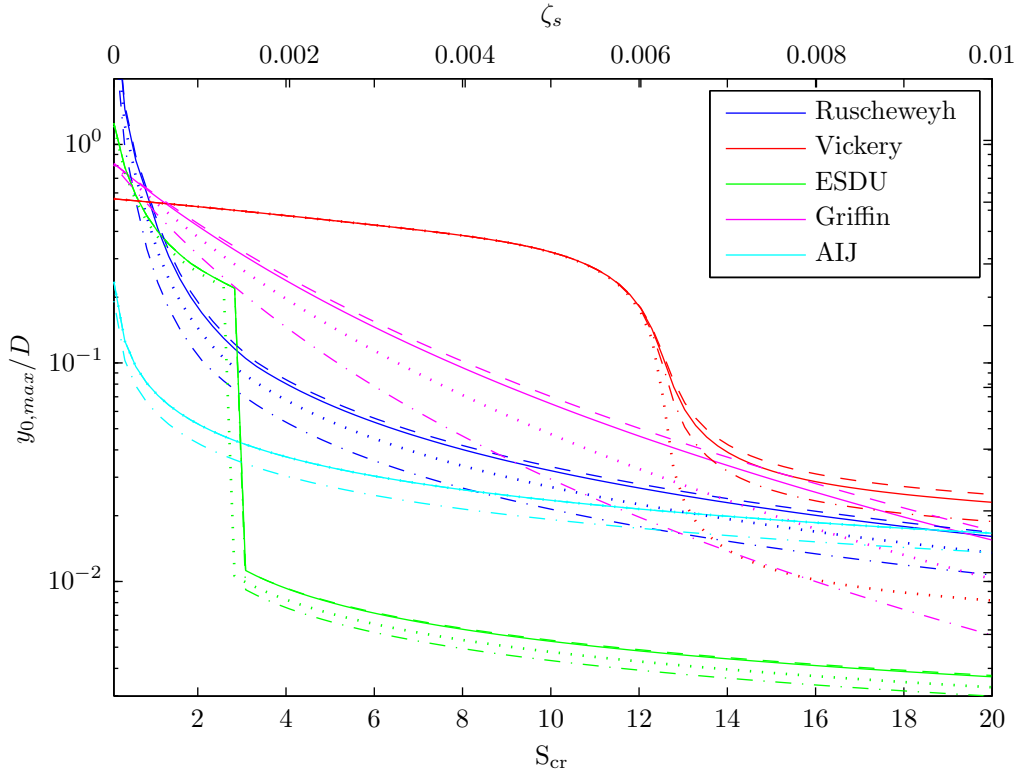

Figure 3.1 – Behavior of the approaches studied in the damping ratio domain; dotted lines represent $n_j D^2/\nu \cdot 0.5$; dashed lines represent $n_j D^2/\nu \cdot 1.5$; dash-dot lines represent $m/\rho/D^2 \cdot 1.5$.

3.2.1 Ruscheweyh

Looking at Fig. 3.1, we see the function obtained by Ruscheweyh's approach marked by a solid line is very strongly declining as the structural damping ratio ζ_s rises, the fact that we use S_{cr} is irrelevant as we are computing the structural reaction for a fixed value $m/\rho/D^2$ which is of course valid for all approaches. Furthermore, the Ruscheweyh method shows that changing the structural mass in terms of $m/\rho/D^2$ marked by a dash-dot line causes the result to shift downwards as the value of interest increases. This becomes clear when remembering that this factor is part of the Scruton number S_{cr} and thus the effect is like computing the structural response at a higher Scruton number; the same effect is reversed, when decreasing the term $m/\rho/D^2$.

$$\lim_{\zeta_s \to 0} \frac{y_{0,max}}{D} = \lim_{S_{cr} \to 0} K_\phi K_w \frac{c_{lat}}{S_{cr} \, St^2} = \infty$$

$$\lim_{\zeta_s \to \infty} \frac{y_{0,max}}{D} = \lim_{S_{cr} \to \infty} K_\phi K_w \frac{c_{lat}}{S_{cr} \, St^2} = 0; \text{ decay } \propto \frac{1}{\zeta_s}$$

$$(3.2)$$

Continuing with Ruscheweyh, we notice a fairly smaller influence when changing $n_j D^2/\nu$, where decreasing the value marked by a dotted line has a higher impact than increasing the value marked by a dashed line. This influence is caused by the lift coefficient c_{lat} and the Strouhal number St, remember $n_j D^2/\nu = \text{Re} \cdot \text{St}$. We find the limits in Eq. (3.2) which show no existence of an auto-limitation and having a decay proportional to $1/\zeta_s$ shows the model to be deterministic.

A further very interesting point is how the function's derivative behaves, see Fig. 3.2. It shows an exponentially growing gradient for small Scruton numbers. The gradient limits indicated are therefore for high S_{cr} values, close to each other, e.g. for $10^{-2} \to S_{cr} \sim 6$ and $5 \cdot 10^{-2} \to S_{cr} \sim 8$, and for low values of S_{cr} the $10^{-3} \to S_{cr} \sim 18$ the distance increases rapidly.

The approximate range for a high structural damping ratio $\zeta_s > 0.01$ can be found by evaluating maximum and minimum limit conditions

$$\frac{y_{0,max}}{D} = \left.\begin{array}{c} 0.029 \\ 0.003 \end{array}\right\rangle \frac{\rho D^2}{m} \frac{1}{\zeta_s} \tag{3.3}$$

which appears to be quite small, leading to the conclusion that once the structural damping ratio is high the structural configuration only has a minor relevance.

3.2.2 Vickery and Basu

Moving to the approach by Vickery and Basu we see a very different behavior. Starting at low numbers for ζ_s we have a slightly inclined plateau[1] which drops within quite a small range down to a lower, less inclined plateau. Varying $m/\rho/D^2$, marked by a dash-dot line, has two effects as mentioned above; one is a shift to the left which is exclusively caused by changing S_{cr} and the other is the down shift in a high Scruton number range which in a small part is caused by S_{cr} but the main part is caused by the variation on m and additionally the slope becomes steeper. Looking at the limit studies carried out by Vickery and Basu and represented in section 2.5.3, the curve in Fig. 3.1 becomes even clearer; as the narrow band branch is only depending on the structural damping ratio ζ_s and the aerodynamic damping ratio ζ_a, see Eq. (2.42). In addition, we notice that the structural reaction $y_{0,max}/D$ is higher[2] than the value obtained by Ruscheweyh's approach in the high Scruton number range, which is generally distinctive upon the structural configuration.

The influence of different values for $n_j D^2/\nu$ is quite moderate when increasing the value, but considerable when decreasing it and it only effects the high Scruton number range branch, where decreasing $n_j D^2/\nu \cdot 0.5$, marked by a dotted line, shifts the function down and makes the drop nearly vertical; increasing $n_j D^2/\nu \cdot 1.5$, marked by a dashed line, lifts the function in a fairly moderate way.

As the approach is auto-limited, the limit value is independent from the structural configuration and is thus only depending on α being the limiting factor of rms response $y_{0,\sigma}$ in structural dimensions. The limits are

$$\lim_{\zeta_s \to 0} \frac{y_{0,max}}{D} \simeq \lim_{\zeta_s \to 0} g_P \left[1 - \frac{\zeta_s}{\zeta_a}\right]^{\frac{1}{2}} \alpha \simeq \sqrt{2}\alpha$$

$$\lim_{\zeta_s \to \infty} \frac{y_{0,max}}{D} \simeq \lim_{\zeta_s \to \infty} g_P \frac{c_1 c_2}{\left[1 - \frac{\zeta_s}{\zeta_a}\right]^{\frac{1}{2}}} = 0; \text{ decay } \propto \frac{1}{\sqrt{\zeta_s}}. \tag{3.4}$$

---

[1] Note: this is caused by the logarithmic scaling of the structural reaction $y_{0,max}/D$.

[2] This is generally so, but when changing the surface roughness ϵ/D to higher values Vickery drops below Ruscheweyh's approach.

The lower limit shows the model to display probabilistic behavior; the decay is proportional to $1/\sqrt{\zeta_s}$. The Vickery and Basu model shows a quite different behavior in the derived damping ratio domain Fig. 3.2, with a maximal steepness at the point of inflection, which – as has already been mentioned above – increases as $n_j D^2/\nu$ decreases, marked by a dotted line. Looking at the limits of the gradient only in the hight Scruton number range is the model by Vickery and Basu smaller than the gradient limits indicated.

Here the approximate range for a high structural damping ratio $\zeta_s > 0.01$ is

$$\frac{y_{0,max}}{D} = \left.\begin{array}{c} 2.570 \\ 0.066 \end{array}\right\rangle \frac{\rho D^2}{m} \frac{1}{\sqrt{\zeta_s}} \tag{3.5}$$

which is quite large; in contrast to the conclusions drawn for Ruscheweyh in this case the structural configuration is not irrelevant at all.

In order to be able to compare the range from the Ruscheweyh approach to the Vickery and Basu, ESDU and AIJ Recommendations for Loads on Buildings the identity

$$\frac{1}{\sqrt{\zeta_s}} \le \frac{1}{\zeta_s} \quad \text{for} \quad \zeta_s \le 1.0 \tag{3.6}$$
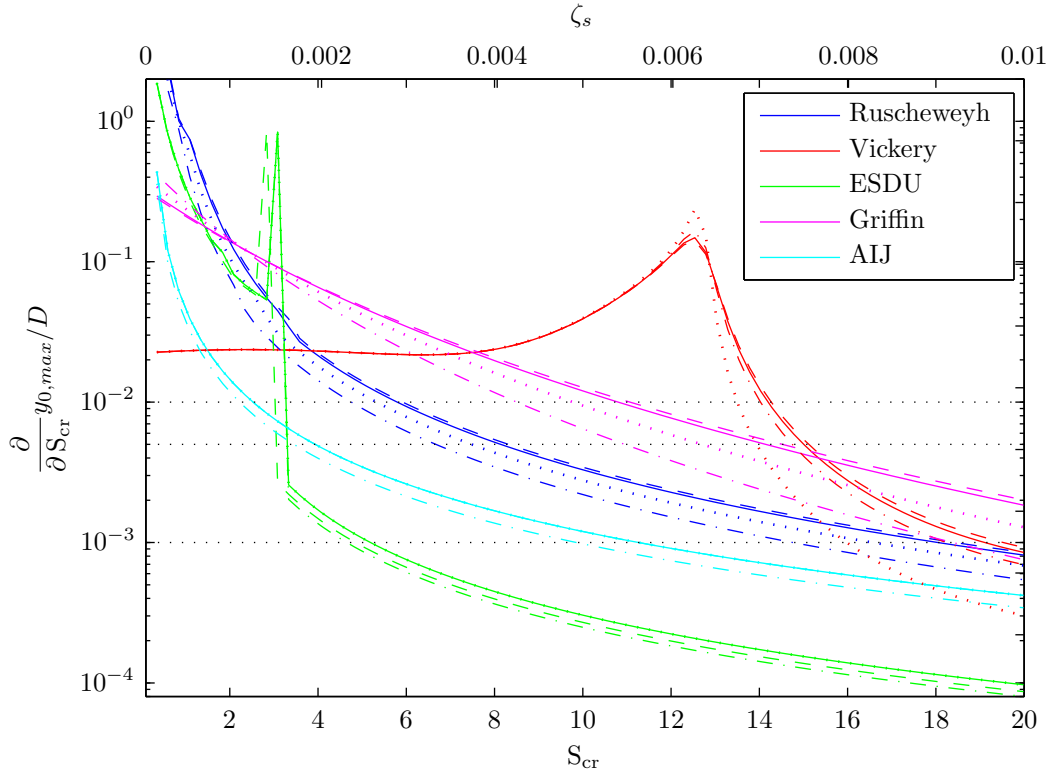
has to be kept in mind.

Figure 3.2 – Numerical derivative of the approaches studied in the damping ratio domain; dotted line means $n_j D^2/\nu \cdot 0.5$; dashed lines represent $n_j D^2/\nu \cdot 1.5$; dash-dot lines represent $m/\rho/D^2 \cdot 1.5$; horizontally doted black lines indicate limits of the gradient at 10^{-2}, $5 \cdot 10^{-3}$ and 10^{-3}.

3.2.3 ESDU

ESDU shows an interesting behavior particularly because it is the most complex approach discussed here and the only one taking buffeting into account. ESDU, based on the

approach by Vickery and Basu, shows a similar behavior in the damping ratio domain Fig. 3.1 with the special feature that the drop in the mixed response region is more or less perpendicular; this is caused by the fact that the narrow band solution is much larger than the broad band solution. The results obtained in the broad band reaction regions does not only start at relatively small Scruton numbers S_{cr}, but is also very small compared to the Vickery and Basu result. ESDU's results are generally smaller than the Vickery and Basu results which leads – together with some later demonstrated effects – to some criticism on the ESDU approach, which will be discussed more extensively in section 3.6.1.

Looking carefully at Fig. 3.1 we see that in the narrow band response case the increase in $y_{0,max}/D$ is very strong when reducing the structural damping ratio ζ_s. But when the structure reacts in the broad band region the response is very small and does vary similarly to the Ruscheweyh approach when varying the structural damping ratio, but is far below the values obtained from Ruscheweyh's approach.

The influence of varying $m/\rho/D^2$ can only be observed on the broad band branch and by altering $n_j D^2/\nu$ on both branches of the ESDU response function, where either variation is very moderate; especially increasing $n_j D^2/\nu \cdot 1.5$, marked by a dashed line, shows nearly no difference to the result. Decreasing $n_j D^2/\nu \cdot 0.5$, marked by a dotted line, shows some effect on the narrow band branch. Increasing $m/\rho/D^2 \cdot 1.5$, marked by a dash-dot line, shows the biggest influence compared to all other changes to the broad band branch.

We find the limits in the damping ratio domain as follows – remember ESDU's approach is not auto-limited,

$$
\lim_{\zeta_s \to 0} \frac{y_{0,max}}{D} = \lim_{\zeta_s \to 0} \frac{g_P}{16\pi^2} \frac{\rho D^2}{m_j \zeta_s} \left(\frac{u}{n_j D} \right)^2 \tilde{C}_{L_j} = \infty
$$
$$
\lim_{\zeta_s \to \infty} \frac{y_{0,max}}{D} = \lim_{\zeta_s \to \infty} \frac{g_P \sqrt{n_j S_{C_F}}}{16\pi^{\frac{3}{2}}} \frac{\rho D^2}{\sqrt{\zeta_s + \zeta_{aero}}} \left(\frac{u}{n_j D} \right)^2 = 0; \ \text{decay} \ \propto \frac{1}{\sqrt{\zeta_s}}
$$

(3.7)

and again we see a probabilistic behavior looking at the decay. That ESDU provides the smallest structural reaction values $y_{0,max}/D$ is a general fact.

In the derivated damping ratio domain, Fig. 3.2, the ESDU model shows a similar behavior to the Vickery and Basu model with the exception that the peak is pointed and due to the nearly perpendicular mixed region very narrow. Here the approximate range for a high structural damping ratio $\zeta_s > 0.01$ is

$$
\frac{y_{0,max}}{D} = \left. \begin{matrix} 0.616 \\ 0.004 \end{matrix} \right\rangle \frac{\rho D^2}{m} \frac{1}{\sqrt{\zeta_s}}
$$

(3.8)

which is smaller than the one obtained by Vickery and Basu but with a smaller possible value and the upper limit very improbable to reach.

3.2.4 Wake Oscillator

Moving to the approach by Griffin we see the response to be a slightly convex function[3] which is retained as $m/\rho/D^2$ increases, marked by a dash dot-line, and the function rotates clockwise and the convexity increases. This phenomenon of rotation and increasing convexity can also be observed in a moderate way for changes in $n_j D^2/\nu$, marked by a

---

[3]Again with a logarithmic scaled $y_{0,max}/D$ axis.

dotted line for decreasing and the dashed line for increasing values. The limits show the approach to be auto-limited

$$\lim_{\zeta_s \to 0} \frac{y_{0,max}}{D} = \lim_{S_{cr} \to 0} \frac{1.29 \, \gamma_j}{\left[1 + 0.43 \left(2\pi \, St^2 \, S_{cr}\right)\right]^{3.35}} = 1.29 \, \gamma_j$$

$$\lim_{\zeta_s \to \infty} \frac{y_{0,max}}{D} = \lim_{S_{cr} \to \infty} \frac{1.29 \, \gamma_j}{\left[1 + 0.43 \left(2\pi \, St^2 \, S_{cr}\right)\right]^{3.35}} = 0; \; \text{decay} \propto \frac{1}{\zeta_s^{3.35}}$$

(3.9)

and having a non-clear behavior as the decay is proportional to $1/\zeta_s^{3.35}$. In the derivative plot, Fig. 3.2, we can see the wake oscillator approach to show a behavior similar to the Ruscheweyh approach just less convex and upshifted, thus if we would have to fulfill a gradient condition the obtained S_{cr} value would be higher than the one of Ruscheweyh.

Here the approximate range for a high structural damping ratio $\zeta_s > 0.01$ is not computed because they will not be directly comparable due to the 3.35 power.

Furthermore, the solution functions used are found empirically for structures in water and adjusted with a small set of aeroelastic experiments on models and thus this approach is not further investigated. As the fundamental idea is ingenious an interesting research idea would be to find these solution functions analytically and adjust them with the help of proper aeroelastic experiments.

3.2.5 AIJ Recommendations for Loads on Buildings

The AIJ approach has a similar shape to the Ruscheweyh approach, but is situated lower in the low Scruton number range and intersects the Ruscheweyh function at high Scruton numbers. The AIJ approach is gradually sensitive to changes of $n_j D^2/\nu$, see Tab. 2.2, and has the same behavior as the Ruscheweyh model when varying $m/\rho/D^2$. We find the limits

$$\lim_{\zeta_s \to 0} \frac{y_{0,max}}{D} = \lim_{\zeta_s \to 0} \frac{20}{4\pi^2} \frac{\rho D^2}{m} \left(\frac{0.53}{\sqrt{\zeta_s}} + \frac{0.02}{\zeta_s} \frac{\rho D^2}{m}\right) = \infty$$

$$\lim_{\zeta_s \to \infty} \frac{y_{0,max}}{D} = \lim_{\zeta_s \to 0} \frac{20}{4\pi^2} \frac{\rho D^2}{m} \frac{0.57}{\sqrt{\zeta_s}} = 0; \; \text{decay} \propto \frac{1}{\sqrt{\zeta_s}}$$

(3.10)

and it shows to be a probabilistic model with a decay proportional to $1/\sqrt{\zeta_s}$ even though it was developed on a semi-empirical basis. When studying the behavior of this approach in the derived damping ratio domain, Fig. 3.2, we again observe nearly identical characteristics to the ones in the Ruscheweyh model with the difference that the function is downshifted and for small Scruton numbers has a less steep gradient.

Here the approximate range for a high structural damping ratio $\zeta_s > 0.01$ is

$$\frac{y_{0,max}}{D} = \left.\frac{0.861}{0.289}\right\rangle \frac{\rho D^2}{m} \frac{1}{\sqrt{\zeta_s}}$$

(3.11)

which appears to be somewhere in-between the Vickery and Basu approach, but considerably smaller than the range found for the Vickery and Basu approach.

3.2.6 General Observation

What can be observed for all approaches is a decreasing response if $n_j D^2/\nu \cdot 0.5$ decreases, marked by a dotted line, and an increasing response, marked by a dashed line, for increasing values of $n_j D^2/\nu \cdot 1.5$, which can be observed in the same way for $m/\rho/D^2 \cdot 1.5$ values,

taking additionally into account all made comments on the different applications. We can see that only Vickery and Basu as well as the wake oscillator approach represent the auto-limitation behavior of a vortex excited structure, which can be physically observed but is of no special importance in engineering applications as structures should not even be designed near the narrow band region. Vickery and Basu and ESDU are the two approaches which do separate the narrow band from the broad band region and give results for all critical velocity ratios u/u_{crit}. From a physical point of view the Vickery and Basu approach is the most convincing one due to the advanced studies carried out in [Vickery and Clark, 1972] which in parts are also valid for the ESDU approach. Ruscheweyh's, Griffin's and AIJ's Recommendations for Loads on Buildings only give results for critical velocity ratios $u/u_{crit} = 1.0$ and allow no variation of the turbulence intensity I_u, therefore they only give indicative results.

When investigating a structure with a high Scruton number S_{cr}, it is more or less even which ever approach one uses, however if the structure is badly damped, the best choice is definitely the Vickery and Basu approach.

3.3   Limits in the Slenderness Domain, H/D

Looking at the influence of the slenderness onto the result we see that it is only influenced by the height H since $1/D$ appears in both expressions H/D and $y_{0,max}/D$. For all approaches[4] the same behavior can be observed: as H/D decreases the response $y_{0,max}/D$ increases, this effect is caused due to the relatively bigger correlation length; consequently for great values of H/D the structural response $y_{0,max}/D$ decreases, but both variations are in a very small and moderate way.

3.4   Representation of Measured Values

Initially, one remark has to be made: comparing the computed values of just 11, not very detailed measurements, should not be overstated, but allows us to get at least an idea of where the different approaches are located in the field of measurement representation.

In order to see how the different approaches capture the measured data the computed results are represented relative to the measured values in Fig. 3.3, by subtracting the measured value from the computed value and then dividing it by the measured value; leading to positive values if the result is overestimated and negative values if the result is underestimated. Thus in Fig. 3.3 we can analyze how the different approaches represent the measured values for every single measurement. Looking at measurement 7 we notice that all approaches, except ESDU, overestimate the measured structural reaction. This leads to the conclusion that the value was maybe measured in less critical circumstances as imposed for the calculations. A further observation concerning ESDU is that it generally gives a too low value, but in case of chimneys 4 and 11 it is quite close to the value obtained by the measurement – numerical values for ESDU can be found in Tab. 3.3. In section 3.6.1 a detailed review of the ESDU model is given.

Furthermore, no precise behavior for one single model can be read from Fig. 3.3 because they vary from measurement to measurement. What can be noticed is that the Ruscheweyh and the wake oscillator approaches have the smallest maximal discrepancy to the measured values and both rather underestimate the measured values.

---

[4]The wake oscillator and the AIJ approach do not depend on H/D and logically show no influence on any variation.
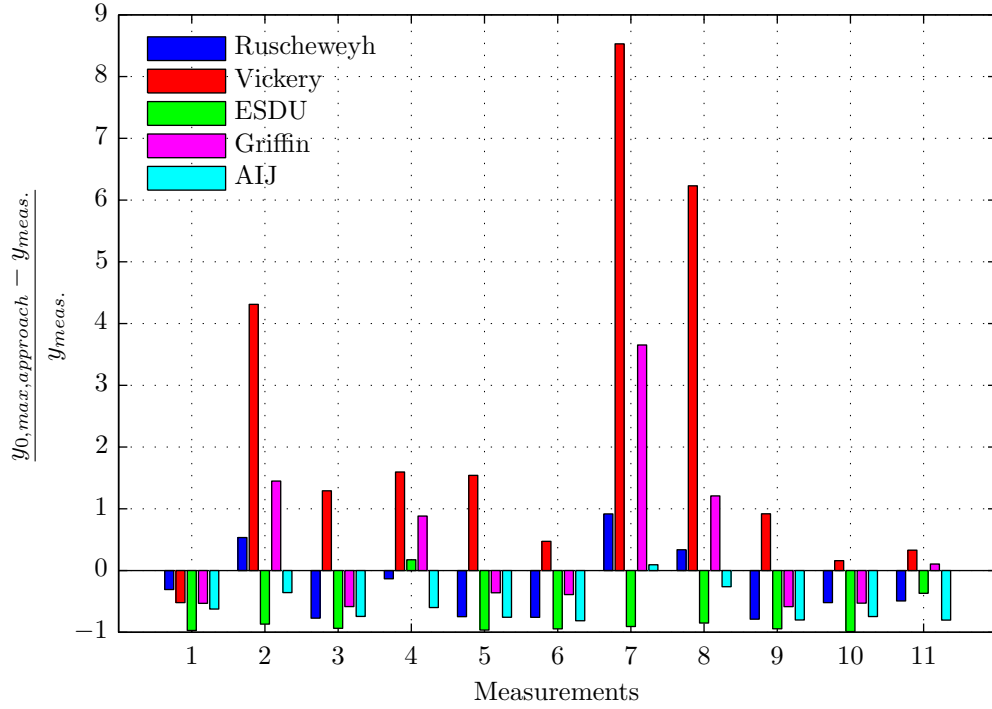
Figure 3.3 – Comparison of the computed values to the measured values: Computed values minus the measured values, all divided by the measured values.

With the help of model class selection, introduced in section 1.4, we try to obtain additional probabilistic information from the computation – measurement relations. Performing the model class selection we obtain the results shown in Tab. 3.2.

Maximum likelihood underlines in a quantitative form what can be observed in Fig. 3.3 – Ruscheweyh and the wake oscillator fit the measured data the best, Vickery and Basu fits them the worst, but generally overestimates the structural reaction values what improves the approach's overall quality. Additionally to this information we are finding the Ockham factor based on the Fisher matrix [Taylor and Kitching, 2010] and are considering every single model to be a parameter update in the context of evidence.

The Ockham factor based on the Fisher matrix does not only penalize the overparameterization, but also includes the bad fit to the data which can be clearly seen in the case of AIJ recommendations. Consequently, the Ockham factor for Vickery and Basu and ESDU are the lowest because of the determining parameters and the bad fit to the data. In case of the AIJ recommendations the bad fit to the data lowers the Ockham factor slightly.

Table 3.2 – Probabilities of different model classes comparing computed and measured data.

	Ruscheweyh	Vickery & Basu	ESDU	Wake Oscillator	AIJ
ln likelihood	-2.8765	-3.8650	-3.2226	-2.8221	-3.1236
ln Ockham	37.3123	34.9320	36.4987	37.0923	36.7972
ln evidence	34.4358	31.0669	33.2761	34.2702	33.6736
$p(\mathcal{D}|\mathcal{M}_j,\mathcal{U})$	0.3756	0.0129	0.1178	0.3183	0.1753

By basing the judgement on the prior plausibility $P(\mathcal{M}_j|\mathcal{U})$ of the model class for all models equal to 0.20, we obtain the evidence and the even more significant plausibility

of a single model class $P(\mathcal{M}_j|\mathcal{D},\mathcal{U})$. The plausibility of a single model class is 38% for Ruscheweyh, 1% for Vickery and Basu, 12% for ESDU, 32% for the Wake Oscillator and 18% for the AIJ recommendations. This shows Ruscheweyh to be the best, however arguments such as number of underestimations have to be taken into account still when evaluating the single models. In case of Vickery and Basu's approach this is especially important as it is the model with the best physical representation of vortex shedding phenomena. Taking this into account and increasing the prior model probability $P(\mathcal{M}_j|\mathcal{U})$ for the Vickery and Basu approach to 0.60 and reducing the other approaches to 0.10, leads to 35% for Ruscheweyh, 7% for Vickery and Basu, 11% for ESDU, 30% for the Wake Oscillator and 16% for the AIJ recommendations. Even when we underline the trust in the Vickery and Basu model, due to the bad fit of the data it is still the worst. This is a disadvantage of the model class selection scheme used in this form as it does not distinguish between overestimating and underestimating, anyhow the model class selection allows us to enrich our knowledge on the different models.

In order to improve the model selection analysis one main goal would be to increase the number of measured data and add information about the actual atmospheric stratification condition. E.g. by varying the turbulence intensity I_u imposed for the single measurements the result of the model class selection changes for the Vickery and Basu and ESDU approach significantly. Choosing an appearance probability $P = 0.95$ for the turbulence intensity I_u shows to create the most reasonable and realistic results for the model class selection. The second important point would be to introduce a penalty term for underestimating the measured results.

3.5 Model Response Analysis

With the help of model response analysis the behavior over selected parameter domains can be visualized and thus can easily be compared for the different vortex shedding models. Furthermore, some qualitative behavior on the sensitivity of the different determining parameters can be gained and this provides a good basis to check if the sensitivity analysis performed in chapter 5 is valid. For the three-dimensional representation introduced to fix the other dimensions in context of parameters the in Eq. (3.1) given values are used again. The model response surfaces are created for the following parameter combinations: Scruton number S_{cr} versus slenderness H/D, Scruton number S_{cr} versus ratio of critical velocity u/u_{crit} for different turbulence intensities I_u, Scruton number S_{cr} versus turbulence intensity I_u and ratio of critical velocity u/u_{crit} versus turbulence intensity I_u for different structural damping ratios ζ_s. Additionally, the measured values marked by a black dot, and computed values marked by a colored dot, for the chimneys given in Tab. 3.1 are included in the graphs. For the wake oscillator and the AIJ recommendations approaches no model response surface graphs were made as both can be studied sufficiently in the two-dimensional graph which is shown in Fig. 3.1.

3.5.1 Ruscheweyh

For the approach by Ruscheweyh we only have the Scruton number S_{cr} versus slenderness H/D model response surface plot, Fig. 3.4, as the structural slenderness H/D is the only independent parameter related to the Scruton number. Looking at Fig. 3.4 shows that when slenderness is decreased relatively, the correlation length and thus the force applied on the structure due to vortex shedding increase which yields a higher structural reaction $y_{0,max}/D$. This phenomenon is obviously very moderate and has generally no relevance.
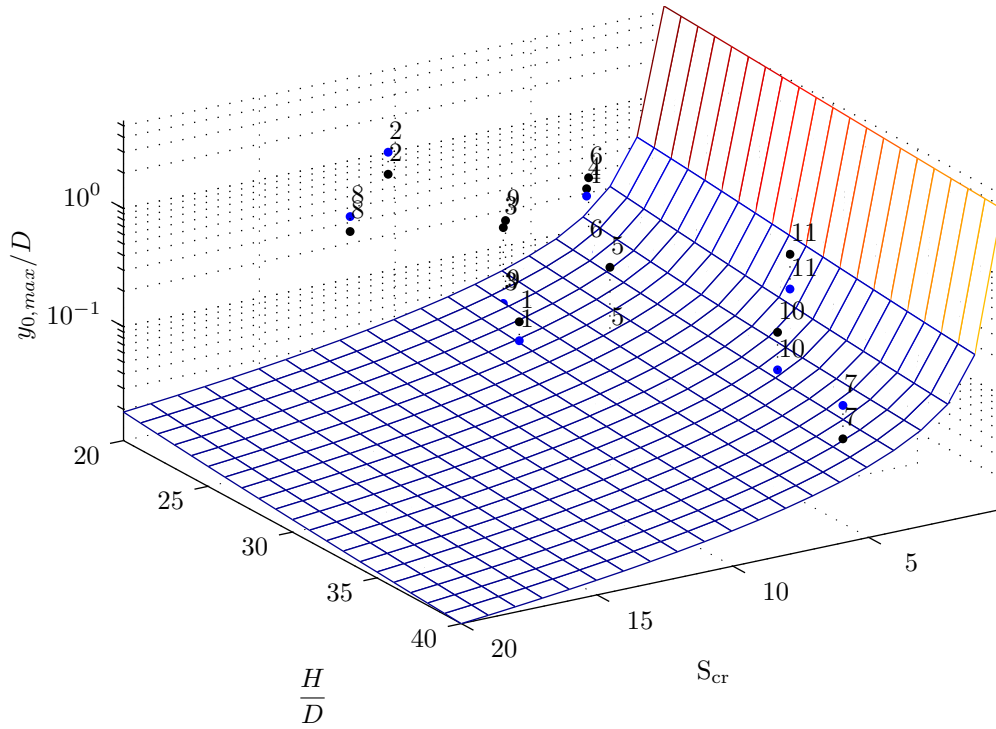
Figure 3.4 – Model response surface Ruscheweyh; Scruton number S_{cr} versus slenderness H/D showing $y_{0,max}/D$; other parameters fixed.
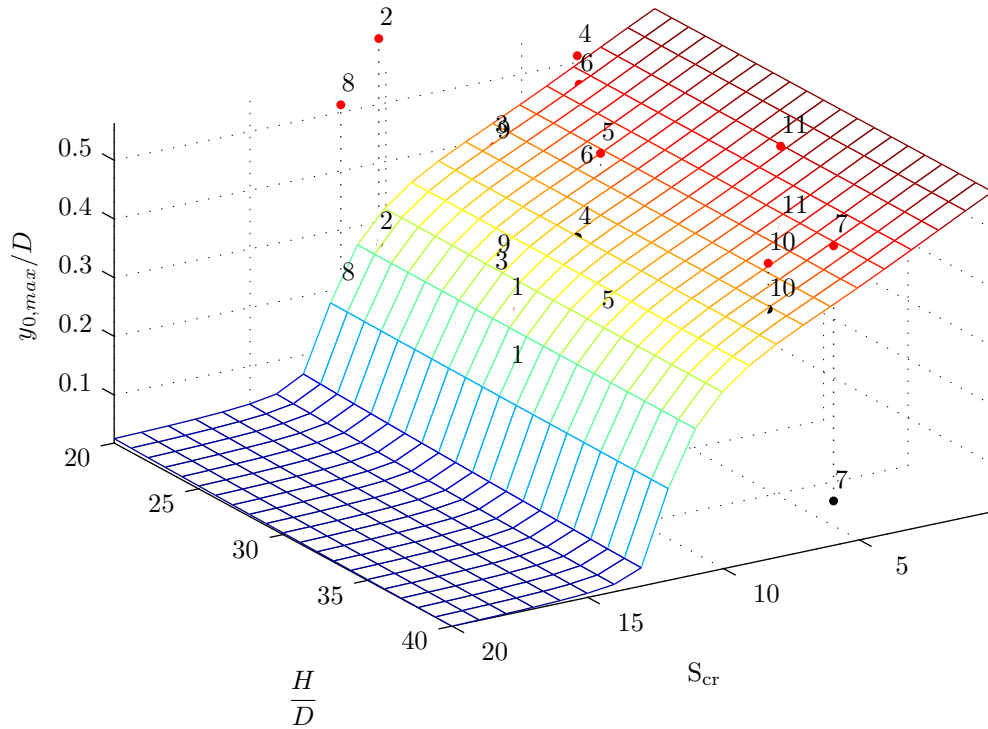
3.5.2   Vickery and Basu

Figure 3.5 – Model response surface Vickery and Basu; Scruton number S_{cr} versus slenderness H/D showing $y_{0,max}/D$; other parameters fixed.

Vickery and Basu is one of the more complex approaches studied here, so with the help of model response surfaces we are able to figuratively show how the model behaves in the
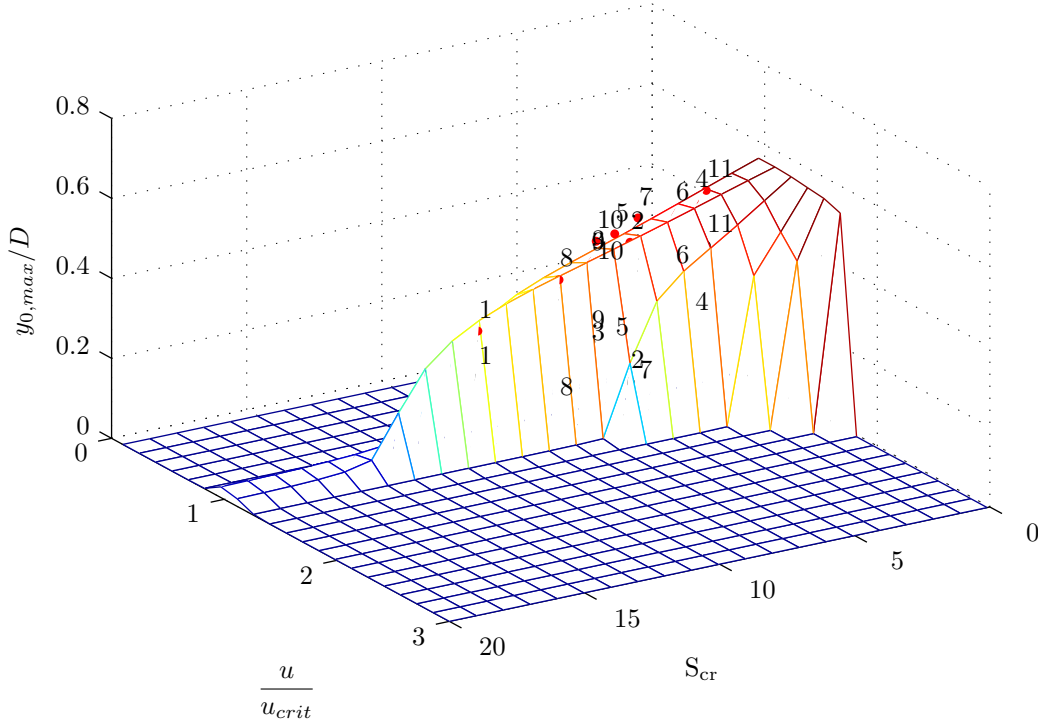
parameter domains.

Figure 3.6 – Model response surface Vickery and Basu; Scruton number S_{cr} versus ratio of critical velocity u/u_{crit} showing $y_{0,max}/D$; other parameters fixed and $I_u = 0.05$.
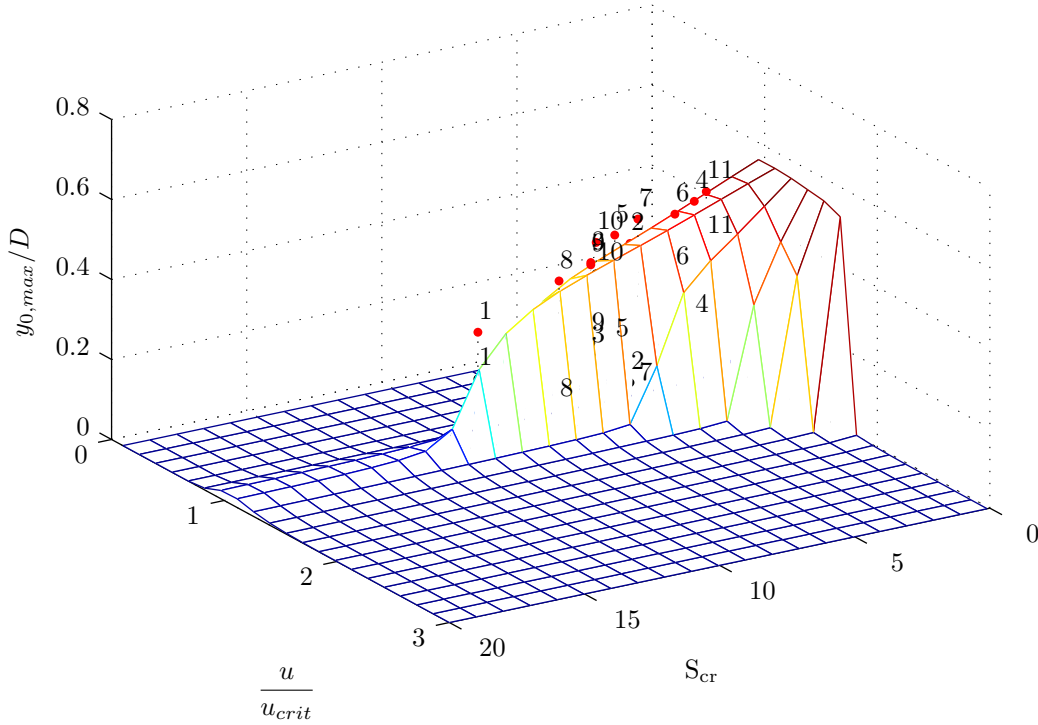

Figure 3.7 – Model response surface Vickery and Basu; Scruton number S_{cr} versus ratio of critical velocity u/u_{crit} showing $y_{0,max}/D$; other parameters fixed and $I_u = 0.1$.

We are starting again with the Scruton number S_{cr} versus slenderness H/D graph, Fig. 3.5, followed by the Scruton number S_{cr} versus ratio of critical velocity u/u_{crit} for

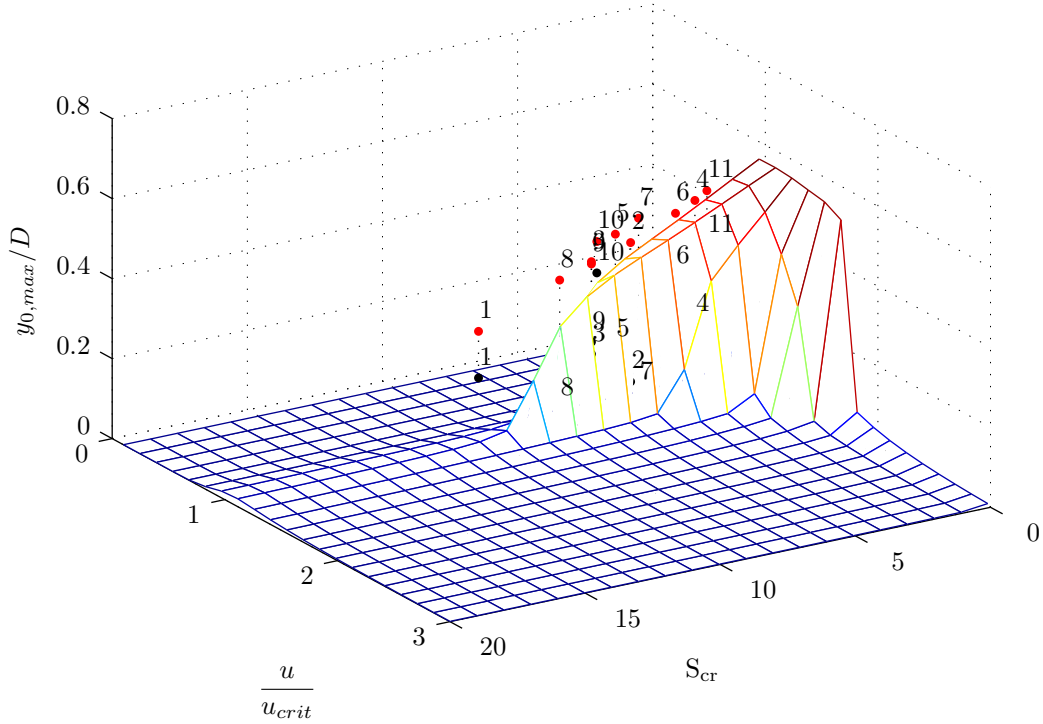different turbulence intensities; $I_u = 0.05$, Fig. 3.6, $I_u = 0.1$, Fig. 3.7, and $I_u = 0.15$, Fig. 3.8.

Figure 3.8 – Model response surface Vickery and Basu; Scruton number S_{cr} versus ratio of critical velocity u/u_{crit} showing $y_{0,max}/D$; other parameters fixed and $I_u = 0.15$.
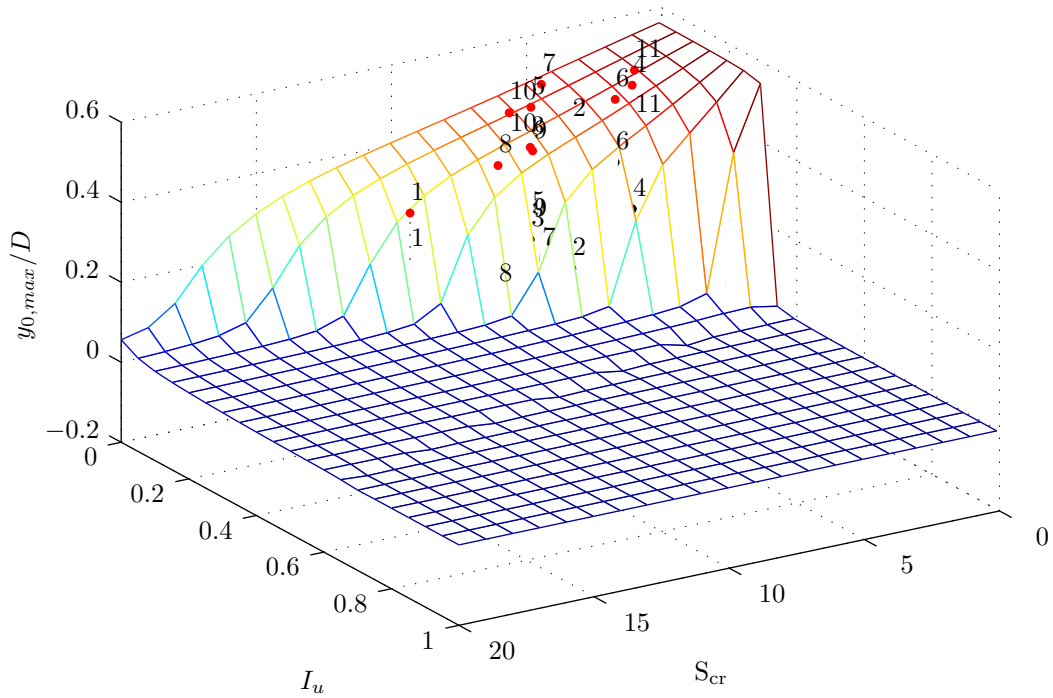

Figure 3.9 – Model response surface Vickery and Basu; Scruton number S_{cr} versus turbulence intensity I_u showing $y_{0,max}/D$; other parameters fixed.

Then the graph of Scruton number S_{cr} versus turbulence intensity I_u, Fig. 3.9, and the graphs ratio of critical velocity u/u_{crit} versus turbulence intensity I_u for different structural

damping ratios, $\zeta_s = 0.0021$, Fig. 3.10, $\zeta_s = 0.0042$, Fig. 3.11, and $\zeta_s = 0.0084$, Fig. 3.12, are shown.

As for the Ruscheweyh approach the slenderness H/D has a minor effect on the result, see Fig. 3.5; in the case of the Vickery and Basu approach it is even smaller than in the case of Ruscheweyh, based on the Reynolds number depending spanwise correlation parameter.

The three graphs of Scruton number S_{cr} versus ratio of critical velocity u/u_{crit}, Fig. 3.6, Fig. 3.7 and Fig. 3.8 have to be discussed together. What becomes imminently obvious is that for low structural damping ratios ζ_s the effect of vortex shedding is dominant in higher Scruton number ranges too. The surface being half cone-like shaped in low Scruton number ranges causes a cross-section parallel to the critical velocity ratio axis to have a big area. This area represents the energy induced in the system by vortex shedding which is especially critical for lightly damped structures and even worse if the structure additionally suffers from fatigue.

In Fig. 3.9 the important effect of the turbulence intensity I_u becomes obvious, especially in weakly damped structures; absence of turbulence can lead to extreme responses.

Fig. 3.10, Fig. 3.11 and Fig. 3.12 form an entity and show which important impact the turbulence intensity I_u has on the result. For a low structural damping ratio ζ_s, Fig. 3.10, the response is not only quite big but also in a fairly large range of u/u_{crit}; increasing the damping ratio nearly extincts these effect, Fig. 3.12. Remember that these low values for the turbulence intensity I_u appear only in stable stratification conditions.

The effect on the vertex for a high ratio of critical velocity u/u_{crit} and for high values for the turbulence intensity I_u, as seen in Fig. 3.10, Fig. 3.11 and Fig. 3.12, is based on two effects: one is high velocities imply high energy in the fluid flow and second high turbulence intensities I_u which would cause buffeting are covered by the influence of the bandwidth function $\phi(B, k)$, Eq. (2.5.1), see [Vickery and Basu, 1983c].
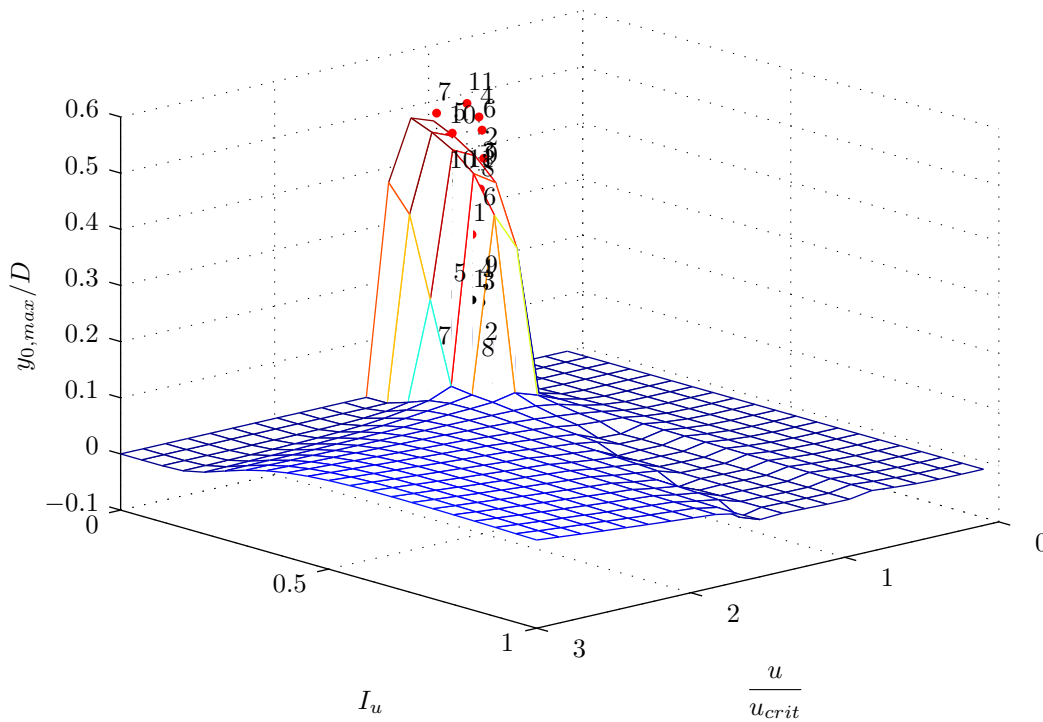

Figure 3.10 – Model response surface Vickery and Basu; ratio critical velocity u/u_{crit} versus turbulence intensity I_u showing $y_{0,max}/D$; other parameters fixed and $\zeta_s = 0.0021$.

Figure 3.11 – Model response surface Vickery and Basu; ratio critical velocity u/u_{crit} versus turbulence intensity I_u showing $y_{0,max}/D$; other parameters fixed and $\zeta_s = 0.0042$.

Figure 3.12 – Model response surface Vickery and Basu; ratio critical velocity u/u_{crit} versus turbulence intensity I_u showing $y_{0,max}/D$; other parameters fixed and $\zeta_s = 0.0084$.
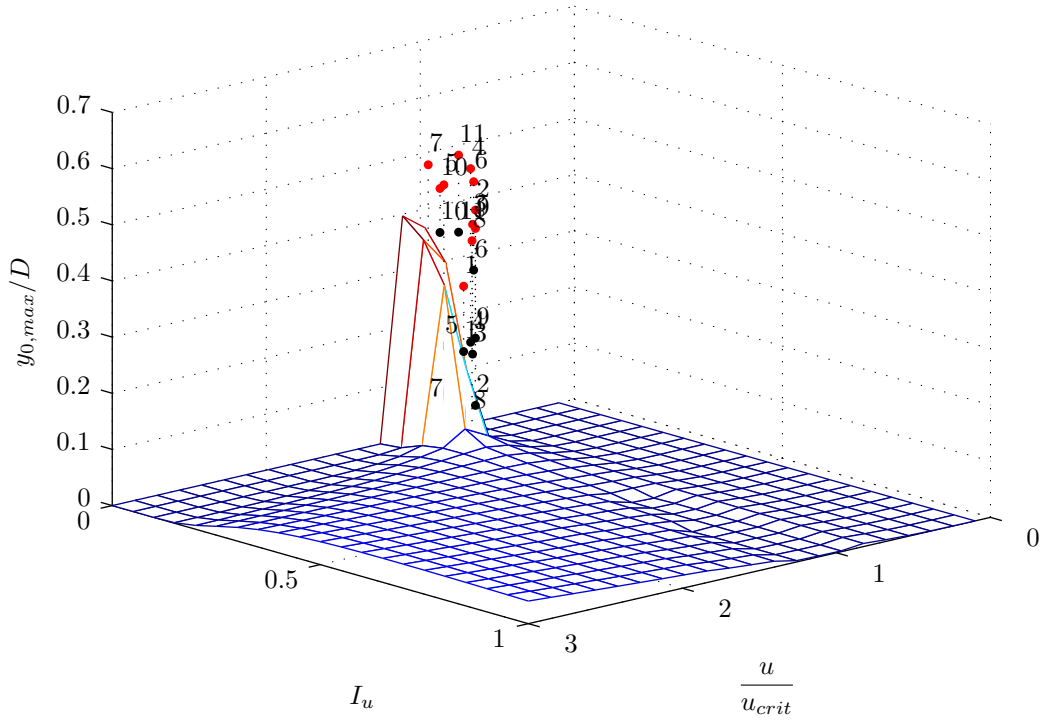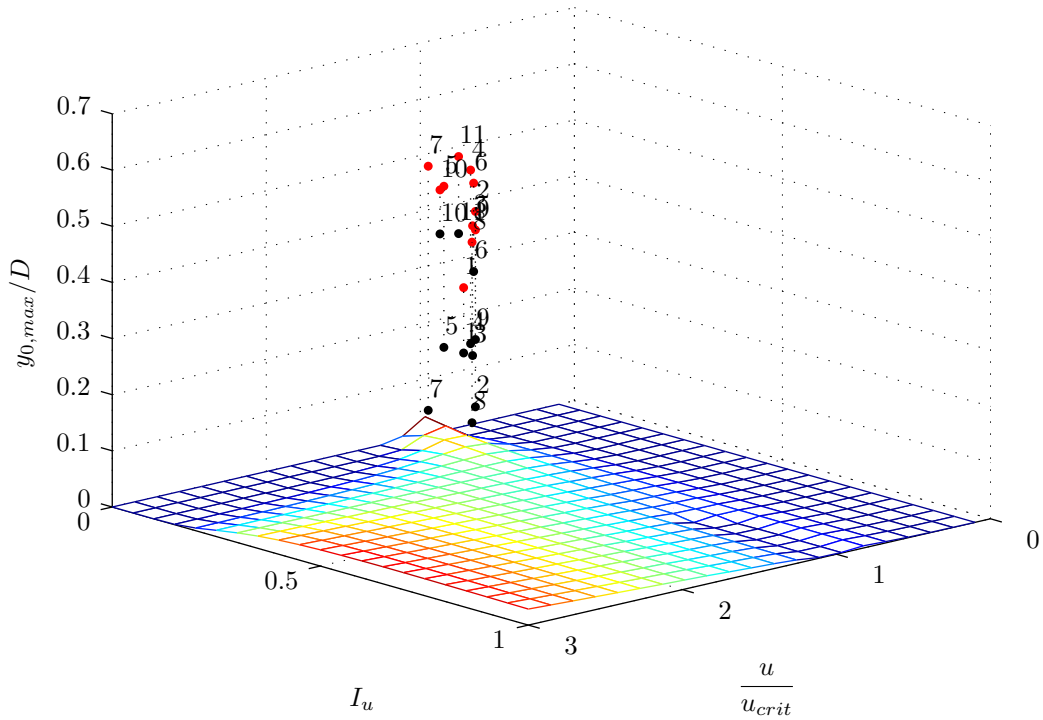
Summing up, the content of the model response surface graphs, the physically expected behavior of vortex shedding, seems to be well represented. Furthermore, the sensitive impact of the turbulence intensity I_u is proven and underlined by the model response surface graphs.

3.5.3 ESDU

As mention in [ESDU96030, 1996], one main disadvantage is the numerical instability in the narrow band response region, remember section 2.6.2. Unfortunately this effect becomes visible and distorts the surface partly to become meaningless. The same model response surfaces as for the Vickery and Basu approach, see section 3.5.2, are represented and thus a direct comparison of these two advanced vortex shedding models is feasible, see the review of the ESDU approach in section 3.6.1 for detailed explanations too.

What is obvious, since the ESDU approach is based on the work done by Vickery and Basu, is that the model response surfaces are very similar except for the inclusion of the buffeting effect in the ESDU approach. This buffeting is caused by the lateral component of the turbulence and thus with the increase of turbulence intensity I_u the effect of buffeting increases as well. In case of the ESDU approach the buffeting effect dominates the effect of vortex shedding under stable atmospheric stratification conditions, see Fig. 3.18, Fig. 3.19 and Fig. 3.20.
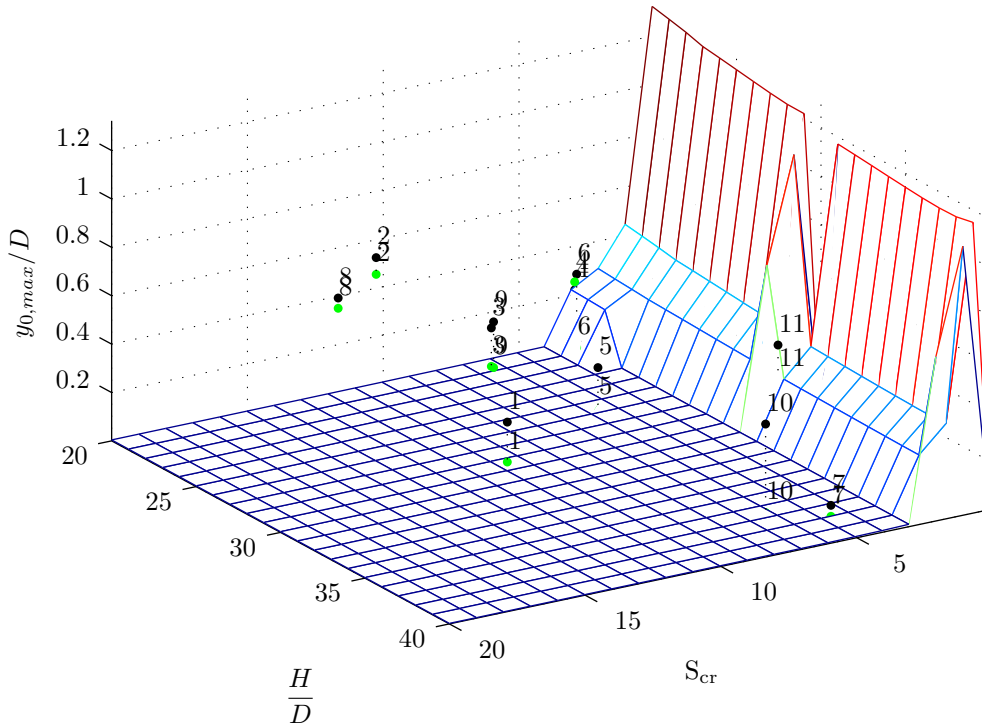

Figure 3.13 – Model response surface ESDU; Scruton number S_{cr} versus slenderness H/D showing $y_{0,max}/D$; other parameters fixed.

For the slenderness behavior the same observations as for Ruscheweyh and Vickery and Basu can be made for ESDU, Fig. 3.13, where the slenderness of the structure has nearly no influence on the outcome. The gap in Fig. 3.13 is caused by the mentioned numerical instabilities.

The set of Fig. 3.14, Fig. 3.15 and Fig. 3.16 show the same half cone-like shape as Vickery and Basu does. The valleys we can see in these graphs, are not caused by the numerical instabilities – only the bottom values are affected – but are formed by the combination of the vortex shedding spectrum with the buffeting due to the lateral component of the turbulence spectrum. Furthermore, the same effect of increasing the half cone as for Vickery and Basu, is observed for small structural damping ratios ζ_s.
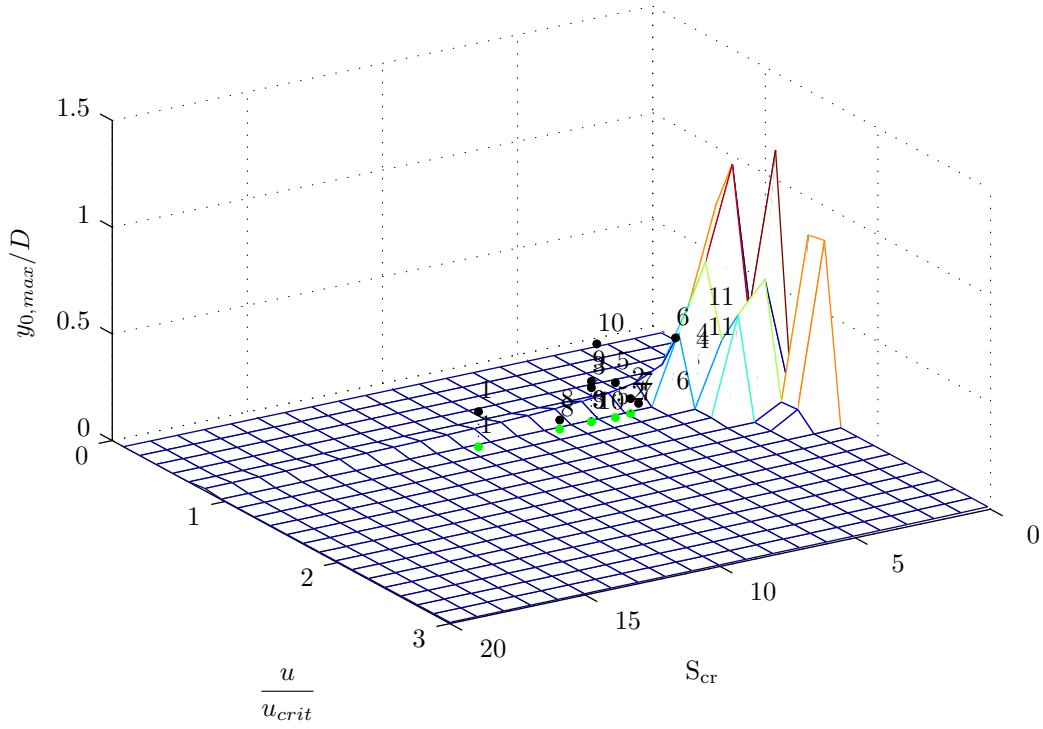
Figure 3.14 – Model response surface ESDU; Scruton number S_{cr} versus ratio of critical velocity u/u_{crit} showing $y_{0,max}/D$; other parameters fixed and $I_u = 0.05$.

Figure 3.15 – Model response surface ESDU; Scruton number S_{cr} versus ratio of critical velocity u/u_{crit} showing $y_{0,max}/D$; other parameters fixed and $I_u = 0.1$.

The model response surface S_{cr} versus the turbulence intensity I_u indeed is very interesting and confounding, see Fig. 3.17. The step in the graph is caused by the separation into broad band and narrow band region, this becomes clear when remembering Fig. 3.1. Looking at Eq. (2.53) we see that for the narrow band response only the spectral density

of $\tilde{C}_{L0}$ integrated over the length scale of vortex shedding and the slenderness H/D of the structure are influencing the response. Comparing Eq. (2.53) with the Ruscheweyh approach underlines the similarities which can also be seen in the graphs, see Fig. 3.1 and related text.

Figure 3.16 – Model response surface ESDU; Scruton number S_{cr} versus ratio of critical velocity u/u_{crit} showing $y_{0,max}/D$; other parameters fixed and $I_u = 0.15$.
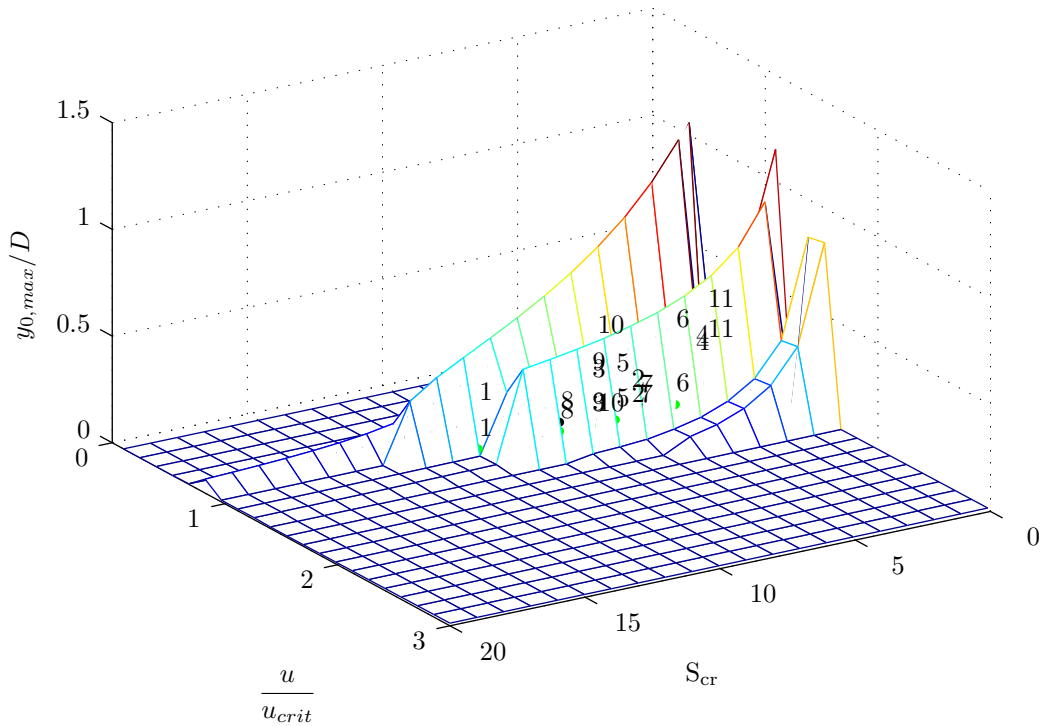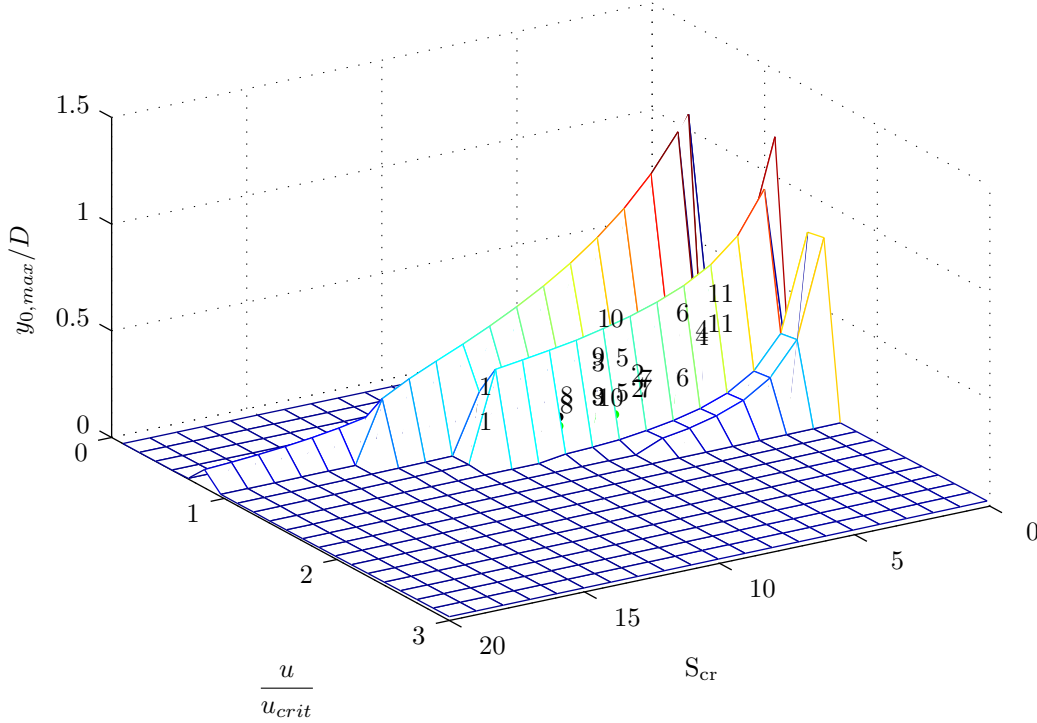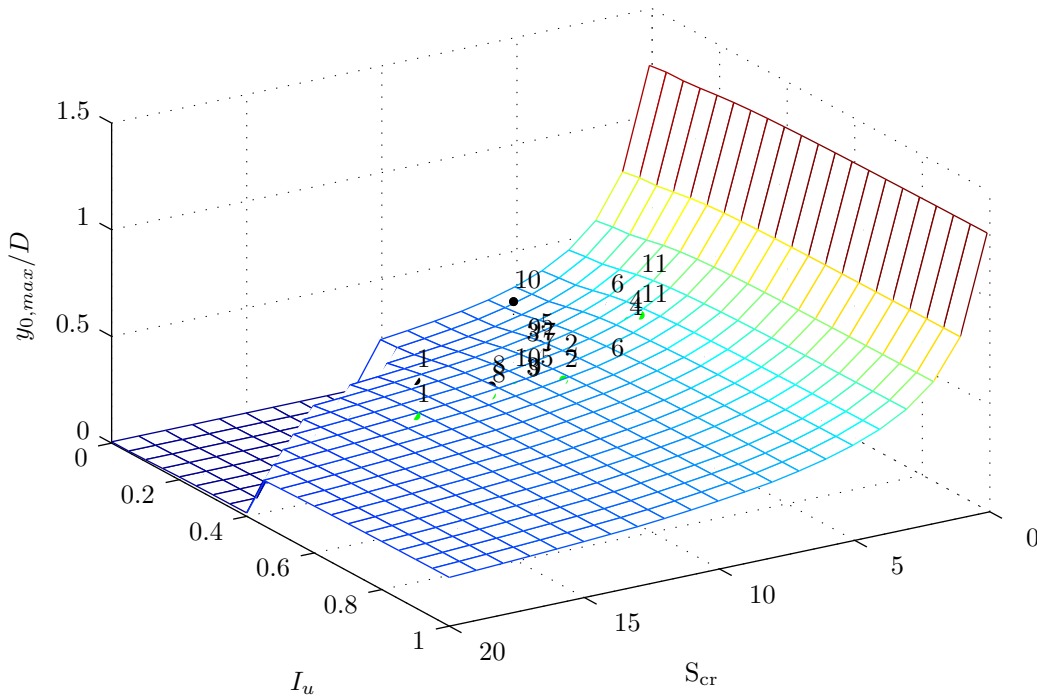

Figure 3.17 – Model response surface ESDU; Scruton number S_{cr} versus turbulence intensity I_u showing $y_{0,max}/D$; other parameters fixed.

Figure 3.18 – Model response surface ESDU; ratio critical velocity u/u_{crit} versus turbulence intensity I_u showing $y_{0,max}/D$; other parameters fixed and $\zeta_s = 0.0021$.
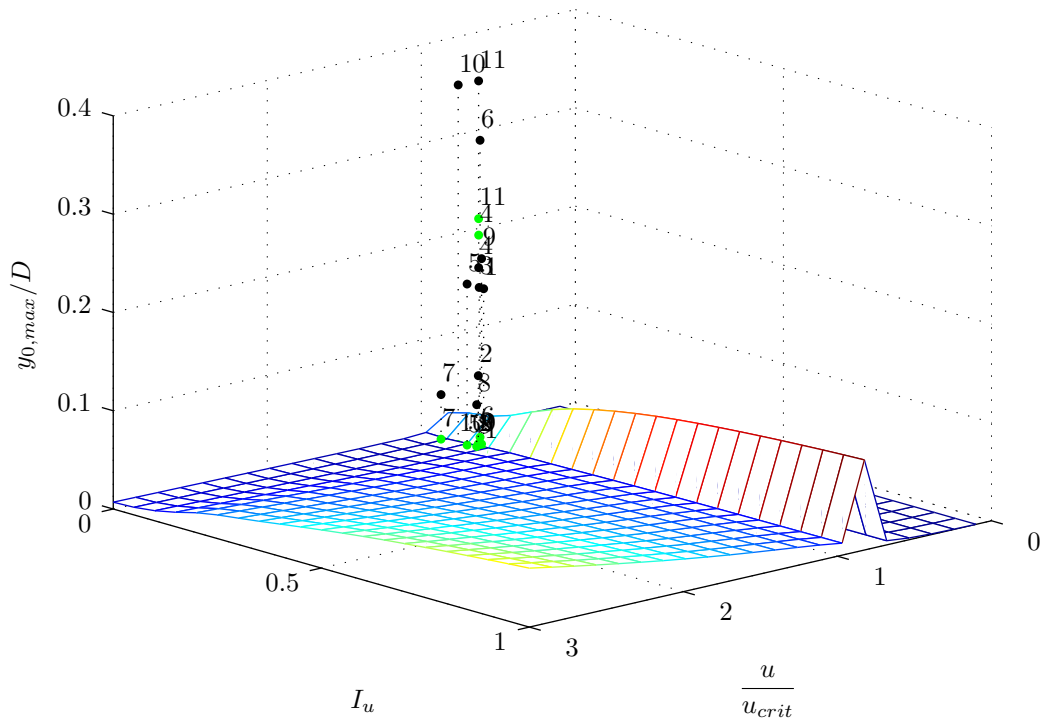
Figure 3.19 – Model response surface ESDU; ratio critical velocity u/u_{crit} versus turbulence intensity I_u showing $y_{0,max}/D$; other parameters fixed and $\zeta_s = 0.0042$.

To understand Fig. 3.18, Fig. 3.19 and Fig. 3.20 some further considerations have to be made. Remembering the equivalent graphs for Vickery and Basu and comparing them to the ones from the ESDU approach shows two main differences to appear: firstly, for Vickery and Basu the low turbulence intensities I_u gave a higher structural response

and secondly for high turbulence intensity values nearly no structural reaction can be observed. For ESDU this is different due to the included buffeting term. The bandwidth parameter used in ESDU is similar to the on in Vickery and Basu but is directly related to the spectral density $\tilde{C}_{L0}$. Integrating the spectral density of $\tilde{C}_{L0}$ over the length scale of vortex shedding and adding up the resulting spectrum with the integrated spectrum due to lateral buffeting results in the buffeting part to be dominant for high turbulence intensities I_u. Here a preview to chapter 5 can be given such that when performing the sensitivity analysis for the ESDU approach the turbulence intensity I_u will have a smaller influence on the result in case $u/u_{crit} = 1.0$ than for the Vickery and Basu approach.
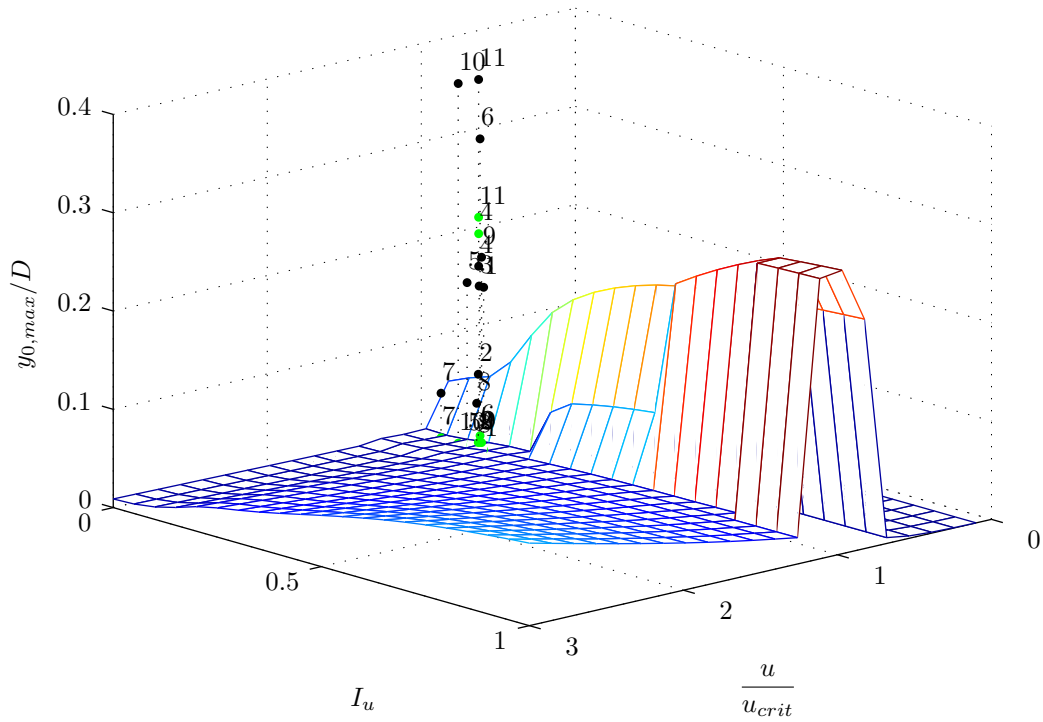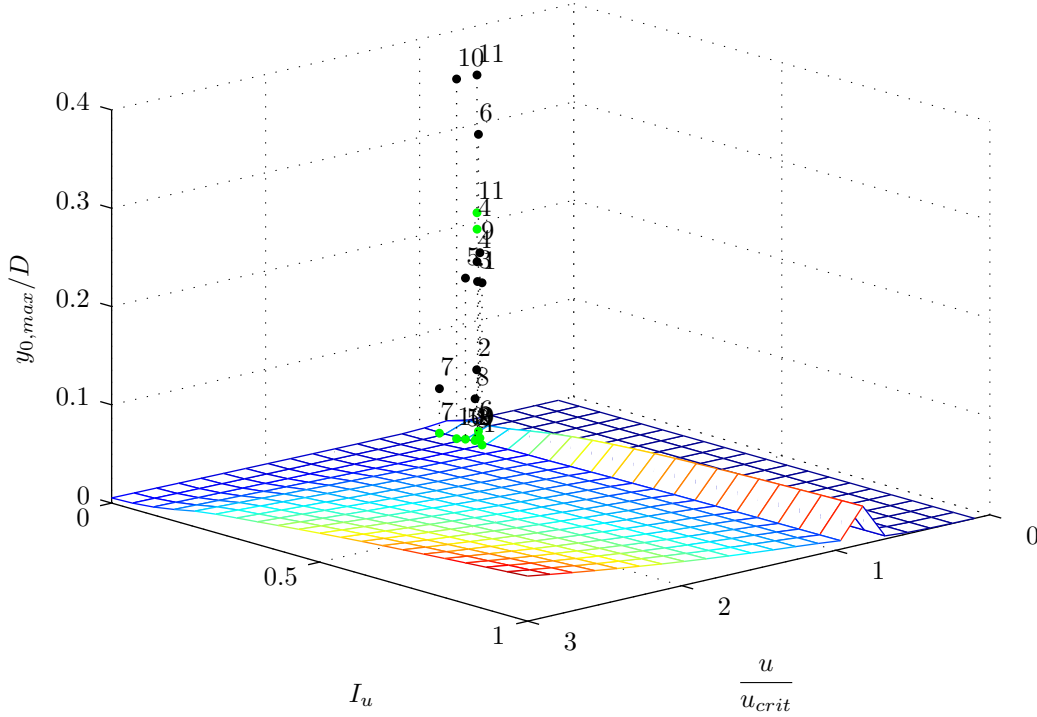

Figure 3.20 – Model response surface ESDU; ratio critical velocity u/u_{crit} versus turbulence intensity I_u showing $y_{0,max}/D$; other parameters fixed and $\zeta_s = 0.0084$.

3.6   Conclusion

Analyzing the behavior of the different models in the damping ratio domain gives us a first impression of how the different models work and by finding limit ranges a certain comparison between them can be done. With the help of model class selection the approaches could be tested on the measured data and the plausibility of a single model class gave an additional information how the models work in terms of measured reality. The response surfaces concluded the analysis of the approaches in a sophisticated manner and allowed us to see the response $y_{0,max}/D$ in different sub parameter spaces and thus gave the possibility to analyze parameter influences right away. Summing up, all observations made in this chapter allow us to identify the Vickery and Basu model to be the physically most meaningful approach regardless of Vickery and Basu being the worst in representing the measured data. Ruscheweyh and the AIJ Recommendations for Loads on Buildings are both acceptable in physical and phenological representation in high Scruton number S_{cr} ranges, but can only give evidence for structures at critical velocity ratio $u/u_{crit} = 1.0$ and with no influence of the turbulence intensity I_u. The Griffin model has – as has

already been mentioned – a physically very reasonable base, but the solution function has to be improved in order to obtain a valuable model.

3.6.1   Review of the ESDU Approach

Summing up the observations made in chapter 3 and especially in section 3.5 leads to the need of reviewing the ESDU approach in more detail with an accurate study of the describing equations. This review will be broken down into three points: the first will be a general criticism, the second a more accurate study of how ESDU represents the measured data, see section 3.4, and the third an analysis where these differences are caused in the formulas and general assumptions underlying the approach.

General criticism

- When carefully studying the document [ESDU96030, 1996] errors in the formulas can be found.[5]

- A more ideological criticism is why the ESDU approach considers the phenomenon non-linearity with a non-linear lift term $\tilde{C}_{L_j}$. Finding the solution with a non-linear lift term $\tilde{C}_{L_j}$ does not only imply making a quite complicated iteration, but as mentioned in [ESDU96030, 1996] too, gives very sensitive results for intermediate values.[6] Using a non-linear aerodynamic damping term as done in the Vickery and Basu approach allows to find an analytical solution to the problem.

- To reduce the input parameters for the ESDU approach to the dimensionless quantities found in section 2.2 provides some difficulties and a clear separation was not possible. The different terms themselves respect all criteria of being dimensionless, however it still seems strange as this could be achieved for all other approaches. In this context a second point has to be mentioned: many formulas used have strange constants in them, like the formulas for the lock-in region p. 74-75 in [ESDU96030, 1996]. This can be justified by representing the reality as best as possible but raises the doubt if the data became over-fitted.

- Maybe a less serious point is the comparison of the ESDU approach with experimental results, shown on p. 27-31 in [ESDU96030, 1996]. Especially the experimental results shown on p. 27-28 remind one more of the Vickery and Basu approach results.[7]

- A slightly curious fact is that the broad band response includes a vortex shedding spectrum, see p. 44-46 in [ESDU96030, 1996] and the narrow band response uses a non-linear term $\tilde{C}_{L_j}$ to cover the vortex shedding.[8]

---

[5]E.g. in [ESDU96030, 1996] *Eq. (5.7)* the modal mass m_j as divisor is missing; *Eq.(B4.6)* is missing a square over B_e in the exponential expression and following the text a square is missing in the expression of B_e over I_u

[6]The explanations made on p. 17-18 in [ESDU96030, 1996] describe the problem well, but do not directly mention that the iteration result is influenced by the structural damping ratio ζ_s which is a very uncertain parameter and in the code provided the iteration is only done with the narrow band solution η_N and not with the total response η as requested.

[7]Here of course just a conjecture can be made as a very detailed study on the experimental results has to be done in relation to the ESDU approach.

[8]This is clear from a conceptual point of view as the ESDU approach separates the narrow band and broad band part strictly – the broad band part based on the Vickery and Basu approach and the

    – Comparing the Visual Basic code provided in [ESDU96031, 2000] with the documentation [ESDU96030, 1996] some differences can be found between the constants given in the documentation and the program itself.[9]

Representation of measured data

In order to underline this criticism we study the results obtained in section 3.4 more closely. In Tab. 3.3 the parameters and the measured values for the different erected chimneys are represented. Looking at the results obtained by the ESDU approach we see that for nine out of eleven we get a too small result. Especially interesting is that comparing the obtained values with each other the results seem to be adequate as for higher Scruton number we obtain lower reaction values $y_{0,max}/D$. The cases of chimneys number 4, 6 and 11 are especially interesting as the chimneys 4 and 11 give a response in the narrow band region and thus are quite close to the measured result, the solution for chimney 6, however, is computed in the broad band region and thus is far too small compared to the measured value. To understand this we will have to analyses the formulas step by step which is done in the next point.

Table 3.3 – Parameters and measured values for erected chimneys associated with section 3.1 and results obtained by the ESDU approach.

No.	D	H/D	n_j	ζ_s	m	S_{cr}	I_u	$\dfrac{y_{0,max}}{D}_{meas.}$	$\dfrac{y_{0,max}}{D}_{ESDU}$
1	0.60	28.33	2.00	0.004	95	10.61	0.150	0.17	0.00
2	3.30	11.52	1.58	0.005	1080	4.99	0.140	0.08	0.01
3	1.50	20.67	1.60	0.006	240	6.43	0.139	0.17	0.01
4	1.80	19.44	1.51	0.003	280	2.61	0.138	0.19	0.22
5	1.80	25.56	0.87	0.004	447	5.55	0.110	0.17	0.01
6	1.40	20.71	1.71	0.003	216	3.32	0.141	0.32	0.02
7	1.58	37.97	0.50	0.005	233	4.69	0.047	0.05	0.00
8	3.04	13.49	1.15	0.006	1166	7.61	0.133	0.05	0.01
9	1.25	20.80	1.88	0.005	200	6.43	0.145	0.20	0.01
10	0.82	36.59	1.06	0.003	139	6.23	0.089	0.37	0.00
11	0.91	30.77	1.72	0.002	89	2.16	0.138	0.38	0.24

Generally, the observations made on the results in Tab. 3.3 underline the sensitivity of the ESDU approach not only on the single parameters of the chimneys but additionally of the relations and constellation between the different parameters.

Formula analysis

As the ESDU approach is based on the Vickery and Basu approach as our first step we are trying to compare the basic formulas of both approaches. Comparing the ESDU formula on the left side in Eq. (3.12) with the Vickery and Basu formula on the right side in the case of a broad band response[10] – generally proper designed structures should not enter

---

non-linearity in the narrow band part is covered by $\tilde{C}_{L_j}$ – but seems a bit inconsistent.

   [9]E.g. in *Eq. (B5.10)* instead of $1.1 \rightarrow 1.65$, instead of $0.08 \rightarrow 0.63$ and instead of the power $1.9 \rightarrow 2$; in *Eq. (B5.11)* instead of $0.03 \rightarrow 0.1$; the reason is nowhere given. Furthermore, the code includes some mistakes which could cause the program to compute futile results.

   [10]In the case of a narrow band response the formulas are not comparable at all.

the narrow band region –

$$\frac{\dfrac{\sqrt{n_j S_{C_F}}}{16\pi^{\frac{3}{2}} \mathrm{St}^2}\dfrac{\rho D^2}{m}}{\dfrac{1}{H}\displaystyle\int_H \phi_j^2 \, \mathrm{d}z \sqrt{\zeta_s + \zeta_{aero}}} \leftrightarrow \frac{\dfrac{c_l \phi_j(H)}{8\pi^2 \mathrm{St}^2}\dfrac{\rho D^2}{m}\sqrt{\dfrac{\sqrt{\pi} l}{2\frac{H}{D}}}\phi(B,k)}{\left[\dfrac{1}{H}\displaystyle\int_H \phi_j^2 \, \mathrm{d}z\right]^{\frac{1}{2}}\sqrt{\zeta_s - \zeta_a}} \tag{3.12}$$

we see that both approaches have similarities in the main parameters but a clear determination cannot be done. Even when dividing the terms further and further we end with a term being a combination of the vortex shedding spectrum and the correlation length which are differently defined in the approaches and thus are not directly comparable. Therefore, we start expressing the aerodynamic damping ratio[11] ζ_a and ζ_{aero} and define the mixed spectral and correlation length parameters,

$$par_{ESDU} = \frac{\dfrac{\sqrt{n_j S_{C_F}}}{16\pi^{\frac{3}{2}}}}{\dfrac{1}{H}\displaystyle\int_H \phi_j^2 \, \mathrm{d}z} \quad \text{and} \quad par_{Vickery} = \frac{\dfrac{c_l \phi_j(H)}{8\pi^2}\sqrt{\dfrac{\sqrt{\pi} l}{2\frac{H}{D}}}\phi(B,k)}{\left[\dfrac{1}{H}\displaystyle\int_H \phi_j^2 \, \mathrm{d}z\right]^{\frac{1}{2}}}. \tag{3.13}$$

In order to understand the aerodynamic damping parameters and the mixed spectral correlation length terms properly, numerical values are inevitable.
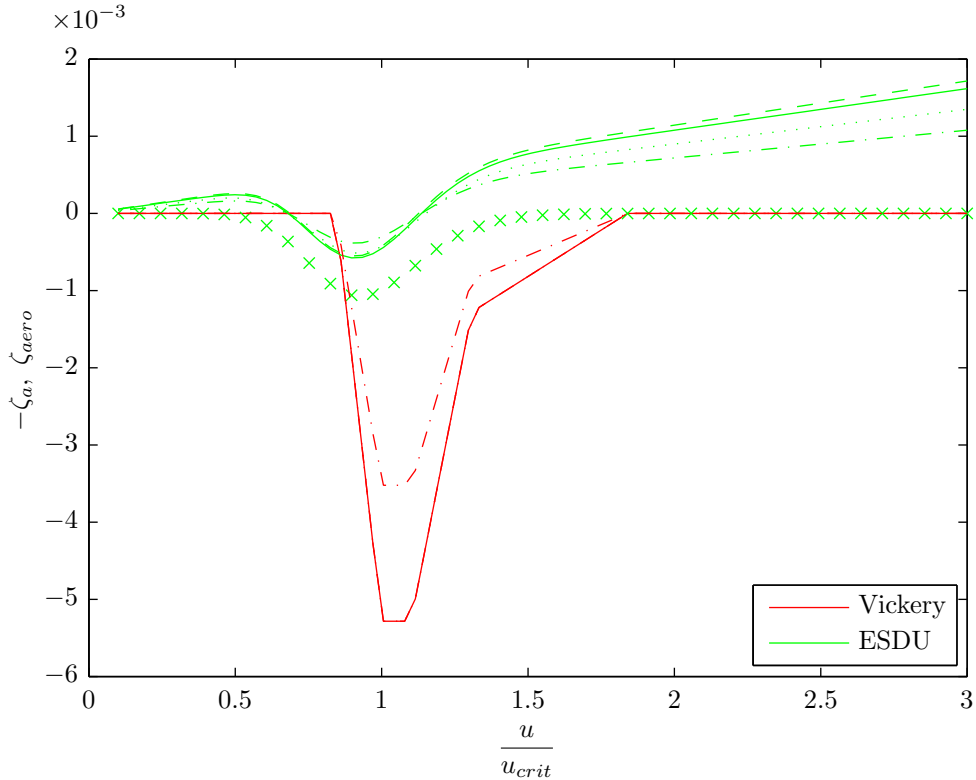
Figure 3.21 – Aerodynamic damping ratios $-\zeta_a$ for Vickery and Basu and ζ_{aero} for the ESDU approach as functions of the critical velocity ratio u/u_{crit}. Crosses represent the ESDU approach without buffeting term; dotted line represents $n_j D^2/\nu \cdot 0.5$; dashed line represents $n_j D^2/\nu \cdot 1.5$; dash-dot line represents $m/\rho/D^2 \cdot 1.5$.

---

[11]N.B. that in the Vickery and Basu approach ζ_a is defined positive; in order to compare both approaches we have to use $-\zeta_a$.

Again, the values shown in Eq. (3.1) are used to create the numerical values which are represented in Fig. 3.21 and Fig. 3.22. Here immediately the great difference in shape and value of the two approaches becomes visible.

Taking a closer look at Fig. 3.21 and comparing the aerodynamic damping parameter $-\zeta_a$ from Vickery and Basu with ζ_{aero} from the ESDU approach without buffeting, marked by crosses, shows two main differences: one is the left shift along the u/u_{crit} axis of the ESDU approach, which has to be criticized for the reason that the vortex shedding phenomena maxima can be physically observed around $1.0 \leq u/u_{crit} \leq 1.1$, [Vickery and Clark, 1972] and [Vickery and Basu, 1983c]. Secondly the positive contribution to the structure damping ratio ζ_s through a positive aerodynamic damping ratio seems to be exaggerated by the buffeting term in the ESDU approach; clearly the total neglect as done in the Vickery and Basu approach is conservative, but derives from the basic assumption of not considering buffeting. The mixed spectral and correlation length parameters $par_{Vickery}$
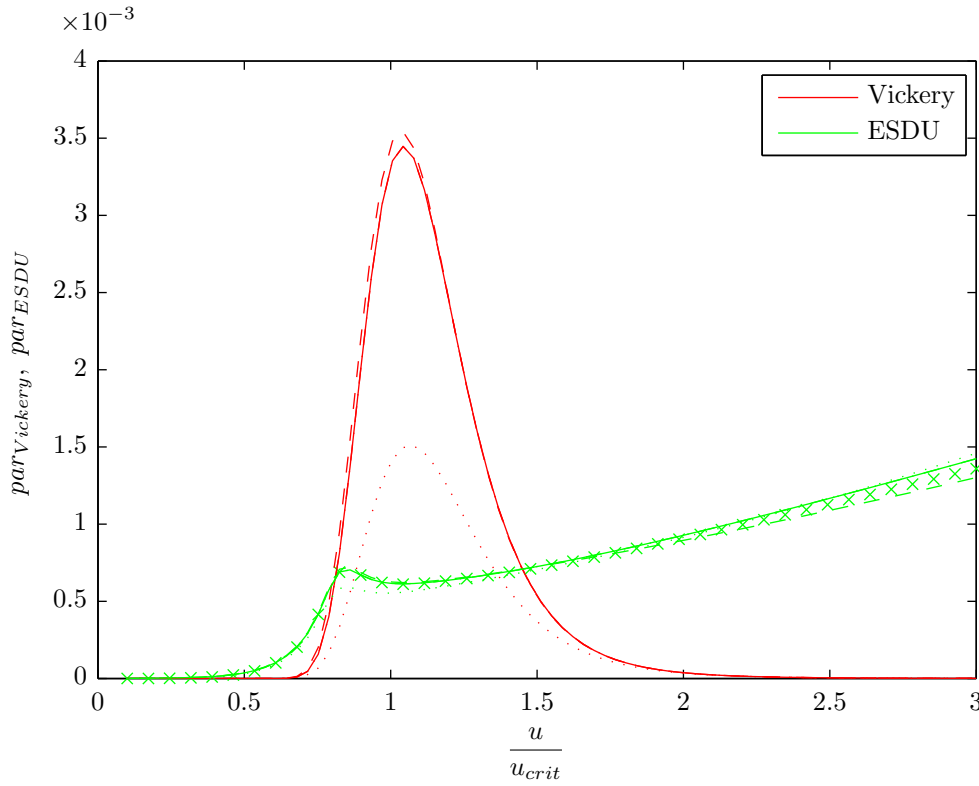

Figure 3.22 – Mixed spectral and correlation length parameter $par_{Vickery}$ and par_{ESDU} as functions of the critical velocity ratio u/u_{crit}. Crosses represent the ESDU approach without buffeting term; dotted line represents $n_j D^2/\nu \cdot 0.5$; dashed line represents $n_j D^2/\nu \cdot 1.5$; dash-dot line represents $m/\rho/D^2 \cdot 1.5$.

and par_{ESDU} in Fig. 3.22 show a similar behavior to the aerodynamic damping ratios: we have a left shift of the parameters where the same criticism as above applies. As in the ESDU approach the spectral part of buffeting is considered as an overall structural buffeting term; the effect of buffeting is very small and only noticeable in the high velocity range.

Studying the size of the numerical values shows differences in varying order of magnitude. In this case the aerodynamic damping ratios at the critical velocity $u/u_{crit} = 1.0$ are for Vickery and Basu $\zeta_a = -0.00528$ and for ESDU $\zeta_{aero} = -0.00044$, the mixed spectral and correlation length parameters are $par_{Vickery} = 0.00335$ and $par_{ESDU} = 0.00062$. As the influence of the aerodynamic damping ratio is foremost in reducing the structural

damping ratio ζ_s this leads to the inequality

$$\frac{1}{\sqrt{\zeta_s + \zeta_{aero}}} \leq \frac{1}{\sqrt{\zeta_s - \zeta_a}} \quad \text{as} \quad \zeta_s \geq \zeta_{aero} \geq -\zeta_a \quad \text{and} \quad \zeta_s \leq 1.0. \qquad (3.14)$$

Multiplying the result with an again smaller mixed spectral and correlation parameter increases the differences in the approaches too. Even if we would compute the structural reaction for the ESDU approach at a lower critical velocity ratio $u/u_{crit} \leq 1.0$, the maximum for the structural damping ratio ζ_{aero} and the mixed spectral and correlation term par_{ESDU} would still be a smaller value due to the small size of the aerodynamic damping ratio ζ_{aero}; whether with or without buffeting term does not matter at all. This leads to the conclusion that once a structure drops out the narrow band response solution region ESDU provides far too small responses. In case the solution is found in the narrow band domain the values are considerably good, see chimney 4 and 11 in Tab. 3.3.

Finally some comments on Fig. 3.21 and Fig. 3.22 related to the changes to the dimensionless quantities $n_j D^2/\nu$ and $m/\rho/D^2$ should be made. In Fig. 3.21 we see that changing $n_j D^2/\nu$ has no influence on the aerodynamic damping ration ζ_a for the Vickery and Basu approach, but changes in $m/\rho/D^2$ are directly visible which is obvious when looking at how ζ_a is defined in Eq. (2.32). A similar behavior can be seen for the ESDU approach where only in the high critical velocity ratios u/u_{crit} distinctive differences for different $n_j D^2/\nu$ values can be observed. Moving to Fig. 3.22, as a consequence from Eq. (3.13) we see no effect of changing $m/\rho/D^2$ as it does not appear, instead changes to $n_j D^2/\nu$ are well visible. This shows how well separated the different parameters or dimensionless quantities are in the Vickery and Basu approach. ESDU again shows for both $n_j D^2/\nu$ and $m/\rho/D^2$ differences due to changes in the parameters, see Fig. 3.22, but again only at high critical velocity ratio values.

Chapter 4

Parameters

On the following pages a composition of all parameters and their distribution is presented; these are needed in order to create populations of data to perform the sensitivity analysis and to use them further in the probabilistic models.

As in section 1.3 requested we need a population of size N of parameters in order to establish a sensitivity analysis. We will create these populations by taking random samples based on the different distributions for the various determining parameters, which lead us to obtain for every base sample a vector and thus N vectors $\mathbf{X}_1, \ldots, \mathbf{X}_N$,

$$\mathbf{X}_1, \ldots, \mathbf{X}_N = [D, H/D, \rho_{steel}, n_{j_{dis}}, \zeta_s, \rho, \nu, I_u, \mathrm{St}_{dis}, c_{dis}, K_{a,max_{dis}}]^T. \tag{4.1}$$

The sensitivity analysis will be carried out for the condition $u/u_{crit} = 1.0$. Also, we take the variation of the natural frequency, the aerodynamic parameters, into account in a fairly special way by multiplying the value with the given distribution density function for a possibly made error, see section 4.4. The reason for this is to still have the variables independent from each other which is one basic condition to use the sensitivity analysis as introduced. The idea is based on the fact that an error in the experimental estimation of a value is seen to be systematic and not depending on the value itself, this observation is made in [Kareem, 1983] and can be re-observed in [Jones and al., 1969]. Doing so, obviously does not allow us to compute the value sensitivity itself, but the sensitivity of a possibly made measurement error which is providing the variation of the parameter in the end.

4.1 Geometrical Parameters

As geometrical parameters we have the structure height H, the diameter D and the surface roughness ϵ. As recommended in [JCSS, 2001] the dimension of the structures can be considered deterministic values. These are not only an outcome of the proper erection of the structure but more than that the single variances of the values are relatively small compared to variances in all other parameters. Furthermore, we are mainly not interested in the variation of the dimensions for a certain value but we are interested to create a population of possible structures.

Starting with these assumptions we create a population of possible structures described by the parameter H/D as uniform continuos distribution $[20, 40]$; as we need to know the D separately we create a second uniform continuos distribution $[0.5, 4.0]$ and group them together.

The structure surface roughness ϵ is a less meaningful parameter and only makes a difference in the Strouhal number St and the lift coefficient c_l; by doing some considerations we fix $\epsilon/D = 0.0001$, this is based on [ESDU96030, 1996] where this value is selected for unknown surface roughness.

4.2 Dynamic Parameters

Mass per unit length m

For steel we find the density ρ_{steel} to be Gaussian distributed with mean 7700kg m^{-3} and coefficient of variance 0.01 according to [JCSS, 2001].

Applying the material density to the model can be done in two ways: one is by creating a possible mass per unit length m population which has to still fulfill the orthogonality condition for sensitivity analysis. It is a quite tricky task to find a suitable distribution which will not create super-heavy slender chimneys and vice versa.

So the author used the following hypothesis: the mass per unit length will be a function of the diameter D; thinking of an annulus[1] we can write

$$m = 0.0625 D^2 \rho_{steel} \cdot 1. \tag{4.2}$$

Natural frequency n_j

Trying to find a population of the natural frequency n_j of the structure leads to some intricacies: first of all it is depending on the structural geometry which is forming the stiffness, the structural flexibility, the structural mass itself depending on the geometry, as seen before, and on the boundary condition of the structure.

One helping argument is found in [Kareem, 1983] where it is shown that the natural frequency n_j of a structure itself can be computed deterministically and can be multiplied with a random variable.

$$n_j = n_{j_{det}} \cdot n_{j_{dis}} \tag{4.3}$$

This idea was picked up and we find the deterministic first natural frequency for a cantilever beam [Clough and Penzien, 1995],

$$n_{1_{det}} = 1.875^2 \sqrt{\frac{EI}{mH^4}} \tag{4.4}$$

we set Young's modulus $E = 200 \cdot 10^9$Pa as deterministic value according to [JCSS, 2001] and compute the cross section moment of inertia I with a wall thickness $D/100$. The mass per unit length m is used as found in Eq. (4.2) with $\rho_{steel} = 7700$kg m^{-3}. Using the mean value, with broad rounding gives

$$n_{1_{det}} \simeq 750 \frac{D}{H^2}. \tag{4.5}$$

Now we have to find the distribution of $n_{j_{dis}}$ and we use a uniform continuous distribution [0.83, 1.17], the variance according to [Kareem, 1983] where the uncertainty of the stiffness and the mass was added and an extra uncertainty of 0.10 was added in order to take the soil-structure interaction into account.

---

[1]The factor 0.0625 can be found by thinking of a wall thickness of $D/100$ and some additional structural parts; the total mass is four times the mass of the wall.

Structural damping ζ_s

Moving to creating a population for the structural damping ζ_s we again refer to [Kareem, 1983] where we can find a uniform continuous distribution to be chosen; applying this for steel structures leads to a uniform continuous distribution $[0.001, 0.007]$, again the considerations made for the natural frequency n_j are valid.

4.3 Fluid Parameters

Looking at the two determining fluid parameters, in our case the fluid is obviously air, density ρ and kinematic viscosity ν we could assume both to be deterministic, this is what is done in [JCSS, 2001] and in most other publications.

After some considerations the fact that the two values to be deterministic can not be satisfied as by varying the mean atmospheric temperature $\bar{T}$ the density ρ changes from $\bar{T} = 260°K$, $\rho = 1.341$kg m^{-3} to $\bar{T} = 320°K$, $\rho = 1.089$kg m^{-3} at fluid pressure $P = 0.1$MPa; reducing the fluid pressure would reduce the density and for higher pressure it would rise.

The kinematic viscosity ν varies for different atmospheric temperatures from $\bar{T} = 260°K$, $\nu = 16.55 \cdot 10^{-6}$m^2 s^{-1} to $\bar{T} = 320°K$, $\nu = 19.49 \cdot 10^{-6}$m^2 s^{-1} at fluid pressure $P = 0.1$MPa; again, at lower pressures the kinematic viscosity would reduce and gain for higher pressures, data found in [Lide, 2010].

The standard values used for air are: density $\rho = 1.25$kg m^{-3} and kinematic viscosity $\nu = 15 \cdot 10^{-6}$m^2 s^{-1}, [CNR, 2009].

To check that varying these parameters has no impact on the results, we represent both values as truncated normal distribution density functions, in case of density with mean 1.25kg m^{-3}, variance 0.125 and the two limits $[1.0$kg m$^{-3}, 1.5$kg m$^{-3}]$ and the kinematic viscosity with mean $15 \cdot 10^{-6}$m^2 s^{-1}, variance $1.5 \cdot 10^{-6}$ and the two limits $[10 \cdot 10^{-6}$m^2 s$^{-1}, 20 \cdot 10^{-6}$m^2 s$^{-1}]$. The variances and the limits are chosen by the author trying to produce reasonable data population for the sensitivity analysis.

4.4 Aerodynamic Parameters

We find the aerodynamic parameters all to be depending on the structure diameter D, the Reynolds number Re and the fluid density ρ. The fluid kinematic viscosity ν shows the need of using an error distribution instead of a parameter distribution. Furthermore, this helps to satisfy the orthogonality condition by considering all values to be deterministic and applying a uniform continuous distribution for the possibly made experimental error; this leads to quite reasonable results when performing a sensitivity analysis.

The other aerodynamic parameters – correlation length Le in Ruscheweyh's approach and l in Vickery and Basu, limiting factor of rms response α in Vickery and Basu and the bandwidth parameter in Vickery and Basu as well as in ESDU – are considered to be deterministic for they are dimensions.

Strouhal number St

In [Kareem, 1983] based on [Jones and al., 1969] values for the variation of the Strouhal number St can be found; again, a uniform continuous distribution $\text{St}_{dis} = [0.89, 1.11]$ is used, thus we have

$$\text{St} = \text{St}_{det} \cdot \text{St}_{dis}. \tag{4.6}$$

Lift coefficient c_l and c_{lat}

Looking at the lift coefficients c_l and c_{lat}, we have one rms value c_l and a rms max value c_{lat}; for both an order of magnitude is given in [Kareem, 1983]; we select for $c_{l_{dis}}$ a uniform continuous distribution $[0.85, 1.15]$ and for $c_{lat_{dis}}$ as well a uniform continuos distribution with $[0.93, 1.07]$, again we can express

$$c_l = c_l \cdot c_{l_{dis}}, \quad c_{lat} = c_{lat} \cdot c_{lat_{dis}}. \tag{4.7}$$

Negative aerodynamic damping $K_{a,max}$

The variation of the negative aerodynamic damping parameter $K_{a,max}$ used in Vickery and Basu can be found to be similar to the rms lift coefficient, [Vickery and Basu, 1983b] and thus, set by the author, $K_{a,max_{dis}}$ is a uniform distribution $[0.85, 1.15]$ and accordingly

$$K_{a,max} = K_{a,max_{det}} \cdot K_{a,max_{dis}}. \tag{4.8}$$

4.5 Atmospheric Parameters

Since we found the different approaches not being dependent on the fluid velocity u by carrying out dimensional analysis, section 2.2, we got rid of finding the distribution of the fluid velocity u. In our case u is depending of the structural dimension D and the investigated structural state n_j/n_s, but we have to find the distribution of possible atmospheric turbulence values I_u related to a certain fluid velocity u given by the structure's configurations. As explained in section 1.1.2, we are able to express a continuous distribution for $1/L$ as function of u; remember L to be the Monin-Obukhov length.

So, now we have to accomplish two tasks: firstly we have to find a probability density distribution for $1/L$ as function of u and secondly we have to sample possible values for I_u. Here we make some additional considerations as mentioned in section 1.2: a total absence of turbulence will be best for the vortex shedding phenomenon and thus worst for the structure. Remembering section 1.1.1, we know positive values of $1/L$ to represent a stable atmosphere with low values for the atmospheric turbulence I_u. Using a uniform continuous distribution $[0.50, 0.9995]$ for the appearance probability $I_{u_{dis}}$ allows us to find reasonable values for the atmospheric turbulence I_u and being quite confident of staying in the stable atmospheric condition range. Furthermore, this allows us to find values taking the different distributions for different fluid velocities into account,

$$I_u = P^{-1} \left(I_{u_{dis}} \right), \tag{4.9}$$

which is described in detail in the following section.

4.5.1 Random Variable Generation

To generate random variables for an arbitrary probability density function we find a quite simple method in [Devroye, 1986] that if F is a continuous distribution function on $\mathbb{R}$ with inverse F^{-1} defined by $F^{-1} = \inf\{x : F(x) = u, 0 < u < 1\}$, it is shown that if U is a uniform $[0, 1]$ random variable, then $F^{-1}(U)$ has the distribution function F.

So first of all we have to integrate the probability density function in order to obtain the appearance probability

$$P[x \leq 1/L](u) = \int_{-\infty}^{1/L} p[x](u) =$$

$$\begin{cases} \dfrac{\gamma_n}{\beta_n} e^{-\beta_n(1/L_{o,n} - x)} + \dfrac{\gamma_d}{\beta_d} e^{-\beta_d(1/L_{o,d} - x)} & \text{if } x < 1/L_{o,d}, \\ \dfrac{\gamma_n}{\beta_n} e^{-\beta_n(1/L_{o,n} - x)} + \dfrac{\gamma_d}{\beta_d} + \dfrac{\gamma_d}{\alpha_d} e^{-\alpha_d(x - 1/L_{o,d})} & \text{if } 1/L_{o,d} \leqslant x < 1/L_{o,n}, \\ \dfrac{\gamma_n}{\beta_n} + \dfrac{\gamma_n}{\alpha_n} e^{-\alpha_n(x - 1/L_{o,n})} + \dfrac{\gamma_d}{\beta_d} + \dfrac{\gamma_d}{\alpha_d} e^{-\alpha_d(x - 1/L_{o,d})} & \text{if } x \geqslant 1/L_{o,n}, \end{cases} \quad (4.10)$$

which is shown graphically in Fig. 4.1. After that we would like to find the inverse P^{-1} which can not be found in a closed form; what we will do instead is to find the single values via search method.[2] Thus we are able to create a random set of variables respecting the probability density function $p[x](u)$.
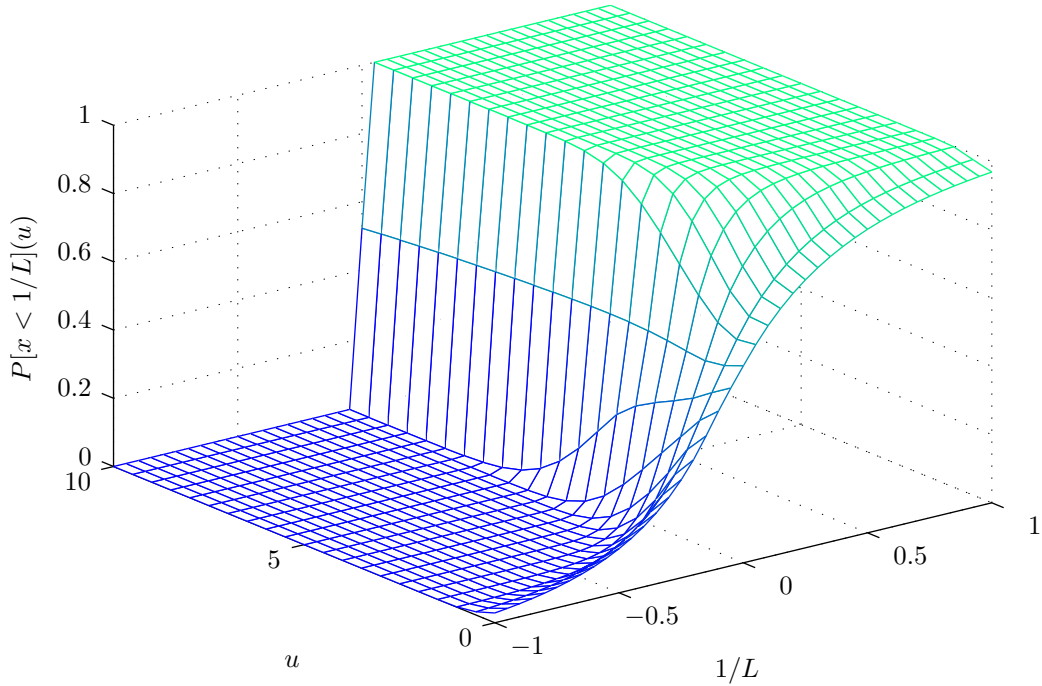
Figure 4.1 – Cumulative distribution function $P[x \leq 1/L](u)$ for the turbulence intensity I_u as function of the fluid velocity u and the Monin-Obukhov L.

4.6   Conclusion

By using the idea of combining a deterministic computed value with an error distribution allows us to handle the sensitivity analysis in a simple and practical form. For a general survey we collect all determining parameters in Tab. 4.1.

---

[2]We do this with the help of the bisection method, which decreases the size of the search interval until the error is small enough; using the mean value of the interval leads to the result, see [Råde and Westergren, 2000].

Table 4.1 – Measured values of erected chimneys with the computed dimensionless quantities.

Parameter	Distr. type	Implementation
D diameter	deterministic, range $[0.5, 4.0]$	set of uniformly distributed population
H/D *slenderness*	deterministic, range $[20, 40]$	set of uniformly distributed population
ϵ/D *roughness*	fixed	$\epsilon/D = 0.0001$
m, ρ_{steel} mass	normal, mean 7700 variance 0.01	$m = 0.0625 D^2 \rho_{steel} \cdot 1$
$n_{j_{dis}}$ struc. frequency	uniform, range $[0.83, 1.17]$	$n_j = n_{j_{det}} \cdot n_{j_{dis}}$
ζ_s struc. damping	uniform, range $[0.001, 0.007]$	
ρ density	normal, mean 1.25 variance 0.125 limits $[1.0, 1.5]$	
ν viscosity	normal, mean $15 \cdot 10^{-6}$ variance $1.5 \cdot 10^{-6}$ limits $[10 \cdot 10^{-6}, 20 \cdot 10^{-6}]$	
St_{dis} Strouhal no.	uniform, range $[0.89, 1.11]$	$St = St_{det} \cdot St_{dis}$
$c_{l_{dis}}$ $c_{lat_{dis}}$ lift coefficient	uniform, range $[0.85, 1.15]$ uniform, range $[0.93, 1.07]$	$c_l = c_l \cdot c_{l_{dis}}$ $c_{lat} = c_{lat} \cdot c_{lat_{dis}}$
$K_{a,max_{dis}}$ aedyn. damping	uniform, range $[0.85, 1.15]$	$K_{a,max} = K_{a,max_{det}} \cdot K_{a,max_{dis}}$
I_u turbulence	appearance probability $[0.50, 0.9995]$	I_u distrib. parameter func. of Re
Further Parameters		
u/u_{crit} rel. critical velocity	deterministic	set to $u/u_{crit} = 1$
ϕ_j mode shape	deterministic	shape is fixed
B, B_e, δ_B bandwidth	random as functions of I_u, functional dependency error free	
L_s, l corr. length	deterministic	
α limit factor	deterministic, as no structures should be exposed to this excitation	

Chapter 5

Sensitivity Analysis

> The analysis of the approaches is concluded with a variance based sensitivity
> analysis in order to find the importance of any parameter distinguished in the
> context of the individual approaches, and in a general context independent of
> the approach and with the help of [Sobol' et al., 2007] to estimate the pos-
> sibly made error by fixing a parameter. Pearson's correlation coefficient and
> Spearman's rank correlation coefficient are computed in order to understand
> the dependencies and correlations of the parameters.

The first order S_{X_i} and total effect S_{T,X_i} sensitivity indices were computed as described
in section 1.3 where the number of base samples N was increased until the sensitivity
indices reached a stable value and thus N is different for every approach. The second
order sensitivity indices were not computed due to the high computation cost and due to
the fairly low gain of knowledge.

All main determining parameters in every approach were set to be varying, according
to the considerations and conventions made in chapter 4. Thus not only the generally
known fact that the physical properties of the fluid are insignificant could be proven but
also that the variance based sensitivity analysis is able to reproduce them too. Again, we
remember that the structural dimensions are not set to be probabilistic values but only
varied in order to cover all possible configurations of chimneys and we make the sensitivity
analysis with the condition that the ratio critical velocity $u/u_{crit} = 1.0$.

The Pearson's correlation coefficient $r_{\mathbf{X},\mathbf{Y}}$ and Spearman's rank correlation coefficient
$\rho_{\mathbf{X},\mathbf{Y}}$ where used for checking the results of the sensitivity analysis in a qualitative way,
to prove the independence of the single parameter populations and with the help of the
Spearman's rank correlation coefficient to prove if the model's result population can be
described using a function. Spearman's rank correlation coefficient provides this at least
for a monotonic function which at least gives an idea of how feasible it is.

Nota bene, that for certain variables that we used to compute the sensitivity indices
for the influence of varying the parameter, this is not the influence of the parameter itself.
However, it allows us to have evidence of the importance of changes in the parameter due
to measurement or model errors.

Fig. 5.2, Fig. 5.4, Fig. 5.6, Fig. 5.8 and Fig. 5.10 are read in the following way: The
diagonal represents the histogram of the single parameter, thus the distribution type is
visible. On the other position scatter plots of the parameter values are plotted. In order
to reduce the quantity of points only 500 randomly selected base samples are represented;
this is disadvantageous for the histogram plots as more values would clearly enable the
histograms to reproduce the initial probability distributions better.

5.1   Ruscheweyh

In the Ruscheweyh approach we varied 9 parameters and with $N = 40\,000$ base samples we obtained stable values for the sensitivity indices.

In Fig. 5.1 the sensitivity indices are shown and we can see straight away that the structural damping ratio ζ_s is the most important factor. All the other non-geometric factors are of such minor importance that even when setting them fixed the possibly made error $\delta(X_i)$ according to [Sobol' et al., 2007] and Eq. (1.3.3) is smaller < 0.07 for an exceeding probability of $\delta(X_i) < 0.50$.
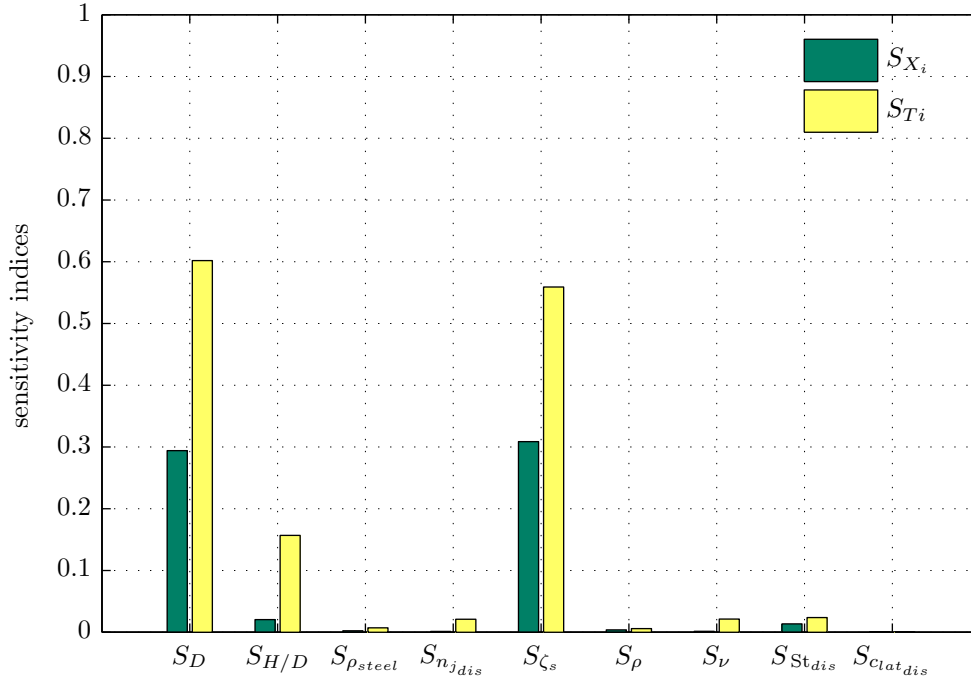

Figure 5.1 – Ruscheweyh; first order and total effect sensitivity indices

By looking at the sum of the first order sensitivity indices we see the first order cover 0.65 of the whole possible variation combinations which will be covered by the higher order sensitivity indices.

$$
\begin{array}{llll}
S_D = 0.2941 & S_{H/D} = 0.0205 & S_{\rho_{steel}} = 0.0024 & S_{n_j} = 0.0013 \\
S_{\zeta_s} = 0.3087 & S_\rho = 0.0038 & S_\nu = 0.0015 & S_{\mathrm{St}_{dis}} = 0.0136 \\
S_{c_{lat_{dis}}} = 0.0008 & \Sigma S_{X_i} = 0.6467 &
\end{array}
\tag{5.1}
$$

Following this, the values for the total effects underline in numbers what can already be seen in Fig. 5.1 and which provides the information for the exceeding probability when fixing a parameter.

$$
\begin{array}{llll}
S_{T,D} = 0.6019 & S_{T,H/D} = 0.1568 & S_{T,\rho_{steel}} = 0.0071 & S_{T,n_j} = 0.0210 \\
S_{T,\zeta_s} = 0.5591 & S_{T,\rho} = 0.0059 & S_{T,\nu} = 0.0213 & S_{T,\mathrm{St}_{dis}} = 0.0238 \\
S_{T,c_{lat_{dis}}} = 0.0001 &
\end{array}
\tag{5.2}
$$

The correlation coefficients have to be read together with Fig. 5.2 where the first horizontal scatter plot line is corresponding to the correlation values.

$$
\begin{array}{lll}
r_{Y_A,Y_D} = -0.4879 & r_{Y_A,Y_{H/D}} = 0.1342 & r_{Y_A,Y_{\rho_{steel}}} = 0.0045 \\
r_{Y_A,Y_{n_j}} = -0.0743 & r_{Y_A,Y_{\zeta_s}} = -0.4861 & r_{Y_A,Y_\rho} = 0.0908 \\
r_{Y_A,Y_\nu} = 0.0770 & r_{Y_A,Y_{\mathrm{St}_{dis}}} = -0.1141 & r_{Y_A,Y_{c_{lat_{dis}}}} = 0.0382
\end{array}
\tag{5.3}
$$

What can be seen from the Pearson's correlation coefficient $r_{\mathbf{X},\mathbf{Y}}$ is that the obtained sensitivity indices are qualitatively right and, in addition, looking at the Spearman's rank correlation coefficient $\rho_{\mathbf{X},\mathbf{Y}}$ we see the representation using a monotonic function to be quite appropriate.

$$
\begin{aligned}
\rho_{Y_A,Y_D} &= -0.5955 & \rho_{Y_A,Y_{H/D}} &= 0.1584 & \rho_{Y_A,Y_{\rho_{steel}}} &= -0.0008 \\
\rho_{Y_A,Y_{n_j}} &= -0.0951 & \rho_{Y_A,Y_{\zeta_s}} &= -0.6123 & \rho_{Y_A,Y_\rho} &= 0.1106 \\
\rho_{Y_A,Y_\nu} &= 0.0955 & \rho_{Y_A,Y_{\mathrm{St}_{dis}}} &= -0.1591 & \rho_{Y_A,Y_{c_{latdis}}} &= 0.0458
\end{aligned}
\tag{5.4}
$$

Of course the Spearman's rank correlation coefficients are quite low but this is due to the effect that there is a band of functions for every base sample.
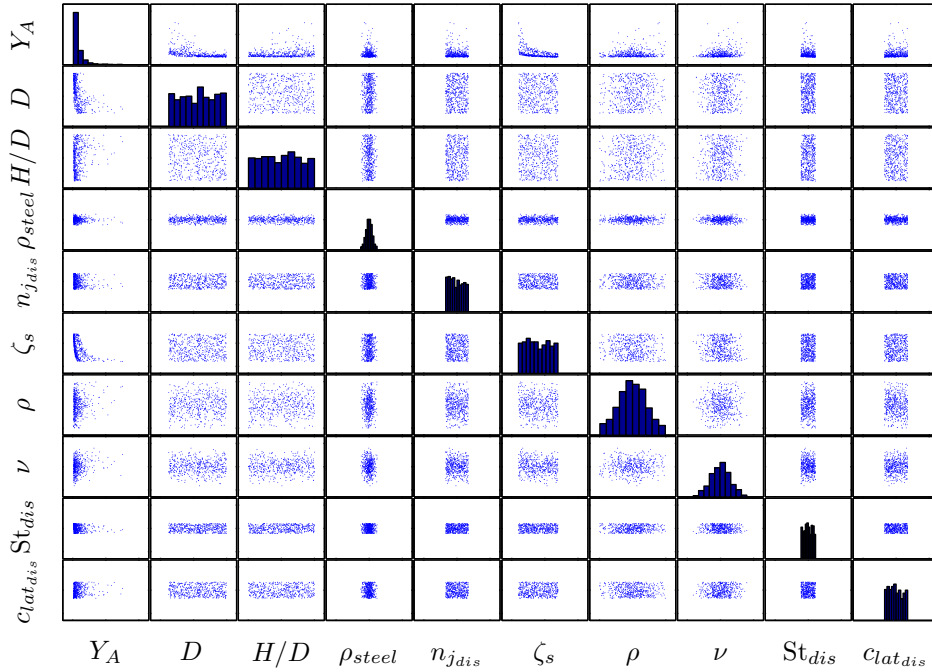

Figure 5.2 – Ruscheweyh; scatter plot of 500 randomly selected parameter vectors $\mathbf{X}$ plotted against each other; on the diagonal: histogram of the individual parameters

5.2   Vickery and Basu

Vickery and Basu was analyzed by varying 11 parameters; to reach stable values $N = 60\,000$ base samples had to be used.

As for the Ruscheweyh approach the structural damping ratio ζ_s plays an important role and, in addition, in the Vickery and Basu approach the turbulence intensity I_u has a considerable impact on the result, see Fig. 5.3. Computing the exceeding probability $\delta(X_i)$ again shows that all other non-geometric parameters are below the < 0.07 threshold for $\delta(X_i) < 0.5$.

$$
\begin{aligned}
S_D &= 0.0186 & S_{H/D} &= 0.0652 & S_{\rho_{steel}} &= 0.0061 & S_{n_{j_{dis}}} &= 0.0074 \\
S_{\zeta_s} &= 0.3690 & S_\rho &= 0.0111 & S_\nu &= 0.0064 & S_{I_{u_{dis}}} &= 0.0746 \\
S_{\mathrm{St}_{dis}} &= 0.0060 & S_{c_{l_{dis}}} &= 0.0062 & S_{K_{a,max_{dis}}} &= 0.0095 & \Sigma S_{X_i} &= 0.5799
\end{aligned}
\tag{5.5}
$$

The sum of the first order sensitivity indices are in case of Vickery and Basu with 0.58 below the value of Ruscheweyh but still covering the major part of the total sum including

the higher order sensitivity indices.

$$
\begin{array}{llll}
S_{T,D} = 0.1935 & S_{T,H/D} = 0.2821 & S_{T,\rho_{steel}} = 0.0000 & S_{T,n_{j_{dis}}} = 0.0151 \\
S_{T,\zeta_s} = 0.8093 & S_{T,\rho} = 0.0300 & S_{T,\nu} = 0.0000 & S_{T,I_{u_{dis}}} = 0.3342 \\
S_{T,\mathrm{St}_{dis}} = 0.0000 & S_{T,cl_{dis}} = 0.0000 & S_{T,K_{a,max_{dis}}} = 0.0326
\end{array}
\tag{5.6}
$$

The total effect sensitivity indices for the structural damping ratio $S_{T,\zeta_s} = 0.81$ is even more distinctive than the one in case of the Ruscheweyh approach $S_{T,\zeta_s} = 0.56$. Looking at the turbulence intensity I_u sensitivity index being $S_{T,I_{u_{dis}}} = 0.33$ and thus of a considerable significance to the approach's results.
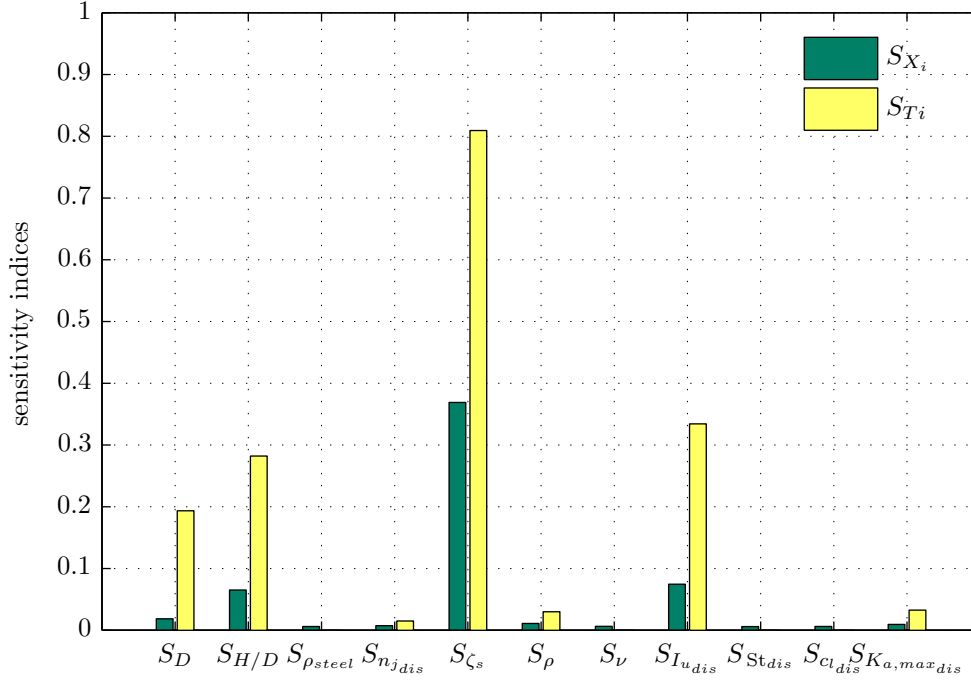

Figure 5.3 – Vickery and Basu; first order and total effect sensitivity indices

Remarkable is that the distribution for negative aerodynamic damping $K_{a,max}$ is the most sensitive parameter to the result and that the total sensitivity index for the fluid density $S_{T,\rho} = 0.03$ is the second largest index.

$$
\begin{array}{lll}
r_{Y_A,Y_D} = 0.1116 & r_{Y_A,Y_{H/D}} = 0.2453 & r_{Y_A,Y_{\rho_{steel}}} = -0.0021 \\
r_{Y_A,Y_{n_{j_{dis}}}} = -0.0425 & r_{Y_A,Y_{\zeta_s}} = -0.4887 & r_{Y_A,Y_\rho} = 0.0657 \\
r_{Y_A,Y_\nu} = 0.0122 & r_{Y_A,Y_{I_{u_{dis}}}} = 0.2605 & r_{Y_A,Y_{\mathrm{St}_{dis}}} = -0.0041 \\
r_{Y_A,Y_{cl_{dis}}} = -0.0087 & r_{Y_A,Y_{K_{a,max_{dis}}}} = 0.0634
\end{array}
\tag{5.7}
$$

The conclusions made, based on the Pearson correlation coefficient $r_{\mathbf{X,Y}}$ and Spearman's rank correlation coefficient $\rho_{\mathbf{X,Y}}$ and assisted by Fig. 5.4, again approve the quality of the performed sensitivity analysis.

$$
\begin{array}{lll}
\rho_{Y_A,Y_D} = -0.0453 & \rho_{Y_A,Y_{H/D}} = 0.5268 & \rho_{Y_A,Y_{\rho_{steel}}} = -0.0040 \\
\rho_{Y_A,Y_{n_{j_{dis}}}} = -0.1048 & \rho_{Y_A,Y_{\zeta_s}} = -0.3458 & \rho_{Y_A,Y_\rho} = 0.0840 \\
\rho_{Y_A,Y_\nu} = 0.0452 & \rho_{Y_A,Y_{I_{u_{dis}}}} = 0.4311 & \rho_{Y_A,Y_{\mathrm{St}_{dis}}} = -0.0811 \\
\rho_{Y_A,Y_{cl_{dis}}} = 0.0634 & \rho_{Y_A,Y_{K_{a,max_{dis}}}} = 0.0218
\end{array}
\tag{5.8}
$$

Due to a non-monotonic functional tendency of the response to the structural damping ratio the Spearman's rank correlation coefficient is not very high $\rho_{Y_A,Y_{\zeta_s}} = -0.3458$ and all other coefficients lack a bit of information due to this effect too.
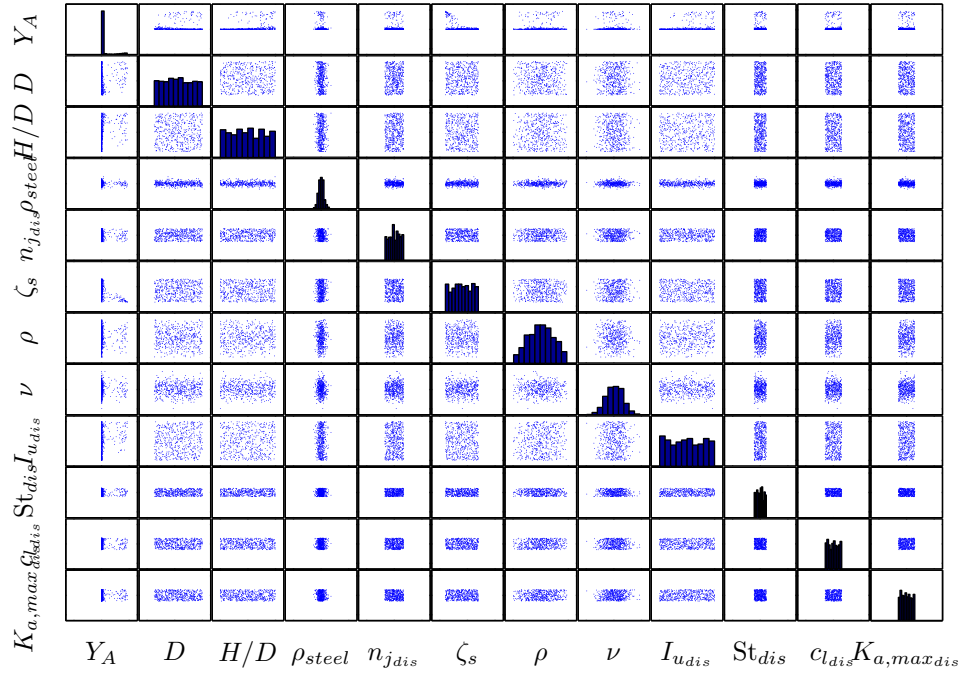
Figure 5.4 – Vickery and Basu; scatter plot of 500 randomly selected parameter vectors **X** plotted against each other; on the diagonal: histogram of the individual parameters

5.3   ESDU

Analyzing ESDU was carried out with the main 11 parameters; the number of base samples $N = 70\,000$ leads to stable sensitivity indices.

Again, in ESDU the structural damping ratio ζ_s is the most sensitive parameter to the result, surprisingly the distribution of turbulence intensity has nearly no influence but the distribution of the Strouhal number St_{dist} plays an important role. Regarding the turbulence intensity I_u we have already made a comment when analyzing the response surfaces in Fig. 3.18, Fig. 3.19 and Fig. 3.20 where the variation of the turbulence intensity I_u along a constant ratio critical velocity $u/u_{crit} = 1.0$ is indeed not significant.

$$
\begin{array}{llll}
S_D = 0.1393 & S_{H/D} = 0.0081 & S_{\rho_{steel}} = 0.0023 & S_{n_{j_{dis}}} = 0.0024 \\
S_{\zeta_s} = 0.3529 & S_\rho = 0.0043 & S_\nu = 0.0026 & S_{I_{u_{dis}}} = 0.0033 \\
S_{\mathrm{St}_{dis}} = 0.0546 & S_{c_{l_{dis}}} = 0.0025 & \Sigma S_{X_i} = 0.5723 &
\end{array}
\tag{5.9}
$$

But this does not mean that the turbulence intensity I_u generally has no importance, which can be seen when studying its response surfaces, Fig. 3.18, Fig. 3.19 and Fig. 3.20. This disadvantage should be noticed when using the idea to not vary the parameter itself but rather applying a distribution function to it.

$$
\begin{array}{llll}
S_{T,D} = 0.4517 & S_{T,H/D} = 0.0124 & S_{T,\rho_{steel}} = 0.0490 & S_{T,n_{j_{dis}}} = 0.0460 \\
S_{T,\zeta_s} = 0.7297 & S_{T,\rho} = 0.0058 & S_{T,\nu} = 0.0407 & S_{T,I_{u_{dis}}} = 0.0355 \\
S_{T,\mathrm{St}_{dis}} = 0.2338 & S_{T,c_{l_{dis}}} = 0.0390 & &
\end{array}
\tag{5.10}
$$

The non-geometric first order sensitivity indices are all below the < 0.07 threshold for $\delta(X_i) < 0.5$, except from the above mentioned, and the sum $\Sigma S_{X_i} = 0.57$ covers the main part of the influences. As clearly shown in Fig. 5.5, the structural damping ratio $S_{T,\zeta_s} = 0.73$ and the distribution of the Strouhal number $S_{T,\mathrm{St}_{dis}} = 0.23$ are the main determining parameters in the approach.
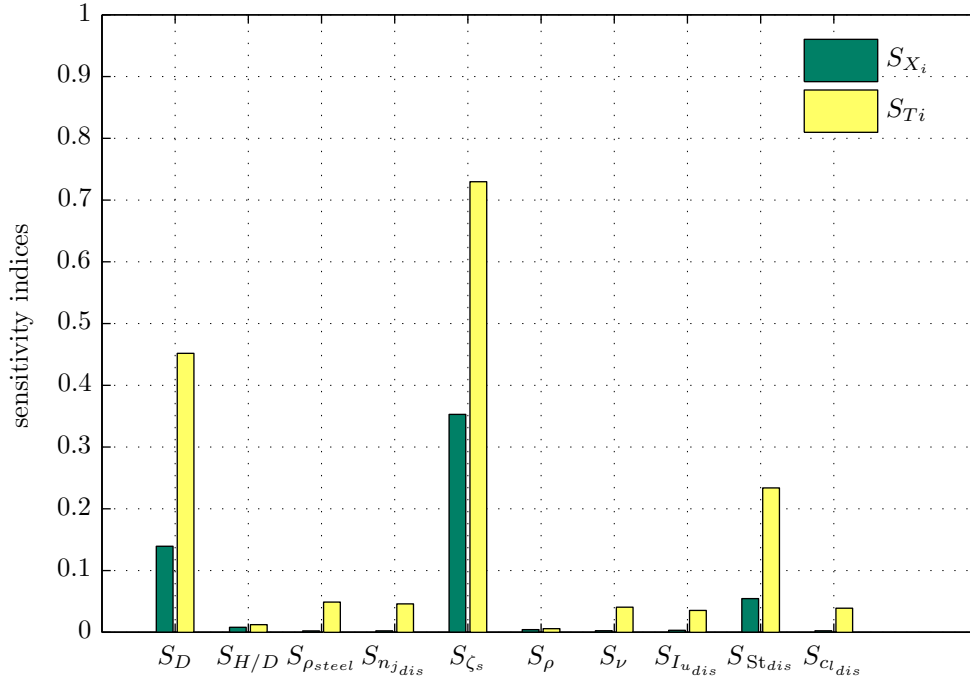
Figure 5.5 – ESDU; first order and total effect sensitivity indices

The reason for the distribution of the Strouhal number St_{dist} to be of importance becomes clear when looking at the sensitivity analysis results of the other approaches and the mathematical models of the individual approaches where in all mathematical models the result is divided by the square of the Strouhal number St and it being a value around ~ 0.2 variation effects the results significantly.

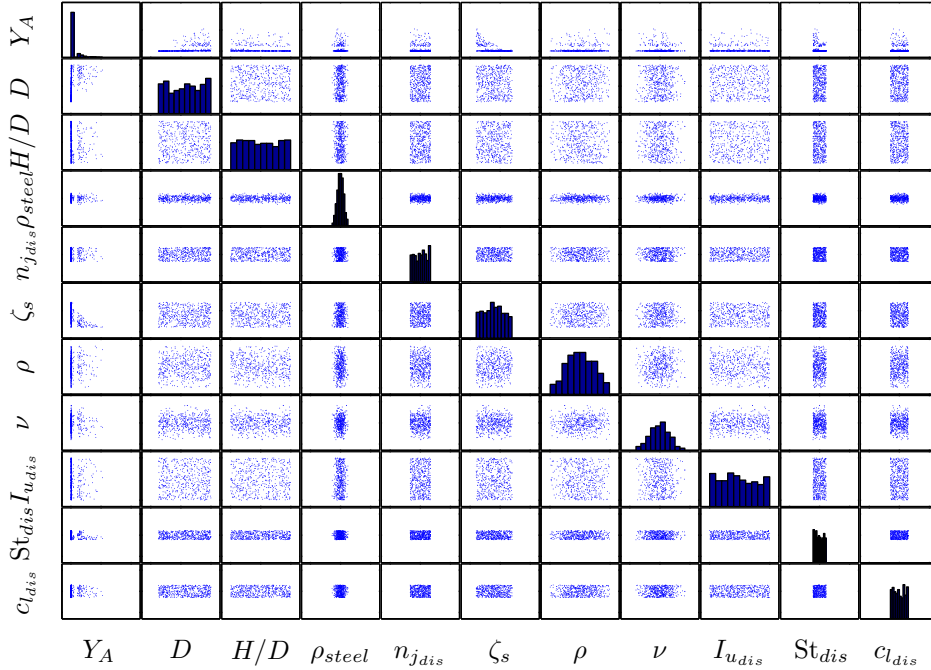**Figure 5.6** – ESDU; scatter plot of 500 randomly selected parameter vectors **X** plotted against each other; on the diagonal: histogram of the individual parameters

The correlation of the parameter population again underlines the outcome of the sensitivity analysis. From Fig. 5.6 and the Pearson's correlation coefficient $r_{\mathbf{X},\mathbf{Y}}$ and Spearman's

rank correlation coefficient $\rho_{\mathbf{X},\mathbf{Y}}$ we see that we have a non-defined monotonic represen-
tation as a correlation of the result and the structural damping ration $\rho_{Y_A,Y_{\zeta_s}} = -0.4329$.

$$
\begin{array}{llll}
r_{Y_A,Y_D} = & 0.3705 & r_{Y_A,Y_{H/D}} = -0.0835 & r_{Y_A,Y_{\rho_{steel}}} = & 0.0013 \\
r_{Y_A,Y_{n_{j_{dis}}}} = & 0.0068 & r_{Y_A,Y_{\zeta_s}} = -0.4937 & r_{Y_A,Y_\rho} = & 0.0691 \\
r_{Y_A,Y_\nu} = & -0.0114 & r_{Y_A,Y_{Iu_{dis}}} = -0.0231 & r_{Y_A,Y_{St_{dis}}} = & -0.2122 \\
r_{Y_A,Y_{c_{l_{dis}}}} = & 0.0153 & &
\end{array}
\tag{5.11}
$$

ESDU's approach is a very complex and numerically instable approach due to the iteration
needed for the narrow band response and thus when the sensitivity analysis is performed
special care to the base sample vectors and the resulting sensitivity indices has to be
given.

$$
\begin{array}{llll}
\rho_{Y_A,Y_D} = & 0.7655 & \rho_{Y_A,Y_{H/D}} = -0.2830 & \rho_{Y_A,Y_{\rho_{steel}}} = & 0.0009 \\
\rho_{Y_A,Y_{n_{j_{dis}}}} = & 0.0184 & \rho_{Y_A,Y_{\zeta_s}} = -0.4329 & \rho_{Y_A,Y_\rho} = & 0.0997 \\
\rho_{Y_A,Y_\nu} = & -0.0214 & \rho_{Y_A,Y_{Iu_{dis}}} = -0.0684 & \rho_{Y_A,Y_{St_{dis}}} = & -0.1368 \\
\rho_{Y_A,Y_{c_{l_{dis}}}} = & 0.0214 & &
\end{array}
\tag{5.12}
$$

5.4   Wake Oscillator

The wake oscillator approach has 7 parameters which were all included in the sensitivity
analysis and to reach stable indices $N = 20\,000$ base samples were needed.

Fig. 5.7 clearly shows that again the structural damping ratio ζ_s is the most important
factor and as for the ESDU approach the distribution for the Strouhal number St_{dis} also
has a significant impact on the result. All the other non-geometric parameters are again
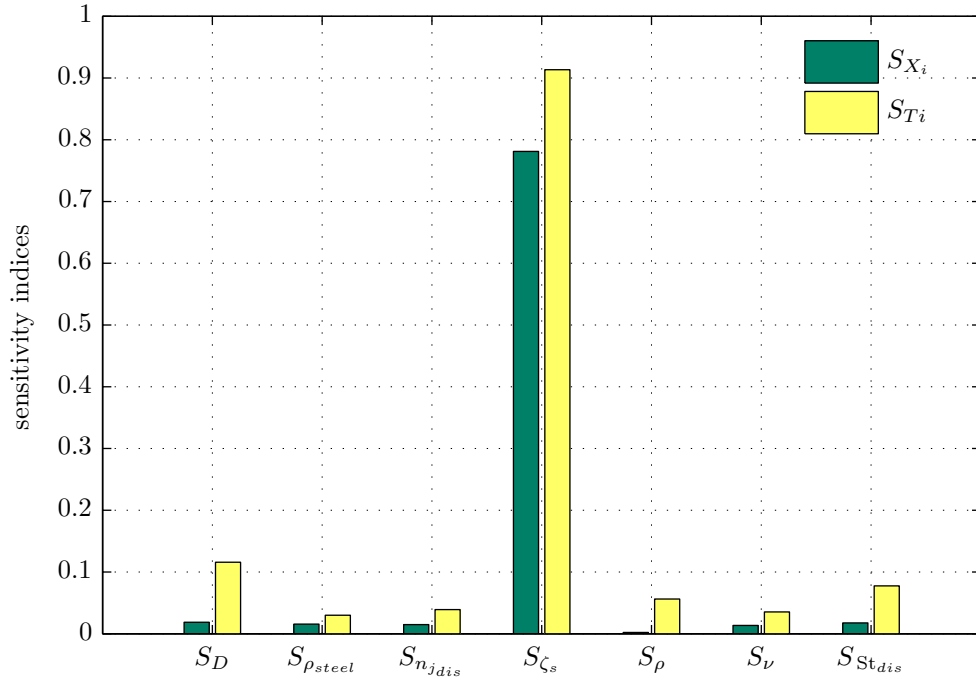below a < 0.07 threshold for $\delta(X_i) < 0.5$.

Figure 5.7 – Wake oscillator; first order and total effect sensitivity indices

The sum of the first order sensitivity indices $\Sigma S_{X_i} = 0.86$ implies that the higher order
sensitivity terms have no big importance. $S_{T,\zeta_s} = 0.91$ is very dominant and in a certain

way this becomes clear looking at Eq. (2.7.1) where definitely the structural damping ratio ζ_s together with the Strouhal number St are the ones which vary.

$$S_D = 0.0186 \quad S_{\rho_{steel}} = 0.0156 \quad S_{n_{j_{dis}}} = 0.0148 \quad S_{\zeta_s} = 0.7811$$
$$S_\rho = 0.0021 \quad S_\nu = 0.0134 \quad S_{\mathrm{St}_{dis}} = 0.0176 \quad \Sigma S_{X_i} = 0.8632 \tag{5.13}$$

Of course the fluid viscosity ν only has an indirect influence in this approach and thus only changes the Reynolds number Re which effects the Strouhal number St.

$$S_{T,D} = 0.1159 \quad S_{T,\rho_{steel}} = 0.0300 \quad S_{T,n_{j_{dis}}} = 0.0391 \quad S_{T,\zeta_s} = 0.9134$$
$$S_{T,\rho} = 0.0562 \quad S_{T,\nu} = 0.0353 \quad S_{T,\mathrm{St}_{dis}} = 0.0775 \tag{5.14}$$

The correlation coefficients once more underline the sensitivity analysis and due to the simplicity of Eq. (2.7.1) they have a big validity.

$$r_{Y_A,Y_D} = -0.1709 \quad r_{Y_A,Y_{\rho_{steel}}} = -0.0032 \quad r_{Y_A,Y_{n_{j_{dis}}}} = -0.0384$$
$$r_{Y_A,Y_{\zeta_s}} = -0.7438 \quad r_{Y_A,Y_\rho} = 0.1189 \quad r_{Y_A,Y_\nu} = 0.0308 \tag{5.15}$$
$$r_{Y_A,Y_{\mathrm{St}_{dis}}} = -0.1736$$

Fig. 5.8 makes visually clear how conservative the structural reaction is due to the input parameters.

$$\rho_{Y_A,Y_D} = -0.2316 \quad \rho_{Y_A,Y_{\rho_{steel}}} = 0.0004 \quad \rho_{Y_A,Y_{n_{j_{dis}}}} = -0.0368$$
$$\rho_{Y_A,Y_{\zeta_s}} = -0.8849 \quad \rho_{Y_A,Y_\rho} = 0.1482 \quad \rho_{Y_A,Y_\nu} = 0.0443 \tag{5.16}$$
$$\rho_{Y_A,Y_{\mathrm{St}_{dis}}} = -0.2182$$

An interesting observation is that the simpler the model analyzed by the sensitivity analysis is the easier and better are the results; the same is valid for the sensitivity analysis done in case of Ruscheweyh and the AJI recommendations approach.
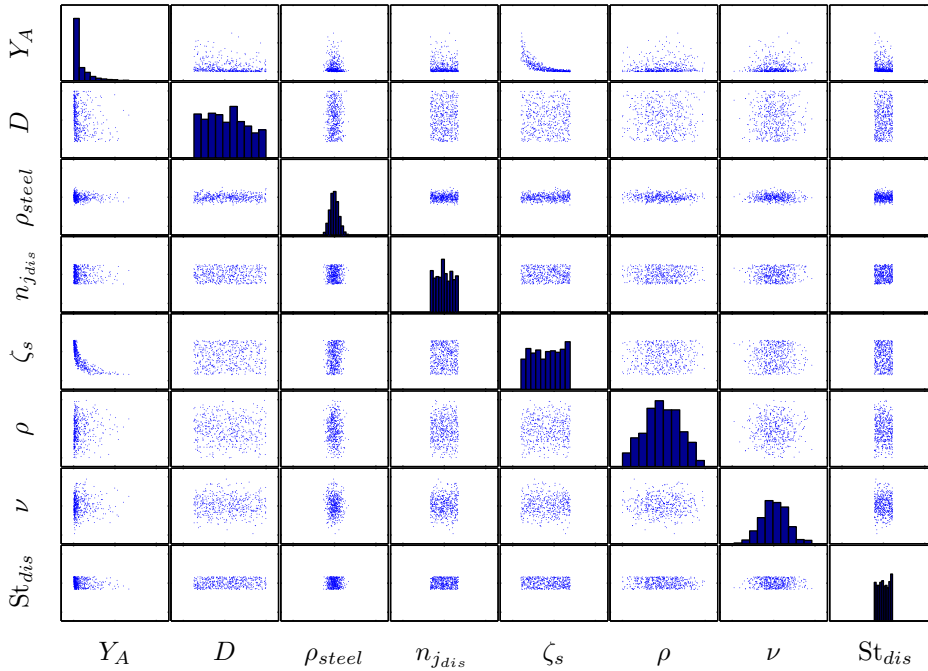

Figure 5.8 – Wake oscillator; scatter plot of 500 randomly selected parameter vectors **X** plotted against each other; on the diagonal: histogram of the individual parameters

5.5 AJI Recommendations for Loads on Buildings

The AJI recommendations for loads on buildings where analyzed using the 7 model parameters and $N = 25\,000$ base samples were needed in order to obtain stable sensitivity indices.

The sensitivity of the individual parameters are more equilibrated but still the major importance is ascribed to the structural damping ratio ζ_s, see Fig. 5.9, all the other non-geometric parameters, except for the distribution of the structural natural frequency term, fall under a < 0.07 threshold for $\delta(X_i) < 0.5$.
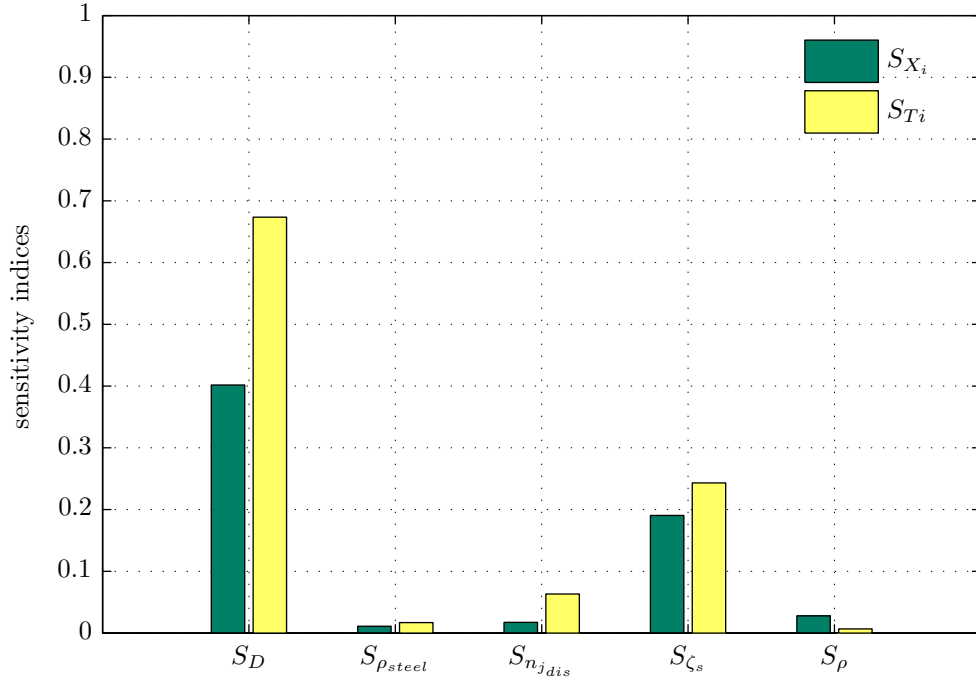

Figure 5.9 – AJI recommendations; first order and total effect sensitivity indices

The total effect sensitivity index $S_{T,n_{j_{dis}}} = 0.0632$ for the distribution of the structural natural frequency is the second most important factor. This is due to the effect that when computing the wind force coefficient at resonance C_r it is directly depending on the natural frequency n_j, see Tab. 2.2.

$$
\begin{aligned}
&S_D = 0.4017 \quad S_{\rho_{steel}} = 0.0111 \quad S_{n_{j_{dis}}} = 0.0174 \quad S_{\zeta_s} = 0.1905 \\
&S_\rho = 0.0278 \quad \Sigma S_{X_i} = 0.6484
\end{aligned} \tag{5.17}
$$

As has already been mentioned the total sensitivity indices are not very distinctive showing the approach to be very well equilibrated to the parameters. Looking at the sum of the first order sensitivity indices $\Sigma S_{X_i} = 0.65$, it shows a good coverage of the possible parameter combined sensitivities.

$$
\begin{aligned}
&S_{T,D} = 0.6735 \quad S_{T,\rho_{steel}} = 0.0169 \quad S_{T,n_{j_{dis}}} = 0.0632 \quad S_{T,\zeta_s} = 0.2431 \\
&S_{T,\rho} = 0.0068
\end{aligned} \tag{5.18}
$$

Before looking at the correlation coefficients, examining Fig. 5.10 shows the separation of the results based on the two cases for the wind force coefficient at resonance C_r, $m/D^2\sqrt{\zeta_s} < 0.5$ and $m/D^2\sqrt{\zeta_s} \geq 0.5$ in Tab. 2.2.

$$
\begin{aligned}
&r_{Y_A,Y_D} = -0.5813 \quad r_{Y_A,Y_{\rho_{steel}}} = -0.0080 \quad r_{Y_A,Y_{n_{j_{dis}}}} = -0.0690 \\
&r_{Y_A,Y_{\zeta_s}} = -0.4018 \quad r_{Y_A,Y_\rho} = 0.1296
\end{aligned} \tag{5.19}
$$

Furthermore the lower branch has less variation due to the fact that the wind force coefficient at resonance C_r is $1.7/\sqrt{\zeta_s}$ or $0.57/\sqrt{\zeta_s}$, see Tab. 2.2.

$$
\begin{aligned}
\rho_{Y_A,Y_D} &= -0.5297 & \rho_{Y_A,Y_{\rho_{steel}}} &= -0.0058 & \rho_{Y_A,Y_{n_{j_{dis}}}} &= -0.0612 \\
\rho_{Y_A,Y_{\zeta_s}} &= -0.5533 & \rho_{Y_A,Y_\rho} &= 0.1905
\end{aligned}
\tag{5.20}
$$

This leads the correlation coefficients to lose some quality; it would be better if the two branches were calculated separately; despite this, they underline the results of the sensitivity analysis.
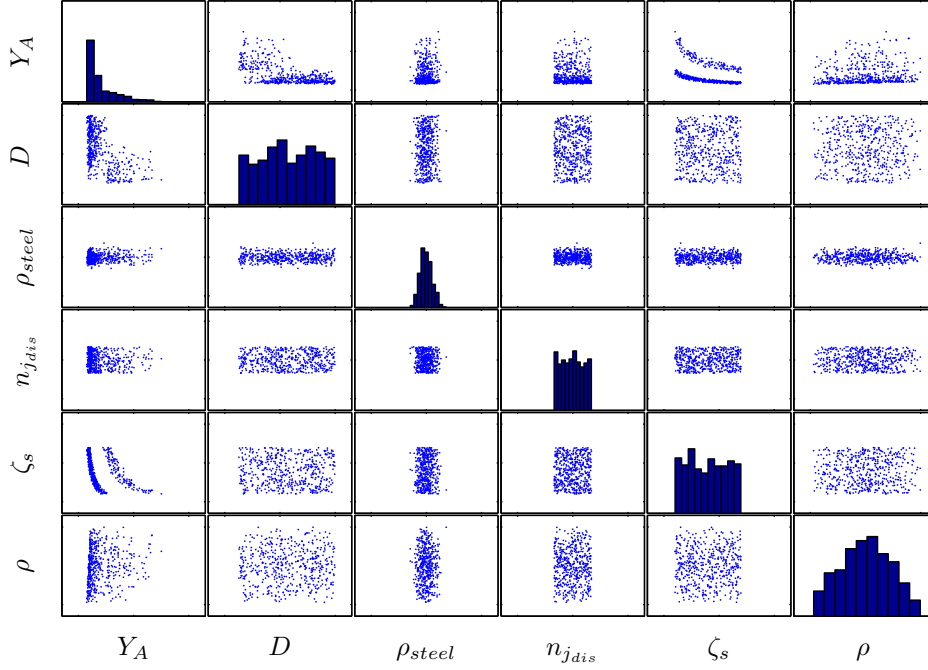
Figure 5.10 – AJI recommendations; scatter plot of 500 randomly selected parameter vectors **X** plotted against each other; on the diagonal: histogram of the individual parameters

5.6   Conclusion

The sensitivity analysis allowed us to figure out the main determining parameters in the different approaches. Based on this the structural damping ratio ζ_s could be figured out to be the most important factor in all approaches. In the case of having numerically cheap approaches the sensitivity analysis is a very effective tool which proved the minor influence of the physical properties of the fluid and confirmed the usability of sensitivity analysis for these kind of models. Furthermore, by not directly varying depending parameters, like the Strouhal number St or the lift coefficients c_l or c_{lat}, but rather applying a distribution function to these parameters, as described in chapter 4, allowed us to conserve the fundamental condition of uncorrelated parameter populations.

Chapter 6

Evolving Probability Models

> This chapter now uses the gained knowledge of the previous chapters and introduces the parameter probability to the obtained results for the different models. This is done in three steps: the first step examines the probability of the mean fluid velocity to reach the critical velocity u_{crit} for all possible natural frequencies n_j, the second step evolves the probability density distribution of the structural reaction $y_{0,max}/D$ due to uncertainties in the structural damping ratio ζ_s and the structural natural frequency n_j, the third and last step combines the structural reaction probability with the probability of the mean fluid velocity in order to obtain a probabilistic damage value for fatigue analysis. Everything is shown in a general way but due to the conclusions made in section 3.6 the generally expressed functions are given only for the Vickery and Basu approach.

Dealing with real structures one main challenge is to introduce the distribution of all determining parameters to the analysis as well as the model uncertainty itself. The first big issue is to understand the distribution of the different model parameters, which can be found in chapter 4 and to secondly introduce them to the deterministic models, for example the ones in chapter 2. A further and even more complicated step is to find the model error distribution and take it into account as well when performing analysis, some ideas to that extend can be found in [Solari, 1997].

In terms of vortex shedding mostly not the occurrence of vortex shedding itself is the main failure criterium for a structure but, when thinking of steel structures, fatigue specifics are a significant criterium for structural failure. This chapter should lead from general considerations if vortex shedding occurs, to model response due to parameter uncertainties and model errors and concludes by introducing the probabilistic models found into a yet deterministic fatigue framework.

6.1 Occurrence Probability of Vortex Shedding

The first step now is to understand properly if vortex shedding appears. This is irrelevant for the first natural frequency mode[1] but is of high importance if deciding to involve higher natural frequencies.

---

[1]If a structure is sensitive to vortex shedding – a slender and/or weakly damped structure – it will generally always suffer from vortex shedding in the first natural frequency mode.
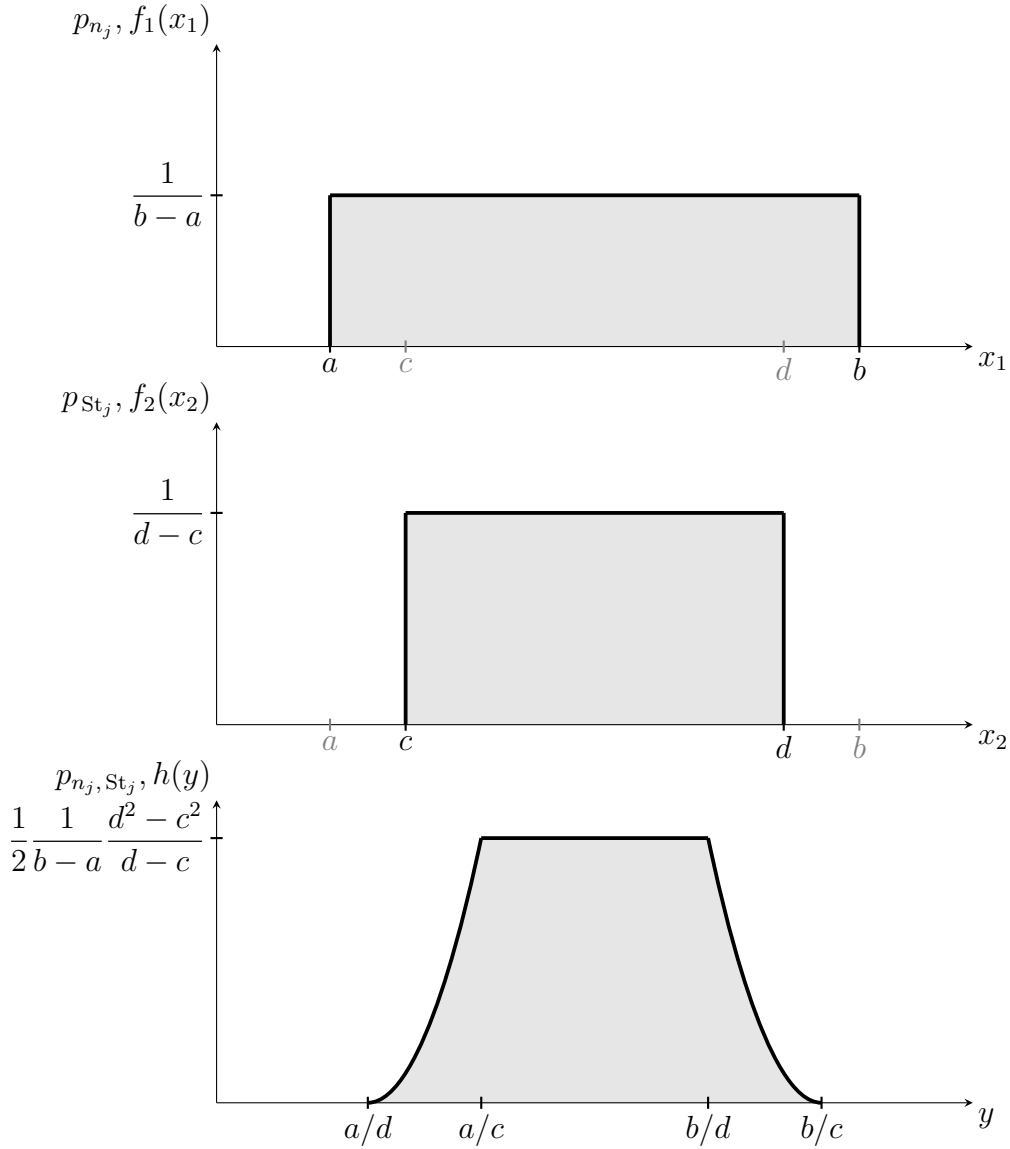
Figure 6.1 – Graphical representations of the probability density function $h(y)$ of two uniformly distributed random variables $f_1(x_1)$ and $f_2(x_2)$.

As the critical velocity u_{crit} is independent of the vortex shedding model it can be derived from the Strouhal number, see section 1.2.1.

$$u_{crit} = \frac{n_j D}{\text{St}} \tag{6.1}$$

This is so far a deterministic description, introducing the distributions for the different parameters found in chapter 4 and with the same idea, by multiplying the deterministic value by a probability density function, Eq. (6.1) transforms to Eq. (6.2). Here the deterministic part $y(u)$ shifts the function to the deterministic point of vortex shedding occurrence, the meaning of the $\lambda(I_u, \text{S}_{\text{cr}})$ function is explained later in detail.

$$p_{u_{crit}}(u) = p_{n_j, \text{St}_j}(y), \quad y(u) = u - \frac{n_{j_{det}} D_{det}}{\text{St}_{j_{det}}} \lambda(I_u, \text{S}_{\text{cr}}) \tag{6.2}$$

$\lambda(I_u, \text{S}_{\text{cr}})$ is the critical velocity u_{crit} reduction function due to the vortex shedding spectrum which is an introduction of the used vortex shedding model to the critical velocity probability density function $p_{u_{crit}}(u)$. The function $\lambda(I_u, \text{S}_{\text{cr}})$ describes the flare of the

response function of the model versus the critical velocity ratio u/u_{crit}. This becomes even clearer when thinking of cutting Fig. 3.6 into slices along the critical velocity ratio u/u_{crit} axis and thus the half-cone becomes narrower the larger the Scruton number S_{cr} becomes. Looking at Fig. 3.6, Fig. 3.7 and Fig. 3.8 makes the functional dependency of $\lambda(I_u, S_{cr})$ on the turbulence intensity I_u and the Scruton number S_{cr} obvious. This function will be discussed further in section 6.1.1.

In the case of p_{n_j} and p_{St_j} being uniformly continuously distributed in the intervals p_{n_j} $[a, b]$ and p_{St_j} $[c, d]$ and $0 < a < c < d < b$ the quotient of p_{n_j}/p_{St_j} can be found analytically by the Mellin convolution integral which is demonstrated in section A.4 and it results in

$$\frac{p_{n_j}(x_1)}{p_{St_j}(x_2)} = p_{n_j, St_j}(y) = \frac{1}{2}\frac{1}{b-a}\frac{1}{d-c} \cdot \begin{cases} 0 & \text{if } \quad 0 < y \leq a/d \\ d^2 - \dfrac{a^2}{y^2} & \text{if } a/d < y \leq a/c \\ d^2 - c^2 & \text{if } a/c < y \leq b/d \\ \dfrac{b^2}{y^2} - c^2 & \text{if } b/d < y \leq b/c \\ 0 & \text{if } b/c < y \end{cases} \tag{6.3}$$

where $p_{n_j, St_j}(y)$ in consequence only gives values greater than zero in the interval a/d to b/c, see Fig. 6.1 for a graphical representation of the problem.

Now the critical velocity is represented as a density function $p_{u_{crit}}(u)$ and, when knowing the distribution function of the fluid velocity in the lifetime of the structure, the occurrence probability of vortex shedding can be computed.

6.1.1 Critical Velocity u_{crit} Reduction Function $\lambda(I_u, S_{cr})$

The critical velocity reduction function $\lambda(I_u, S_{cr})$, as has already been mentioned, introduces the widening of the structural reaction function along the critical velocity ratio u/u_{crit} axis and thus consequently introduces the model to the evaluation of the critical velocity probability density function $p_{u_{crit}}(u)$.

So why do we need do to this? When computing the probability of vortex shedding occurrence we cannot only look at the density function of the critical velocity u_{crit} itself, but we have to take into account that vortex shedding and concomitants do not only appear at a critical velocity ratio $u/u_{crit} = 1.0$. Shifting the critical velocity density function $p_{u_{crit}}(u)$ to the left increases the vortex shedding occurrence probability Eq. (6.7) and thus takes the phenomenon into account. Generally the critical velocity reduction function $\lambda(I_u, S_{cr})$ will be between $0 < \lambda(I_u, S_{cr}) < 1.0$ and is smaller for low Scruton numbers and decreases when increasing the turbulence intensity I_u.

Critical velocity reduction function $\lambda(I_u, S_{cr})$ for Vickery and Basu

In the case of the Vickery and Basu approach the critical velocity reduction function $\lambda(I_u, S_{cr})$ can be found making some considerations to the model equation, Eq. (2.34) where we want to find the values for $y_{0,\sigma}/D$ to be zero for turbulence intensity I_u, Scruton number S_{cr} and critical velocity ratio u/u_{crit}. Setting Eq. (2.34) equal to zero would result in $\zeta_a c_1^2 c_2^2 = 0$ as all terms are greater than zero[2] this condition cannot be fulfilled. But

---

[2] ζ_a of course could be zero but to obtain numerical stability it is set to a very small value instead; remember in Eq. (2.34) ζ_a is used as divisor.

what is feasible is to fulfill the condition $y_{0,\sigma}/D \le \varepsilon$, with a small ε e.g. $\varepsilon = 10^{-3}$, it showed to be more convenient to find the values by a numerical search method.
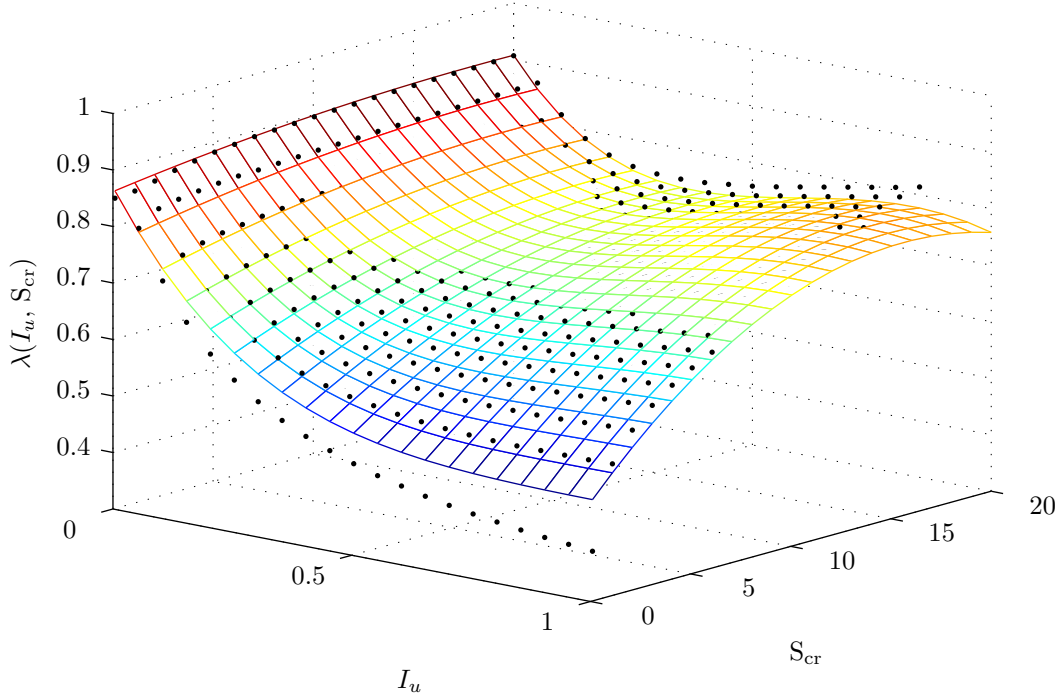

Figure 6.2 – Critical velocity reduction function $\lambda(I_u, \mathrm{S_{cr}})$ for the Vickery and Basu approach; dots indicate numerically obtained values and polynomial surface fit

This was done for discrete values of turbulence intensity I_u and Scruton number $\mathrm{S_{cr}}$ which are shown in Fig. 6.2 as dots; to have continuous values a polynomial surface function of order two for the Scruton number $\mathrm{S_{cr}}$ and order four for the turbulence intensity I_u were fitted to the discrete points by the Levenberg Marquardt minimization method. The obtained polynomial function is expressed in Eq. (6.4) and shown in Fig. 6.2.

$$\begin{aligned}
\lambda(I_u, \mathrm{S_{cr}}) =& 0.8617 - 1.41 I_u + 0.005097\,\mathrm{S_{cr}} + 1.98 I_u^2 + 0.03542 I_u \,\mathrm{S_{cr}} - 0.0001395\,\mathrm{S_{cr}}^2 \\
& - 1.272 I_u^3 + 0.0218 I_u^2 \,\mathrm{S_{cr}} - 0.001128 I_u \,\mathrm{S_{cr}}^2 + 0.3157 I_u^4 - 0.02283 I_u^3 \,\mathrm{S_{cr}}
\end{aligned} \tag{6.4}$$

Due to the complexity the polynomial function $\lambda(I_u, \mathrm{S_{cr}})$, Eq. (6.4), can be reduced to a one dimensional function which is valid for a Scruton number $\mathrm{S_{cr}} > 5$ and results to be

$$\lambda(I_u, \mathrm{S_{cr}} = 5.0) = 0.8836975 - 1.261100 I_u + 2.0890 I_u^2 - 1.38615 I_u^3 + 0.3157 I_u^4. \tag{6.5}$$

This function will show slightly lower values for the critical velocity ratio u/u_{crit} too and thus gives conservative results. We remember section 1.1 where the stratification conditions for the atmosphere where studied with the conclusion that for high wind velocities the atmosphere enters into a neutral condition which has to be taken into account; in chapter 7 this procedure is shown in detail.

6.1.2 Maximum Wind Velocity Distribution

In order to be able to compute the occurrence probability of vortex shedding the distribution of the fluid velocity has to be known. Talking about wind the distribution function for the mean wind velocity is known, as well as the distribution of the maximum wind velocity $F_{\hat{u}}$ in the structure's lifetime. In [Solari, 2000], a selection of the most common

distribution functions are found along with criticism for each of them. Based on the conclusions made in [Solari, 2000] using a Gumbel distribution[3] has two main advantages: firstly when the parent distribution is represented by the Weibull model the tail of the Gumbel distribution falls off in an exponential form as demanded by the Weibull model and secondly the parameters for a Gumbel distribution can be estimated quite easily. The cumulative distribution function for a Gumbel distribution is

$$F_{\hat{u}}(u) = e^{-e^{-\beta(u-\mu)}}, \quad -\infty < u < \infty \tag{6.6}$$

with β and μ being distribution parameters; the mean found by $\mu + \gamma/\beta$, γ is the Euler Mascheroni constant [Abramowitz and Stegun, 1972]; the standard deviation is found by $\pi/(\beta\sqrt{6})$; the distribution function can be found in [Bucher, 2009].

6.1.3 Occurrence Probability of Vortex Shedding for Different Natural Frequencies n_j

Now the last step is to calculate the occurrence probability p_f of vortex shedding, this can be analytically expressed accordingly to [Fellin and Lessmann, 2005] with a single integral involving the maximum wind velocity distribution function $F_{\hat{u}}$, Eq. (6.6), and the probability density function $p_{u_{crit}}(u)$, Eq. (6.2), of the critical velocity u_{crit}; remember $y = f(u)$, for simplicity in Eq. (6.7) y is directly notated.

$$p_f = P\left(u_{crit} < \hat{u}_{max}\right) = \int_{-\infty}^{\infty} [1 - F_{\hat{u}}(u)] \, p_{u_{crit}}\left(u - \frac{n_{j_{det}}D_{det}}{\mathrm{St}_{j_{det}}}\lambda\left(I_u, \mathrm{S_{cr}}\right)\right) \mathrm{d}u \tag{6.7}$$

The reduction to a single integral is possible due to the effect that the two functions $F_{\hat{u}}$ and $p_{u_{crit}}(u)$ can be considered independent. With the occurrence probability p_f we now have a measure of how likely vortex shedding occurs and can compare the values of p_f with regulations given in the different codes.

With Eq. (6.7) we are able to compute the occurrence probability p_f of vortex shedding, where in $p_{u_{crit}}(u)$ also the model's uncertainty of the Strouhal model [Strouhal, 1878] is included through the uncertainty of the Strouhal number St. What is missing is the model's uncertainty of the Vickery and Basu model which impacts through $\lambda(I_u, \mathrm{S_{cr}})$. As we are mainly interested in knowing the occurrence probability $p_f > 0$ in this case the model's uncertainty of the Vickery and Basu model was set to be zero.

6.2 Probability Distribution due to Varying Structural Parameters

After evaluating the vortex shedding occurrence probability in a second step the behavior of vortex shedding due to variation of the structural parameters is studied to obtain a sophisticated basis for the probabilistic fatigue analysis, see section 6.3. By extracting the structural parameters – the structural damping ratio ζ_s and the structural natural frequency n_j – the idea is to see if a generally valid distribution can be applied in order to represent the distribution density function of the structure's response $y_{0,max}/D$.

---

[3]Or Type I largest distribution. As in recent research different distribution functions are found to be more sophisticated, this new distribution function can also be used without any limitation.

In chapter 5 the structural damping ratio ζ_s for all analyzed models could be identified as one of the most influential parameters, in the case of the critical velocity ratio $u/u_{crit} = 1.0$. The fatigue analysis in section 6.3 introduces the wind velocity as a probability density function and thus the influence of variations in the structural damping ratio has to be analyzed for values of the critical velocity ratio other than one too.
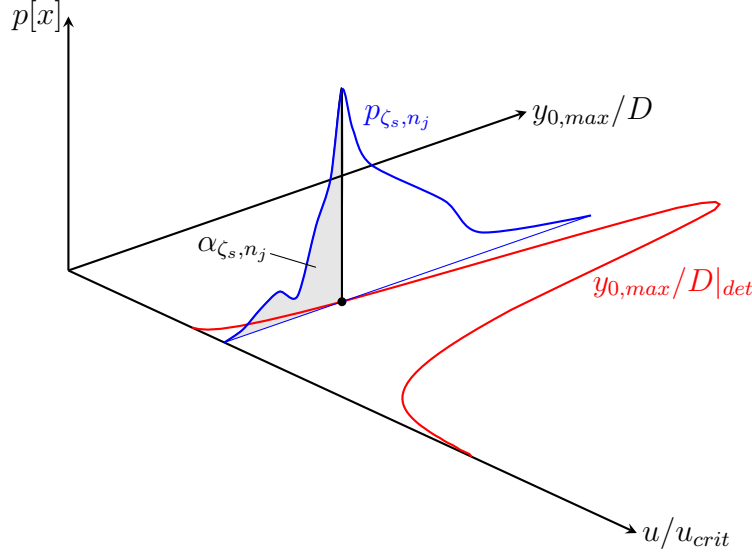

Figure 6.3 – Illustration of the quantile value α_{ζ_s,n_j} as gray shaded area for a certain critical velocity ratio u/u_{crit} along the deterministic reaction value $y_{0,max}/D|_{det}$ – red line; The probability density function p_{ζ_s,n_j} obtained due to variations in the structural damping ratio ζ_s and the structural natural frequency n_j is drawn in blue.

For this reason we analyze two different aspects, first of all if a generally valid probability density function to describe the variations in the structural damping ratio ζ_s and the structural natural frequency n_j can be found for all different critical velocity ratios u/u_{crit} and second the quantile value for the reaction obtained by using the deterministic parameters for the structural damping ratio ζ_s and the structural natural frequency n_j. The aim of the second step is to create a quantitative measure of the importance of using distributed parameters for describing the structure.

As illustrated in Fig. 6.3 we can compute the quantile value α_{ζ_s,n_j} for every critical velocity ratio u/u_{crit} due to variations in the structural damping ratio ζ_s and the structural natural frequency n_j with

$$\alpha_{\zeta_s,n_j} = P\left[y_{0,max}/D(p_{\zeta_s,n_j}) \leq y_{0,max}/D|_{det}\right]. \tag{6.8}$$

Of course the quantile value could be evaluated separately for the parameters, but due to the computation cost both parameters are varied simultaneously.

6.2.1   General Introduction to the Quantile Value α_{ζ_s,n_j}

As the approaches are too complex to find the probability density function p_{ζ_s,n_j} analytically using algebra of random variables as done in section 6.1, we use numerical methods to find the discrete probability density and then compute a closed form probability density function based on the *kernel* approach smoothing technique [Bowman and Azzalini, 1997].

The basic idea of the *kernel* approach according to [Bowman and Azzalini, 1997] and [Whittle, 1958] is that instead of using intervals, as done by histograms, a smooth

function is used which respects the assumption of the underlying density function to be smooth too. Furthermore, the dependence on the histogram interval width has no influence on the shape of the probability density function. As a base building block a smooth *kernel* function is used instead of a box-like one for histograms and every single smooth function is centered directly over each observation. Detailed descriptions can be found in [Parzen, 1962], [Whittle, 1958] and in [Rosenblatt, 1956] which gives some remarks on non-parametric estimates of density functions. The analysis was carried out with Gaussian normal probability density functions as *kernel* functions.

Following a short and general introduction to the numeric evaluation of the quantile value α_{ζ_s,n_j} of the deterministic model reaction value is given, the introduction of the single values are enriched by forecasts to the numerical procedure in order to rise the comprehensibility.

6.2.2 Numerical Evaluation of the Quantile Value α_{ζ_s,n_j}

In a first step the idea is to generate a discrete probability density for varying structural damping ratios ζ_s and structural natural frequencies n_j around a deterministically chosen value, which is shown in a figurative way in Fig. 6.3 and in an idealized way in Fig. 6.4 where the ranges of variation are exaggerated to underline the phenomenon and make the discrete probability density function more visible.

To guarantee a general validity a set of 500 chimneys is created over a physically meaningful parameter range by a Sobol' quasi random set [Sobol', 1967] and then all 500 chimneys are evaluated for different critical velocity ratios u/u_{crit}.
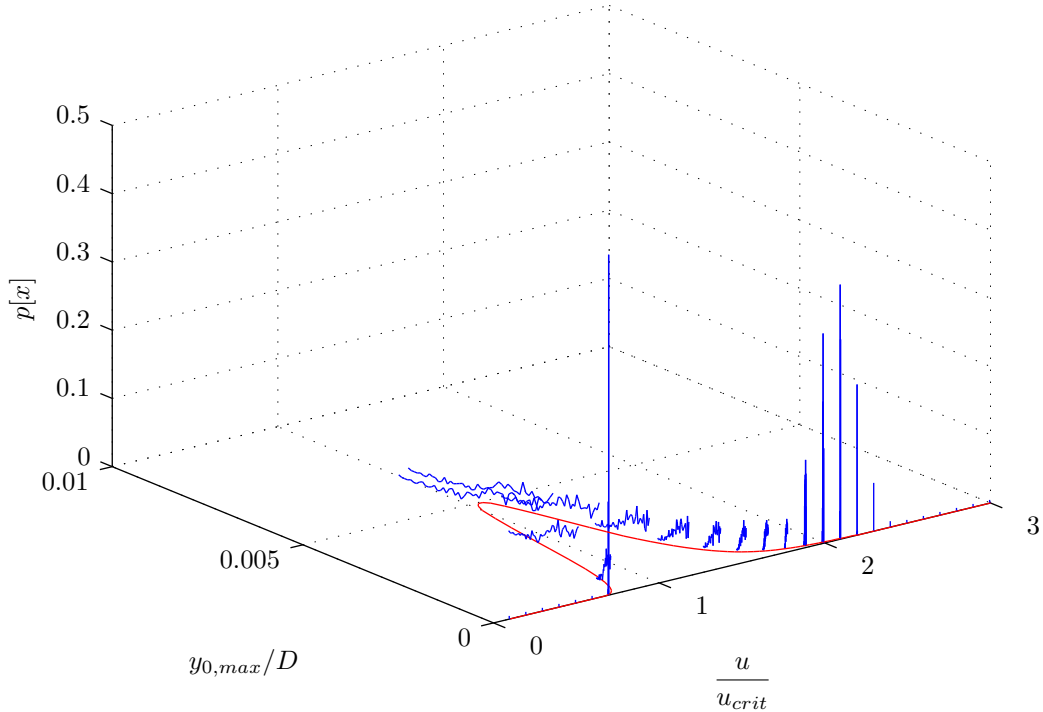
Figure 6.4 – Model reaction function with deterministically chosen values in red and blue the obtained numerical discrete probability density function for random variables ζ_s and n_j

In Fig. 6.4 the red line represents the solution with deterministically chosen structural values for different critical velocity ratios u/u_{crit}, the blue lines draw the discrete probability density function around the fixed values for u/u_{crit} due to contemporaneous variations in

ζ_s and n_j. The idealized representation in Fig. 6.4 allows to see the general behavior of the distribution, which the closer the critical velocity ratio u/u_{crit} goes to 1.0 the wider the probability density function p_{ζ_s, n_j} becomes, which was already predicted in chapter 3. To raise the compressibility and underline this behavior in Fig. 6.5 the 0.25 and 0.75 confidence interval as well as the variance of the discrete probability density function is shown for different values of u/u_{crit}.

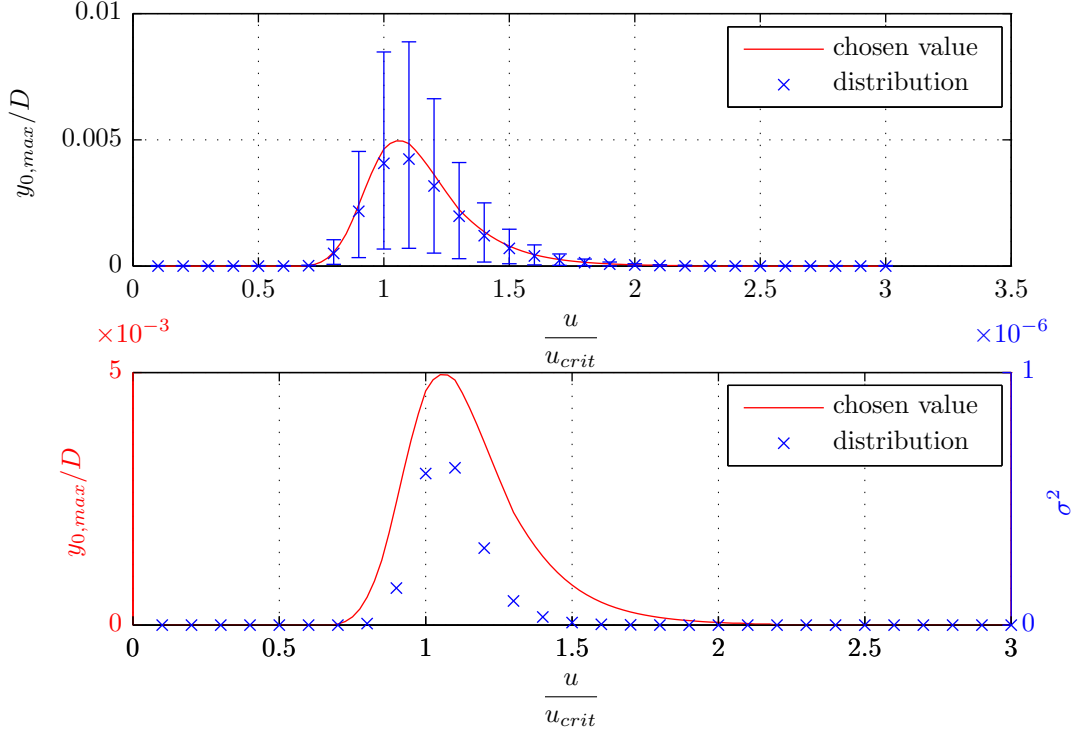**Figure 6.5** – Top: model reaction function with deterministically chosen values, mean and 0.25 and 0.75 confidence intervals for random parameters. Bottom: model reaction function with deterministically chosen values and the variance of the reaction due to random parameters.

The second step is to find the appropriate *kernel* smoothing function for the discrete probability density function for a fixed value of u/u_{crit} due to contemporaneous variations in ζ_s and n_j. The obtained probability density function p_{ζ_s, n_j} from the *kernel* approach is in closed from thus if a certain shape for all critical velocity ratios u/u_{crit} is conserved it would be easily identified. Unfortunately this is not true and so no direct correlation between the critical velocity ratio u/u_{crit} and the shape of the probability density function p_{ζ_s, n_j} can be derived.

Anyhow, the generated probability density function p_{ζ_s, n_j} can be used to evaluate the quantile value α_{ζ_s, n_j} of the deterministic model reaction value. Of course the quantile value α_{ζ_s, n_j} can alternatively be calculated in discrete form by dividing the number of samples smaller than the deterministic value by the total number of samples. Here, the more sophisticated approach based on the *kernel* smoothing function is used.

The advantage of using a numerical method to generate discrete data and then finding the probability density function using a smoothing technique shows to be a fast and comfortable way to obtain probabilistic information out of complex models, without the need of studying in detail possibly suitable probability density functions, which becomes obvious when looking at Fig. 6.4. As a first attempt using known probability density functions was tried, which lead to unsatisfying results.

6.2.3   The Quantile Value α_{ζ_s,n_j} for the Vickery and Basu Model

As the approach is numerically based, a computed example is essential; starting with the first step of computing the quantile value α_{ζ_s,n_j} of the deterministic model reaction value based on a set of 500 chimneys. The chimneys where generated with a Sobol' quasi random set [Sobol', 1967], as has already been mentioned. The single parameter variations are for the structural damping ratio $\zeta_s \in [0.001, 0.01]$, for $m/\rho/D^2 \in [100, 300]$, for $n_j D^2/\nu \in [10^5, 10^6]$, for the slenderness $H/D \in [20, 40]$ and the turbulence intensity $I_u \in [0.0, 0.5]$ where the regulation of an at least neutral atmospheric condition was introduced; this is explained in detail in section 4.5. All 500 chimneys where analyzed in 11 steps for the critical velocity ratio u/u_{crit} in the range $[0.1, 3.0]$. The surface roughness of the chimneys was set to $\epsilon/D = 0.001$.
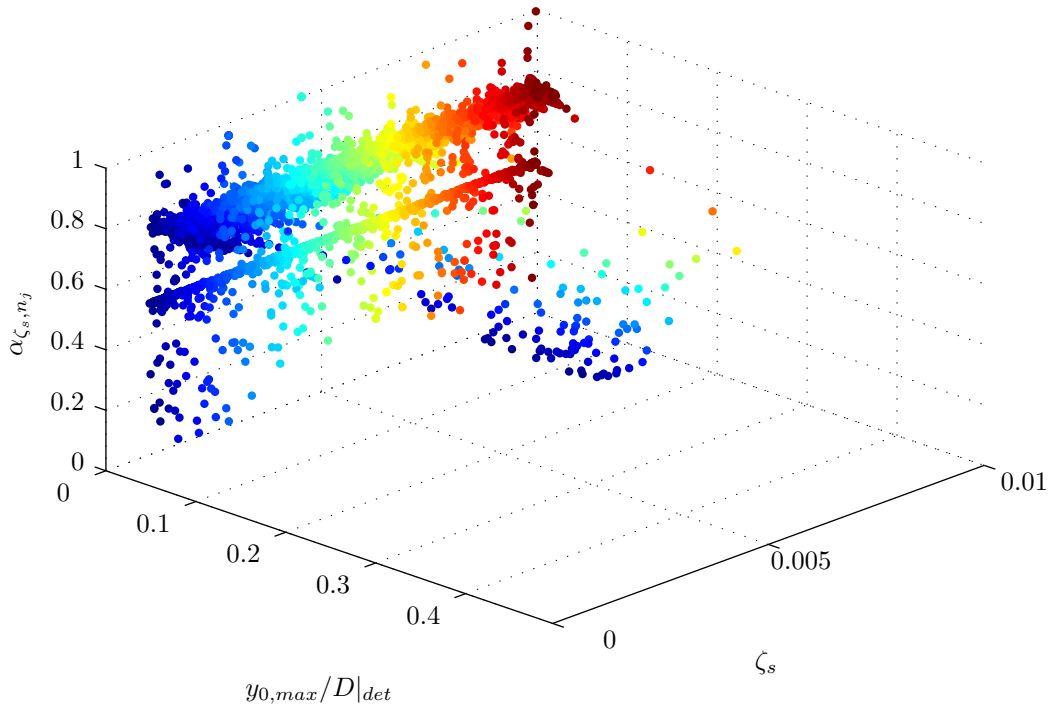

Figure 6.6 – The quantile value α_{ζ_s,n_j} of the deterministic model reaction value for 500 randomly selected chimneys for all different critical velocity ratios u/u_{crit} vs the deterministic model reaction value $y_{0,max}/D|_{det}$ and the structural damping ratio ζ_s.

In order to obtain the quantile value α_{ζ_s,n_j} the chosen values the structural damping ratio ζ_s was multiplied by a factor $\zeta_{s_{dis}} \in [0.5, 2.5]$ and the natural frequency n_j by a factor $n_{j_{dis}} \in [0.83, 1.17]$. Both values were varied simultaneously 1000 times in order to save some computational effort and the obtained discrete probability density function was smoothed with the *kernel* approach and then integrated to obtain the quantile value α_{ζ_s,n_j} for every deterministic model reaction value $y_{0,max}/D$.

   Fig. 6.6 shows the quantile value α_{ζ_s,n_j} of the deterministic model reaction value for all 500 chimneys for all 11 critical velocity ratios u/u_{crit} which thus form a cloud of 5 500 data points. The dots where shaded from dark blue for small values of ζ_s to dark red for high values of ζ_s to indicated the structural damping ratio, hereby the shading becomes clear. Fig. 6.7 shows the represented sample obtained by a Sobol' quasi random set. Both figures, Fig. 6.6 and Fig. 6.7, do not really give further information other than that big deterministic structural reaction values $y_{0,max}/D|_{det}$ result from weakly damped chimneys – blueish shaded dots – and for these chimneys the quantile value α_{ζ_s,n_j} of

the deterministic model reaction value seems to be considerably high. Sorting the dots according to the critical velocity ratio u/u_{crit} as shown in Fig. 6.8 allows us to obtain more information from the computed data. Now, in every critical velocity interval we see 500 dots, one dot for every chimneys. Clearly, for small critical velocity ratios u/u_{crit} the deterministic structure reaction $y_{0,max}/D|_{det}$ is small and as the critical velocity ratio is increased the structural reaction increases with maximum responses for a critical velocity ratio $u/u_{crit} = 1.0$.
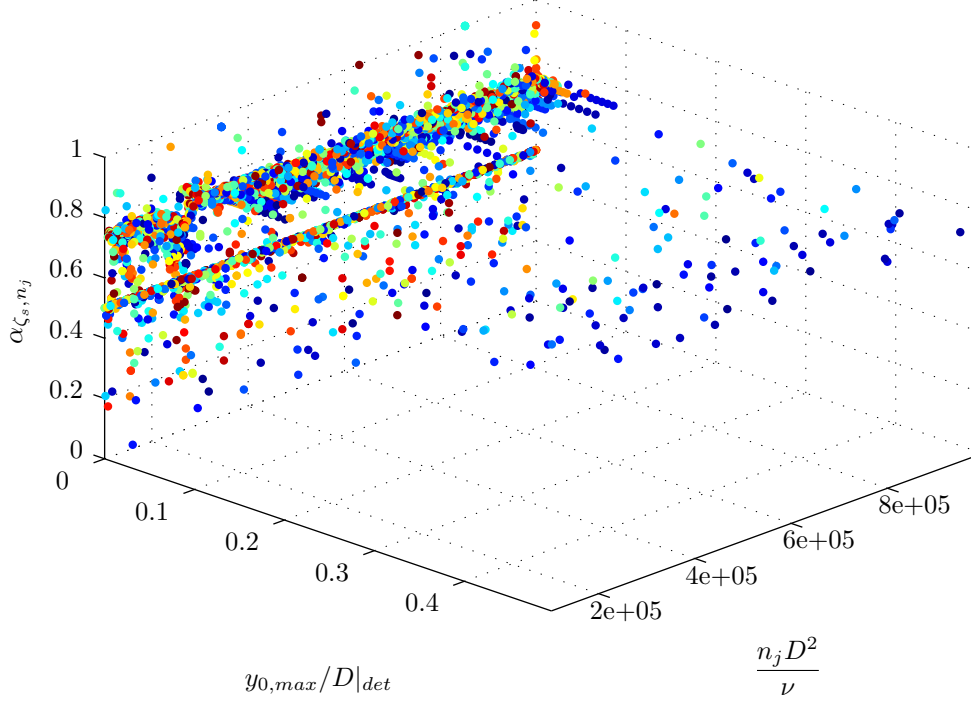

Figure 6.7 – The quantile value α_{ζ_s,n_j} of the deterministic model reaction value for 500 randomly selected chimneys for all different critical velocity ratios u/u_{crit} vs the deterministic model reaction value $y_{0,max}/D|_{det}$ and the dimensionally independent quantity $n_j D^2/\nu$.

Obviously the weakly damped structures give the highest deterministic reaction $y_{0,max}/D|_{det}$ but what is very interesting is that the quantile value α_{ζ_s,n_j} for these values is far higher – they are greater than 0.75 – this becomes visibly clearer when looking at Fig. 6.9 which is a frontal projection of Fig. 6.8. The reason for this is explained later in the text.

But to guarantee structural safety and economic design we cannot allow such high reaction values; actually we try to keep them below $y_{0,max}/D = 0.10$ or $y_{0,max}/D = 0.05$. Looking at the dot cloud, below these thresholds, Fig. 6.9, we see that no unique level for the quantile value α_{ζ_s,n_j} of the deterministic model reaction value can be obtained.

Consequently, the possible variation in the structural parameters – the structural damping ratio ζ_s and the structural natural frequency n_j – has to be taken into account to obtain a full sophisticated design chain, remember Fig. 1.2. As has already been mentioned when trying to find the quantile value α_{ζ_s,n_j} of the deterministic model reaction value, no generally valid distribution can be found to describe the probability density function of the obtained structural reaction value $y_{0,max}/D$ due to the variations in the structural parameters. As shown later, see section 7.1.5, the author chose to sample a set of possible structures around the structure described by deterministic parameters. Thus for every individual sample a deterministic lifetime is evaluated, which results together with all the samples in a discrete probability density function for the structural lifetime

due to fatigue damage. This discrete probability density function can be used further for structural reliability analysis, or to show for which parameters further investigation would be appropriate to improve the structural design.
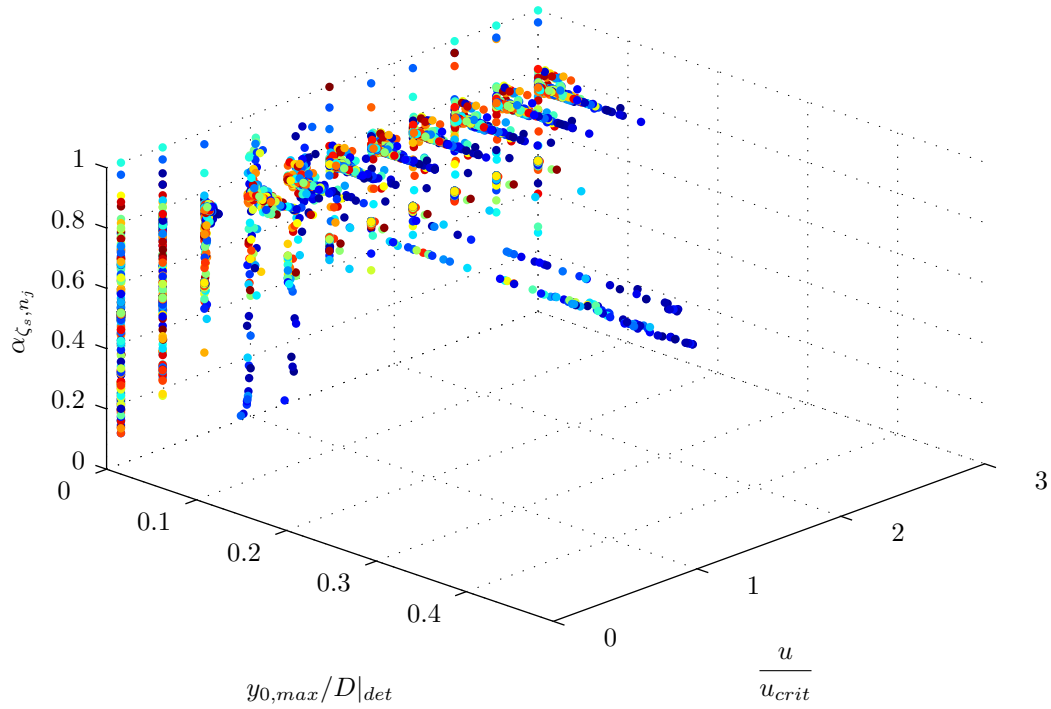

Figure 6.8 – The quantile value α_{ζ_s, n_j} of the deterministic model reaction value for 500 randomly selected chimneys vs the different critical velocity ratios u/u_{crit} and the deterministic model reaction value $y_{0,max}/D|_{det}$.

Some further comments should be made about the results visualized in Fig. 6.8 and Fig. 6.9. As has already been mentioned we identified two different regimes in the process of vortex shedding, a region with small structural reaction which is randomly Gaussian distributed and a region with high reaction values which is sinusoidal and nearly deterministic, see [Vickery and Clark, 1972] and chapter 2. Now, analyzing the results shown in Fig. 6.8 and Fig. 6.9 represents this phenomenon visually. Fig. 6.8 makes clear that in case of critical velocity ratios u/u_{crit} smaller than one we are in the broad band and thus Gaussian regime, the dots are distributed nearly uniformly between zero and one. The nearer the critical velocity ratio tends to one and we reach the lock-in region – or narrow band region – the reaction increases and for large values enters into the sinusoidal regime and the deterministic behavior is proven through the constant[4] quantile values α_{ζ_s, n_j} of the deterministic model reaction values. For critical velocity ratios greater than one a mixed behavior can be seen: the dots are somehow cumulated around a constant value but still with a considerable variation.

Fig. 6.9 sums up and shows the results expected when varying the structural damping ratio ζ_s and the structural natural frequency n_j; for small reaction values the Vickery and Basu model working in a Gaussian regime produces random results; for intermediate reactions the model works in a mixed Gaussian and deterministic regime which leads to a cumulation of the points around a constant value and for large reaction values the

---

[4]If the lower limit of $\zeta_{s_{dist}}$ is reduced to 0.10 the limit falls from 0.75 to 0.50 and thus the dependency on the interval size of ζ_s is given. But the values still stay constant which proves the deterministic characteristics of the process.

variations in the input parameters is reduced to a nearly deterministic output caused by the model working in a sinusoidal regime.
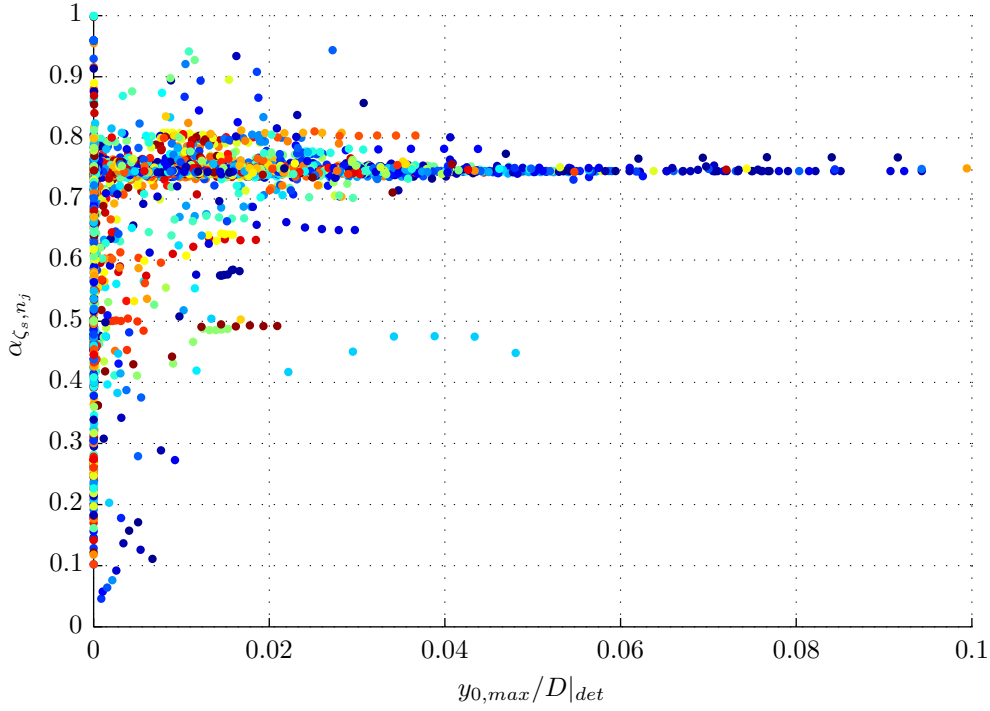

Figure 6.9 – The quantile value α_{ζ_s, n_j} of the deterministic model reaction value for 500 randomly selected chimneys for all different critical velocity ratios u/u_{crit} vs the deterministic model reaction value $y_{0,max}/D|_{det}$.

6.3   Fatigue Analysis with Probabilistic Model Reaction Values

As our final step probabilistic fatigue analysis is introduced in order to evaluate not only if vortex shedding occurs, but if the continuously induced vibrations lead to a fatigue failure of the structure. The here represented approach is mainly based on [Repetto and Solari, 2002] and [Repetto and Solari, 2007] where the concept of introducing the wind velocity $\bar{u}$ and the turbulence intensity I_u as functions of the Monin-Obukhov length L and thus as probabilistic values has ben developed but the structure properties are set as deterministic. To consider the structures together with their distributed parameters, the fatigue approach is evaluated for a set of possible similar structures, respecting the found distribution function for the structural natural frequency and the damping ratio. The author also refers to [Repetto and Solari, 2004] which provides another valuable contribution to this topic.

6.3.1   Preliminaries in Fatigue Analysis

When dealing with time periods T greater than the spectral gap [van der Hoven, 1957] interval ΔT,[5] – in this spectral gap period ΔT the characteristic parameters of the wind

---

[5]What is done here is to subdivide time into intervals ΔT which fall into the spectral gap [van der Hoven, 1957] where the mean fluid velocity and the atmospheric stratification can be set constant, see [Repetto and Solari, 2004].

field are derived – the only way to do this is probabilistically, since the probabilistic characteristics in the spectral gap period ΔT can be mapped onto the whole analysis time period T. In our case the probabilistic characteristics are a two variant random vector which contains the mean fluid velocity $\bar{u}$ and the inverse of the Monin-Obukhov length $1/L$.[6] We are considering the mean fluid velocity $\bar{u}(z)$ at different heights as function of the reference fluid velocity $\bar{u}_{ref}$ for which we create a possible series $\bar{u}_h = (2h - 1)\delta\bar{u}/2$ with $h = 1, 2, \ldots$ and $\delta\bar{u}$ velocity steps. We make the same consideration for the inverse Monin-Obukhov length $1/L$ and create a series in analogy $(1/L)_l = (2l - 1)\delta L^{-1}/2$ with $l = \ldots, -1, 0, 1, \ldots$ and δL^{-1} the inverse Monin-Obukhov length step.

In probabilistic terms now the joint probability that $\bar{u}_{ref}$ belonging to the h-th velocity interval $\Delta\bar{u}_h = (h - 1, h]\delta\bar{u}$ and $1/L$ belonging to the lth interval $\Delta L_l^{-1} = (l - 1, l]\delta L^{-1}$ is defined as $P_{hl} = [\bar{u}_{ref} \in \Delta\bar{u}_h \cap 1/L \in \Delta L_l^{-1}]$. This wind field configuration joint probability P_{hl} is a function of the territorial position, local site properties and the thermal atmospheric stratification.

Since the joint probability P_{hl} is based on parameters derived in the time period ΔT, P_{hl} describes the probabilistic characteristic in this time period for the loading condition when $\bar{u}_{ref} \in \Delta\bar{u}_h$ and $1/L \in \Delta L_l^{-1}$ and we can map these characteristics onto the effective duration time T by considering the effective time T to be a continuous sequence of time intervals ΔT and thus the effective duration time $T_{hl} = T \cdot P_{hl}$.

The next step is to compute the wind loading effect e associated with the hl-th loading condition. Considering a linear behavior of the structure we can express the loading condition $e_{hl} = \bar{e}_{hl} + e'_{hl}$ as a sum of the mean loading effect $\bar{e}_{hl}$ and the fluctuation of the loading effect e'_{hl}. Following [Repetto and Solari, 2007] the damage induced by the wind loading during the whole structural life is evaluated by collecting the wind load cycles in a discrete cycle histogram.

By using an *S-N* approach to evaluate the damage due to wind induced loading, the nominal stress s and the corresponding mean stress cycles $\bar{n}$ have to be known. The nominal wind induced stress is assumed to be $s_{hlk} = e_{hlk}$ and the corresponding mean cycles $\bar{n}_{hkl}$ can be found with an approbated cycle counting method, see section 6.3.2. Again, we create a series of possible stress amplitudes ${}^s\Delta_k = (2k - 1)\delta^s\Delta/2$ with $k = 1, 2, \ldots$ and $\delta^s\Delta$ the stress amplitude step. Combining the mean stress $\bar{s}_{hlk}$ with the mean number of cycles $\bar{n}_{hkl}$ and with the amplitude $\delta^s\Delta$ gives the cycle histogram. Based on this, for the different cycles at different stress states the damage to the structure can be computed. As mentioned in [Repetto and Solari, 2007] the Palmgren-Miner linear rule seems to be the appropriated one, see [Haibach, 2006] for further details on fatigue analysis. So we can compute the mean damage $\bar{d}_{hlk}$ created due to the hlk-th loading condition

$$\bar{d}_{hlk}(T) = \frac{\bar{n}_{hlk}(T)}{\bar{N}_{hlk}} \tag{6.9}$$

where $\bar{N}_{hlk}$ is the mean number of cycles which will lead to failure for the stress amplitude ${}^s\Delta_k$ and mean stress $\bar{s}_{hlk}$. The standard Wöhler curves [Haibach, 2006] are given for the case of a zero mean stress $\bar{s}_{hl} = 0$. Since this is normally not the case, the Goodman's relation has to be applied to transform the amplitude ${}^s\Delta_k$ into an equivalent amplitude ${}^e\Delta_{hlk}$.

$$^e\Delta_{hlk} = \frac{{}^s\Delta_k s_u}{s_u - \bar{s}_{hl} - \bar{s}_P} \tag{6.10}$$

---

[6]Of course this random vector can be of any order; as shown in [Repetto and Solari, 2004] where the wind direction is included in the analysis.

with s_u being the ultimate stress strength of the material and $\bar{s}_P$ being the stress due to permanent loads. In [Haibach, 2006] and [Repetto and Solari, 2007] we find the Wöhler curve, see Fig. 6.10, separated into three segments and we can thus compute the number of cycles $\bar{N}_{hlk}$ which lead to failure

$$
\begin{aligned}
\bar{N}_{hlk} &= \infty && \text{for} && {}^e\Delta_{hlk} \leq s_D, \\
\bar{N}_{hlk} &= \frac{a_1}{e\Delta_{hlk}^5} && \text{for} && s_D < {}^e\Delta_{hlk} < s_L, \\
\bar{N}_{hlk} &= \frac{a_2}{e\Delta_{hlk}^3} && \text{for} && s_L \leq {}^e\Delta_{hlk},
\end{aligned}
\tag{6.11}
$$

where s_L and s_D are the stress bending points and a_1 and a_2 are curve parameters which depend on the structural detail and material considered.
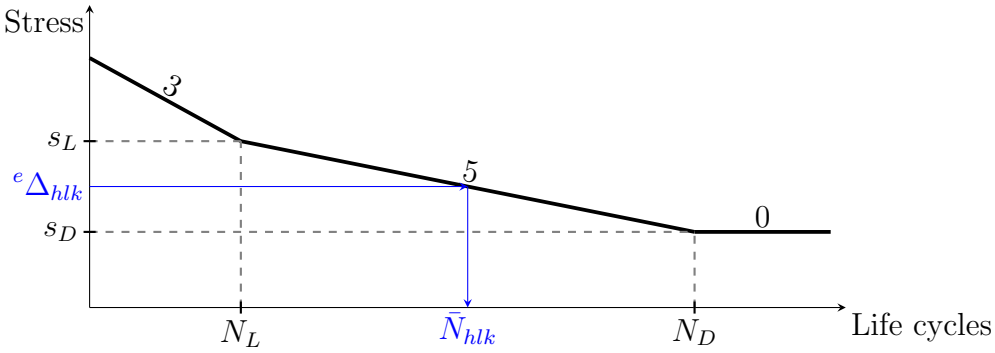

Figure 6.10 – Idealistic stress-cycle diagram (Wöhler curve) with path of finding the number of cycles $\bar{N}_{hlk}$ which lead to failure in blue.

The total mean damage $\bar{D}(T)$ for a time interval T can be computed by the sum over the cycle histogram

$$
\bar{D}(T) = \sum_h \sum_l \sum_k \bar{d}_{hlk}(T)
\tag{6.12}
$$

and based on the Palmgren-Miner linear rule $\bar{D}(T) = 1.0$ in case of failure the mean fatigue life $\hat{T}_F$ can be estimated by

$$
\hat{T}_F = \frac{1}{\bar{D}(1)}
\tag{6.13}
$$

with $\bar{D}(1)$ being the mean damage per unit time.

6.3.2   Wind Induced Stress and Cycle Counting

Returning to the structure as defined in section 2.3 and Fig. 2.2 and remembering the considerations made for the Vickery and Basu model in section 2.5 the aerodynamic wind action in the hl-th loading condition can be modeled as a stochastic stationary Gaussian process, see [Piccardo and Solari, 2000],

$$
F_{\varepsilon,hl}(z,t) = \bar{F}_{\varepsilon,hl}(z) + F'_{\varepsilon,hl}(z,t)
\tag{6.14}
$$

where ε stand for x in case of along wind forces, y in case of crosswind forces and φ for torsional moments. Again we separate the aerodynamic wind force $F_{\varepsilon,hl}(z,t)$ into a mean

$\bar{F}_{\varepsilon,hl}(z)$ and a fluctuating part $F'_{\varepsilon,hl}(z,t)$. As we consider the system to be linear we can express the stresses in a point R in analogy to the force

$$s_{\varepsilon,hl}(R,t) = \bar{s}_{\varepsilon,hl}(R) + s'_{\varepsilon,hl}(R,t) \tag{6.15}$$

which also represents a stochastic stationary Gaussian process. Furthermore, in the case of crosswind forces $\varepsilon = y$ we know the mean force term $\bar{F}_{y,hl}(z) = 0$ and also the mean stress term $\bar{s}_{y,hl}(R) = 0$. The fluctuating part of the force term $F'_{y,hl}(z,t)$ can be split into a contribution due to lateral turbulence ${}^{v}F'_{y,hl}(z,t)$ and one due to wake contribution ${}^{w}F'_{y,hl}(z,t)$.

$$F'_{y,hl}(z,t) = {}^{v}F'_{y,hl}(z,t) + {}^{w}F'_{y,hl}(z,t) \tag{6.16}$$

According to [Piccardo and Solari, 2000] and applying the quasi steady theory and considering the turbulence to be small we find the contribution due to lateral turbulence

$$ {}^{v}F'_{y,hl}(z,t) = \frac{1}{2}\rho\left(c_D + c_L{}'\right)DI_v(z)\bar{u}^2(z)v^*(z,t) \tag{6.17}$$

and the wake contribution

$$ {}^{w}F'_{y,hl}(z,t) = \frac{1}{2}\rho c_l D\bar{u}^2(z)w^*(z,t) \tag{6.18}$$

where $v^*(z,t)$ and $w^*(z,t)$ are the reduced lateral and wake excitation components. Their cross power spectrum can be expressed generally in the form

$$S^*_{\varepsilon,\varepsilon}(z,z',n) = \sqrt{S^*_{\varepsilon}(z,n)S^*_{\varepsilon}(z',n)}\,\mathrm{C}_{\varepsilon,\varepsilon}(z,z',n) \tag{6.19}$$

where $\varepsilon = v,w$ and $\mathrm{C}_{\varepsilon,\varepsilon}(z,z',n)$ is the coherence function at height z and z'

$$\mathrm{C}_{\varepsilon,\varepsilon}(z,z',n) = e^{-\kappa_\varepsilon(z,z',n)\frac{|z-z'|}{h}} \tag{6.20}$$

with κ_ε being a suitable non-dimensional quantity and h a suitable length.

Since ${}^{v}F'_{y,hl}(z,t)$ is a linear function of $v^*(z,t)$ and ${}^{w}F'_{y,hl}(z,t)$ is a linear function of $w^*(z,t)$ both force terms are random stationary Gaussian processes due to the fact that $v^*(z,t)$ and $w^*(z,t)$ are random stationary Gaussian processes which are independent from each other too. This condition allows the summation of the force terms as assumed at the beginning; the fundamental proof can be found in [Solari, 1985].

The variance of the stress process in a structural point R results to be

$$ {}^{s}\sigma_{hl}(R) = \sqrt{\mathcal{S}^2(R)\left[\chi_v^2\left(Q_v + D_v\right) + \chi_w^2\left(Q_w + D_w\right)\right]} \tag{6.21}$$

where $\mathcal{S}(R)$ maps the along wind mean force $\bar{F}_{y,hl}(z)$ to the stress in a structural point R

$$\mathcal{S}(R) = \frac{\phi_j''(0)E\rho HD^2\bar{u}^2(z_s)\phi_j(z_s)c_D\bar{K}_{yu}}{16\pi^2 M_j n_j^2} \tag{6.22}$$

with $z_s = 0.8H$ according to [Piccardo and Solari, 2000]; some further considerations will be made in the second example. χ_v, χ_w are non-dimensional quantities

$$\chi_v = \frac{\left(c_D + c_L{}'\right)I_v(z_s)K'_v}{c_D\bar{K}_{yu}}, \quad \chi_w = \frac{c_l K'_w}{c_D\bar{K}_{yu}} \tag{6.23}$$

with non-dimensional coefficients[7] K_v', K_w' and $\bar{K}_{yu}$ derived from the fluctuating part of the force term,

$$K_v' = \frac{\int_H \bar{u}^2(z) I_v(z) \phi_j(z)\, dz}{H \bar{u}^2(z_s) I_v(z_s)}, \quad K_w' = \bar{K}_{yu} = \frac{\int_H \bar{u}^2(z) \phi_j(z)\, dz}{H \bar{u}^2(z_s)}. \tag{6.24}$$

Q_v, Q_w are non-dimensional quantities related to the quasi static part and D_v, D_w are non-dimensional quantities derived from the resonant part of the structural response excitation component via the reduced generalized equivalent spectra [Piccardo and Solari, 1998]

$$Q_\varepsilon = \int_0^{n_j} S_{\varepsilon,eq}^*(n)\, dn, \quad D_\varepsilon = \frac{\pi n_j}{4\left(\zeta_s - \zeta_a\right)} S_{\varepsilon,eq}^*(n), \tag{6.25}$$

defined in appendix A.5. All these quantities are related to the lh-th load configuration; to increase the readability no additional lh subscripts where added. The expected frequency of the stress process is given by – see [Repetto and Solari, 2002] –

$$^s\nu_{hl} = \sqrt{\frac{n_j^2\left(\chi_v^2 D_v + \chi_w^2 D_w\right)}{\chi_v^2\left(Q_v + D_v\right) + \chi_w^2\left(Q_w + D_w\right)}}. \tag{6.26}$$

Appendix A.5 provides closed form solutions for all quantities and coefficients not shown above. Based on the closed form solutions represented above we obtain the expected frequency $^s\nu_{hlk}$ of the stress process and the variance of the stress process $^s\sigma_{hl}$ analytically. In consequence, this allows us to compute the mean number of cycles $\bar{n}_{hlk}(T)$ for any hlk-th load configuration

$$\bar{n}_{hlk}(T) = T P_{hl}{}^s\nu_{hl}\left[\exp\left(-\frac{(k-1)^2\delta^s\Delta^2}{2^s\sigma_{hl}^2}\right) - \exp\left(-\frac{k^2\delta^s\Delta^2}{2^s\sigma_{hl}^2}\right)\right] \tag{6.27}$$

in a closed form and thus the fatigue life time of the structure in closed form as well.

6.3.3 Wind Field Configuration Joint Probability P_{hl}

The wind field joint configuration probability P_{hl} is obtained by the combination of the mean wind velocity occurrence probability P_h and the occurrence probability of the atmospheric stratification condition P_l. In [Repetto and Solari, 2007] the mean wind velocity occurrence probability P_h is expressed using a Weibull model

$$P_h = (1 - F_0)\left[\exp\left(-\left[\frac{(h-1)\delta\bar{u}}{c}\right]^a\right) - \exp\left(-\left[\frac{h\delta\bar{u}}{c}\right]^a\right)\right] \tag{6.28}$$

where F_0 is the probability for $\bar{u} = 0$, a and c are model parameters. The probability of the atmospheric stratification condition P_l in the interval δL^{-1} we obtain in analogy, remember the atmospheric stratification distribution to be a function of $\bar{u}$ – see Eq. (4.10)

$$P_l(\bar{u}) = P[l\delta L^{-1} \leq 1/L](\bar{u}) - P[(l-1)\delta L^{-1} \leq 1/L](\bar{u}) \tag{6.29}$$

and due to the independence of the two probabilities $P_{hl} = P_h \cdot P_l(\bar{u})$.

---

[7]The identity of $K_w' = \bar{K}_{yu}$ is true if the v shape function is a unity function for all directions; see [Repetto and Solari, 2004] and [Piccardo and Solari, 2000] for detailed explanations.

6.3.4 Annotations

To sum up the process of evaluating the fatigue life of a structure we create three sequences: one for the mean velocity $\Delta \bar{u}_h$, one for the inverse Monin-Obukhov length ΔL_l^{-1} and one for the stress amplitude ${}^s\Delta$. Based on the probability distribution for the mean velocity P_h, Eq. (6.28), and the probability of the atmospheric stratification condition P_l, Eq. (6.29), we obtain the wind field joint configuration probability P_{hl}. With the single values $\Delta \bar{u}_h$ and ΔL_l^{-1} and the theory from section 1.1.2 and section 6.3.2 we compute the variance of the stress process ${}^s\sigma_{hl}(R)$ and the expected frequency of the stress process ${}^s\nu_{hl}$. By using the aerodynamic damping ζ_a as defined in section 2.5.2 for any hlk-th load configuration this leads to the mean damage $\bar{d}_{hlk}$ and to the mean fatigue life $\hat{T}_F$ of the structure. As this approach is expressed in closed form the probability distribution for varying structural parameters can easily be computed by numerical sampling; a closed analytical solution cannot be found due to the complexity of the evolved functions.

6.4 Conclusion

The three steps performed in this chapter allow us to characterize a structure immersed in a wind field with regards to vortex shedding. The first step provides a very easy way to evaluate whether vortex shedding occurs and in case it does, how many higher modes have to be taken into account.

The second and more academic step underlines numerically that for large structural reaction values $y_{0,max}/D$ the deterministic model reaction probability P_{ζ_s,n_j} is constant due to the deterministic characteristics of the process. Furthermore, it results in the fact that variations of the structural parameters have to be taken into account in order to guarantee a full sophisticated design.

Concluding with the fatigue analysis of the structure with distributed structural parameters in step three, the effect of vortex shedding is mapped onto an engineering design basis.

Chapter 7

Examples

The penultimate chapter should be dedicated to two examples: one which especially shows the usage of in chapter 6 evolved probabilistic models and demonstrates the usage and utility in applied engineering and one which deals with the occurrence and structural reaction due to vortex shedding.

7.1 Industrial Chimney

Since all approaches described in chapter 2 are representative for constant diameter chimneys an industrial chimney with exactly these characteristics is chosen. The principal parameters of the chimney as well as all other parameters for the atmosphere and the fatigue are represented in Tab. 7.2.

7.1.1 Project Definition and First Considerations

The chimney has to be analyzed whether vortex shedding occurs and if so, whether in the critical point R, see diagram in Tab. 7.2, a fatigue analysis has to be carried out if the structure's life time of 50a is to be secured with sufficient reliability. The structure is erected in Genoa, Italy and all characteristics of the wind field can be found in Tab. 7.2.

First Considerations

In a first step we analyze the chimney with the approaches from chapter 2 and try to understand if the chimney suffers from vortex shedding. The results are represented in Tab. 7.1.[1] The turbulence intensity $I_u = 0.1484$ for the Vickery and Basu and the ESDU approach was computed at a height $0.8H$ and in stable atmospheric stratification condition with a Monin-Obukhov length of $1/L = 0.01$, which is definitely on the safe side. With $u_{crit} = 7.62\text{m s}^{-1}$ we obtain $P[0.01 \leq 1/L](7.62) = 0.9813$, see Eq. (4.10).

Table 7.1 – Results of vortex shedding approaches
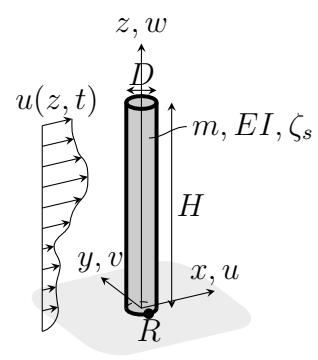
ζ_s	S_{cr}		Ruscheweyh	Vickery	ESDU	Griffin	AJI
0.009	10.05	$y_{0,\sigma}/D$	0.0299	0.0520	0.0084	0.0570	0.0342
		$y_{0,\sigma}$ [m]	0.0359	0.0624	0.0101	0.0684	0.0411
		$y_{0,\sigma}/H$	0.0012	0.0021	0.0003	0.0023	0.0014

---

[1]N.B. in Tab. 7.1 more decimal place are given than is meaningful for engineering applications.

With a Scruton number $S_{cr} = 10.05$ we would not suspect any great difficulties with vortex shedding and looking at the results in Tab. 7.1 we see that in case of the critical velocity ratio $u/u_{crit} = 1.0$ we obtain reaction values $y_{0,\sigma}$ below a possibly critical value $H/300$. Looking at the values in the last two rows in Tab. 7.1 we only see that the Vickery and Basu as well as the Griffin approach gives values near the limit of $H/300$ and that the ESDU approach is far too small compared to the other results.

7.1.2   Parameters

Table 7.2 – Parameters for the industrial chimney and diagram

Structural						Diagram				
D	1.2	m								
H	30.0	m								
ϵ/D	0.001	–								
ζ_s	0.009	–	$\zeta_{s_{dist}}$	[0.50, 1.50]						
n_1	1.27	Hz	$n_{1_{dist}}$	[0.83, 1.17]						
m	160.0	kgm^{-1}								
$\phi_1(z)$	$1 - \cos\left(\dfrac{\pi z}{2H}\right)$	–								
$\dfrac{d^2\phi_1}{dz^2}$	$z = 0 \rightarrow \dfrac{\pi^2}{4H^2}$	m^{-2}								
Atmospheric						Aerodynamic				
ρ	1.25	kg m^{-3}	C	1/6	–	c_D	0.7	–	St	0.2	–
ν	$15 \cdot 10^{-6}$	m^2 s^{-1}	b	0.10	–	$c_L{'}$	0.0	–			
κ	0.4	–	d	0.25	–	c_l	0.3	–			
z_0	0.1	m	F_0	0.1943	–	C_{zv}	6.5	–			
z_{ref}	10.0	m	a	1.549	–	l	1.0	–			
f	$6.8 \cdot 10^{-5}$	s^{-1}	c	4.629	m^{-1}s	B_0	0.05	–			
Fatigue						Material				
s_D	14.0	MPa				E	210	GPa			
s_L	26.0	MPa				s_u	510	MPa			
a_1	$6.109 \cdot 10^{13}$	MPa^5									
a_2	$8.933 \cdot 10^{10}$	MPa^3									

7.1.3   Occurrence Probability of Vortex Shedding

The values obtained by the simple vortex shedding analysis, Tab. 7.1, especially the one from Vickery and Basu, let us expect some problems with fatigue due to vortex shedding. Therefore we firstly compute the occurrence probability of vortex shedding in allusion to section 6.1. A critical velocity of $u_{crit} = 7.62\text{ms}^{-1}$ already suggests a high occurrence probability. Using Eq. (6.5) and the turbulence intensity $I_u = 0.1484$, again computed at height $0.8H$ and a Monin-Obukhov length of $1/L = 0.01$, we obtain $\lambda(I_u, S_{cr}) = 0.7382$. The simplified function from Eq. (6.5) could be used as we have a Scruton number greater than five. For the Strouhal number St we use a variability of [0.89, 1.11] and for the structure's natural frequency n_j the variability given in Tab. 7.2.

For the maximum wind velocity distribution we use the Gumbel distribution from Eq. (6.6) with the parameters $\beta = 0.8057\text{m}^{-1}\text{s}$ and $\mu = 4.92\text{ms}^{-1}$ according to [Pagnini and Solari, 2009] which gives values for a 50a return period of extreme winds. By solving the integral in Eq. (6.7) with the parameters given above, we obtain an occurrence probability of vortex shedding $p_f = 0.2237$ in the structure's lifetime and thus it is quite probable that vortex shedding will occur during the lifetime of the structure; see section 7.1.6 for some additional considerations on this behalf.

7.1.4 Fatigue Analysis

In order to perform the fatigue analysis some more conditions have to be set: first of all we have to set the interval size of the parameter ranges; for the wind velocity $\Delta \bar{u}_h$ the interval is $[0.0\text{ms}^{-1}, 30.0\text{ms}^{-1}]$ with a step width of $\delta \bar{u} = 1.0\text{ms}^{-1}$, for the inverse Monin-Obukhov length ΔL_l^{-1} the interval extends from $[-0.5\text{m}^{-1}, 0.5\text{m}^{-1}]$ and the interval step $\delta L^{-1} = 0.01\text{m}^{-1}$ and for the stress amplitude ${}^s\Delta$ an interval $[0.0\text{MPa}, 50.0\text{MPa}]$ with steps of $\delta^s\Delta = 2.0\text{MPa}$ is chosen. The analysis time period T is set to one year.

When we perform the method described in section 6.3, in Eq. (A.29) the aerodynamic damping ratio ζ_a has to be computed. We do this according to Eq. (2.32) with the speciality that when evaluating ζ_a we use a turbulence intensity for neutral atmospheric stratification condition at a height $0.8H$ based on the idea that otherwise we would take the atmospheric stratification condition into account twice which is already quite conservative in the Vickery and Basu approach.[2]
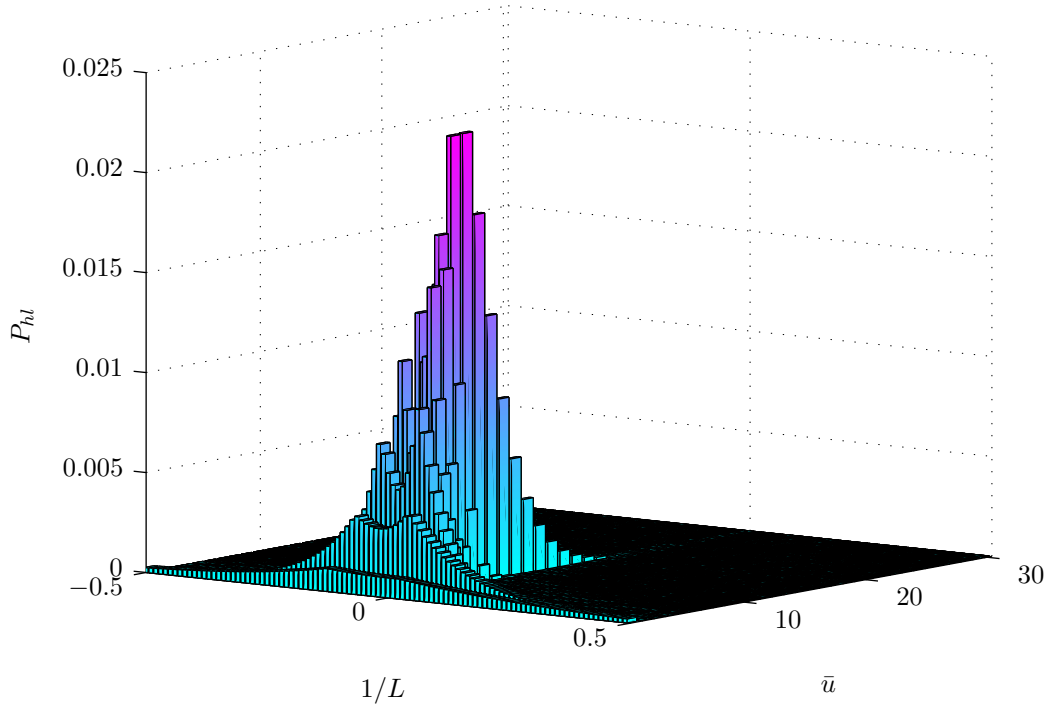

Figure 7.1 – Wind field joint configuration probability P_{hl}

In Fig. 7.1 the wind field joint configuration probability P_{hl}, see section 6.3.3, is shown which does not give much more information as to how the joint probability of the mean

---

[2]If not doing so the result will get very conservative as the term $\zeta_s - \zeta_a$ will be nearly zero for more or less all configuration cases $\Delta \bar{u}_h$ around the critical velocity u_{crit} and $\Delta L_l^{-1} > 0.1$; this was observed when studying the approach and during implantation. By using a neutral atmospheric stratification condition very sophisticated results can be obtained and this is what the author recommends to do.

wind velocity occurrence probability P_h and the probability of the atmospheric stratification condition P_l looks like.
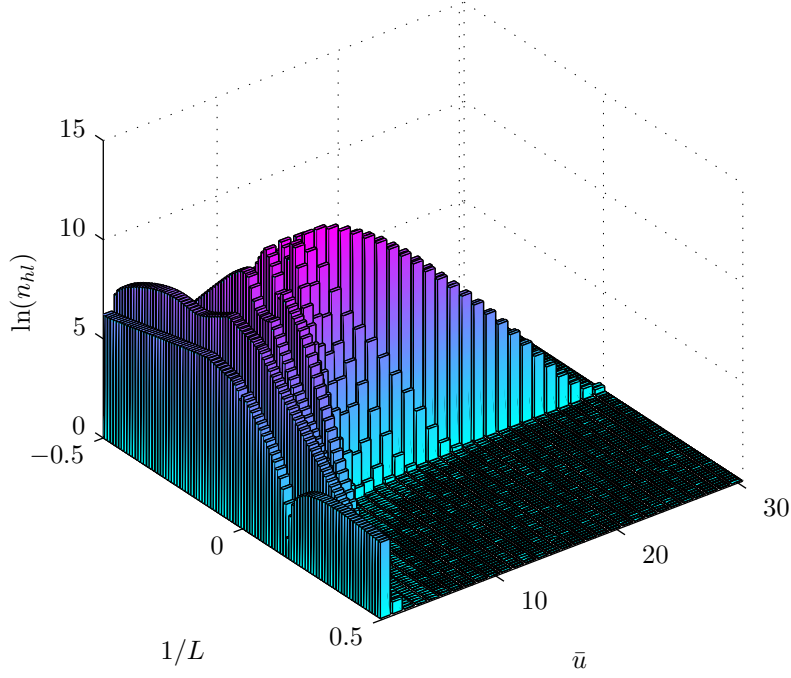

Figure 7.2 – Logarithm of mean number of cycles $\bar{n}_{hl}(T)$

Fig. 7.2 shows the logarithm of the mean number of cycles $\bar{n}_{hl}(T)$ where $\bar{n}_{hl}(T)$ means that the mean number of cycles is summed up over the stress amplitude step $^s\Delta$. A clear interpretation of Fig. 7.2 is not possible due to the smoothing by summing over the stress amplitude step $^s\Delta$.
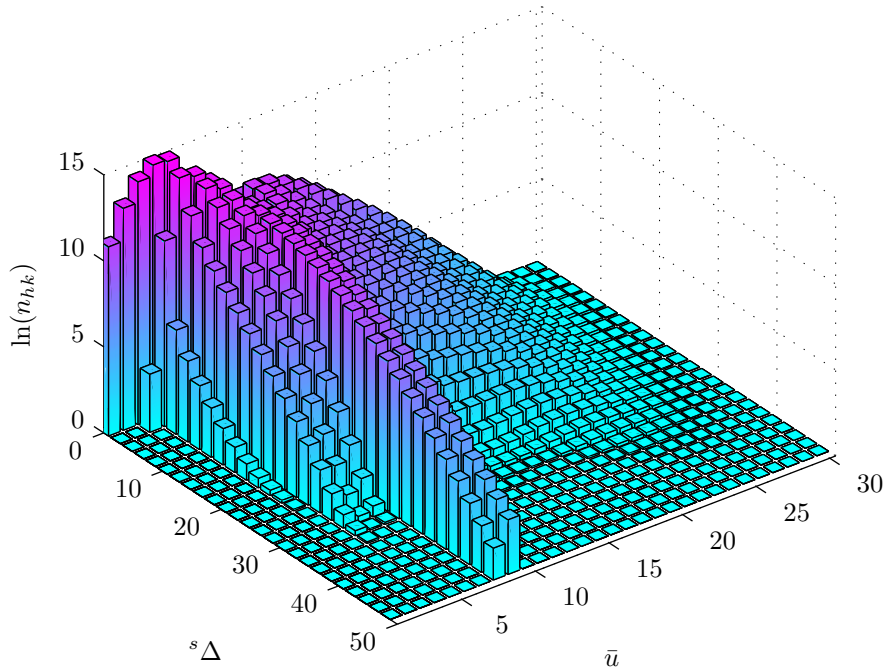

Figure 7.3 – Logarithm of mean number of cycles $\bar{n}_{hk}(T)$

Definitely more interesting is Fig. 7.3 where $\bar{n}_{hk}(T)$ means to have summed up over the different atmospheric stratification condition steps ΔL_l^{-1}. Here, clearly the vortex

shedding effect becomes visible, $\Delta\bar{u}_h$ being around $u_{crit} = 7.62\text{ms}^{-1}$. Furthermore, the reaction due to buffeting is visible in the high wind velocity region. What is obvious and is visibly proven is that the number of cycles for small stresses are the highest, as they are more probable and looking back at Fig. 7.1 we see the most probable values being around $\Delta\bar{u}_h = 6.0 - 8.0\text{ms}^{-1}$.
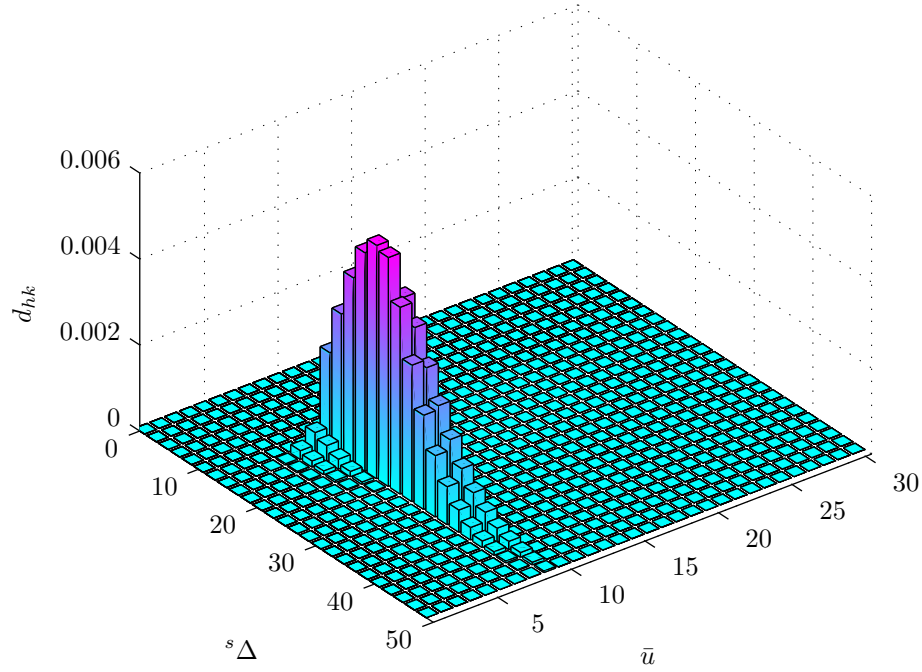

Figure 7.4 – Mean damage $\bar{d}_{hk}$

Following up this observation the mean damage $\bar{d}_{hk}$ in Fig. 7.4 becomes even clearer and looking at Fig. 7.5 we can notice this again. $\bar{d}_{hk}$ and $\bar{d}_{hl}$ are obtained in analogy to $\bar{n}_{hk}$ and $\bar{n}_{hl}$.
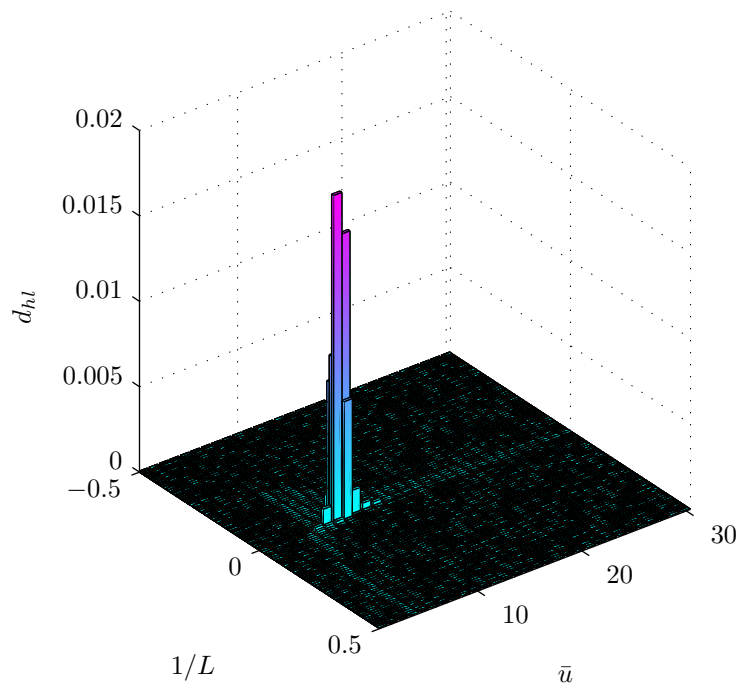

Figure 7.5 – Mean damage $\bar{d}_{hl}$

Furthermore, in Fig. 7.4 we can check whether the interval for the stress amplitude $^s\Delta$ is large enough, here this is the case as no damage seems to happen at higher stress amplitudes, see Fig. 7.4.

Combining the information from Fig. 7.1, Fig. 7.4 and the critical velocity $u_{crit} = 7.62\text{ms}^{-1}$, we see that the critical velocity of the structure falls right into the region of most probable wind velocities and so excitation happens quite frequently which increases the mean number of stress cycles $\bar{n}_{hlk}$ and due to the resonant effect increases the stress amplitudes $^s\Delta$ in the resonate region of the structure. In Fig. 7.5 additionally the importance of considering stable atmospheric stratification conditions becomes clear, as the most damage occurs right at the border between neutral and stable condition. If only neutral atmospheric stratification conditions would have been considered the damage contribution in stable condition would not have been taken into account, which would have lead to a bad underestimation of induced damage.

What becomes immediately obvious from Fig. 7.4 is that the structure suffers from fatigue due to vortex shedding.

7.1.5 Results, Reliability

After having performed the fatigue analysis we obtain a deterministic structural lifetime of the structure $\hat{T}_{F,det} = 13.12\text{a}$ which is definitely smaller than the requested lifetime of 50a. As a deterministic analysis provides no information about the probability of the result we generate a Sobol' set [Sobol', 1967] of 1 000 points in the given intervals in Tab. 7.2 for the structural damping ratio ζ_s and the structural natural frequency n_j and recompute the structural live time $\hat{T}_F$ for every reconfigured chimney.
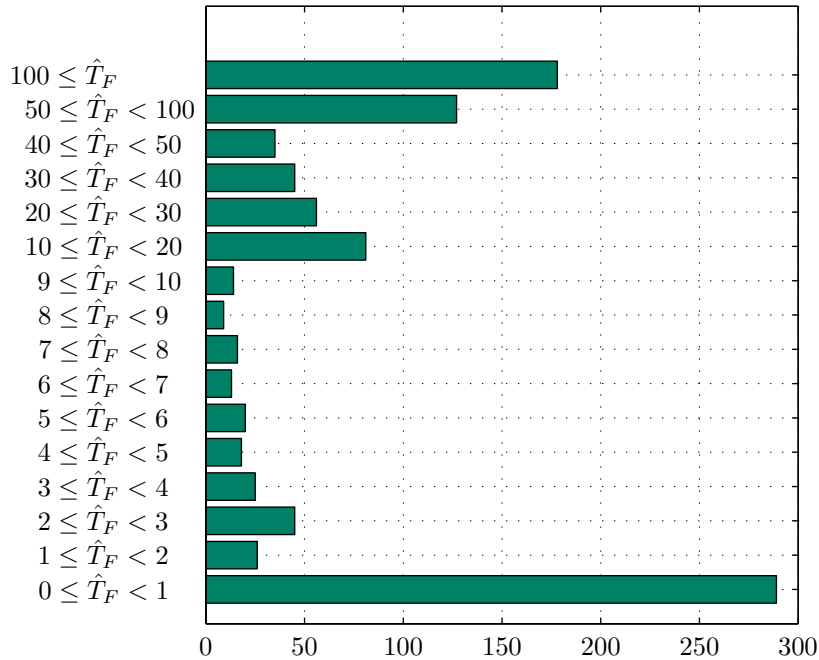
Figure 7.6 – Bar plot of structural lifetime $\hat{T}_F$ for 1 000 differently configured chimneys due to varying ζ_s and n_j.

In Fig. 7.6 the obtained fatigue lifetimes are sorted into intervals and we see that nearly one third of the chimneys don't even survive a year. The probability $P[\hat{T}_F \leq \hat{T}_{F,det}]$ is computed by dividing the number of results smaller than or equal to $\hat{T}_F$ by the total

number of samples; in this case $P[\hat{T}_F \leq \hat{T}_{F,det}] = 0.507$ and the probability to be smaller than the requested lifetime is $P[\hat{T}_F \leq 50\text{a}] = 0.695$.

As it is obvious that the structure does not fulfill the requirements we try to optimize the structure. We do this by increasing the structural damping ration ζ_s by applying a mass spring damper. Another way would be to increase the mass m which is quite difficult and more expensive with fairly less effect. The analysis was done for two more configurations: one with $\zeta_s = 0.016$ and one with $\zeta_s = 0.030$, the results are shown in Tab. 7.3.

Table 7.3 – Probabilistic fatigue lifetime results for the original and optimized structures.

ζ_s	$\hat{T}_{F,det}$	$P[\hat{T}_F \leq \hat{T}_{F,det}]$	$P[\hat{T}_F \leq 50\text{a}]$
0.009	13.12a	0.507	0.695
0.016	716.86a	0.502	0.174
0.030	92153.48a	0.545	–

Increasing the value for the structural damping ratio ζ_s increases the deterministic structural lifetime $\hat{T}_{F,det}$ drastically. Computing the structural failure probability $P[\hat{T}_F \leq 50\text{a}]$ due to fatigue we see the decrease is very moderate. Still a satisfying reliability can be achieved with a structural damping ratio $\zeta_s = 0.03$. Additionally, the importance of considering both the structural damping ratio ζ_s and the structural natural frequency n_j as random structural parameters becomes obvious by this example.

7.1.6   Conclusion

This example shows how difficult it is to predict the behavior of the structure in a wind field by only computing the maximum response of the structure in neutral atmospheric stratification condition. This can only be an indication, whether it is not too sensitive to vortex shedding per se due to a too low Scruton number.

With the help of the occurrence probability of vortex shedding a useful tool is provided not only to check how many higher modes have to be taken into account, but also to give an idea of how probable vortex shedding is. Studying Eq. (6.7) shows that a maximum $p_f \simeq 0.99$ occurs if the critical velocity $u_{crit,det} = 0.00\text{m s}^{-1}$; which is clear since the probability for small wind velocities is nearly 1.00. So, in our case with $p_f = 0.2237$, we are very close to the maximum value. The ratio of obtained occurrence probability p_f to the maximal value can be interpreted as an indicator whether the structure will suffer fatigue from vortex shedding or not; maximizing the occurrence probability means that the wind will most probably blow at the critical velocity of the structure and thus vortex shedding effects will be present with a high probability in the time domain too.

The in section 6.3 presented procedure is quite easy and gives sophisticated results, by varying the structural parameters in a given range. With a small effort probabilistic information related to distributed structural parameters can also be obtained. The randomness of the wind field is very well covered by the procedure itself and as shown in [Repetto and Solari, 2004] introducing the wind direction will require nearly no additional effort.

7.2   Stonecutters Bridge Freestanding Tower

The second example is the prediction of vortex shedding on the freestanding tower of the Stonecutters Bridge and compare them with aeroelastic wind tunnel test results. The

example deals especially with the problem of very high and tapered structures. Again all parameters of the tower and the atmospheric parameters for the different conditions considered[3] are shown in Tab. 7.4.

7.2.1 Project Definition

During the erection of the bridge vortex shedding on the tower is always interfered as there is erection equipment beside it and later the stay cables are present and thus the importance of vortex shedding phenomena will be minor. An aeroelastic model of the totally freestanding tower was tested in the wind tunnel. This test result should be compared with the results of the Vickery and Clark approach, section 7.2.2, and the approach described in section 6.3.2 based on [Piccardo and Solari, 2000].

In Tab. 7.4 the tower is represented as a simple truncated cone which is not true for both directions, as looking from the bridge deck on the tower the part below the bridge deck is an oval cone. The exact geometry as well as the mass distribution are not represented here but were respected when performing the calculations. Furthermore, the lowest part of the tower is oval, which was treated as a circle with the small dimension of the oval as we study the perpendicular wind effect on the bridge.

7.2.2 Preliminaries in Vortex Shedding on Tapered Structures

Dealing with a non-constant diameter structure, the first consideration is whether we can map this structure to a constant shaft structure as both approaches provide good results for constant shaft structures. The validity of the solution for constant diameter structures is assured for structures with little or no taper $D(z = H)/D(z = 0) > 0.5$ in [Vickery and Clark, 1972] when using $\bar{D}_{ref}$, the top third mean diameter of the structure.

For the case $D(z = H)/D(z = 0) \leq 0.5$ Vickery and Clark provide a closed form solution in [Vickery and Clark, 1972] where the basic idea is to find a reference height z_e where the mean wind velocity $\bar{u}(z)$ is equal to the critical velocity u_{crit} of the structure's section and consider the region around this section as the domain of vortex shedding excitation. Remembering Eq. (2.32), we can reformulate c_1 and c_2 as follows

$$c_1 = \frac{c_l \overline{\phi_j(ze)}}{8\pi^2 \, \mathrm{St}^2} \frac{\rho D^3(z_e)}{m_{e,j}}, \quad c_2 = \frac{\sqrt{\dfrac{\pi l}{2t}}}{\displaystyle\int_H \phi_j^2 \, \mathrm{d}z} \tag{7.1}$$

in allusion to [Vickery and Basu, 1983c]; all the other variables remain as they were defined in Eq. (2.32) and thus with Eq. (2.34) the solution is provided even for a tapered structure. The missing variables are

$$z_e \text{ is height where } \bar{u}(z) = \frac{n_j D(z)}{\mathrm{St}}, \quad t = -\frac{\mathrm{d}D(z)}{\mathrm{d}z}\Big|_{z=z_e} + \alpha_{prof} \frac{D(z_e)}{z_e}, \tag{7.2}$$

where α_{prof} is the power law exponent of the vertical wind profile, since a power law wind profile is an underlying assumption in [Vickery and Clark, 1972],

$$\overline{\phi_j(ze)} = \left[\frac{1}{2\Delta} \int_{z_e-\Delta}^{z_e+\Delta} \phi_j(z) \, \mathrm{d}z \right]^{\frac{1}{2}} \text{ with } \Delta = \frac{1}{6t} D(z_e). \tag{7.3}$$
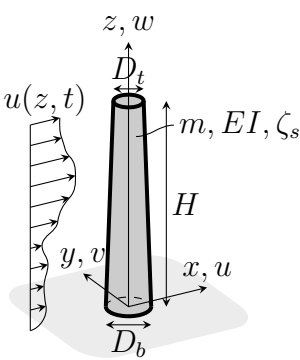
---

[3]The parameters for the structure, the atmospheric conditions and the aeroelastic wind tunnel test results were kindly provided by Prof. G. Morgenthal, BU Weimar.

A similar concept is used also by the approach shown in section 6.3.2 based on [Piccardo and Solari, 2000] where the reference heights z_{zv} and z_{zw} are derived from the mode shape function. These reference heights vary in between $0.5H$ and $0.8H$; their influence will be studied in section 7.2.5. As we are interested in the displacements we need a mapping function $\mathcal{S}(R)$ which maps the along wind mean force $\bar{F}_{y,hl}(z)$ to the top displacement of the structure,

$$\mathcal{S}(R) = \frac{\rho H \bar{D}_{ref}^2 \bar{u}^2(z_s)\phi_j(z_s)c_D \bar{K}_{yu}}{16\pi^2 M_j n_j^2}. \tag{7.4}$$

7.2.3 Parameters

Table 7.4 – Parameters for the freestanding tower of Stonecutters Bridge

Structural						Diagram
D_t	7.0	m	$\bar{D}_{ref}$	8.62	m	
D_b	18.0	m	D_t/D_b	0.39	–	
H	293.0	m				
ϵ/D	0.001	–				
ζ_s	0.01	–	$\zeta_{s_{dist}}$	$[0.50, 1.50]$		
n_1	0.183	Hz	$n_{1_{dist}}$	$[0.83, 1.17]$		
$m_{e,1}$	$3.8\cdot 10^4$	kgm^{-1}				
M_1	$2.5\cdot 10^6$	kg				
$\phi_1(z)$	$\left(\dfrac{z}{H}\right)^\xi$	–	ξ	1.9	–	

Atmospheric *sea fetch*						Aerodynamic *sea fetch*					
ρ	1.25	kg m^{-3}	$u(z)$	$u_{ref}\cdot(z/10)^{0.19}$		c_D	0.74	–	l	1.00	–
ν	$15\cdot 10^{-6}$	m^2 s^{-1}	$I_u(z)$	$0.175\cdot(z/10)^{0.19}$		c_L'	0.00	–	B_0	0.05	–
z_0	0.03	m	$I_v(z)$	$0.74\cdot I_u(z)$		c_l	0.30	–	St	0.20	–

Atmospheric *land fetch*						Aerodynamic *land fetch*					
ρ	1.25	kg m^{-3}	$u(z)$	$u_{ref}\cdot(z/10)^{0.29}$		c_D	0.52	–	l	1.00	–
ν	$15\cdot 10^{-6}$	m^2 s^{-1}	$I_u(z)$	$0.437\cdot(z/10)^{0.29}$		c_L'	0.01	–	B_0	0.05	–
z_0	0.001	m	$I_v(z)$	$1.00\cdot I_u(z)$		c_l	0.25	–	St	0.20	–

Atmospheric *smooth fetch*						Aerodynamic *smooth fetch*					
ρ	1.25	kg m^{-3}	$u(z)$	u_{ref}	ms^{-1}	c_D	0.90	–	l	1.00	–
ν	$15\cdot 10^{-6}$	m^2 s^{-1}	$I_u(z)$	0.01	–	c_L'	0.02	–	B_0	0.05	–
z_0	0.001	m	$I_v(z)$	0.01	–	c_l	0.35	–	St	0.20	–
z_{ref}	10.0	m				C_{zv}	6.5	–			

7.2.4 Occurrence Probability of Vortex Shedding

The second preliminary step is to compute the vortex shedding probability according to section 6.1 and again the need for a reference diameter is obvious. The probability for vortex shedding is computed with the parameters for smooth flow, see Tab. 7.4. Using the reference diameter $\bar{D}_{ref} = 8.62$m and a critical velocity of $u_{crit,1} = 7.89$m s^{-1} for the first mode, the vortex shedding probability $p_{f,1} = 0.0884$ is found.

For the second mode $n_2 = 0.625$Hz the critical velocity results in $u_{crit,2} = 26.94$m s^{-1} and the $p_{f,2} = 1.4414 \cdot 10^{-7}$. The missing parameter $\lambda(I_u, S_{cr})$ is computed in analogy to Eq. (6.5) and with a turbulence intensity of $I_u = 0.01$ we obtain $\lambda(I_u, S_{cr}) = 0.7382$. Using $I_u = 0.01$ stays in contradiction to the high wind velocity but only effects the vortex shedding occurrence probability in obtaining a too large value. The Gumbel distribution from Eq. (6.6) with the parameters $\beta = 0.8057$m^{-1}s and $\mu = 4.92$ms^{-1} according to [Pagnini and Solari, 2009] is needed too.

The vortex shedding probability $p_{f,1} = 0.0884$ is quite small compared to the probability obtained for the industrial chimney, examined in our first example in section 7.1. Thus we would not expect difficulties from vortex shedding excitation for the second mode with $p_{f,2} = 1.4414 \cdot 10^{-7}$ as vortex shedding is very unlikely.

7.2.5 Structural Reaction due to Vortex Shedding

In Fig. 7.7 the vortex shedding top displacement reaction of the freestanding tower is represented for different reference wind velocities u_{ref}. The results obtained by the Vickery and Clark model were computed with parameters for smooth fetch and it clearly shows structural reactions in a wide reference velocity range. This is caused by distinctive searching of the lock-in region on the structure; regardless, the peak value underestimates the measured result slightly.
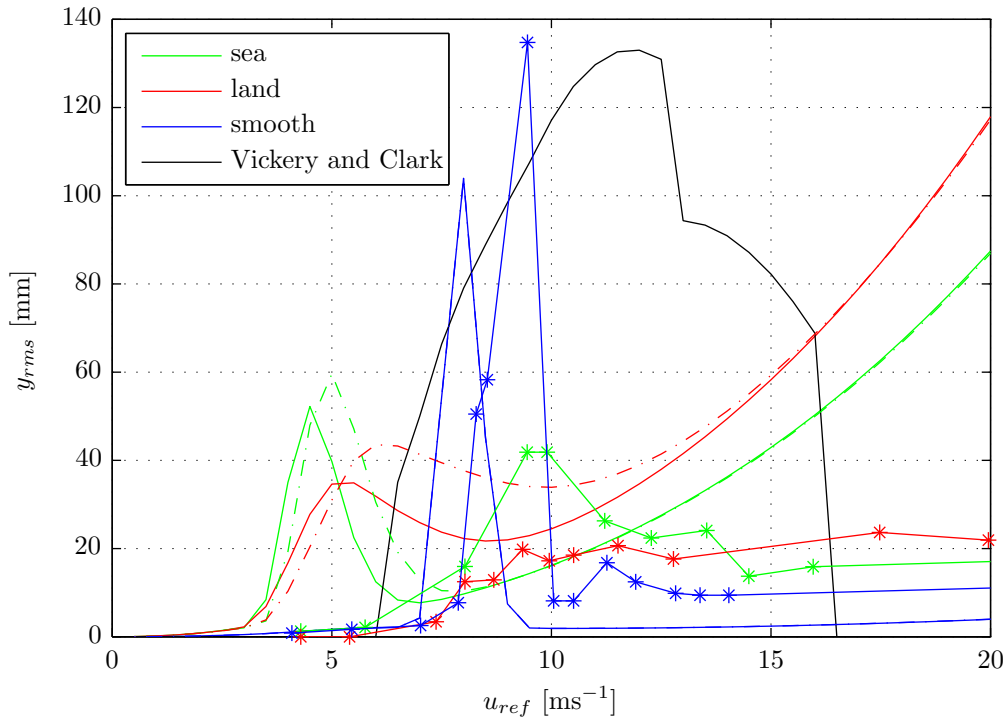

Figure 7.7 – Structural reaction due to vortex shedding for the reference wind velocity u_{ref} domain for the different approaches; the dash-dot line indicates results with reduced reference heights; the lines with asterisks are the values measured in the aeroelastic wind tunnel test digitalized from the report, and therefore no exactness can be guaranteed.

Looking at the results obtained based on [Piccardo and Solari, 2000] and described in section 6.3.2, we see that in case of *sea fetch* and *land fetch* the results represent the maximum measured response very well; green and red line. When varying the reference heights z_s, z_{zv} and z_{zw} to $0.5H$ the obtained result functions for both the *sea fetch* and

land fetch increase and shift to the right; green and red dash-dot line. This increase and right shift is due to the changes in the used reference velocity and turbulence intensity see appendix A.5. Moving to the *smooth fetch*, blue line, first we note that there is no difference depending on what reference height is chosen, as for the *smooth fetch* the wind velocity and the turbulence intensity is the same for every evaluation height. What is a bit problematic is that in case of the *smooth fetch* the peak value is not obtained and so the structural reaction due to vortex shedding is underestimated, but at least the overall critical velocity can be found very well.

The increase of the response for *sea fetch* and *land fetch* for high wind velocities u_{ref} is due to a differently designed power spectrum used in [Piccardo and Solari, 2000] to the one configured in the aeroelastic wind tunnel test; but since we are mainly interested in the vortex shedding response, we can neglect this difference.

Generally, with both approaches fairly valid predictions of the behavior of the free-standing tower can be made, but with the disadvantage that the position of the overall critical velocity cannot be found and in case of smooth flow the maximum peak value cannot be quantified. Varying the reference height allows us to make ulterior studies which help investigate the problem further. One important point is to select ξ, Tab. 7.4, with particular care in order to have a mode shape function $\phi_j(z)$ which represents the real structural behavior the best.

Chapter 8

Conclusion

> This last chapter sums up and comments the elaborated work and additionally
> a chapterwise outlook on open research fields is enclosed.

Chapter 1

As a first step the atmospheric stratification condition is discussed and a suitable and very sophisticated probability distribution is given, see Eq. (1.4). The description of the wind field itself is quite complicated but allows to represent adequately the atmospheric condition in every regime. As shown in [Repetto and Solari, 2007] the difference in the wind profile is minor, if using the more complex model provided by [Arya, 1984] and represented in section 1.1. But neglecting the probability of atmospheric stratification condition, see [Benedetti et al., 2010] and section 1.1, in the fatigue analysis, see section 6.3, will lead to unexpected failure due to vortex shedding, as documented in [Verboom and van Koten, 2010] and [Hansen, 1998].

A remark concerning the probability distribution of the atmospheric stratification condition has to be made: in [Repetto and Solari, 2007] a simple Gaussian distribution is used which is further developed in [Benedetti et al., 2010] and even an enhanced curve fitting was performed by the author see appendix B. The only problem is that the existing data set with 59 684 entries, is still far too small and a more selective analysis for different locations should be made. Regardless of this, the in Eq. (1.4) given atmospheric stratification condition density distribution is highly valid and represents the reality sophisticatedly.

Chapter 2

The powerful tool of dimensional analysis carried out in section 2.2 demonstrated what was already know: the fluid velocity can be introduced by a dimensionless critical velocity ratio. Combining the Strouhal number and the Reynolds number, see Eq. (2.7), eliminates the critical velocity but conserves the explicit solution for the structural reaction.

By describing the different models their strengths and weakness becomes clear, which is quite extensively discussed in chapter 3. Two specialties should be mentioned: one is the Vickery and Basu model which in its original form [Vickery and Clark, 1972] can be considered to be the best model. Using the model given in [Vickery and Basu, 1983c] with the added descriptions from [Simiu and Scanlan, 1996], see section 2.5, is more or less at the level of the original model in [Vickery and Clark, 1972].

The wake oscillator approach based on [Griffin and Votaw, 1972] is very powerful, section 2.7, but the solutions provided in [Griffin, 1975] do not convince at all. Due to this discrepancy the author is beginning a study trying to obtain the solution function

analytically by creating solutions in forced fluid flow conditions with a numerical flow solver based on the vortex particle method [Morgenthal, 2002].

Chapter 3

Studying the behavior of the presented models in the damping ratio domain shows, as was also noticed in [Verboom and van Koten, 2010] and [Ruscheweyh and Sedlacek, 1988], that the structural reaction obtained by the different models can differ up to an order of magnitude. Studying the limits and finding result ranges for high Scruton numbers for all models allowed us to evaluate and understand the reasons for this discrepancy in a better way. Computing the numerical derivative in the damping ratio domain, Fig. 3.2, created an initial idea of how sensitive the models are to changes to the structure damping ratio or the Scruton number respectively.

Using the model class selection does not provide a convincing result due to not taking into account overestimation or underestimation of the measured value. However, it showed in a sophisticated probabilistic way how likely the different models reach the measured results.

The response surfaces helped to analyze the behavior of the individual approaches qualitatively over a defined parameter space and underlined the particular behavior of the Vickery and Basu model well. The ESDU model on the other hand showed some defects concerning the turbulence intensity which were discussed in detail and the buffeting term could be identified as the reason.

As a final part a detailed review of the ESDU approach was elaborated due to the many inconsistencies found in the model when implementing it. This review showed some problems in the spectral formulation and the definition of a far too small aerodynamic damping ratio.

Chapter 4

The collection of parameters given in chapter 4 is mainly based on [Kareem, 1983] and, checking with current publications proves that they are still and extraordinarily valid. Using distributed multiplicands for selected parameters allowed us to fulfill the condition of parameter independence imposed by the variance based sensitivity analysis [Saltelli, 2008].

Chapter 5

With variance based sensitivity analysis the influence of the different parameters could be shown easily in a quantitative way. Estimating the approximate error made by fixing a parameter based on [Sobol' et al., 2007] gave ulterior information about which parameters can be used deterministically and which have to be taken into account with its probabilistic characteristics.

In the case of the Vickery and Basu model the sensitivity proved the high importance of the atmospheric turbulence intensity; on the contrary, for the ESDU model the buffeting term kills the strong influence of the turbulence intensity.

A further step would be to study the sensitivity not only for a critical velocity ratio equal to one, but also for other values. Since the variance based sensitivity index, defined according to [Saltelli, 2008], has the defect to be unusable if the variance of a process increases when fixing a parameter, a modified sensitivity model must be used.

Chapter 6

The developed vortex shedding occurrence probability is based on the Strouhal law [Strouhal, 1878] where the distributions for the structural natural frequency and Strouhal number are introduced analytically using algebra of random variables. The so found distribution for the critical velocity is adjusted by a term which considers the effect of vortex shedding, starting for critical velocity ratios lower than one. Choosing common, extreme value distributions for the wind velocity allows us to evaluate the probability of vortex shedding occurrence with a single integral, see Eq. (6.7), for every natural frequency of the structure. Thus a sophisticated model was evolved to determine how many natural frequencies of a structure have to be considered.

Studying the probability distribution of model reaction values in the critical velocity ratio domain due to variations in the structural natural frequency and the damping ratio allowed us to analyze if considering the variations of these parameters is necessary. Furthermore, the behavior of the Vickery and Basu model to work in random and deterministic regimes could be regenerated and in consequence for small reaction values – which a proper design aims for – possible variations of the structural parameters have to be considered.

Combining the fatigue analysis developed in [Repetto and Solari, 2007], which does already take into account the distribution of atmospheric stratification conditions and thus the distribution of the turbulence intensity and the mean wind velocity with distributed structural parameters, allowed us to obtain a full probabilistic tool for evaluating the structural lifetime due to fatigue damage. This is achieved by sampling possible similar structures respecting the distributions of the chosen parameters – the structural natural frequency and the damping ratio – and evaluating the fatigue lifetime for every one of them. Thus a discretized distribution of the structural lifetime is available, from which the structural reliability can be derived.

Chapter 7

The two examples both showed how complex the task of evaluating vortex shedding is. Especially in the first example the fatigue analysis is demonstrated and also how important it is to consider the structural natural frequency and the structural damping ratio as distributed parameters. Furthermore, the example showed that a small reaction amplitude due to vortex shedding does not mean the structure to be save against vortex shedding induced fatigue.

The second example underlines, what is expressed in [CNR, 2009], that for complex problems there is no way around aeroelastic wind model tests. The different approaches do represent the measured values, but a very accurate study has to be carried out, which is normally not possible a priori without any measured values. With experience and an accurate parameter study and variation at least very good results for smaller structures can be achieved without aeroelastic wind tunnel tests.

Conclusion

This work gives a valuable contribution in the field of vortex shedding model analysis and for the probabilistic fatigue analysis. Especially the dimensional analysis allowed us to find generally valid dimensionless quantities on which basis the different models could be compared. The found combination of Strouhal number and Reynolds number gives a

valuable contribution to the comparability and understanding of parameter configurations and of how to determine the vortex shedding model's outcome.

A further specialty of this work is that it studied five different models, beginning with very simple models like Ruscheweyh [Sockel, 1994] and the AIJ recommendations [AIJ, 2006], going over to the very sophisticated models from Vickery and Basu [Vickery and Basu, 1983c] and ESDU [ESDU96030, 1996] and concludes with a very promising, but not very well developed, model of wake oscillators [Griffin and Votaw, 1972].

Analyzing the individual models in the damping ratio domain and with the response surface as well as by performing a model class selection allowed us to demonstrate the behavior for the models in a clear and general way. The performed variance based sensitivity analysis ulteriorly showed how the different parameters determine the computed results obtained by the models. This variance based sensitivity analysis used by the author describes an innovative way of judging the quality and usability of vortex shedding models and allows to understand the behavior of all individual models over the whole parameter domain of possible structures.

The presented method to evaluate the vortex shedding occurrence probability is very sophisticated, but as shown in the examples, still simple to use. Studying the probability of model reaction values was a more academic step, but showed how the deterministically evaluated structural reactions are situated in a probabilistic framework. By adding a sampling procedure to the fatigue analysis approach [Repetto and Solari, 2007], distributed structural parameters could be taken into account and thus an enhanced structural reliability analysis could be carried out.

During this work three major opened fields for further research could be identified; one are the above mentioned missing solution functions for the wake oscillators in a high Reynolds number range, second would be trying to further improve the relation between the atmospheric stratification condition and the turbulence intensity and thirdly to study the parameter sensitivities over the whole critical velocity domain and to identify the parameter sensitivity in relation to the size of the model reaction.

Finally a short statement in the context of structural engineering seems to be necessary to underline the relevance of this work for real structures; the first and most important point is that different models do exist which do provide very different results thus it is up to the engineer to chose the *best* model. This work should give a valuable contribution and a decision basis to allow to chose always the most sophisticated and so *best* model on an elaborated and generally valid basis; here the statement at the beginning of this work has to be remembered; simplicity can and should not be an argument for a model formulation, [Verboom and van Koten, 2010]. As a second point the importance of considering distributed parameters becomes especially clear when looking at the examples in chapter 7. There the randomness in the structural damping ratio determines on the structural lifetime dominantly and not considering the turbulence intensity in terms of atmospheric stratification conditions may hide away possible fatigue problems of the structure, [Repetto and Solari, 2007].

Appendix A

Proofs and Calculus

All in the document not shown proofs and further calculus are shown here in sequence of appearance.

A.1   Proof Concerning Eq. (1.26)

Lemma

$$A \text{ grows faster than } B \text{ in case of limit } \lim_{1/L \to -\infty} \tag{A.1}$$

Proof

$$\lim_{1/L \to -\infty} \frac{h}{L} = C \frac{u_*}{|f|L} \left[1 + d \sqrt{\frac{u_*}{|fL|}} \right] = -A \to -\infty \text{ as } 1/\text{L} \to -\infty \tag{A.2}$$

$$\tag{A.3}$$

we see that $-A$ grows with

$$-A \sim \left(\frac{1}{L} \right)^{\frac{3}{2}} \tag{A.4}$$

$$\lim_{1/L \to -\infty} \ln \left(\frac{1 + x^2}{2} \right) + 2 \ln \left(\frac{1 + x}{2} \right) - 2 \arctan(x) + \frac{\pi}{2} = B \to \infty \text{ as } 1/\text{L} \to -\infty,$$
$$x = \left(1 - 16 \frac{z}{L} \right)^{1/4}, \tag{A.5}$$

and we see B grows with

$$B \sim \ln \left[\frac{1}{L} \right] \tag{A.6}$$

A.2   Proof Concerning Eq. (2.9)

Lemma

$$\int_h \phi_1^n \, \mathrm{d}z = const. \cdot h, \quad n \in \mathbb{N}_0 \text{ for } \phi_1 = 1 - \cos \left(\frac{\pi z}{2h} \right). \tag{A.7}$$

Proof

$$\int_h \left[1 - \cos\left(\frac{\pi z}{2h}\right) \right]^n \mathrm{d}z = h \int_0^1 \left[1 - \cos\left(\frac{\pi x}{2}\right) \right]^n \mathrm{d}x = const. \cdot h, \quad x = \frac{z}{h} \tag{A.8}$$

Corollary

$$\begin{aligned}
\int_h \left[1 - \cos\left(\frac{\pi z}{2h}\right) \right]^n \mathrm{d}z &= 2^n \int_h \sin^{2n}\left(\frac{\pi z}{4h}\right) \mathrm{d}z = \\
\frac{8^n h}{\pi} \cos\left(\frac{\pi z}{4h}\right) \, _2F_1 &\left[\frac{1}{2}, \frac{1-2n}{2}, \frac{3}{2}, \cos^2\left(\frac{\pi z}{4h}\right) \right] \Big|_h = \\
\frac{8^n h}{\pi} \frac{1}{\sqrt{2}} \, _2F_1 \left[\frac{1}{2}, \frac{1-2n}{2}, \frac{3}{2}, \frac{1}{2} \right] &- \frac{8^n h}{\pi} \, _2F_1 \left[\frac{1}{2}, \frac{1-2n}{2}, \frac{3}{2}, 0 \right] = \\
\frac{8^n h}{\pi} \left\{ \frac{1}{\sqrt{2}} \, _2F_1 \left[\frac{1}{2}, \frac{1-2n}{2}, \frac{3}{2}; \frac{1}{2} \right] \right. &- \left. _2F_1 \left[\frac{1}{2}, \frac{1-2n}{2}, \frac{3}{2}, 0 \right] \right\} = const. \cdot h
\end{aligned} \tag{A.9}$$

Useful Cases

$$\int_h \phi_1^0 \, \mathrm{d}z = h, \quad \int_h \phi_1^1 \, \mathrm{d}z = 0.3634 h, \quad \int_h \phi_1^2 \, \mathrm{d}z = 0.2268 h, \quad \int_h \phi_1^4 \, \mathrm{d}z = 0.1309 h \tag{A.10}$$

A.3   AIJ Recommendations for Loads on Buildings

Lemma

$$\frac{y_{0,max}}{D} = \frac{W_r(z)}{m\omega_1^2 D} \tag{A.11}$$

Demonstration

$$q(z) = \phi_1(z) P_1, \quad \ddot{P_1} + 2\zeta_s \dot{P_1} + \omega_j^2 P_1 = \frac{1}{m_1} \int_h f(z) \phi_1(z) \, \mathrm{d}z \tag{A.12}$$

in the static case

$$P_1 = \frac{1}{m_1 \omega_1^2} \int_h f(z) \phi_1(z) \, \mathrm{d}z = \frac{1}{\omega_1^2} \frac{\int_h f(z) \phi_1(z) \, \mathrm{d}z}{\int_h m(z) \phi_1^2(z) \, \mathrm{d}z} \tag{A.13}$$

and we find with $f(z) = \alpha \phi_1(z)$, $\alpha = const.$ and $m = m(z) = const.$

$$q(z) = \frac{\phi_1(z)}{\omega_1^2} \frac{\int_h \alpha \phi_1(z) \phi_1(z) \, \mathrm{d}z}{\int_h m(z) \phi_1^2(z) \, \mathrm{d}z} = \frac{\alpha \phi_1(z)}{m\omega_1^2} = \frac{f(z)}{m\omega_1^2} = \frac{W_r(z)}{m\omega_1^2} \tag{A.14}$$

A.4   Distribution of Quotients of Random Variables

Theorem

As shown in [Springer, 1979] the quotient $Y = X_1/X_2$ of two distribution density functions $f_1(x_1)$ and $f_2(x_2)$ can be found by the Mellin convolution integral

$$h(y) = \int_0^\infty x_2 f_1(y x_2) f_2(x_2) \, \mathrm{d}x_2, \quad y = x_1/x_2. \tag{A.15}$$

Calculus

Suppose the distribution functions to be uniformly continuously distributed over an arbitrary interval, see Fig. 6.1

$$f_1(x_1) = \begin{cases} 1/(b-a) & \text{if } a \le x_1 \le b \\ 0 & \text{else} \end{cases}, \quad f_2(x_2) = \begin{cases} 1/(d-c) & \text{if } c \le x_2 \le d \\ 0 & \text{else} \end{cases} \tag{A.16}$$

and $0 < a < c < d < b$ thus the Mellin integral splits into 5 parts, remember $y = x_1/x_2$; for the first part $0 < y < a/d$, a/d is the smallest possible quotient value

$$h_1(y) = \int_0^a x_2 f_1(y x_2) f_2(x_2) \, \mathrm{d}x_2 = 0, \quad x_2 < c \to f_2(x_2) = 0 \tag{A.17}$$

the second interval $a/d < y < a/c$

$$h_2(y) = \int_{a/y}^d x_2 f_1(y x_2) f_2(x_2) \, \mathrm{d}x_2 = \frac{1}{2} \frac{1}{b-a} \frac{1}{d-c} \left[d^2 - \frac{a^2}{y^2} \right] \tag{A.18}$$

the third interval $a/c < y < b/d$

$$h_3(y) = \int_c^d x_2 f_1(y x_2) f_2(x_2) \, \mathrm{d}x_2 = \frac{1}{2} \frac{d+c}{b-a} \tag{A.19}$$

the fourth interval $b/d < y < c/b$

$$h_4(y) = \int_c^{b/y} x_2 f_1(y x_2) f_2(x_2) \, \mathrm{d}x_2 = \frac{1}{2} \frac{1}{b-a} \frac{1}{d-c} \left[\frac{b^2}{y^2} - c^2 \right] \tag{A.20}$$

and the fifth interval $b/c < y$, b/c is the largest possible quotient value

$$h_5(y) = \int_b^\infty x_2 f_1(y x_2) f_2(x_2) \, \mathrm{d}x_2 = 0, \quad x_2 > d \to f_2(x_2) = 0. \tag{A.21}$$

Result

Combined and rewritten

$$h(y) = \frac{1}{2} \frac{1}{b-a} \frac{1}{d-c} \cdot \begin{cases} 0 & \text{if } 0 < y \le a/d \\ d^2 - \dfrac{a^2}{y^2} & \text{if } a/d < y \le a/c \\ d^2 - c^2 & \text{if } a/c < y \le b/d \\ \dfrac{b^2}{y^2} - c^2 & \text{if } b/d < y \le b/c \\ 0 & \text{if } b/c < y \end{cases} \tag{A.22}$$

A.5 Analytic Vortex Shedding Spectrum Formulas

Power spectrum and coherence function

The following spectrum and coherence function for the reduced turbulence component v^* are found in [Solari and Piccardo, 2001]

$$S_v^*(z', n) = \frac{9.434 \dfrac{L_v(z)}{\bar{u}(z)}}{\left[1 + 14.151 \dfrac{nL_v(z)}{\bar{u}(z)}\right]^{\frac{5}{3}}}, \quad C_{v,v}(z, z', n) = e^{-\dfrac{2nC_{zv}|z - z'|}{\bar{u}(z) + \bar{u}(z')}} \tag{A.23}$$

where L_v is the integral scale of v^* in the y direction and C_{zv} is the exponential decay of v^* along z.

The spectrum for the reduced wake excitation is already given in Eq. (2.26) according to [Vickery and Clark, 1972] and the coherence function is taken from [ESDU96030, 1996]

$$S_w^*(z', n) = \frac{1}{\sqrt{\pi}B(z)n_s(z)} e^{-\left[\dfrac{1 - n/n_s(z)}{B(z)}\right]^2}, \quad C_{w,w}(z, z', n) = e^{-\dfrac{|z - z'|}{lD}}. \tag{A.24}$$

We compute the generalized equivalent spectrum as shown in [Piccardo and Solari, 1998]

$$S_{v,eq}^*(n) = S_v^*(z_{yv}, n)\mathcal{Q}\left(k_{yv}\frac{nC_{zv}H}{\bar{u}(z_{yv})}\right), \quad S_{w,eq}^*(n) = S_w^*(z_{yw}, n)\mathcal{Q}\left(\frac{k_{yw}H}{lD}\right) \tag{A.25}$$

where the function $\mathcal{Q}$ and the later used function $\mathcal{E}$ are defined as

$$\mathcal{Q}(x) = \frac{1}{x} - \frac{1}{2x^2}\left[1 - e^{-2x}\right] \text{ for } x > 0; \mathcal{Q}(0) = 1, \quad \mathcal{E}(x) = \frac{x^4}{x^4 - 3x^2 + 4}. \tag{A.26}$$

Non-dimensional quantities and coefficients

We find the non-dimensional quantities Q_v, Q_w, D_v and D_w based on [Piccardo and Solari, 2000]

$$Q_v = \frac{1}{1 + 0.25\left[\dfrac{k_{yv}C_{zv}H}{L_v(z_{vy})}\right]^{0.63}}, \quad Q_w = \mathcal{Q}\left(\frac{k_{yw}H}{lD}\right)\mathcal{E}\left(\frac{n_j}{n_s(z_{yw})}\right), \tag{A.27}$$

$$D_v = \frac{\pi}{4\zeta_s} \frac{9.434 \dfrac{n_j L_v(z_{yv})}{\bar{u}(z_{yv})}}{\left[1 + 14.151 \dfrac{n_j L_v(z_{yv})}{\bar{u}(z_{yv})}\right]^{5/3}} \mathcal{Q}\left(k_{yv}\frac{n_j C_{zv}H}{\bar{u}(z_{zv})}\right), \tag{A.28}$$

$$D_w = \frac{\pi}{4(\zeta_s - \zeta_a)} \frac{\dfrac{n_j}{n_s(z_{yw})}}{\sqrt{\pi}B(z_{yw})} e^{-\left[\dfrac{1 - \dfrac{n_j}{n_s(z_{yw})}}{B(z_{yw})}\right]^2} \mathcal{Q}\left(\frac{k_{yw}H}{lD}\right), \tag{A.29}$$

with $z_{zv} = 0.6H$, $z_{zw} = 0.8H$,

$$k_{yv} = k_{yw} = \frac{1}{2}\left[\frac{1}{H}\int_H |\phi(z)|\,\mathrm{d}z\right]^{0.55} \text{ and } L_v(z) = 0.25 + 300\left[\frac{z}{200}\right]^{0.67 + 0.05\ln(z_0)}. \tag{A.30}$$

Appendix B

Atmospheric Stratification Condition Density Distribution

This short chapter shows the work carried out by the author based on the well- prepared and developed work [Benedetti et al., 2010]. The author used the data and the general ideas and improved the functions used to fit the measured data. To fully understand this short introduction [Benedetti et al., 2010] is indispensable and without the kind allowance of the authors of the publication of making the data used in [Benedetti et al., 2010] available, this improvement would not have been possible to achieve.

Starting with the preprocess data from the measurements made in different locations, the 59 684 data points with the daytime t, the mean wind velocity u and the Monin-Obukhov length L are analyzed if they separated into day and night as described in [Stull, 1988], see Fig. B.1.
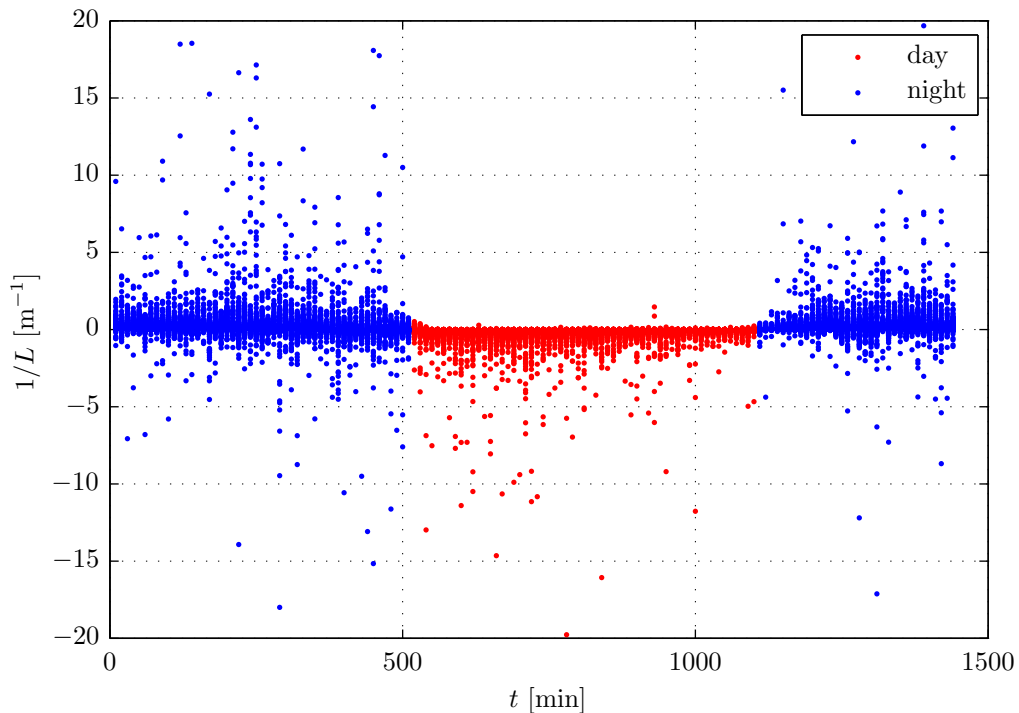

Figure B.1 – Preprocess data from the measurements; distribution over the day

In Fig. B.1 it becomes visibly clear that during the day[1] a stable atmospheric stratification does not establish, but during the night the probability of a stable and unstable atmospheric stratification condition is nearly equal.
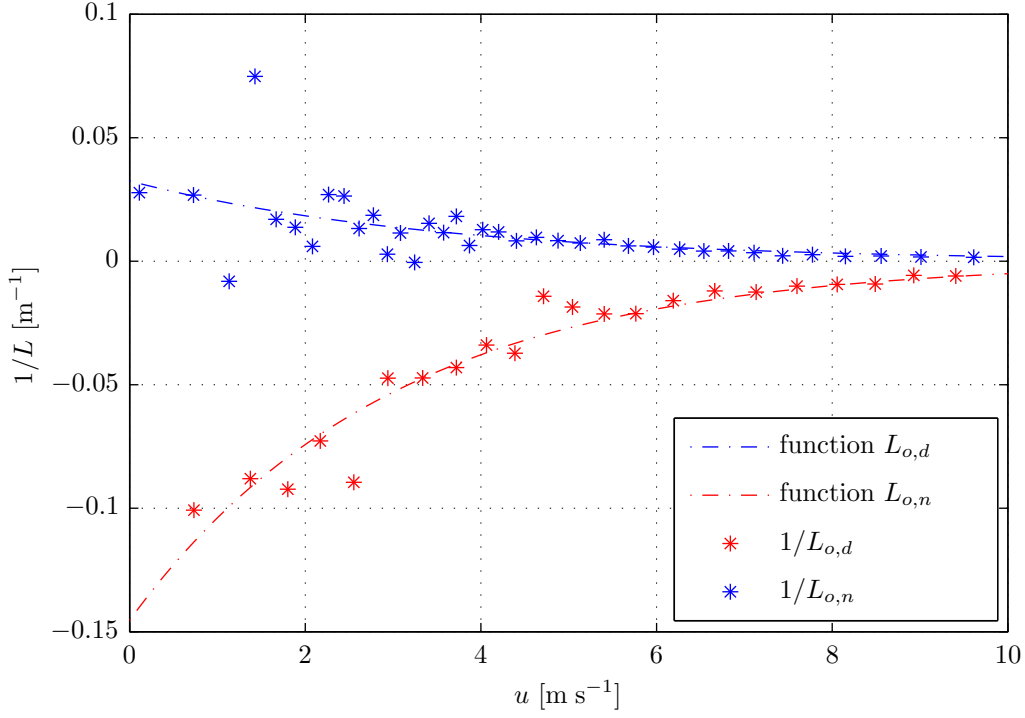

Figure B.2 – Fitted parameter functions for $1/L_{o,d}$ and $1/L_{o,n}$ and measured data
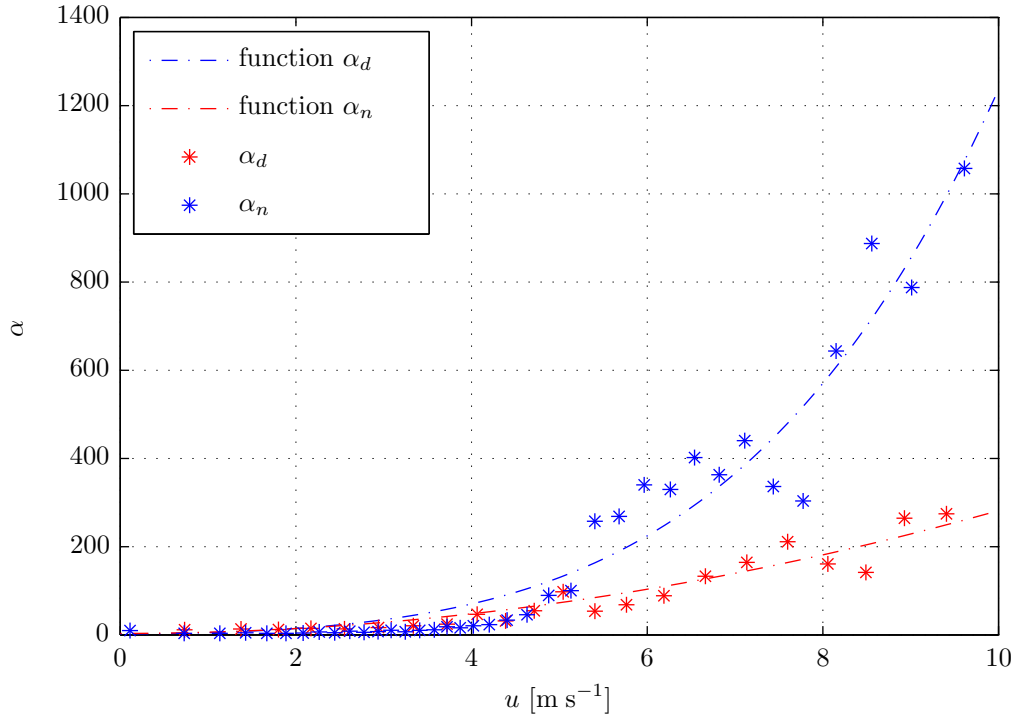

Figure B.3 – Fitted parameter functions for α_d and α_n and measured data

The second step is to create discrete distribution functions of the data for different velocities separated for the day and night values. This is done by filling single velocity intervals

---

[1]Day is defined to be between 510min and 1100min after midnight.

with an equal number, in this case 1 000, of measured values and referring them to the mean velocity of the in this interval contained data. Following the in [Benedetti et al., 2010] recommended analytic functions to represent the found discrete density functions, these are used as imposed separated for day and night. This leads to finding the right parameters for the recommended analytic functions which are functions of u and for day and night are

$$p[1/L](u) = \begin{cases} \gamma\, e^{-\beta(1/L_{o,\varepsilon} - 1/L)} & \text{if } 1/L < 1/L_{o,\varepsilon}, \\ \gamma\, e^{-\alpha(1/L - 1/L_{o,\varepsilon})} & \text{if } 1/L \geqslant 1/L_{o,\varepsilon} \end{cases} \tag{B.1}$$

where the ε in $1/L_{o,\varepsilon}$ stands for d day or n night. In order to find the parameters it is best to start with finding the location $1/L$ of maximum values of the discrete function which correspond to the $1/L_{o,\varepsilon}$ parameters. The asterisks in Fig. B.2, Fig. B.3, Fig. B.4 and Fig. B.5 represent the numerically derived parameters from the measurements after creating the velocity intervals. The irregularity of the asterisks on the velocity axis u is due to the effect of the regular velocity interval size.
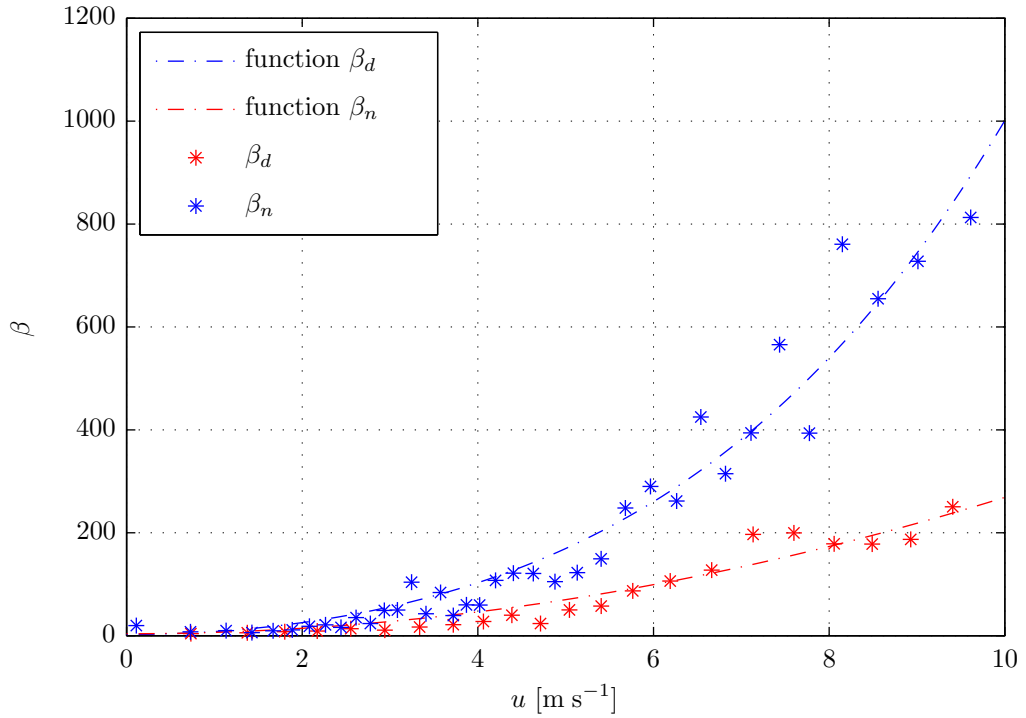

Figure B.4 – Fitted parameter functions for β_d and β_n and measured data

Before starting to fit functions to the obtained data points –asterisks– the starting parameters have to be found, otherwise the physical meaning in the low velocity range could be lost through the curve fitting which will take all data points into account. In case of day we use all values in the range $0 \leq u < 0.5$, which are 184 values, in case of night we use all values with $u = 0$ and thus we obtain 155 values; for both, day and night, we recreate the discrete density distribution function and obtain so the following starting parameters for α and β parameter functions;

$$\begin{aligned} \alpha_{0,d} &= 3.4009 & \alpha_{0,n} &= 2.3052 \\ \beta_{0,d} &= 3.7919 & \beta_{0,n} &= 2.3962. \end{aligned} \tag{B.2}$$
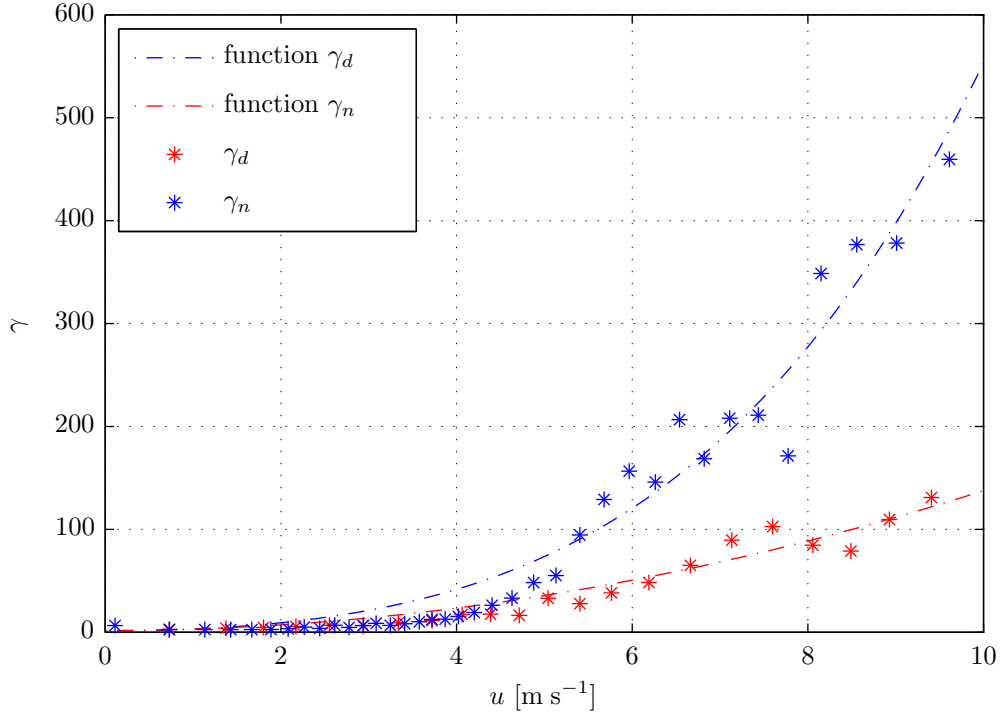
Figure B.5 – Parameter functions for γ_d and γ_n and measured data

The parameter functions represented in [Benedetti et al., 2010] are expanded with some terms in order to capture the computed data better and especially the γ parameter functions were not fitted as in [Benedetti et al., 2010], but the functional dependency is found via the condition that the infinite integral of the distribution density function has to be equal to one for every velocity u.

Remembering the time separation of day and night, which in probabilistic terms means the probability to happen during the daytime is 0.55 and to happen during the nighttime is 0.45. Combining all obtained results the final distribution density function is

$$p[1/L](u) =$$
$$\begin{cases} \gamma_n \, e^{-\beta_n(1/L_{o,n} - 1/L)} + \gamma_d \, e^{-\beta_d(1/L_{o,d} - 1/L)} & \text{if } 1/L < 1/L_{o,d}, \\ \gamma_n \, e^{-\beta_n(1/L_{o,n} - 1/L)} + \gamma_d \, e^{-\alpha_d(1/L - 1/L_{o,d})} & \text{if } 1/L_{o,d} \leqslant 1/L < 1/L_{o,n}, \\ \gamma_n \, e^{-\alpha_n(1/L - 1/L_{o,n})} + \gamma_d \, e^{-\alpha_d(1/L - 1/L_{o,d})} & \text{if } 1/L \geqslant 1/L_{o,n}. \end{cases} \quad \text{(B.3)}$$

Where the functions for the daily peak $1/L_{o,d}$ and the nightly peak $1/L_{o,n}$ are

$$1/L_{o,d} = -0.1454 \, e^{-0.3363u},$$
$$1/L_{o,n} = 0.0325 \, e^{-0.2847u} \quad \text{(B.4)}$$

and the function for the α, β and γ parameters again for day and night are

$$\begin{aligned} \alpha_d &= 2.7833u^2 + 3.4009, & \alpha_n &= 0.0964u^4 + 2.7043u^2 + 2.3052, \\ \beta_d &= 2.6504u^2 + 3.7918, & \beta_n &= 0.0441u^4 + 5.5791u^2 + 2.3962, \\ \gamma_d &= \frac{0.55}{1/\alpha_d + 1/\beta_d}, & \gamma_n &= \frac{0.45}{1/\alpha_n + 1/\beta_n}. \end{aligned} \quad \text{(B.5)}$$

Bibliography

[Abramowitz and Stegun, 1972] Abramowitz, M. and Stegun, I. A. (1972). *Handbook of Mathematical Functions with Formulas, Graphs and Mathematical Tables*, volume 55. Courier Dover Publications.

[AIJ, 2006] AIJ (2006). *Recommendations for Loads on Buildings*. Architectural Institute of Japan.

[Arya, 1984] Arya, S. P. S. (1984). "Parametric Relations for the Atmospheric Boundary Layer". *Boundary Layer Meteorology*, 30(1-4), pp. 57–73.

[Barenblatt, 1996] Barenblatt, G. I. (1996). *Scaling, Self-Similarity, and Intermediate Asymptotics*. Cambridge University Press.

[Beck and Katafygiotis, 1998] Beck, J. L. and Katafygiotis, L. S. (1998). "Updating Models and their Uncertainties. I: Bayesian Statistical Framework". *J. Eng. Mech. - ASCE*, 124(4), pp. 455–461.

[Beck and Yuen, 2004] Beck, J. L. and Yuen, K. (2004). "Model Selection Using Response Measurements: Bayesian Probabilistic Approach". *J. Eng. Mech. - ASCE*, 130, pp. 192–203.

[Benedetti et al., 2010] Benedetti, R. D.; Repetto, M. P.; and Solari, G. (2010). "Neutralità e non neutralità atmosferica: caratterizzazione probabilistica e risposta al vento delle strutture". In *Atti XI Convegno Nazionale di Ingegneria del Vento*, Spoleto. IN-VENTO 2010.

[Blackburn and Melbourn, 1993] Blackburn, H. M. and Melbourn, W. H. (1993). "Cross Flow Response of Slender Circular-Cylindrical Structures: Prediction Models and Recent Experimental Results". *J. Wind Eng. Ind. Aerodyn.*, 49, pp. 167–176.

[Blevins, 2001] Blevins, R. D. (2001). *Flow-Induced Vibration*. Krieger Publishing Company, second edition.

[Bowman and Azzalini, 1997] Bowman, A. W. and Azzalini, A. (1997). *Applied Smoothing Techniques for Data Analysis, The Kernel Approach with S-Plus Illustrations*, volume 18 of *Oxford Statistical Science Series*. Clardon Press Oxford.

[Bucher, 2009] Bucher, C. (2009). *Computational Analysis of Randomness in Structural Mechanics*, volume 3 of *Structures and Infrastructures Book Series*. Taylor and Francis Group, LLC.

[CICIND, 1999] CICIND (1999). *CICIND Model Code for Steel Chimneys Revision 1*. CICIND, Zurich.

[Clough and Penzien, 1995] Clough, R. W. and Penzien, J. (1995). *Dynamics of Structures*. Computers & Structures, Inc., 3rd edition.

[CNR, 2009] CNR (2009). *Istruzioni per la valutazione delle azioni e degli effetti del vento sulle costruzioni*. Consiglio Nazionale Delle Richerche.

[Colaiuda and Currarino, 2007] Colaiuda, G. and Currarino, A. (2007). "Il problema del distacco dei vortici nelle ciminiere: aspetti teorici e risvolti progettuali". Master's thesis, Università degli Studi di Genova, Italy.

[Daly, 1986] Daly, A. F. (1986). "Evaluation of Methods of Predicting the Across Wind Response of Chimneys". *CICIND Report*, 2(1), pp. 9–46.

[Devroye, 1986] Devroye, L. (1986). *Non-Uniform Random Variate Generation*. Springer.

[ESDU96030, 1996] ESDU96030 (1996). *Response of Structures to Vortex Shedding. Structures of Circular or Polygonal Cross Section.* Engineering Science Data Unit International plc, London.

[ESDU96031, 2000] ESDU96031 (2000). *Computer Program for Response of Structures to Vortex Shedding. Structures of Circular or Polygonal Section.* Engineering Science Data Unit International plc, London.

[Fellin and Lessmann, 2005] Fellin, W. and Lessmann, H. (2005). *Analyzing Uncertainty in Civil Engineering*. Springer.

[Griffin, 1975] Griffin, O. M. (1975). "The Resonant, Vortex-Excited Vibrations of Structures and Cabel Systems". *Offshore Technology Conference, 5-8 May , Houston, Texas*.

[Griffin, 1985] Griffin, O. M. (1985). "Vortex Induced Vibrations of Marine Cables and Structures". *NRL Memorandum Report 5600*.

[Griffin and Skop, 1973a] Griffin, O. M. and Skop, R. A. (1973a). "Measurements of the Response of Bluff Cylinders to Flow-Induced Vortex Shedding". *Offshore Technology Conference, 29 April-2 May , Houston, Texas*.

[Griffin and Skop, 1973b] Griffin, O. M. and Skop, R. A. (1973b). "The Vortex Excited Resonant Vibrations of Circular Cylinders". *J. Sound Vibrat.*, 31(2), pp. 235–249.

[Griffin and Votaw, 1972] Griffin, O. M. and Votaw, C. W. (1972). "The Vortex Street in the Wake of a Vibrating Cylinder". *J. Fluid Mech.*, 51(1), pp. 31–48.

[Gull, 1988] Gull, S. F. (1988). "Bayesian Inductive Inference and Maximum Entropy". In Erickson, G. J. and Smith, C. R., editors, *Maximum-Entropy and Bayesian Methods in Science and Engineering*, volume 1, pages 53–74. Kluwer Academic Publishers.

[Haibach, 2006] Haibach, E. (2006). *Betriebsfestigkeit, Verfahren und Daten zur Bauteilberechnung*. Springer, 3rd edition.

[Hansen, 1998] Hansen, S. O. (1998). "Vortex Induced Vibrations of Line Like Strucutures". *CICIND Report*, 15(1), pp. 15–23.

[Hazewinkel, 1987] Hazewinkel, M. (1987). *Encyclopaedia of Mathematics*, volume 8. Kluwer Academic Publishers.

[JCSS, 2001] JCSS (2001). *Probabilistic Model Code*, volume 1-3. Joint Committee on Structural Safety.

[Jones and al., 1969] Jones, G. W. and al. (1969). "Aerodynamic Forces on a Stationary and Oscillating Circular Cylinder at high Reynolds numbers". *NASA Technical Report*, TR R-300.

[Kareem, 1983] Kareem, A. (1983). "Reliability of Concrete Chimneys Under Winds". Technical Report 83-4, University of Houston Dept. of Civil Engineering.

[Kawecki and Żurański, 2005] Kawecki, J. and Żurański, J. A. (2005). "Cross Wind Vibrations of Steel Chimneys - A New Case History". In Náprstek, J. and Fischer, C., editors, *EACW4- The Fourth European & African Conference on Wind Engineering*.

[Lide, 2010] Lide, D. R. (2010). *CRC Handbook of Chemistry and Physics*. Taylor and Francis Group, LLC, 90th internet edition.

[MacKay, 1992] MacKay, D. J. C. (1992). "Bayesian Interpolation". *Neural Computation*, 4, pp. 415–447.

[Morgenthal, 2002] Morgenthal, G. (2002). *Aerodynamic Analysis of Structures Using High-resolution Vortex Particle Methods*. PhD thesis, University of Cambridge.

[Obukhov, 1971] Obukhov, A. M. (1971). "Turbulence in an Atmosphere with a Non-Uniform Temperature". *Boundary-Layer Meteorology*, 2, pp. 7–29.

[Pagnini and Solari, 2009] Pagnini, L. C. and Solari, G. (2009). "Preliminary elements for an innovative wind map of Italy". In *5th European-African Conference on Wind Engineering*.

[Panofsky and Dutton, 1983] Panofsky, H. A. and Dutton, J. A. (1983). *Atmospheric Turbulence Models and Methods for Engineering Applications*. John Wiley & Sons, Inc.

[Papadimitriou et al., 1997] Papadimitriou, C.; Beck, J. L.; and Katafygiotis, L. S. (1997). "Asymptotic Expansions for Reliability and Moments of Uncertain Systems". *J. Eng. Mech. - ASCE*, 123(12), pp. 1219–1229.

[Parzen, 1962] Parzen, E. (1962). "On Estimation of a Probability Density Function and Mode". *The Annals of Mathematical Statistics*, 33(3), pp. 1065–1076.

[Piccardo and Solari, 1998] Piccardo, G. and Solari, G. (1998). "Generalized Equivalent Spectrum Technique". *Wind and Structures*, 1(2), pp. 161–174.

[Piccardo and Solari, 2000] Piccardo, G. and Solari, G. (2000). "3D Wind-Excited Response of Slender Structures: Closed-Form Solution". *J. Struct. Eng. - ASCE*, 126(8), pp. 936–943.

[Plate, 1982] Plate, E. J. (1982). *Engineering Metrorology*. Elsevier.

[Råde and Westergren, 2000] Råde, L. and Westergren, B. (2000). *Springers Mathematische Formeln*. Springer.

[Repetto and Solari, 2002] Repetto, M. P. and Solari, G. (2002). "Dynamic Crosswind Fatigue of Slender Vertical Structures". *Wind and Structures*, 5(6), pp. 527–542.

[Repetto and Solari, 2004] Repetto, M. P. and Solari, G. (2004). "Directional Wind-Induced Fatigue of Slender Vertical Structures". *J. Struct. Eng. - ASCE*, 130(7), pp. 1032–1040.

[Repetto and Solari, 2007] Repetto, M. P. and Solari, G. (2007). "Wind-Induced Fatigue of Structures Under Neutral and Non-Neutral Atmospheric Conditions". *J. Wind Eng. Ind. Aerodyn.*, 95, pp. 1364–1383.

[Rodgers and Nicewander, 1988] Rodgers, J. L. and Nicewander, W. A. (1988). "Thirteen Ways to Look at the Correlation Coefficient". *The American Statisticien*, 42(1), pp. 59–66.

[Rosenblatt, 1956] Rosenblatt, M. (1956). "Remarks on Some Nonparametric Estimates of a Density Function". *The Annals of Mathematical Statistics*, 27(3), pp. 832–837.

[Ruscheweyh, 1985] Ruscheweyh, H. (1985). "Neuvorschalag für die grundsätzliche Neufassung nach Ruscheweyh". *RWTH Aachen*.

[Ruscheweyh, 1990] Ruscheweyh, H. (1990). "Practical Experiences with Wind-Induced Vibrations". *J. Wind Eng. Ind. Aerodyn.*, 33(1-2), pp. 211–218.

[Ruscheweyh, 1996] Ruscheweyh, H. (1996). "Full-scale measurements of wind-induced oscillations of chimneys". *J. Wind Eng. Ind. Aerodyn.*, 65, pp. 55–62.

[Ruscheweyh and Sedlacek, 1988] Ruscheweyh, H. and Sedlacek, G. (1988). "Crosswind Vibrations of Steel Stacks. –Critical Comparison Between some Recently Proposed Codes–". *J. Wind Eng. Ind. Aerodyn.*, 30, pp. 173–183.

[Saltelli, 2004] Saltelli, A. (2004). *Sensitivity Analysis in Practice: A Guide to Assessing Scientific Models.* John Wiley & Sons Ltd.

[Saltelli, 2008] Saltelli, A. (2008). *Global Sensitivity Analysis. The Primer.* John Wiley & Sons Ltd.

[Scruton, 1963] Scruton, C. (1963). "On the Wind Excited Oscillations of Stacks, Towers and Masts". *Symposium on Wind Effects on Buildings and Structures*, II, pp. 798–832.

[Simiu and Scanlan, 1996] Simiu, E. and Scanlan, R. H. (1996). *Wind Effects on Structures.* John Wiley & Sons, Inc., 3rd edition.

[Skop and Griffin, 1973] Skop, R. A. and Griffin, O. M. (1973). "An Heuristic Model for Determining Flow-Induced Vibration of Offshore Structure". *Offshore Technology Conference, 29 April-2 May , Houston, Texas.*

[Sobol', 1967] Sobol', I. M. (1967). "On the Distribution of Points in a Cube and Approximate Evaluation of Integrals". *U.S.S.R. Computational Mathematics and Mathematical Physics*, 7, pp. 86–112.

[Sobol' et al., 2007] Sobol', I. M.; Tarantola, S.; Gatelli, D.; Kucherenko, S. S.; and Mauntz, W. (2007). "Estimating the Approximation Error when Fixing Unessential Factors in Global Sensitivity Analysis". *Reliability Engineering and System Safety*, 92(7), pp. 957–960.

[Sockel, 1994] Sockel, H. (1994). *Wind-Excited Vibrations of Structures.* Springer.

[Solari, 1985] Solari, G. (1985). "Mathematical Model to Predict 3-D Wind Loading on Buildings". *J. Eng. Mech. - ASCE*, 111(2), pp. 254–276.

[Solari, 1997] Solari, G. (1997). "Wind-Excited Response of Structures with Uncertain Parameters". *Probabilistic Eng. Mech.*, 12(2), pp. 75–87.

[Solari, 2000] Solari, G. (2000). *Wind Excited and Aeroelastic Vibrations of Structures*. University of Genova.

[Solari and Piccardo, 2001] Solari, G. and Piccardo, G. (2001). "Probabilistic 3-D Turbulence Modeling for Gust Buffeting of Structures". *Probabilistic Eng. Mech.*, 16(1), pp. 73–86.

[Springer, 1979] Springer, M. D. (1979). *The Algebra of Random Variables*. John Wiley & Sons, Inc.

[Strouhal, 1878] Strouhal, V. (1878). "Über eine besondere Art der Tonerregung". *Annalen der Physik und Chemie*, 241(10), pp. 216 – 251.

[Stull, 1988] Stull, R. B. (1988). *An Introduction to Boundary Layer Meteorology*. Kluwer Academic Publishers.

[Taylor and Kitching, 2010] Taylor, A. N. and Kitching, T. D. (2010). "Analytic Methods for Cosmological Likelihoods". *Monthly Notices of the Royal Astronomical Society*, 000, pp. 1–12.

[van der Hoven, 1957] van der Hoven, I. (1957). "Power Spectrum of Horizontal Wind Speed in the Frequency Range from 0.0007 to 900 Cycles per Hour". *Journal of Meteorology*, 14(2), pp. 160–164.

[Verboom and van Koten, 2010] Verboom, G. K. and van Koten, H. (2010). "Vortex excitation: Three design rules tested on 13 industrial chimneys". *J. Wind Eng. Ind. Aerodyn.*, 98, pp. 145–154.

[Vickery and Basu, 1983a] Vickery, B. J. and Basu, R. (1983a). "Across-Wind Vibrations of Structure of Circular Cross-Section. Part II. Development of a Mathematical Model for Full-Scale Application". *J. Wind Eng. Ind. Aerodyn.*, 12(1), pp. 75–97.

[Vickery and Basu, 1983b] Vickery, B. J. and Basu, R. (1983b). "Across-Wind Vibrations Of Structures of Circular Cross-Section. Part I. Development of a Mathematical Model for Two-Dimensional Conditions". *J. Wind Eng. Ind. Aerodyn.*, 12(1), pp. 49–73.

[Vickery and Basu, 1983c] Vickery, B. J. and Basu, R. (1983c). "Simplified Approaches to the Evaluation of the Across-Wind Response of Chimneys". *J. Wind Eng. Ind. Aerodyn.*, 14(1-3), pp. 153–166.

[Vickery and Basu, 1984] Vickery, B. J. and Basu, R. I. (1984). "The Response of Reinforced Concret Chimneys to Vortex Shedding". *Engineering Structures*, 6(4), pp. 324–333.

[Vickery and Clark, 1972] Vickery, B. J. and Clark, A. W. (1972). "Lift or Across Wind Response of Taper Stacks". *J. Struct. Div. - ASCE*, 98(1), pp. 1–20.

[Whittle, 1958] Whittle, P. (1958). "On the Smoothing of Probability Density Functions". *J. R. Stat. Soc. Series B Stat. Methodol.*, 20(2), pp. 334–343.